



UNIVERSITEIT VAN PRETORIA  
UNIVERSITY OF PRETORIA  
YUNIBESITHI YA PRETORIA

Denkleiers • Leading Minds • Dikgopolo tša Dihlalefi

# **Structural and functional validation of S-adenosylmethionine decarboxylase as a novel drug target in the malaria parasite, *Plasmodium falciparum***

by

Dina Coertzen

Submitted in partial fulfilment of the requirements for the degree

*Philosophiae Doctor*  
(Specialisation in Biochemistry)

In the Faculty of Natural and Agricultural Sciences  
Department of Biochemistry  
University of Pretoria  
Pretoria  
South Africa

September 2014



UNIVERSITEIT VAN PRETORIA  
UNIVERSITY OF PRETORIA  
YUNIBESITHI YA PRETORIA  
Denkleiers • Leading Minds • Dikgopolo tša Dihlalefi

## **SUBMISSION DECLARATION**

I, Dina Coertzen declare that the thesis/dissertation, which I hereby submit for the degree at *Philosophiae Doctor* (Specialisation in Biochemistry) the University of Pretoria, is my own work and has not previously been submitted by me for the degree at this or any other tertiary institution.

SIGNATURE:.....

DATE:.....



## **PLAGIARISM DECLARATION**

Full names of student: Dina Coertzen

Student number: 27041612

### Declaration

1. I understand what plagiarism is and I am aware of the University's policy in this regard.
2. I declare that this thesis is my own original work. Where other people's work has been used (either from a printed source, Internet or any other source), this has been properly acknowledged and referenced in accordance with departmental requirements.
3. I have not used work previously produced by another student or any other person to hand in as my own.
4. I have not allowed, and will not allow, anyone to copy my work with the intention of passing it off as his or her own work.

SIGNATURE STUDENT:.....

DATE:.....

## Acknowledgements

I would like to acknowledge the following individuals and institutions:

My supervisor, Prof. L Birkholtz, for her support, guidance and insight during this project, as well as all the conference, research and collaborative opportunities she provided me.

My co-supervisor, Prof. A. I. Louw, for always providing support and input as well as bringing new ideas to the challenges I faced during this project.

The NRF Innovation bursary, which gave me the opportunity to continue my studies at the University of Pretoria.

Dr. Marni Williams and Janina Sprenger, for their advice and sharing their knowledge and expertise. Prof. Lo Persson, for inviting me to visit Lund University in Sweden, as well as his research input and his hospitality during the visit. Dr. Pieter Burger for his *in silico* work. Dr. Salome Smit from the Central analytical facility at Stellenbosch University for her Mass-Spectrometry analysis. Prof. Trevor Sewell and Dr. Brandon Webber at the Structural Biology Group, IDM, University of Cape Town for their advice and assistance in protein crystallography studies. Dr. Robert Barker from the Genzyme Corporation for donating the Genzyme compounds. Desiree Wilken from North-west University for synthesis of Pheroids™. Patricia Urbán from the Nanobioengineering group at the Institute for Bioengineering of Catalonia, University of Barcelona, Spain, for the synthesis of the immunoliposomes.

The students and staff of the Malaria Parasite Molecular Laboratory (M<sup>2</sup>PL); not only for their advice and assistance but also for their friendship and support.

My parents, parents-in-law and grandparents for their prayers and support, as well as my husband, Rudolf, for his love, care and encouragement during this endeavour.

The Lord, my complete trust in Him always provided me with the strength and eternal hope – all praise unto Him.

## Summary

*“Nobody can go back and start a new beginning, but everyone can start today and make a new ending”- Maria Robinson*

Malaria is considered the most prevailing human parasitic disease. Despite various chemotherapeutic interventions being available, the parasite responsible for the most lethal form of malaria, *Plasmodium falciparum*, is continuously developing resistance towards drugs targeted against it. This, therefore, necessitates the need for validation of new antimalarial development. Polyamine biosynthetic enzymes, particularly S-adenosylmethionine-L-decarboxylase (*PfAdoMetDC*), has been identified as a suitable drug target for protozoan parasitic diseases due to its essential role in cell proliferation. Furthermore, in *Plasmodium* polyamine biosynthesis, *PfAdoMetDC* is organised into a unique bifunctional complex with ornithine decarboxylase (*PfAdoMetDC/ODC*) covalently linked by a hinge region, distinguishing this enzyme as unique a drug target. However, inhibitors targeting this pathway have not been successful in clinical assessment, creating the need for further research in identifying novel inhibitors. This study focused on the structural and functional characterisation of protein-specific properties of the AdoMetDC domain in *P. falciparum* parasites, as well as identifying novel inhibitors targeting this enzyme as a potential antimalarial therapeutic intervention.

In order to develop novel inhibitors specifically targeting *PfAdoMetDC* through a structure-based drug discovery approach, the three-dimensional structure is required. However, due to a lack of structural and functional characterisation, determination of the crystal structure has been challenging. Heterologous expression of monofunctional *PfAdoMetDC* was achieved from a wild-type construct of the *PfAdoMetDC* domain including the covalently linked hinge region. In chapter 2, deletion of a large non-homologous, low-complexity parasite-specific insert (A3) in monofunctional *PfAdoMetDC* resulted in an increased yield, purity and sample homogeneity, whilst maintaining protein functionality and structural integrity. However, truncation of the proposed non-essential hinge region resulted in low-level expression of insoluble protein aggregates and a complete loss of protein activity, indicating that the hinge region is essential for monofunctional *PfAdoMetDC*.

However, in the absence of the three-dimensional *PfAdoMetDC* crystal structure, novel derivatives of a well-known AdoMetDC inhibitor, MDL73811, were tested for their activity against heterologous *PfAdoMetDC*, as well as their potency against *P. falciparum* parasites, in chapter 3. The compound Genz-644131 was identified as a lead inhibitor of *PfAdoMetDC*, however, the poor membrane permeability of the compound resulted in low *in vitro* activity. Drug permeability of Genz-644131 into *P. falciparum* infected erythrocytes and its potency was significantly improved by its encapsulation into a novel immunoliposome based drug delivery system.

The results presented here provide essential information for development of a unique strategy in obtaining sufficient levels of fully active recombinant *PfAdoMetDC* of sufficient purity for crystallisation studies and subsequent structure-based drug design efforts. The combination of Genz-644131 with the novel drug delivery system, which markedly improved its potency against *PfAdoMetDC* may prove to be a viable antimalarial chemotherapeutic strategy for future investigations.

## Table of contents

<b>List of Figures</b>	<b>x</b>
<b>List of Tables</b>	<b>xii</b>
<b>Abbreviations</b>	<b>xiii</b>
<b>Chapter 1: Introduction</b>	<b>1</b>
1.1 Malaria	1
1.2 The life cycle and pathogenesis of the malaria parasite, <i>Plasmodium falciparum</i>	2
1.3 Malaria control	4
1.3.1 Malaria elimination and eradication strategies	5
1.3.2 Vector control	5
1.3.3 Vaccine development	6
1.3.4 Diagnosis	7
1.3.5 Malaria chemotherapy	7
1.3.5.1 Quinolines	8
1.3.5.2 Antifolates	9
1.3.5.3 Atovaquone	9
1.3.5.4 Artemisinin	10
1.3.5.5 Antibiotics	11
1.3.5.6 Antimalarial combination therapies	11
1.4 Novel drug targets in parasitic protozoa	13
1.4.1 Role of polyamines in eukaryotic cells	13
1.4.2 Polyamine biosynthesis in the human host and parasitic protozoa	14
1.4.3 Polyamine biosynthetic enzymes as drug targets in parasitic protozoa	18
1.4.3.1 ODC inhibitors	18
1.4.3.2 AdoMetDC inhibitors	19
1.4.3.3 SpdS inhibitors	19
1.4.3.4 Polyamine analogues	20
1.4.4 Structural and functional characteristics of <i>PfAdoMetDC</i> /ODC	22
1.5 Research objectives	27
1.6 Research outputs	28
<b>Chapter 2: Structural and functional characterisation of monofunctional <i>PfAdoMetDC</i></b>	<b>30</b>
2.1 Introduction	30
2.2 Materials and Methods	35
2.2.1 <i>In silico</i> analysis of <i>PfAdoMetDC</i>	35
2.2.2 Cloning of codon harmonised <i>PfAdoMetDC</i> constructs	35
2.2.3 Analysis of recombinantly expressed and purified <i>PfAdoMetDC</i>	38
2.2.4 <i>PfAdoMetDC</i> activity determination	39
	vii

2.2.5 Analysis of mutated <i>PfAdoMetDC</i> secondary structure content with far-UV Circular Dichroism spectroscopy	40
2.2.6 Analysis of <i>PfAdoMetDC</i> protein flexibility with small angle X-ray scattering	40
2.2.7 Determination of the polydispersity index of SEC purified proteins with Dynamic light scattering	41
2.2.8 Determination of optimal protein crystallisation conditions with differential scanning fluorimetry	41
2.2.9 $\Delta A3$ <i>PfAdoMetDC</i> crystallisation trials	42
2.2.10 Statistical analyses	42
2.3 Results	43
2.3.1 <i>In silico</i> analysis of <i>PfAdoMetDC</i> reveals unique sequence characteristics of the A3 parasite-specific insert and the C-terminal hinge region	43
2.3.2 Expression and purification of deletion constructs reveals unique characteristics of the A3 insert and the hinge region for monofunctional <i>PfAdoMetDC</i>	45
2.3.2.1 Deletion of the A3 insert improves heterologous expression of monofunctional <i>PfAdoMetDC</i> .	45
2.3.2.2 The oligomeric status and sample homogeneity of monofunctional <i>PfAdoMetDC</i>	52
2.3.3 Analysis of $\Delta A3$ <i>PfAdoMetDC</i> reveals novel structural characteristics of the parasite-specific insert	56
2.3.3.1 Deletion of the A3 insert does not influence <i>PfAdoMetDC</i> structural integrity	56
2.3.4 Deletion of residues of the A3 parasite-specific insert aids in protein crystal formation	58
2.4 Discussion	63
2.5 Conclusion	68
<b>Chapter 3: Novel S-adenosyl-L-methionine decarboxylase inhibitors as potent antiproliferative agents against intra-erythrocytic <i>Plasmodium falciparum</i> parasites</b>	<b>69</b>
3.1 Introduction	69
3.2 Methods and materials	71
3.2.1 MDL73811 and derivatives	71
3.2.2 Recombinant <i>PfAdoMetDC</i> enzyme inhibition assays	71
3.2.3 Determination of the inhibition constant of Genz-644131 against <i>PfAdoMetDC</i>	71
3.2.4 Homology modelling and conformational analysis	71
3.2.5 <i>In vitro</i> cultivation of intra-erythrocytic <i>P. falciparum</i> parasites and $IC_{50}$ determination of MDL73811 derivatives	72
3.2.6 Determining parasite recovery following Genz-644131 inhibition	72
3.2.7 Spermidine uptake in intra-erythrocytic <i>P. falciparum</i> parasites	73
3.2.8 Comparative $IC_{50}$ determination of Genz-644131 incorporated with	



Pheriod® technology	73
3.2.9 Comparative IC <sub>50</sub> determination of Genz-644131 with immunoliposomes	74
3.2.10 Statistical analyses	74
3.3. Results	75
3.3.1 Inhibitory effect of MDL73811 derivatives on heterologous monofunctional <i>PfAdoMetDC</i> and bifunctional <i>PfAdoMetDC/ODC</i>	75
3.3.2 Genz-644131 is active against <i>in vitro</i> intra-erythrocytic <i>P. falciparum</i> parasites	79
3.3.3. Effect of Genz-644131 encapsulated in nanovectors on <i>in vitro</i> antiplasmodial activity	83
3.4 Discussion	84
<b>Chapter 4: Concluding discussion</b>	<b>88</b>
<b>References</b>	<b>93</b>
<b>Appendices</b>	<b>i</b>
Appendix 1: Plasmid maps of wild-type, C505S, ΔA3, ΔH and ΔA3ΔH <i>PfAdoMetDC</i> .	i
Appendix 2: PCR products of ΔH and ΔA3ΔH <i>PfAdoMetDC</i> recombinant cloning.	iii
Appendix 3: Restriction enzyme mapping of wild-type, C505S, ΔA3, ΔH and ΔA3ΔH <i>PfAdoMetDC</i> .	iv
Appendix 4: Automated nucleotide sequencing of ΔA3, ΔH and ΔA3ΔH <i>PfAdoMetDC</i> .	vi
Appendix 5: <i>PfAdoMetDC</i> A3 insert amino acid sequence analysis, Kyte and Doolittle hydrophobicity plot, complexity and disorder prediction	viii
Appendix 6: MALDI-TOF MS analysis of ΔA3 <i>PfAdoMetDC</i> .	x
Appendix 7: Supplemental data for novel <i>S</i> -adenosyl-L-methionine decarboxylase inhibitors as potent antiproliferative agents against intra-erythrocytic <i>Plasmodium falciparum</i> parasites.	xv
Appendix 8: Kitz-Wilson enzyme kinetics analysis of MDL73811 against bifunctional and monofunctional <i>PfAdoMetDC</i>	xxi
Appendix 9: Dose response IC <sub>50</sub> curves of MDL73811 derivatives as determined with the SYBR Green I-based assay	xxii
Appendix 10: Scanning Confocal Laser Microscopy (SCLM) of Pheriods® encapsulating Genz-644131	xxiii

## List of Figures

### Chapter 1

Figure 1.1: The global distribution of malaria in 2011.	1
Figure 1.2: Diagram depicting the life cycle of the <i>P. falciparum</i> parasite.	3
Figure 1.3: Malaria control strategies: preventative and curative strategies for vector control, disease transmission and disease development.	5
Figure 1.4: Polyamine biosynthetic pathways in <i>protozoan</i> parasites compared to the human host.	16
Figure 1.5: Intracellular concentrations of polyamines during the intra-erythrocytic lifestage.	17
Figure 1.6: The bifunctional arrangement of <i>PfAdoMetDC</i> /ODC.	24

### Chapter 2

Figure 2.1: Homology model of monofunctional <i>PfAdoMetDC</i> .	32
Figure 2.2: Proposed mechanisms of heterologous monofunctional <i>PfAdoMetDC</i> oligomerisation <i>in vitro</i> .	34
Figure 2.3: Schematic diagram of the <i>PfAdoMetDC</i> wild-type protein and various mutant proteins created in this study to allow comparative structure-activity analyses.	37
Figure 2.4: Secondary structure prediction of <i>PfAdoMetDC</i> .	44
Figure 2.5: Amino acid sequence alignments of wild-type, C505S, $\Delta$ A3, $\Delta$ H and $\Delta$ A3 $\Delta$ H <i>PfAdoMetDC</i> .	46
Figure 2.6: Protein concentration and yield determination of soluble protein from wild-type and mutant (C505S, $\Delta$ A3, $\Delta$ H and $\Delta$ A3 $\Delta$ H) <i>PfAdoMetDC</i> .	47
Figure 2.7: Reducing SDS-PAGE of 5 $\mu$ g affinity chromatography purified wild-type, C505S, $\Delta$ A3, $\Delta$ H and $\Delta$ A3 $\Delta$ H <i>PfAdoMetDC</i> .	48
Figure 2.8: Reducing SDS-PAGE analysis of <i>PfAdoMetDC</i> cell lysates, soluble and insoluble fractions.	49
Figure 2.9: Specific activities of soluble wild-type, C505S, $\Delta$ A3, $\Delta$ H and $\Delta$ A3 $\Delta$ H <i>PfAdoMetDC</i> .	50
Figure 2.10: Detection of $\Delta$ A3 <i>PfAdoMetDC</i> homodimer observed by reducing SDS-PAGE through Western immunodetection and MADLI-TOF MS.	51
Figure 2.11: HMW standard curve for analytical SEC (44-669 kDa).	52
Figure 2.12: Analytical SEC purification under reducing conditions followed by reducing SDS-PAGE of collected peak fractions of wild-type, C505S and $\Delta$ A3 <i>PfAdoMetDC</i> .	54

Figure 2.13: Analytical SEC of affinity chromatography purified $\Delta A3$ <i>PfAdoMetDC</i> under reducing and non-reducing conditions.	55
Figure 2.14: Far-UV CD analysis of C505S and $\Delta A3$ <i>PfAdoMetDC</i> .	56
Figure 2.15: SAXS analysis of C505S and $\Delta A3$ <i>PfAdoMetDC</i> .	57
Figure 2.16: Differential scanning fluorimetry (DSF) of SEC purified $\Delta A3$ <i>PfAdoMetDC</i> under different buffering conditions.	60
Figure 2.17: Reducing SEC of ~4 mg $\Delta A3$ <i>PfAdoMetDC</i> with buffer W and HEPES buffer.	61
Figure 2.18: $\Delta A3$ <i>PfAdoMetDC</i> needle clusters.	62
<b>Chapter 3</b>	
Figure 3.1: The inhibitory activities of MDL73811 derivatives against monofunctional <i>PfAdoMetDC</i> (grey) and the <i>PfAdoMetDC</i> domain of bifunctional <i>PfAdoMetDC/ODC</i> (black).	75
Figure 3.2: Enzyme kinetics of Genz-644131 against monofunctional and bifunctional <i>PfAdoMetDC</i> .	76
Figure 3.3: A predicted binding pose for Genz-644131 to <i>PfAdoMetDC</i> highlighting conserved residues with <i>T. brucei</i> and human protein equivalents.	79
Figure 3.4: Uptake of [ <sup>3</sup> H]spermidine, with rescue and reversibility of Genz-644131 inhibited intra-erythrocytic <i>P. falciparum</i> parasites <i>in vitro</i> .	81
Figure 3.5: The effect of encapsulation of Genz-644131 in different nanovectors on its <i>in vitro</i> anti-plasmodial activity.	83
<b>Chapter 4</b>	
Figure 4.1: The proposed spatial organisation of heterotetrameric bifunctional <i>PfAdoMetDC/ODC</i> .	92

## List of Tables

### Chapter 1

Table 1.1: Current antimalarial drug combination therapies.	12
Table 1.2: Inhibitors of polyamine biosynthetic enzymes.	21

### Chapter 2

Table 2.1: MALDI-TOF MS analysis of ~50 µg affinity chromatography purified soluble $\Delta A3$ PfAdoMetDC.	51
Table 2.2: Protein hydrodynamic radii ( $R_H$ ) and polydispersity index (Pdl) determined under reducing conditions for C505S and $\Delta A3$ PfAdoMetDC.	59
Table 2.3: Protein crystallisation conditions for $\Delta A3$ PfAdoMetDC.	62

### Chapter 3

Table 3.1: Conformational search analysis of MDL73811 and its derivatives.	78
--	----

## Abbreviations

<b>4-MCHA</b>	<i>trans</i> -4-methylcyclohexyl amine
<b>AAR</b>	Amino acid repeats
<b>AbeAdo</b>	5'-([(Z)-4-amino-2-butenyl]methylamino)-5'-deoxyadenosine
<b>ACT</b>	Artemisinin combination therapy
<b>ADME</b>	Absorption, Distribution, Metabolism, Excretion
<b>AdoDATO</b>	S-adenosyl-1,8-diamino-3-thio-octane
<b>AdoMet</b>	S-adenosyl-L-methionine
<b>AdoMetDC</b>	S-adenosyl-L-methioine-L-decarboxylase
<b>AG</b>	aminoguanidine
<b>AHT</b>	anhydrotetracycline
<b>APA-1</b>	aminoxy-3-aminopropane
<b>CAPS</b>	3-(cyclohexylamino)-1-propane
<b>CGP48664</b>	4-amidinoindan-1-one-2'-amidinohydrazone
<b>CHA</b>	cyclohexylamine
<b>CSLM</b>	Confocal laser scanning microscopy
<b>CPM</b>	Counts per minute
<b>CQ</b>	chloroquine
<b>CSP</b>	circumsporozoite protein
<b>DDT</b>	1,1,1-trichloro-2,2-bis(4-chlorophenyl)ethane
<b>dcAdoMet</b>	decarboxylated S-adenosyl-L-methionine
<b>DFMO</b>	DL- $\alpha$ -difluoromethylornithine
<b>DHFR</b>	dihydrofolate reductase
<b>DHPS</b>	dihydropteroate synthase
<b>DLS</b>	Dynamic light spectroscopy
<b>DPM</b>	Degradations per minute
<b>DSF</b>	Differential scanning fluorimetry
<b>DSMO</b>	dimethyl sulfoxide
<b>DTT</b>	dithiotreitol
<b>elf-5a</b>	eukaryotic initiation factor 5A
<b>Far-UV CD</b>	far- ultraviolet circular dichroism
<b>GMAP</b>	Global Malaria Action Plan
<b>gor</b>	glutathione reductase
<b>GSH</b>	glutathione
<b>HABA</b>	4-hydroxyazobenzene-2-carboxylic acid
<b>HEPES</b>	4-(2-hydroxyethyl)-1-piperazineethanesulfonic acid
<b>hFNT1</b>	human facilitative nucleobase transporter
<b>HomoT(SH)<sub>2</sub></b>	homotrypanothione
<b>HPLC-MS</b>	High performance liquid chromatography-mass spectrometry
<b>HRP</b>	horseradish peroxidase
<b>HTS</b>	High throughput screening
<b>IC<sub>50</sub></b>	Inhibitory concentration at 50% parasite proliferation
<b>IDC</b>	Intra-erythrocytic developmental cycle
<b>IDP</b>	Intrinsically disordered regions
<b>IPT</b>	Intermittent preventative treatment
<b>IRS</b>	Indoor residual spraying
<b>ITN</b>	Insecticide treated net
<b>IUR</b>	Intrinsically unstructured regions
<b>K<sub>i</sub></b>	Inhibition constant
<b>LCR</b>	Low complexity region
<b><i>L. infantum</i></b>	<i>Leishmania infantum</i>
<b><i>L. donovani</i></b>	<i>Leishmania donovani</i>

<b>MALDI-TOF MS</b>	Matrix assisted laser desorption ionisation time of flight mass-spectrometry
<b>MES</b>	2-( <i>N</i> -morpholino)ethanesulfonic acid
<b>MDL73811</b>	5'-[( <i>Z</i> )-4-amino-2-butenyl]methylamino)-5'-deoxyadenosine
<b>MDL27695</b>	<i>N,N'</i> -bis{3-[(phenylmethyl)amino]propyl}-1,7-diaminoheptanex
<b>MGBG</b>	Methylglyoxal bis(gaunylhydrazone)
<b>mRNA</b>	messenger RNA
<b>MQ</b>	mefloquine
<b>MSP</b>	Merozoite surface proteins
<b>MTA</b>	5'-methylthioadenosine
<b>MM</b>	molecular mass
<b>ODC</b>	ornithine decarboxylase
<b>pABA</b>	<i>p</i> -aminobenzoic acid
<b><i>P. berghei</i></b>	<i>Plasmodium berghei</i>
<b><i>P. falciparum</i></b>	<i>Plasmodium falciparum</i>
<b><i>P. knowlesi</i></b>	<i>Plasmodium knowlesi</i>
<b><i>P. malariae</i></b>	<i>Plasmodium malariae</i>
<b><i>P. ovale</i></b>	<i>Plasmodium ovale</i>
<b><i>P. knowlesi</i></b>	<i>Plasmodium knowlesi</i>
<b><i>P. vivax</i></b>	<i>Plasmodium vivax</i>
<b>PDI</b>	Polydispersity index
<b>PEG</b>	poly ethylene glycol
<b><i>PfADA</i></b>	<i>P. falciparum</i> adenosine deaminase
<b><i>PfAdoMetDC</i></b>	<i>Plasmodium falciparum</i> S-adenosylmethionine-L-decarboxylase
<b><i>PfAdoMetDC/ODC</i></b>	<i>Plasmodium falciparum</i> S-adenosylmethionine-L-decarboxylase/ ornithine decarboxylase
<b><i>Pfcrt</i></b>	<i>Plasmodium falciparum</i> chloroquine resistance transporter
<b><i>PfDHFR/TS</i></b>	<i>Plasmodium falciparum</i> dihydrofolate reductase/thymidylate synthase
<b><i>PfEMP1</i></b>	<i>Plasmodium falciparum</i> erythrocyte membrane protein 1
<b><i>PfHPPK/DHPS</i></b>	<i>Plasmodium falciparum</i> hydroxymethylpterinyprophospho kinase/dihydropteroate synthase
<b><i>PfLDH</i></b>	<i>Plasmodium falciparum</i> lactate dehydrogenase
<b><i>Pfmdr</i></b>	<i>Plasmodium falciparum</i> multiple drug resistance
<b><i>PfODC</i></b>	<i>Plasmodium falciparum</i> ornithine decarboxylase
<b><i>Pfpgh1</i></b>	<i>Plasmodium falciparum</i> prostaglandin H1
<b><i>PfPFT</i></b>	<i>Plasmodium falciparum</i> farnesyltransferase
<b><i>PfSpdS</i></b>	<i>Plasmodium falciparum</i> spermidine synthase
<b>PK</b>	pharmacokinetic
<b>PLP</b>	pyridoxal-5'-phosphate
<b>Put</b>	putrescine
<b>QN</b>	quinine
<b>RDT</b>	Rapid diagnostic test
<b>R<sub>H</sub></b>	Hydrodynamic radii
<b>ROS</b>	reactive oxygen species
<b>SA</b>	specific activity
<b>SAXS</b>	Small Angle X-ray Scattering
<b>SAMS</b>	S-adenosylmethionine synthase
<b>SEC</b>	size exclusion chromatography
<b>SEM</b>	standard error of the mean
<b>SERCA</b>	Sarcoendoplasmic reticulum (SR) calcium transport ATPase
<b>SDS - PAGE</b>	Sodium dodecyl sulphate - polyacrylamide gel electrophoresis
<b><i>Solanum tuberosum</i></b>	<i>S. tuberosum</i>
<b>Spd</b>	spermidine
<b>SpdS</b>	spermidine synthase
<b>Spm</b>	spermine

<b>SpmS</b>	spermine synthase
<b>SSAT</b>	spermidine/Spermine N1-acetyltransferases
<b>Strep-tag II</b>	Streptavidin tag II
<b>TCEP</b>	Tris-2(carboxyethyl phosphine)
<b><i>T. cruzi</i></b>	<i>Trypanosoma cruzi</i>
<b><i>T. b. brucei</i></b>	<i>Trypanosoma brucei brucei</i>
<b><i>T. b. rhodesiense</i></b>	<i>Trypanosoma brucei rhodesiense</i>
<b>TCA</b>	trichloro-acetic acid
<b>TCEP</b>	tri-(2-carboxymethyl) Phosphine Hydrochloride
<b><i>tet</i></b>	tetracycline
<b><i>trxB</i></b>	thioredoxin reductase
<b>TryR</b>	trypanothione reductase
<b>TS</b>	thymidylate synthase
<b>TS<sub>2</sub></b>	oxidised trypanothione
<b>T(SH)<sub>2</sub></b>	reduced trypanothione
<b>TyrS</b>	trypanothione syntethase
<b>WHO</b>	World health organisation

# Chapter 1

## Introduction

### 1.1 Malaria

Malaria is the most prevalent vector-borne parasitic disease in the world, with 207 million cases reported, which resulted in 627 000 recorded deaths, in 2012. According to the WHO, approximately 90% of these deaths occur in sub-Saharan Africa, most of these being children under the age of five (1, 2).

The disease is endemic to 97 countries, as shown in the world map (Figure 1.1). These include tropical and sub-tropical regions such as equatorial South America, sub-Saharan Africa and Southeast Asia (3, 4), and places 3.4 billion people at risk for transmission. Not only does malaria place significant pressure on public health expenditure in Africa, it accounts for 12-30 billion dollars in lost GDP annually, therefore, having a severe impact on the socio-economic development within these poverty afflicted countries (1, 5).

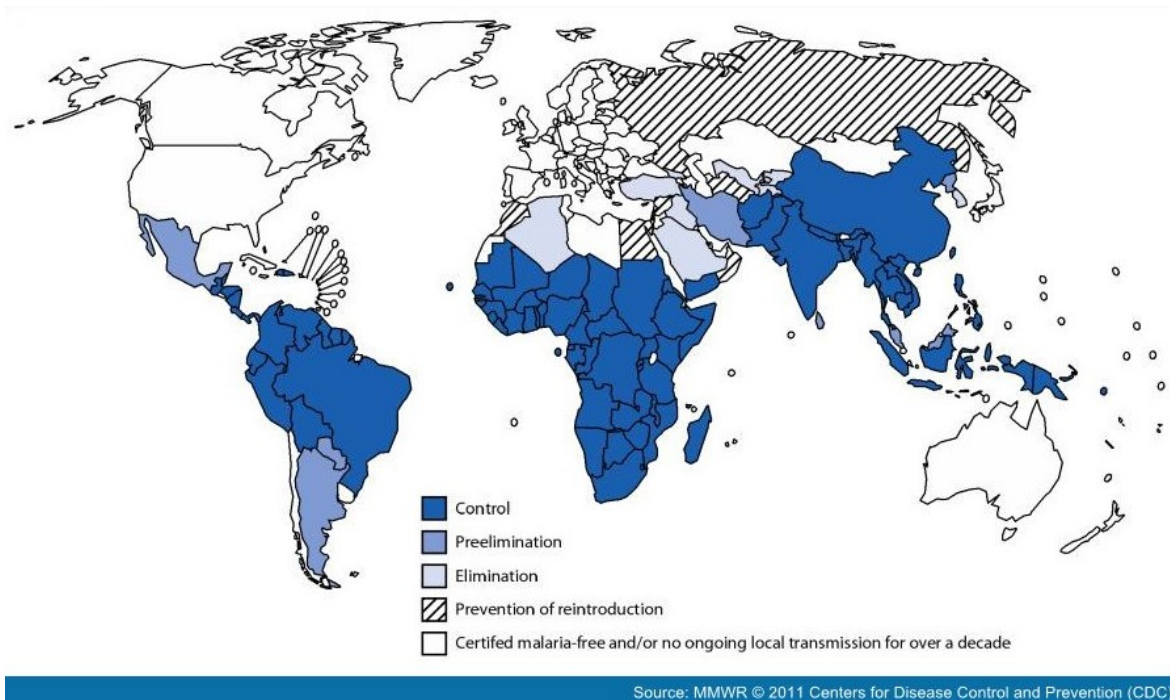


**Figure 1.1: The global distribution of malaria in 2011.** The image depicts the epidemiology of malaria globally. Image obtained from <http://www.cdc.gov>.



## 1.2 The life cycle and pathogenesis of the malaria parasite, *Plasmodium falciparum*

Malaria infections are caused by unicellular, protozoan parasites in the apicomplexan phylum of the *Plasmodium* genus. There are five *Plasmodium* species known to cause malaria infections in humans: *P. malariae*, *P. vivax*, *P. ovale*, *P. knowlesi* (6) and *P. falciparum* (7). *P. falciparum* is clinically the most lethal species being responsible for approximately 90% of recorded deaths (8).

Parasites are transmitted from the vector a female *Anopheles* mosquito to a human host during a blood meal (9) (Figure 1.2). *Plasmodia*, in particular *P. falciparum* parasites, have a complex life cycle involving sexual replication within the mosquito vector and asexual replication within the mammalian host. When a mosquito feeds on a human host, sporozoites (small, haploid, elongated cells) are transmitted from the mosquito salivary glands into the host where they migrate through the bloodstream to infect the host's hepatocytes, initiating the exo-erythrocytic developmental stage (Figure 1.2A). Parasites are rapidly replicated, developing into mature schizonts in the hepatocytes. The hepatocytes rupture releasing thousands of daughter merozoites, which enter the blood stream infecting host erythrocytes, initiating the asexual intra-erythrocytic developmental cycle (IDC) (Figure 1.2B). After *P. falciparum* merozoites have infected erythrocytes, the parasite progresses asexually through the ring, trophozoite and schizont developmental stages. Mature schizonts rupture the erythrocyte membrane releasing 16 to 32 daughter merozoites, which can re-infect erythrocytes for subsequent asexual development cycles increasing host parasitaemia levels. Some parasites differentiate into male or female gametocytes, and these gametocytes are transmitted back to the mosquito vector upon taking its next blood meal.

The formation of gametocytes initiates the sexual stage of the parasite life cycle, known as the sporogonic cycle (Figure 1.2C). Following uptake by the mosquito, gametocytes mature into gametes through fusion of the haploid, flagellated, male microgametocytes and female macrogametocytes, forming zygotes in the mosquito gut. Zygotes mature through ookinesis into an oocyte, rupturing these cells and releasing sporozoites that proliferate rapidly within outer cell walls of the mosquito intestine. Mature sporozoites migrate to the mosquito salivary gland, which are then transmitted back to the human host during a subsequent blood meal (10) (Figure 1.2C).

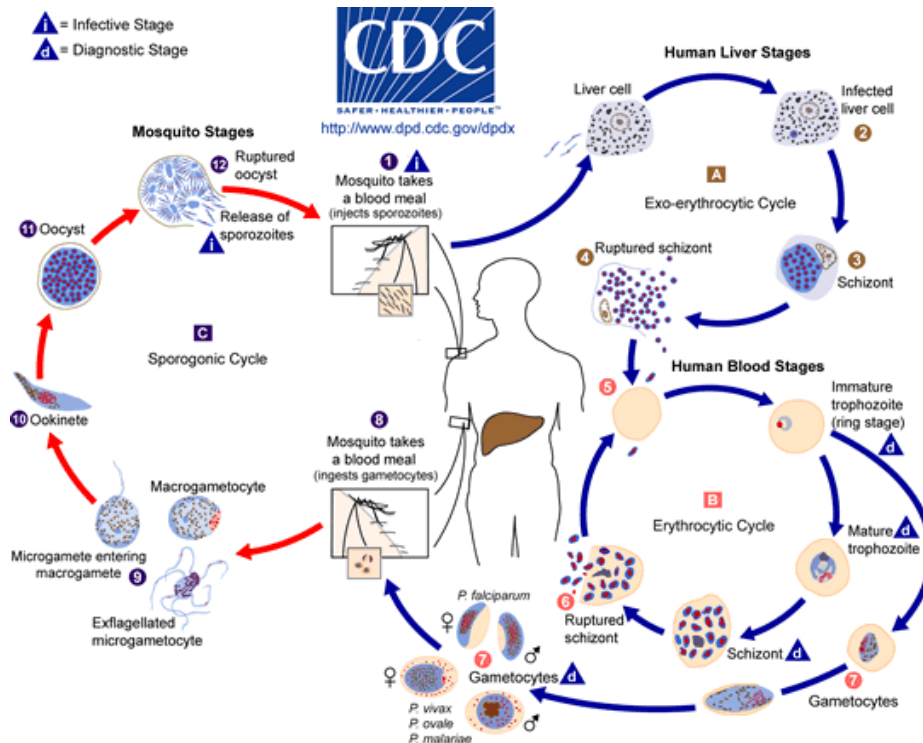


**Figure 1.2: Diagram depicting the life cycle of the *P. falciparum* parasite.** The parasite life cycle alters between sexual replication stages within the gut of the mosquito vector and an asexual stage within the human host. ① Sporozoites infect the human host. **A** The exo-erythrocytic cycle. ② In the hepatocytes, the parasites develop into schizonts. ③ The schizonts mature into merozoites. ④ The merozoites are released from the hepatocytes and enter the blood stream infecting erythrocytes. **B** Asexual life cycle. ⑤ Released merozoites re-infect the erythrocytes. ⑥ Within the erythrocytes, trophozoites mature into schizonts and release merozoites. ⑦ Some merozoites differentiate into female or male gametocytes. ⑧ The mosquito ingests the male and female gametocytes, upon a blood meal in the host. **C** The sexual sporogonic cycle. ⑨ Within the gut of the mosquito, the gametes fuse to become zygotes. ⑩ Zygotes differentiate into ookinetes. ⑪ Within the gut of the mosquito, the ookinetes mature to form oocysts. ⑫ These large oocysts rupture to release sporozoites. Mature sporozoites migrate to the salivary glands. Image obtained from <http://www.cdc.gov/malaria/about/biology/>.

Following transmission to the human host, some *Plasmodium* parasites can remain dormant in the host's hepatocytes. Dormancy and the location of dormant parasites depend on the parasite species for example, *P. vivax* and *P. ovale* have a long latent liver phase (incubation periods of months to years) (11), compared to *P. falciparum* that immediately matures into schizonts, resulting in disease formation (incubation period of 7 days) (12).

Disease symptoms develop within the human host during the parasite's asexual IDC. In uncomplicated malaria cases, symptoms include fever, chills, headaches, muscular aches, vomiting, coughing, diarrhoea and abdominal pain. The febrile nature of these symptoms makes it difficult to detect and diagnose the initial stages of the disease (13). Once an uncomplicated *P. falciparum* infection is left untreated, the disease can progress into severe

complicated malaria, which is characterised as cerebral malaria. At this stage of the disease, parasite-infected erythrocytes start to sequester and rosette in the cerebral microvessels of brain tissue resulting in patients entering a coma, ultimately leading to death or severe brain impairment (13-15).

Owing to the multiple stages of the parasite's life cycle, various disease control strategies have been implemented to assist in the elimination and possible eradication of the disease. These include elimination of vectors, preventing parasite transmission between host and vector, and if parasite transmission occurred, inhibition of parasite proliferation within the host and transmission back to the vector.

### **1.3 Malaria control**

The Global Malaria Action Plan (GMAP) for malaria elimination and eradication, targeting each stage of malaria transmission and progression, was adopted in 2007 to enable comprehensive disease control by 2025 (16). Preventative disease control includes physical and chemical vector control through indoor residual spraying (IRS) and insecticide-treated bed nets (ITNs). Strategies to prevent disease transmission include the use of validated vaccines and intermittent preventative treatments (IPT) and chemoprophylaxis in infants and travellers (Figure 1.3). However, current disease control for infected hosts mostly relies on accurate diagnosis of the disease followed by curative disease control through chemotherapeutic intervention, either as drug mono- or combination therapies (Figure 1.3) (17, 18).

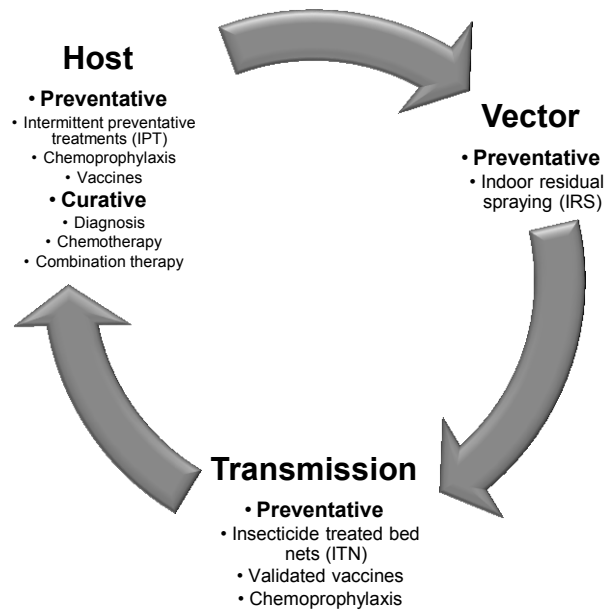


**Figure 1.3: Malaria control strategies: preventative and curative strategies for vector control, disease transmission and disease development.** The preventative strategies for malaria control include: *Anopheles* vector control via IRS, disease transmission is prevented with the use of ITN's, chemoprophylaxis and validated vaccines. Chemoprophylaxis and IPT strategies are in place to prevent disease transmission. However, if transmission occurred and disease symptoms present itself, the use of either drug mono- or combination therapies are in place as a curative strategy, following diagnosis. Chemotherapeutic intervention usually prevents transmission of parasites back into the mosquito vector from an infected host.

### 1.3.1 Malaria elimination and eradication strategies

The GMAP implemented in 2007 by the WHO with the Roll Back on Malaria program, aimed at eliminating (defined as reducing the number of malaria cases of locally acquired infections to zero, in a specific geographic area through deliberate efforts (16)), and eradicating (reducing global malaria incidence to zero) malaria. The WHO World Malaria Report (2013) states that, by the end of 2015, there should be a 75% reduction in malaria cases, with most deaths being eliminated, and the disease eradicated in at least 10 more endemic countries (1). In order to achieve this, monitoring of malaria endemic regions (identified through geographical reconnaissance) and consistent management through preventative and control disease measures, which include diagnosis and vector eradication, vaccination, diagnosis and treatment, would have to be performed (17).

### 1.3.2 Vector control

Physical and chemical vector control aims to prevent disease transmission from *Anopheles* mosquitoes to the host. Chemical vector control through IRS mainly depends on the use of the insecticides: 1,1,1-trichloro-2,2-bis(4-chlorophenyl)ethane (DDT) and pyrethroids. DDT, a broad spectrum insecticide, was the first synthetic insecticide developed during the 1940s for use during World War II to prevent soldiers from contracting insect transmitted diseases (19). DDT successfully eradicated malaria in the 1950s to 1960s in first-world countries (5), but, for various reasons, was not successful in eradicating malaria in the tropical and sub-tropical third-world countries (20). Later, the overuse of DDT for crop spraying was found to have detrimental effects on human health that led to its classification as a persistent organic pollutant at the 2001 Stockholm convention, and its use for commercial purposes was terminated (21). However, due to the prohibited use of DDT, mosquitoes resistant to the exclusively used pyrethroid insecticides spread rapidly, which led to an increase in disease incidence in the 1990s, particularly in sub-Saharan Africa. Therefore, DDT was re-introduced by the WHO global Malaria Eradication Campaign (22, 23), for use as an insecticide for malaria control in countries experiencing pyrethroid resistance. The use of DDT is stringently controlled by regulations recommended by the WHO, which includes limited spraying of residential structures only and no aerial/ mass applications. Conversely, increasing resistance of mosquitoes to DDT and pyrethroids threatens this crucial malaria elimination strategy. Physical vector control aims to prevent disease transmission to the host by using insecticide-treated bed nets (ITNs) or long lasting insecticide treated nets (LLINs). However, most nets only have a three-year lifespan (1), and have to be replaced and regularly maintained, which along with misuse and limited quantities, creates logistical problems in rural sub-Saharan Africa.

### 1.3.3 Vaccine development

For effective malaria control as stipulated by the Roll Back on Malaria program, an effective vaccine is required but to date no reliable malaria vaccine has been developed yet (24, 25). Three approaches for malaria vaccine development are being followed; 1) pre-erythrocytic vaccines (preventing sporozoites from infecting hepatocytes and progressing to the IDC stage), 2) erythrocytic vaccines (reducing parasite levels during the IDC) and 3) transmission blocking vaccines (preventing sequestration of mosquito ingested gametocytes into the mosquito gut) (26). The most advanced pre-erythrocytic vaccine undergoing Phase III clinical trials (27), RTS'S/AS02 from GlaxoSmithKline, consists of an antigenic C-terminus circumsporozoite protein (CSP) fused to a hepatitis B surface antigen expressed as virus-like

particles in *Saccharomyces cerevisiae* (28). Second generation vaccines targeting the asexual stage erythrocytic merozoite surface proteins (MSP) vaccines, MSP/RESA (29) and FMP2.1(AMA-1/AS02) (30) have also been developed and are currently in Phase I and II clinical trials. However, none of these vaccines have been shown to be completely effective in providing successful immunity against malaria in rural settings (24). Although the MSP proteins are the most suitable immunogenic targets for vaccine development, their polymorphic gene characteristics and antigen switching properties in the *Plasmodium* genome (31) creates a unique challenge for vaccine development. Therefore, due to challenges confronting vaccine research, a long-term goal for vaccine deployment has been set for production of a suitable vaccine only by 2025 (32).

#### 1.3.4 Diagnosis

Diagnosis is an essential part of malaria control since accurate and early detection of infections can decrease disease transmission rates and drug resistance development against antimalarials. Numerous diagnostic tools have been developed for recognising malaria infections, however, the requirement for specialised training and equipment for implementing of these diagnostic tools creates challenges in diagnosing malaria especially in rural endemic settings (18). Microscopically analysed Giemsa-stained blood smears remains the standard diagnostic tool for malaria in both rural and urban regions, since it allows for identification of infective stage, species and parasitaemia (33). An alternative malaria diagnostic tool is the use of rapid diagnostic tests (RDTs), providing up to 90% accuracy and requiring minimal training and ease of interpretation (34, 35). However, RDTs are not cost effective and have short-term temperature dependent storage conditions, limiting their use in malaria endemic regions. Other means of diagnosis, although not suitable for rural regions include fluorescent microscopy (34), serological testing, flow cytometry (36), automated pigment detection (37) and polymerase chain reaction (PCR). Diagnosis with PCR is the most sensitive and specific tool for diagnosis but also has limited field applications (7).

#### 1.3.5 Malaria chemotherapy

Malaria prevention and treatment, through chemoprophylaxis and chemotherapy, are the most effective methods for disease control. However, developing novel antimalarials is a challenge in itself, since drugs should have activity against resistant strains, parasite selectivity and low toxicity for pregnant woman and children, with good oral bio-availability, shorter treatment times assisting in drug compliancy, and affordability (38, 39). Three classes of antimalarials

(most of which target the asexual IDC stage of the parasite), Quinolines, Antifolates and Artemisinins, have been identified with derivatives in each class being based on a single chemical backbone structure and a similar mode of action.

#### 1.3.5.1 Quinolines

Quinine (QN), the first antimalarial identified, was isolated from the bark of the *Cinchona ledgeriana* tree in South America in the 17<sup>th</sup> century (40). From this compound a series of derivatives belonging to the quinolone class of compounds have been developed, e.g. the 4-aminoquinoline quinine derivative, chloroquine (CQ), was introduced as the first synthetic antimalarial agent in 1934. Quinolines accumulate within the digestive food vacuole in parasite-infected erythrocytes, inhibiting haem polymerization into haemozoin crystals. The drugs form complex  $\pi$ -stacking with the heterocyclic haem ferriprotoporphyrin (IX) ring between the porphyrin units preventing haemozoin formation, which is toxic to the parasite (41-43).

Resistance to CQ was first detected in 1957 on the Thailand-Cambodian border from where it rapidly spread to sub-Saharan Africa by 1988, rendering the drug largely ineffective for malaria treatment. The mechanism of resistance to CQ is due to a K76T point mutation in the *P. falciparum* chloroquine resistance transporter gene (*Pfcr*t). This mutation of the encoded transmembrane protein in the digestive food vacuole alters the pH of the food vacuole, thus reducing CQ accumulation and allowing haemozoin crystal formation (44, 45). Parasite resistance to CQ resulted in the development of alternative 4-aminoquinoline derivatives; primaquine, amodiaquine, the 8-aminoquinoline; pamaquine (46-48), and the amino alcohols mefloquine (MQ), halofrantine, lumefrantine and piperazine (49). These derivatives are mainly used both therapeutically (50) and prophylactically (48). However, increasing resistance to these derivatives render them largely ineffective as monotherapies. Resistance formation to MQ is due to modifications on the P-glycoprotein homologue (*pgh*1) and the *P. falciparum* multidrug resistance protein-1 (*Pfmdr*1) gene that function as pumps in expelling cytotoxic drugs (51, 52). Presently, quinolones are only used in combination therapies with other classes of antimalarials as shown in Table 1.1 (53). As a result of resistance to this class of drugs, second generation quinolone derivatives are being developed, AQ-13 (54), an amodiaquine derivative, *N*-*tert*-butyl-isoquine (55); a primaquine analogue, tafenoquine (56) and three 4-aminoquinoline derivatives, naphthoquine (57), pyronaridine (58) and ferroquine (59).



### 1.3.5.2 Antifolates

Folate metabolism, associated with DNA synthesis, amino acid and methionine formation in *Plasmodium* parasites, was identified as a suitable antimalarial drug target in the 1930-1940s. Sulphonamides (type 1 antifolates; sulphadoxine, sulphalene and the sulphone, dapsone), are analogues of *p*-aminobenzoic acid (*p*ABA), and inhibit the *P. falciparum* dihydropteroate synthase (DHPS) domain of the bifunctional hydroxymethylpterin pyrophosphokinase (HPPK-DHPS), thus preventing the formation of dihydropteroate from hydroxymethyldihydropterin. Pyrimethamines (type 2 antifolates; biguanides, triazines, quinazolines and proguanil, which is metabolised to cycloguanil *in vivo*) are dihydrofolate analogues inhibiting *P. falciparum* dihydrofolate reductase (DHFR), which forms part of the DHFR-thymidylate synthase (DHFR-TS) bifunctional complex (60, 61). This complex is responsible for NADPH dependent reduction of dihydrofolate to tetrahydrofolate, a cofactor required for the synthesis of nucleotides and specific amino acids (62).

The unique structural and functional differences of these targets in *P. falciparum* such as their bifunctional organisation, folate salvage and *de novo* folate biosynthesis ability of the parasite compared to the monofunctional organisation of human homologues and the absence of *de novo* synthesis ability in humans, provided selectivity for antifolate drugs (63). However, the use of these drugs as monotherapies resulted in rapid drug resistance development (46, 64, 65). Antifolate drug resistance in *P. falciparum* was initially due to single random point mutations, Ser108Asn for *Pf*DHFR (66) and Ala437Gly for *Pf*DHPS (64), which in combination with cumulative point mutations (Asn51Ile and Cys59Arg for *Pf*DHFR (62, 67) and Lys540Glu, Ala581Gly, Ser436Phe/Ala and Ala613Ser/Thr for *Pf*DHPS (64)) resulted in multidrug resistant phenotypes.

Parasite resistance to antifolate drugs led to the co-formulation of pyrimethamine and sulphadoxine, commercially known as Fansidar<sup>®</sup> (Table 1.1). However, this combination therapy was only effective until resistance developed in Southeast Asia in the 1960s that subsequently spread to sub-Saharan Africa (68) and is today mainly used for IPT in pregnant woman. Second-generation derivatives of sulphonamides include sulphamethoxazole and trimethoprim and these are used mainly in combination with other antimalarials (69).

### 1.3.5.3 Atovaquone

Atovaquone is a 2-hydroxynaphthoquinone derivative, developed as an antimalarial from a class of mitochondrial respiration inhibitors. The compound is an analogue of coenzyme Q, the ubiquinone cofactor found in the electron transport chain (ETC) of mitochondria and



inhibits cytochrome b on complex III disrupting the membrane potential required for cellular respiration (70). However, drug resistance was detected via point mutations in the *cytochrome b* gene when used as monotherapy (71). Therefore, atovaquone was introduced as a combination therapy with proguanil in 1997 (Table 1.1) and used successfully in regions with high levels of antimalarial drug resistance (70), as well as a prophylactic agent (72).

#### 1.3.5.4 Artemisinins

Artemisinin, a sesquiterpene trioxane lactone peroxide (endoperoxide) isolated from the Chinese shrub *Artemisia annua*, significantly reduced parasitaemia in infected patients compared to other antimalarials and was introduced as a new class of drugs in 1978 (73). Semi-synthetic derivatives including dihydroartemisinin, artesunate, artemether and arteether (74) have been developed and showed increased potency over the native compound. The mode of action of these drugs involves the cleavage of the peroxide bridge across the seven-membered triple-ring system by ferroheme ferrous-protoporphyrin IX. The cleavage generates free radicals that alkylate several proteins within the parasites (75), for example, the sarco/endoplasmic reticulum calcium-dependent APTase6 (SERCA transporter) in membranes found in the mitochondrial membrane. The transporter maintains intracellular  $Ca^{2+}$  concentrations, which mediate signalling and post-translational protein modifications (76). In addition, studies have revealed that disruption of the membrane potential via the ETC of the mitochondrion further increases artemisinin potency (77).

Despite this class of drugs being the most recent and most effective class of antimalarials, and thus recommended as first-line antimalarial treatments, *P. falciparum* artemisinin resistance was detected at the Thai-Cambodian border in 2009 (78, 79). Resistance has been correlated to point mutations in the PF3D7\_1343700 kelch propeller domain (K13-propeller) of the K13-propeller cluster allele (80).

Consequently, the WHO recommends that artemisinins be used as artemisinin combination therapies (ACTs) (81) to prolong the lifetime of this class of antimalarials since the use of monotherapies resulted in rapid and highly specific drug resistance formation. ACTs are artemisinin-based derivatives formulated in fixed-dosed combinations with other antimalarials, such as lumefrantine, piperaquine and pyrimethamine-sulphadoxine (Table 1.1). Second generation artemisinin derivatives currently in clinical trials include arterolane (OZ277) (82) and artemisone (83, 84).

#### 1.3.5.5 Antibiotics

Antimicrobial agents that have shown potential as antimalarial agents include tetracycline and doxycycline. Both of these inhibitors consist of a four-carbon ring backbone structure, which inhibit parasite growth by repressing apicoplast localized deoxyxylulose reductoisomerase genes responsible for synthesis of isopentenyl diphosphate in daughter merozoites (85). In addition, clindamycin, which consist of pyrrolidine amide sugars, inhibit protein translation by binding to the 50S ribosomal subunit. Second generation antibiotics, fosmidomycin, a tetracycline derivative (86) and azithromycin from clindamycin (87), are currently in clinical trials for use in antimalarial combination therapies, with piperazine, artesunate and other antibiotics (88, 89) (Table 1.1).

#### 1.3.5.6 Antimalarial combination therapies

The WHO encouraged the implementation of antimalarial combination therapies such as pyrimethamine-sulphadoxine and ACT's due to the high rate of drug resistance formation against monotherapy based antimalarials (1). General guidelines for combinations include that the partner drugs should have different mechanisms of action since cross-resistance can arise through shared biological targets and uptake mechanisms (90). The combination should preferably be an additive interaction although synergistic interactions are also accepted (44). An additive interaction is, as a result, of two drugs binding independently with different cellular targets, either targeting the same or different metabolic pathways, and a synergistic interaction is caused by drugs binding to the same target enhancing drug binding (91). However, synergistic combinations might not offer as much protection and effectiveness as an additive interaction since resistance against either component may lead to loss of efficacy of the treatment (92) enabling selection for resistance formation (44).

Being the most recent class of antimalarials, artemisinins are mainly formulated as combination therapies since the use of these drugs as monotherapies are challenged due to recrudescence caused by the short biological half-lives of these compounds (93). The rationale behind an ACT is the rapid parasite clearance by the fast acting artemisinin component followed by a slow acting partner drug, to eradicate residual parasites (94). ACTs include artemisinins in combination with quinolones such as, naphthoquine and artemisinin (ARCO<sup>®</sup>), mefloquine and artesunate, lumefrantine and artesunate (Coartem<sup>®</sup>), amodiaquine and artesunate (Coarsucam<sup>®</sup>), pyronaridine and artesunate (Pyramax<sup>®</sup>) and piperazine and dihydroartemisinin (Euartesim<sup>®</sup>) (Table 1.1) (53).

Antifolate antimalarial combinations that have been developed (Table 1.1), e.g. sulphadoxine-pyrimethamine (Fansidar<sup>®</sup>) has furthermore been combined with atovaquone (95) and artemisinin (96) (Table 1.1). In addition, sulphonamide and pyrimethamine derivatives dapson and proguanil (LapDap<sup>®</sup>) (Table 1.1) (97), have been developed to replace sulphadoxine-pyrimethamine due to drug resistance development. Atovaquone is also used in combination with the antifolate inhibitor proguanil (Malarone<sup>®</sup>) (70) (Table 1.1). Combination therapies are also in development with antibiotics, with several clinical trials with second-generation quinolones and antibiotics being performed to validate novel combinations of these two drug classes (88, 98, 99).

**Table 1.1: Current antimalarial drug combination therapies.** Different classes of current antimalarial drug combination therapies, including ACT's with registered trade names.

Drugs in combination	Product name	Ref.
<b>Antifolate combinations</b>		
pyrimethamine/sulphadoxine	Fansidar <sup>®</sup>	(69)
dapsone/proguanil	LapDap <sup>®</sup>	(97)
sulphalene/pyrimethamine	Metakelfin <sup>®</sup>	(100)
fansidar/atovaquone		(100)
atovaquone/proguanil	Malarone <sup>®</sup>	(70)
fosmidomycin/clindamycin		
<b>ACT's</b>		
naphthoquine/artemisinin	ARCO <sup>®</sup>	
mefloquine/artesunate		(53, 100)
lumefrantine/artesunate	Coartem <sup>®</sup> (Riamet)	(53)
piperazine/dihydroartemisinin	Euartesim <sup>®</sup>	(53)
amodiaquine/artesunate	Coarsucam <sup>®</sup>	(101)
fansidar/artesunate		(32)
pyronaridine/artesunate	Pyramax <sup>®</sup>	(58)
fosmidomycin/artesunate		

Insecticide resistance development as well as the absence of a reliable vaccine, creates dependence on current antimalarials for chemoprophylactic prevention and chemotherapeutic strategies (53). However, drug toxicity and adverse side-effects of treatments results in drug over-and misuse, promoting drug resistance development in *Plasmodium* parasites (62). In combination with this, high parasite proliferation rates and inherited parasite genetic polymorphism (102, 103) further contributes to a high rate of drug resistance development. Antimalarial resistance development indicates that all drugs have a limited life-span, creating the need for a steady pipe-line of antimalarials in sustaining malaria control and elimination (104). However, the development of combination therapies, provides only a temporary solution for reducing the rate of resistance formation, since the drugs being incorporated into these therapies are designed on a limited number of chemical scaffolds, developed on a derivative-based strategy (100). Therefore, a fundamental change is required to prevent untreatable multidrug-resistant malaria infections from developing. This can be achieved by

validating unique and novel drug targets within the parasite, ideal for exploitation by inhibitors, and introducing novel classes of antimalarial agents with high specificities for these targets and diverse mechanisms of action (44, 105).

#### 1.4 Novel drug targets in parasitic protozoa

Drug target identification and validation relies on the dependency of an organism for a specific molecular entity for cellular survival and development. Moreover, this target should preferably be structurally and functionally unique to the organism such that a specific compound can selectively inhibit it. Several metabolic mechanisms exemplifying such characteristics are present in *Plasmodium* parasites including parasite membrane phospholipid replacement mechanisms (106), proteases required by the parasite for host cell invasion (107), microtubular formation (108), guanidine nucleotide regulatory proteins (G-protein coupled receptors) in the erythrocyte membrane (109) and shikimate-(110), isoprenoid-(111), glycolysis-(112), methionine-(113) and polyamine biosynthesis pathways (114).

Polyamine biosynthesis is considered a suitable drug target due to elevated intracellular polyamine levels being associated with highly proliferating cells (115) such as cancer cells (116) and protozoan parasites (114). Inhibition of polyamine biosynthetic enzymes resulted in the decrease of cellular growth and propagation supporting the dependency on these metabolites in the organisms of interest (117). Distinct differences in various aspects of the polyamine biosynthetic pathway compared to the human host have been identified in the asexual stages of *P. falciparum* parasites by functional studies, raising the potential of the pathway as a unique target worth exploiting for drug discovery.

##### 1.4.1 Role of polyamines in eukaryotic cells

Polyamines are present in all living organisms including mammals, plants and unicellular organisms, with the exception of certain orders of *Archaea* (118). Putrescine ( $\text{H}_2\text{N}(\text{CH}_2)_4\text{NH}_2$ ), spermidine ( $\text{H}_2\text{N}(\text{CH}_2)_3\text{NH}(\text{CH}_2)_4\text{NH}_2$ ) and spermine ( $\text{H}_2\text{N}(\text{CH}_2)_3\text{NH}(\text{CH}_2)_4\text{NH}(\text{CH}_2)_3\text{NH}_2$ ), the three most abundant polyamines (Figure 1.5), are small, cationic oligoamines positively charged at physiological pH (119, 120).

Due to their polycationic nature, polyamines form electrostatic interactions with a variety of polyanionic macromolecules. Spermidine and spermine stabilise DNA through electrostatic (121) and hydrophobic interactions (methylene bridging) with the major groove of the DNA

phosphate backbone (122). The binding of these polyamines alters the DNA structure (B- to Z-DNA conformational changes), aiding in euchromatin condensation, which influences gene transcription and protein translation rates in the cell (123-125). These polyamines also modify protein structures by binding to surface residues through reversible hydrophilic interactions, which alter the protein tertiary structure and thereby mediating protein function such as with membrane transglutaminases (126), membrane ion channels (127) and proteinases (123). Other cellular functions of spermidine and spermine include the formation of complexes with phospholipids and membrane proteins in the plasma membrane and increasing plasma membrane rigidity (128). In addition, spermidine forms a ternary complex with ATP-Mg<sup>2+</sup>, which mediates protein kinase phosphorylation (129), disrupting the secondary messenger system in the cell.

The most specific function of spermidine involves the activation of the eukaryotic initiation factor 5A (eIF-5A), a transcription factor required for protein synthesis in eukaryotic cells (130). Deoxyhypusine synthase transfers the aminopropyl moiety from spermidine onto the side-chain amino group of a lysine residue of eIF-5A, forming a hypusine residue, which activates eIF-5A (131, 132). The essential nature of spermidine required for activation of eIF-5A and its interaction with cyclin-dependent kinases (133) indirectly links cell cycle progression to polyamine biosynthesis. A reduction of intracellular polyamine levels in eukaryotic cells, specifically that of spermidine, have been shown to arrest cell progression at the G<sub>1</sub> stage of cell development (134). Polyamine depletion results in the down regulation of DNA synthetic enzymes, preventing DNA synthesis through the appearance of Okazaki-like DNA fragments (134-136), which results in cellular apoptosis by activation of caspase-3 in the mitochondria-mediated apoptotic pathway (137). However, polyamine accumulation also induces cell death (138, 139). The extensive role of polyamine homeostasis on cellular function conveys the importance of these molecules in indirectly mediating cell proliferation and differentiation (120, 140).

#### 1.4.2 Polyamine biosynthesis in the human host and parasitic protozoa

Polyamine biosynthesis in mammalian cells (Figure 1.4) produces putrescine through the decarboxylation of L-ornithine, catalysed by pyridoxal-5'-phosphate-dependent (PLP) ornithine decarboxylase (ODC; EC 4.1.1.17) (141). S-adenosyl-L-methionine decarboxylase (AdoMetDC; EC 4.1.1.50), decarboxylates S-adenosyl-L-methionine (AdoMet), synthesised from methionine and ATP by AdoMet synthase (SAMS), into decarboxylated AdoMet (dcAdoMet) (142). Putrescine and dcAdoMet are the substrates for the subsequent reaction

catalysed by spermidine synthase (SpdS; EC 2.5.1.1), which transfers the aminopropyl moiety from dcAdoMet onto putrescine, producing spermidine. The fourth enzyme in the pathway, spermine synthase (SpmS), catalyses the transfer of a second aminopropyl moiety onto spermidine, producing spermine (119, 143).

The reduced complexity of polyamine biosynthesis in parasitic protozoa makes this pathway evolutionary distinct compared to the human host (144). African sleeping sickness, transmitted via the tsetse fly (Figure 1.4) is caused by two subspecies of protozoan *Trypanosoma brucei* parasites. Similar to the human host, putrescine and spermidine are synthesised by ODC, AdoMetDC and SpdS in *T. brucei* parasites, however, spermine is not synthesised due to the absence of a SpmS synthesis enzyme. A unique distinction between polyamine biosynthesis in these parasites and that of the human host is the role of glutathione (GSH) and a spermidine conjugate, trypanothione ( $N^1, N^9$ -bisglutathionylspermidine) in thiol-based redox metabolism (145) (Figure 1.4). Leishmaniasis is a range of diseases caused by *Leishmania* parasites such as visceral leishmaniasis by *L. donovani* transmitted via sand flies (146). *L. donovani* polyamine biosynthesis shares commonalities with *Trypanosoma* parasites such as the absence of spermine synthesis and trypanothione production (147) (Figure 1.4). *T. cruzi* parasites, transmitted via the kissing bug causes Chagas' disease (148) that is mainly prevalent in South America. *T. cruzi* parasites lack ODC and are, therefore, auxotrophic for putrescine from the extracellular environment. However, the parasites produce spermidine and spermine through the promiscuous action of SpdS. *T. cruzi* parasites also have a polyamine redox-dependent metabolism as observed for *T. brucei* and *L. donovani* parasites. However, *T. cruzi* parasites are able to convert a fourth polyamine, cadaverine, into aminopropylcadaverine, bis(aminopropyl) cadaverine and  $N^1 N^9$ -bis(glutathionyl) aminopropylcadaverine (149) (Figure 1.4). Like *T. cruzi* parasites, *Plasmodium* parasites also produce low levels of spermine through a promiscuous SpdS enzyme (150). Apart from this similarity, *Plasmodium* parasites do not possess a trypanothione redox metabolism. Polyamine biosynthesis in *Plasmodium* parasites is uniquely diverse compared to the human host and other protozoan parasites in that AdoMetDC and ODC are organised into a single bifunctional complex, expressed from a single open reading frame (151, 152) (Figure 1.4). Several other bifunctional proteins have been identified in *P. falciparum* parasites e.g. PfDHFR/TS and PfPPPDK/DHPS begging the question of the evolutionary as well as functional role of the bifunctional organisation of these proteins in the parasite.

A polyamine transporter has not been characterised in mammalian cells or protozoan parasites indicating that *de novo* polyamine biosynthesis is the main source of intracellular polyamines. However, a polyamine uptake system has been characterised for putrescine in



*P. knowlesi* (153), and putrescine and spermidine uptake has been shown for *P. falciparum* parasites (154). The polyamines are taken up across the infected host erythrocyte membrane by endogenous polyamine uptake mechanisms, and cross the parasitophorous vacuolar membrane into the parasite cytoplasm through a concentration gradient dependent electrogenic process (154) (Figure 1.4).

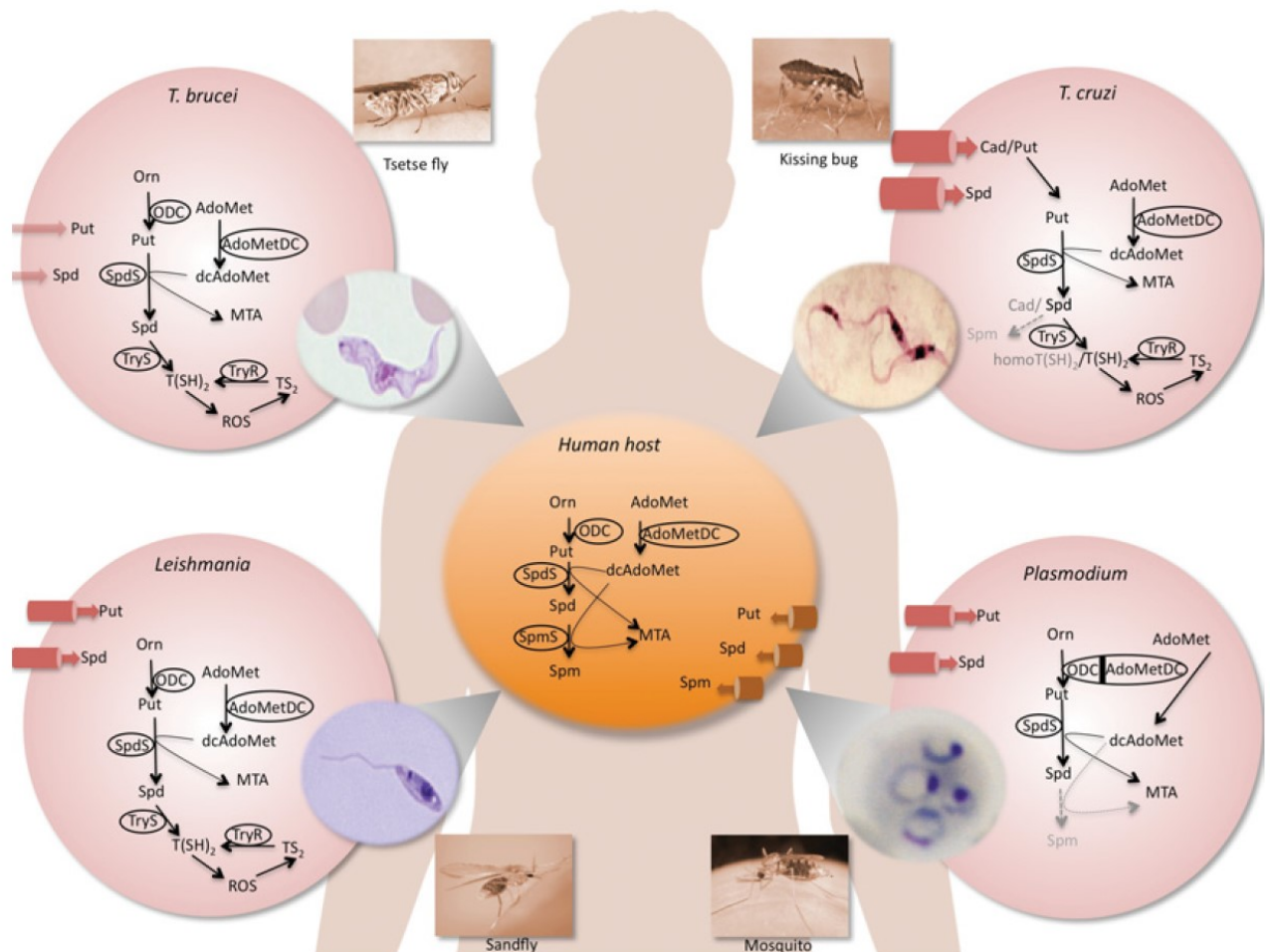


**Figure 1.4: Polyamine biosynthetic pathways in protozoan parasites compared to the human host.** Disease vectors for various protozoan organisms are shown, *T. brucei* is transmitted via tsetse flies, *T. cruzi* via kissing bugs, *L. donovani* via sand flies, and *P. falciparum* via female *Anopheles* mosquitoes. Abbreviations: Cad, cadaverine; homoT(SH)<sub>2</sub>, homotrypanothione; Orn, ornithine; Put, putrescine; ROS, reactive oxygen species; Spd, spermidine; Spm, spermine; MTA, 5'-methylthioadenosine; TyrS, trypanothione synthetase; TryR, trypanothione reductase; TS<sub>2</sub>, oxidised trypanothione; T(SH)<sub>2</sub>, reduced trypanothione. Taken from (144).

In mammalian cells, polyamine pools are not only maintained by *de novo* synthesis and uptake (155) but also through interconversion pathways. Polyamine interconversion is mediated by salvaging methylthioadenosine (MTA), a by-product produced from spermidine and spermine synthesis (Figure 1.4). The metabolite acts as a substrate for adenosine deaminases, N<sub>1</sub>-

acetyltransferases (SSAT) and methylthioadenosine phosphorylase, therein recycling the purine ring of MTA into adenine and methionine pools (156). *Plasmodium* parasites lack these enzymes, salvaging purine rings from MTA with adenosine oxidase and purine nucleoside phosphorylase enzymes (157, 158).

Lastly, human erythrocytes are deficient in the polyamine biosynthetic enzymes and contain only trace amounts of polyamines (Figure 1.5) (159). However, in asexual intra-erythrocytic *P. falciparum* parasites the intracellular polyamine concentration is significantly higher in the trophozoite to schizont stage due to transcriptional upregulation of the polyamine biosynthetic enzymes (Figure 1.5) (151, 160). These elevated intracellular levels of polyamines, spermidine being the most abundant (Figure 1.5), reiterates the requirement of polyamines in the activation of the eIF-5a transcription factor required for macromolecule biosynthesis and cellular development required during trophozoite and schizont stages (159). The distinctive structural and regulatory characteristics between *P. falciparum* and mammalian cells' polyamine biosynthesis make the pathway ideal for exploitation in antimalarial drug development.

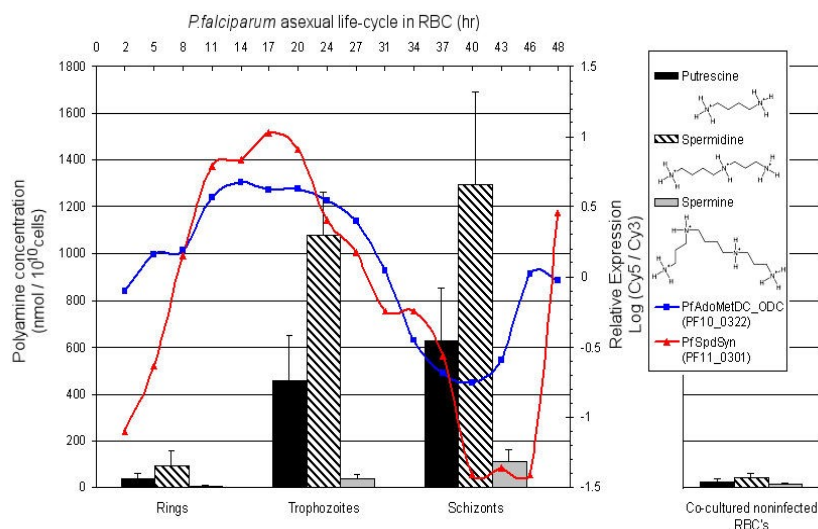


**Figure 1.5: Intracellular concentrations of polyamines during the intra-erythrocytic life stage.** The graph depicts the various intracellular concentrations of polyamines at different stages during the IDC of *P. falciparum*. The red and blue lines indicate the increase in the cellular concentration of transcripts for *PfAdoMetDC/ODC* and *PfSpdS* during ring and trophozoite stages, resulting in increased polyamine levels during the trophozoite and schizont stages, with spermidine being the most abundant polyamine. The intracellular concentration of polyamines in *P. falciparum* parasites is significantly higher compared to that of un-infected erythrocytes. Diagram taken from (161) based on (159, 162).



### 1.4.3 Polyamine biosynthetic enzymes as drug targets in parasitic protozoa

Due to the cellular proliferation and differentiation role of polyamines in parasitic protozoa, inhibition of ODC, AdoMetDC and SpdS results in a decreased rate of cell development and propagation, mostly due to intracellular polyamine depletion (114). Table 1.2 summarises specific inhibitors of polyamine biosynthesis enzymes, with their *in vitro* activities determined against *P. falciparum* parasites and their kinetic constants against their respective target enzymes.

#### 1.4.3.1 ODC inhibitors

DL- $\alpha$ -difluoromethylornithine (DFMO, Table 1.2), an irreversible, suicide inhibitor of ODC, was developed as an anti-cancer treatment (163). Although this drug did not prove to be very effective in treating cancer, it was shown to be highly effective in treating west-African sleeping sickness, caused by *T. b. gambiense* (164) and *T. b. brucei* parasites (165), validating inhibition of this pathway as a viable drug target in protozoan parasites. The dependency of *P. falciparum* parasites on polyamines was verified with DFMO inhibition studies, which cytostatically prevented parasite proliferation *in vitro* (162, 166). However, the use of DFMO as an antimalarial has not been as successful as anticipated, due to its inability to cure *in vivo* *P. berghei* infections in murine malaria models (167). DFMO in combination with the polyamine analogue *N,N'*-bis{3-[(phenylmethyl)amino]propyl}-1,7-diaminoheptanex (MDL 27695, Table 1.2), however, is curative of *P. berghei* infected mice (166).

Most cells are able to recover from the inhibitory effect of DFMO due to uptake of exogenous putrescine, which rescues organisms from drug pressure and is therefore cytostatic rather than cytotoxic during the trophozoite to schizont transition stage (168). The cytostatic arrest in cell development is attributed to spermidine depletion, which prevents eIF-5A activation (169).

A second-generation ODC inhibitor, 1-aminooxy-3-aminopropane (APA), a putrescine analogue (Table 1.2), is a promising inhibitor for ODC in *P. falciparum* parasites. The inhibitory effect of this drug is reversed by exogenous putrescine (162, 170) due to polyamine uptake in *P. falciparum* infected erythrocytes and creates a challenge for developing effective ODC inhibitors. Therefore, strategies are needed to counteract the parasite's ability to replace putrescine following ODC inhibition e.g. development of a compound that not only interferes with putrescine production but also prevents extracellular putrescine uptake.

#### 1.4.3.2 AdoMetDC inhibitors

Methylglyoxal bis(gaunylhydrazone) (MGBG, Table 1.2), a spermidine analogue, was the first AdoMetDC-specific inhibitor identified. However, MGBG displayed low inhibitory capacity against *P. falciparum* parasites (171) and, therefore, two aromatic derivatives, CGP48664A and CGP40215A, were designed (Table 1.2). Compared to MGBG, these compounds showed an improved *in vitro* and *in vivo* antiplasmodial activity (172, 173) and a ~25-100 fold improved potency against *in vitro* *P. falciparum* parasites as well as  $K_i$  values bordering on nM concentrations (162, 174) (Table 1.2). The lead compound, CGP40215A, reduced parasitaemia levels in *P. berghei* murine models significantly, although did not deplete spermidine levels thereby indicating off-target effects in *P. falciparum* parasites (162).

A nucleoside AdoMet analogue, 5' [(Z)-4-amino-2butenyl]-methylamino-5'-deoxyadenosine (MDL73811) also known as AbeAdo was identified in 1989 by the Merrell-Dow institute, as an enzyme acitivated irreversible inhibitor of AdoMetDC (Table 1.2) (175, 176). In contrast to CGP40215A, MDL73811 treated parasites showed a 3-fold increase in putrescine levels and a 67% decrease in spermidine levels (162). In *P. falciparum* parasites, MDL73811 is a 1000-fold more potent than DFMO (162) and 200-fold more active in inhibiting *P. falciparum* parasite proliferation compared to MGBG (Table 1.2). Therefore, MDL73811 is the most effective inhibitor for PfAdoMetDC identified thus far, inhibiting *P. falciparum* development *in vitro* without reversal of the inhibitory effect by exogenous spermidine (162). Although MDL73811 showed promising *in vitro* results, the compound could not be clinically developed as an antimalarial since it was unable to cure *P. berghei* murine infections (177).

#### 1.4.3.3 SpdS inhibitors

SpdS has been shown to be an important polyamine flux control point in the polyamine biosynthesis pathway, making it an ideal target from an inhibition perspective (178). A SpdS specific inhibitor, cyclohexylamine (CHA), and its derivatives, trans-4-methylcyclohexylamine (4-MCHA) and dicyclohexylamine (Table 1.2), are competitive substrate analogues inhibiting the aminopropyl transferase activity of SpdS (150, 179). Inhibition of SpdS results in depletion of spermidine required for hypusine formation in eIF-5A activation (180). Moreover, the inhibitory effect is not reversible by exogenous spermidine due to inefficient uptake of this polyamine by *P. falciparum* infected erythrocytes (181). Of these, 4-MCHA was the most effective inhibitor (182) (Table 1.2), however, it could not inhibit parasite proliferation in *in vivo* *P. berghei* models, probably due to assimilation with host SpdS (183).

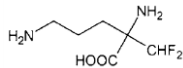
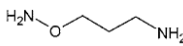
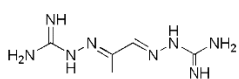
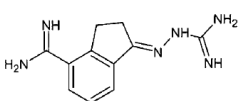
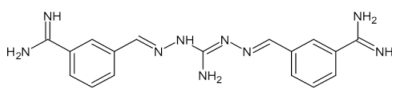
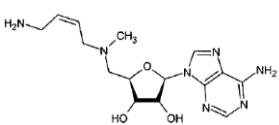
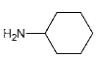
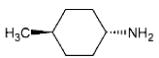
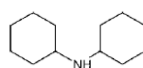
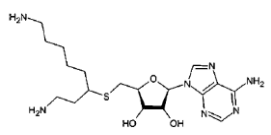
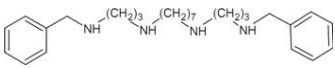
The *in vitro* activity of these inhibitors reflect the dependency of *P. falciparum* parasites on polyamines, although, *in vivo* experiments have not yielded promising results. Therefore, the 3D crystal structure of *P. falciparum* SpdS was obtained to aid in the development of novel compounds displaying high specificity and activity against *P. falciparum* parasites, as well as revealing several structural and functional characteristics of the enzyme (184, 185).

The inhibitor, S-adenosyl-1,8-diamino-3-thioacetate (AdoDATO; Table 1.1), developed through structure-based drug discovery using the crystal structure of SpdS, is a large transition state analogue of SpdS (179, 186) that binds to the entire catalytic centre of the enzyme (184). Although AdoDATO effectively inhibited *in vitro* *P. falciparum* parasite proliferation (Table 1.2) (184), the compound could not cure *P. berghei* infected mice (184).

#### 1.4.3.4 Polyamine analogues

Polyamine analogues aim to perturb polyamine homeostasis by competing for polyamine uptake and/or inhibition of polyamine target sites by replacing the intracellular polyamine pool or by down regulating the rate of polyamine biosynthesis due to allosteric feedback inhibition (116, 187). Spermidine analogues (*N,N'*-bis(benzyl)polyamines) of which MDL27695 proved to be the most potent, effectively inhibited *P. falciparum* parasite proliferation *in vitro* (Table 1.2). In combination with chloroquine, the analogue showed an additive effect and inhibition of parasite proliferation by this analogue could not be reversed by the addition of exogenous spermidine (188). This polyamine analogue was curative of *P. berghei* infected mice when used in combination with DFMO (166). However, due to poor pharmacodynamic properties (189), the compound could not be further taken into clinical studies. Other promising polyamine analogues include 1,3,5-triazine (190) and diamine analogues (191). These inhibitors prevent *P. falciparum* parasite proliferation *in vitro* at low micromolar levels, however, the *in vivo* efficacy has not been determined.

**Table 1.2: Inhibitors of polyamine biosynthetic enzymes.** The IC<sub>50</sub>s (effective drug concentration resulting in 50% of parasite growth inhibition) of polyamine biosynthesis inhibitors against *in vitro* *P. falciparum* parasite cultures and enzyme inhibition constants (*K<sub>i</sub>*) for these inhibitors against recombinant or purified *P. falciparum* biosynthesis enzymes; ODC, AdoMetDC and SpdS. Adapted from (144).

Inhibitor	Chemical structure	<i>P. falciparum</i>	
ODC		IC <sub>50</sub> (μM)	<i>K<sub>i</sub></i> (μM)
DFMO		1250 (162)	87.6 (174)
APA		1 (162)	0.0027 (162)
<b>AdoMetDC</b>			
MGBG		224 (171)	0.46 (188)
CGP48664A		8.8 (162)	3 (162)
CGP40215A		1.8 (162)	1.3 (162)
MDL73811		3 (162)	0.33 (192)
<b>SpdS</b>			
CHA		198 (150)	19.7(150)
<i>Trans</i> -4-MCHA		1.4 (150)	0.18(150)
DHA		>1000 (150)	342(150)
AdoDATO		8.5 (184)	8.5 (184)
<b>Polyamine analogues</b>			
MDL27695		3 (166)	-

Inhibition of polyamine biosynthesis prevents intra-erythrocytic *P. falciparum* parasite proliferation and differentiation, clearly demonstrating the dependence of the parasite on these molecules. However, compounds currently available for targeting polyamine biosynthesis in *P. falciparum* parasites have been unsuccessful in *in vivo* murine models. Failure of these inhibitors could be attributed to the reversal of the inhibitory effect through uptake of exogenous polyamines as well as their incompatible pharmacodynamic properties, creating

the need to identify more specific and potent inhibitors. Therefore, the structures of current inhibitors have to be further optimised either through derivative-based drug design or the identification of alternative inhibitors to develop suitable antimalarial candidates targeting polyamine metabolism.

#### 1.4.4 Structural and functional characteristics of *PfAdoMetDC/ODC*

*PfAdoMetDC/ODC* contains two independent N- and C-terminal protein domains that are covalently linked via a ~ 10 kDa hinge region producing a single ~165 kDa heterodimeric polypeptide. *PfAdoMetDC* resides on the N-terminus of the polypeptide and is a protomer that undergoes post-translational autocatalytic cleavage, yielding active enzyme with a ~9 kDa  $\beta$ -subunit and a ~55 kDa  $\alpha$ -subunit. The protein forms a ~140 kDa homodimer by interacting with an additional processed *PfAdoMetDC*  $\alpha\beta$ -monomer. *PfODC*, which resides on the C-terminus, is a ~90 kDa monomeric protein that interacts with another *PfODC* monomer to yield a ~180 kDa homodimer (151, 152). The quaternary structure of the bifunctional complex consists of two ~165 kDa *PfAdoMetDC/ODC* polypeptides associated through the *PfODC* domain to form a ~330 kDa heterotetrameric complex (Figure 1.6) (151, 152).

Despite the two domains residing on a single polypeptide the decarboxylase activities function independently (151). Unlike human *AdoMetDC*, *PfAdoMetDC* activity is not stimulated by putrescine (193) due to the putrescine binding site having been replaced by internal basic Lys residues simulating bound putrescine (194). However, *PfODC* is susceptible to feedback inhibition by putrescine (152). Furthermore, through means of intra- and interdomain protein-protein interactions functional studies indicated that the *PfODC* domain inhibits the activity of the *PfAdoMetDC* domain (152) while *PfODC* activity is stimulated by the *PfAdoMetDC* domain (174, 192). The specific activities of the two domains are co-ordinately modulated as observed by their similar catalytic efficiencies ( $k_{cat}$ ) (192). Therefore, *PfAdoMetDC* and *PfODC* activities are controlled through their independent product levels, kinetics and specific activities within the complete heterotetrameric complex resulting in coordinated, equimolar production of putrescine and dcAdoMet. The coordinated production of *PfAdoMetDC/ODC* products is thus responsible for modulating polyamine pool flux (152, 192). Apart from this, the bifunctional arrangement of *PfAdoMetDC/ODC* also assists the parasite in coordinated transcription and translation during rapid cellular differentiation required for the IDC stage.

The hinge region (Figure 1.6) has been shown to be essential for the heterotetrameric bifunctional complex conformational stability and quaternary structure formation through interdomain protein-protein interactions with both the *PfAdoMetDC* domain and the *PfODC*

domains (151, 174, 195). These interdomain interactions are proposed to be mediated by two  $\alpha$ -helices and a  $\beta$ -sheet present within the hinge region and are essential for modulating activities of both protein domains, specifically that of *Pf*ODC, although the exact mechanism of interaction has not yet been resolved (174, 195, 196).

An additional unique characteristic of *Pf*AdoMetDC/ODC is the presence of five non-homologous amino acid sequences constituting nearly 26% of the polypeptide, known as parasite-specific inserts. Three inserts have been characterised in the *Pf*AdoMetDC domain (A1, A2 and A3) and two in the *Pf*ODC domain (O1 and O2) (Figure 1.6) (194). Parasite-specific inserts have been found in several *Plasmodium* proteins (197, 198) and are characterised as low complexity regions (LCRs), containing tandem amino acid repeats (TAAs) with selective bias towards hydrophilic residues such as asparagine and lysine (199-201). The crystal structure of *Pf*DHFR/TS indicated that its parasite-specific inserts are non-globular, unstructured domains on the surface of the protein that do not interact with the protein core (202). Although *in silico* predictions of the monofunctional homology models predict the same conformations for *Pf*AdoMetDC/ODC (194, 203), the exact function of these inserts have not been annotated for *Pf*AdoMetDC/ODC. However, functional studies performed by deletion mutagenesis of various inserts from either domains of the *Pf*AdoMetDC/ODC polypeptide resulted in adverse effects on both decarboxylase activities (195). Therefore, it is proposed that these parasite-specific inserts contribute to coordinated catalytic control between the *Pf*AdoMetDC and *Pf*ODC domains through conformational changes brought on by long-range interdomain protein-protein interactions to stabilise the heterotetrameric bifunctional complex (195, 204).

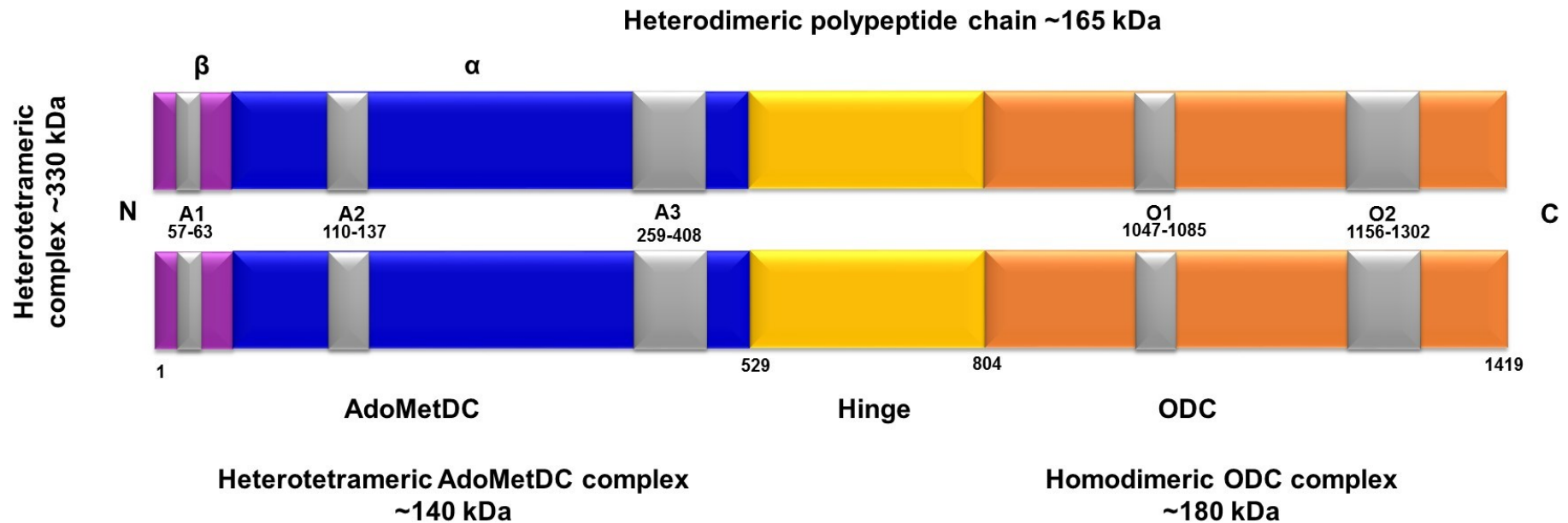


**Figure 1.6: The bifunctional arrangement of *PfAdoMetDC/ODC*.** The bifunctional complex consists of two *PfAdoMetDC/ODC* heterodimeric polypeptides (~165 kDa each) in a ~330 kDa heterotetrameric complex of N-terminal *PfAdoMetDC* (residues 1-529) connected to the C-terminal *PfODC* (residues 804-1419) via a ~10 kDa hinge region (residues 529-804). The two peptides interact via the *PfODC* domain forming independent ~140 kDa and ~180 kDa *PfAdoMetDC* and *PfODC* homodimers. *PfAdoMetDC* undergoes post-translational processing into an  $\alpha\beta$ -monomer. The bifunctional protein polypeptide spans a total of 1419 residues with the *PfAdoMetDC* domain containing three parasite-specific inserts; A1: residues 57-63, A2: residues 110-137 and A3: residues 259-408 with *PfODC* containing two inserts; O1: residues 1047-1085 and O2: residues 1156-1302.



The current study focussed specifically on characterising the *PfAdoMetDC* domain since this enzyme has been shown to catalyse an essential chokepoint reaction to produce dcAdoMet (86) whereby polyamine biosynthesis is linked to methionine metabolism (205). This makes the enzyme uniquely exploitable for inhibition in *P. falciparum* parasites. However, current inhibitors that have been developed against *PfAdoMetDC* display poor *in vitro* and *in vivo* inhibition against *P. falciparum* parasites compared to *T. brucei* parasites (144). Furthermore, due to the lack of structural information available for the bifunctional *PfAdoMetDC*/ODC enzyme complex, development of potent and specific *PfAdoMetDC* inhibitors remains a challenge. Another strategy to identify *PfAdoMetDC* specific inhibitors is via structure-based drug discovery, however, this strategy requires the complete 3D structure of the protein. Identification of novel inhibitors targeting *PfAdoMetDC* can be performed via derivative-based drug design to obtain compounds with a favourable pharmacodynamic profile and the sequential validation of their respective *in vitro* kinetic and parasite inhibition capabilities.

A range of structural and functional characteristics derived from homology models (194, 203) and recombinant cloning and expression studies for *PfAdoMetDC*/ODC have been determined. However, no crystal structure is available for this protein complex. Although active bifunctional *PfAdoMetDC*/ODC has been expressed successfully, low soluble protein yields are obtained with many background contaminating protein aggregates and truncated versions (206-208). Due to the difficulty in studying the structural and functional characteristics of this large bifunctional protein complex and the fact that their active sites function independently, studies of *PfAdoMetDC* and *PfODC* as monofunctional entities were attempted in order to derive their respective structural and functional characteristics. Subsequent cloning and expression of the domains as independent monofunctional proteins, with partial segments of the hinge region attached, yielded protein with variant degrees of solubility and activities. However, recombinant expression of monofunctional *PfAdoMetDC* from a codon harmonised construct produced increased soluble protein yields and improved solubility, purity and specific activity compared to when it is expressed in its bifunctional association with *PfODC* (174, 207). By contrast, monofunctional expression of *PfODC* resulted in a 10-fold decrease in activity compared to its bifunctional counterpart (174). Thus, it was postulated that *PfODC* requires the *PfAdoMetDC* domain as well as specific sequences of the hinge region to be functional (195), similar to the dependence of the *PfTS* domain on *PfDHFR* in *PfDHFR-TS* (202, 209). The low protein activity in combination with poor soluble recombinant protein yields, made deriving the structural and functional characteristics of monofunctional *PfODC* exceedingly difficult. However, the success achieved in expressing active monofunctional *PfAdoMetDC* in a relatively pure soluble form and high recombinant protein yields (207), provides an ideal starting point for possible protein crystallography



studies. Nonetheless, further optimisation of the recombinant expression conditions is required to produce a completely homogenous protein sample amenable to crystallisation. Once available, the crystal structure of *PfAdoMetDC* can be used for structure-based drug discovery to identify novel, specific inhibitors targeting *PfAdoMetDC*.

## 1.5 Research objectives

The main research objective of this study was to identify novel candidate compounds specifically targeting *PfAdoMetDC* as a possible antimalarial treatment strategy.

Firstly, to enable structure-based drug discovery, structure-activity analyses of monofunctional *PfAdoMetDC* was performed to obtain homogenous protein preparations amenable to crystallisation studies.

Secondly, a derivative-based strategy was employed to identify and characterise the *in vitro* potency of novel derivatives of the AdoMetDC inhibitor, MDL73811, against *P. falciparum* parasites.

### **Chapter 2: Structural and functional characterisation of monofunctional *PfAdoMetDC***

A comparative study with recombinantly expressed monofunctional *PfAdoMetDC* from a codon harmonised construct was undertaken in an attempt to improve homogeneous production of the protein for protein crystallography purposes. This included structure-activity analysis of the role of a parasite-specific insert and the hinge connector in the monofunctional protein through a deletion mutagenesis strategy thereof.

### **Chapter 3: Novel S-adenosyl-L-methionine decarboxylase inhibitors as potent antiproliferative agents against intra-erythrocytic *Plasmodium falciparum* parasites**

Pharmacodynamically favourable derivatives of the specific AdoMetDC inhibitor, MDL73811, were tested for their potency against *P. falciparum* parasites. The kinetic properties of these derivatives were derived for the recombinantly expressed protein and their inhibitory concentrations were determined against *P. falciparum* parasite cultures *in vitro*. The specificity of these inhibitors against *P. falciparum* parasites were further verified and characterised, and their probability as a potential antimalarial treatment strategy was considered with novel lipid-based drug delivery systems.

### **Chapter 4: Concluding discussion**

## 1.6 Research outputs

1. **Peer reviewed publication:** Dina le Roux, Pieter Burger, Jandeli Niemand, Robert Barker, Anne Grobler, Patricia Urbán, Xavier Fernández-Busquets, Abraham I. Louw and Lyn-Marie Birkholtz. (2014) Novel derivatives of MDL 73811 inhibit *Plasmodium falciparum* S-adenosyl-L-methionine decarboxylase. International Journal for Parasitology: Drugs and Drug resistance, 4, 28-36.
2. **Conference proceeding:** Dina le Roux, Marni Williams, Janina Sprenger, Abraham I. Louw, Lo Persson and Lyn-Marie Birkholtz. (January 2012) AdoMetDC - A Unique Novel Drug Target in *Plasmodium falciparum*. Poster presentation. South African Society of Biochemistry and Molecular Biology Conference, Drakensberg, South Africa.
3. **Conference proceeding:** Dina le Roux, Lyn-Marie Birkholtz, Abraham I. Louw. (July 2012) Novel properties of S-adenosylmethionine decarboxylase as a drug target in *P. falciparum*. Invited oral presentation. 7<sup>th</sup> biannual symposium on Polyamines in Parasites, Pacific University, Forest Grove, OR, USA.
4. **Conference proceeding:** Dina le Roux, Jandeli Niemand, Anne Grobler, Robert Barker, Patricia Urbán, Abraham I. Louw, Lyn-Marie Birkholtz. (October 2012) Novel MDL 73811 derivatives inhibit *Plasmodium falciparum* S-adenosylmethionine decarboxylase. Poster presentation. H3-D symposium, Cape Town, South Africa.
5. **Conference proceeding:** Dina le Roux, Lyn-Marie Birkholtz, Abraham I. Louw. (July 2013) Novel S-adenosylmethionine decarboxylase inhibitors as potent anti-proliferative agents against *Plasmodium falciparum*. Invited oral presentation. International Gordon seminar: Polyamines. Waterville valley resort, NH, USA. Voted best presentation at seminar.
6. **Conference proceeding:** Dina le Roux, Lyn-Marie Birkholtz, Abraham I. Louw. (July 2013) Novel S-adenosylmethionine decarboxylase inhibitors as potent anti-proliferative agents against *Plasmodium falciparum*. Poster presentation and Oral presentation. International Gordon Conference: Polyamines. Waterville valley resort, NH, USA.

7. **Conference proceeding:** Dina Coertzen, Anne Grobler, Patricia Urbán, Xavier Fernández-Busquets, Robert Barker, Abraham I. Louw, Lyn-Marie Birkholtz. (July 2014) Novel S-adenosylmethionine decarboxylase inhibitors as potent antiproliferative agents against *Plasmodium falciparum*. Poster presentation. South African Society of Biochemistry and Molecular Biology Conference, Goudini Spa, South Africa. Received the award for the most meritorious Poster (1<sup>st</sup> Prize) at the 24<sup>th</sup> SASBMB Conference, Goudini Spa.
  
8. **Conference proceeding:** Dina Coertzen, Marni Williams, Janina Sprenger, Lo Persson, Abraham I. Louw and Lyn-Marie Birkholtz (September 2014) Structural and functional characterization of *Plasmodium falciparum* AdoMetDC. Oral poster presentation. Third International Conference on Polyamines: Biochemical, Physiological and Clinical Perspectives, Itamambuca Eco Resort, Ubatuba-Sao Paulo, Brazil.

## Chapter 2

# Structural and functional characterisation of monofunctional *PfAdoMetDC*

### 2.1 Introduction

Due to increasing insecticide resistance of the mosquito vector, poor compliance to preventative strategies in the affected populations and the absence of a reliable malaria vaccine, effective malaria control is still highly dependent on the use of antimalarial drugs. Current antimalarials rely on a limited set of chemical backbone structures with minor modifications, thus essentially inhibiting parasite proliferation by similar modes of action. The limited range of drug targets and drug diversity, coupled to the highly polymorphic genome of the parasite, has resulted in widespread drug resistance (62, 79, 103). This necessitates the identification of novel drug targets with specific and robust inhibitors in order to contain and diminish the spread of drug resistant malaria parasites.

Polyamines are small ubiquitous molecules that mediate an essential role in parasite cell development and proliferation during the asexual blood stages (114). For this reason, polyamine biosynthesis has been specifically studied and characterised as a drug target in *P. falciparum*, the parasite responsible for the most lethal form of malaria. The intracellular polyamine pool is regulated by the biosynthetic enzymes, S-adenosyl-L-methionine decarboxylase and ornithine decarboxylase (*AdoMetDC/ODC*). These two enzymes are co-expressed from a single open reading frame as a 1419 residue heterodimer, with two polypeptides interacting to yield a heterotetrameric bifunctional complex, a property unique to *Plasmodium* parasites. The two enzymes are organised into individual domains covalently linked by a 275 residue hinge region. The *AdoMetDC* domain resides on the N-terminal region of the polypeptide, and consists of 529 residues and the *ODC* domain on the C-terminal with 614 residues. Although the two protein domains are located on the same polypeptide, their active sites are independent from each other i.e. inhibition of one site does not influence the other active site (151, 152). The enzyme activities however are co-ordinately modulated by each other through interdomain protein-protein interactions mediated by the hinge region and low complexity parasite-specific inserts (195, 199).

This distinctive bifunctional organisation and regulatory mechanisms coupled to the high demand for polyamines by *P. falciparum* parasites for proliferation, makes *PfAdoMetDC/ODC*

a promising drug target (144). However, in order to develop antimalarial candidate molecules specifically targeting this enzyme through a structure-based discovery approach, the detailed three-dimensional structure of the protein is needed, which is the bottleneck (210).

Protein structures representing eukaryotic (211, 212), prokaryotic (213), plant (214) and protozoan (215, 216) polyamine biosynthetic enzymes for AdoMetDC and ODC have been published. However, obtaining a crystal structure for *PfAdoMetDC*/ODC has proven to be problematic mainly due its sizeable heterotetrameric structure, low expression levels of impure protein and an inadequate understanding of the complex's biochemical and biophysical properties (152).

The *PfAdoMetDC* domain was therefore studied here as a monofunctional protein as a first attempt to eventually derive the three-dimensional structure of the *PfAdoMetDC*/ODC complex. Up to this point, limited structural properties of *PfAdoMetDC* have been obtained using structure-function studies on a recombinant protein (192) and a homology model based on plant (214) and human (211) AdoMetDC crystal structures.

The homology model in Figure 2.1 depicts the monomeric form consisting of residues 1-529 of the tertiary structure of monofunctional *PfAdoMetDC* (194). The enzyme presumably forms a unique four layer  $\alpha\beta\beta\alpha$ -sandwich fold as observed for human and *Solanum tuberosum* (211, 214), consisting of two central anti-parallel eight stranded  $\beta$ -sheets with the active site positioned in-between the  $\beta$ -sheets (211), flanked by approximately ten  $3_{10}$   $\alpha$ -helices (194).

*PfAdoMetDC* requires a pyruvoyl cofactor (Figure 2.1), formed post-translationally by non-hydrolytic autocatalytic serinolysis at a Ser73 and Glu72 residue, to catalyse the decarboxylation of AdoMet (152). The processing reaction cleaves the peptide backbone into two independent protein chains ( $\alpha$ - and  $\beta$ -subunit) and a dehydroalanine residue at the N-terminus of the  $\alpha$ -subunit is converted into a covalently bound pyruvoyl cofactor to produce catalytically active *PfAdoMetDC* (217, 218). AdoMet binds to the pyruvoyl group through a Schiff base forming an anionic electron sink with a leaving  $\alpha$ -carboxylate group, which is then reprotonated, resulting in hydrolysis of the Schiff base and release of dcAdoMet (213, 217).

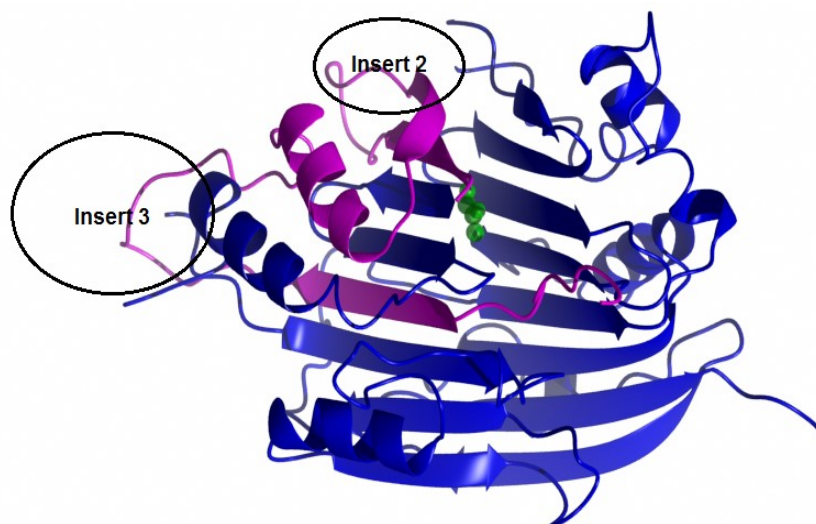


**Figure 2.1: Homology model of monofunctional *PfAdoMetDC*.** The proposed structure consists of two central  $\beta$ -sheets of eight anti-parallel  $\beta$ -strands, flanked by ten  $3_{10}$   $\alpha$ -helices. Autocatalytic processing yields a small  $\beta$ -subunit (purple) and a large  $\alpha$ -subunit (blue) with a covalently bound pyruvoyl cofactor (green) in the catalytic centre between the two central  $\beta$ -sheets. *PfAdoMetDC* contains three parasite-specific inserts of which only insert A1 was modelled in the homology model. Spatial regions of inserts A2 and A3 are surface localised and proposed as large unstructured loops. Model adapted from (194).

Human AdoMetDC autocatalytic processing and activity is allosterically stimulated by putrescine (211, 219, 220). However, in *S. tuberosum* (214) and *Plasmodium* AdoMetDC, the putrescine binding site is substituted with basic amino acid residues Arg11, Lys15 and Lys215, respectively, simulating bound putrescine at the equivalent site (194). Therefore, autocatalytic processing and activity of *PfAdoMetDC* are independent of intracellular putrescine levels (152, 213, 214). However, it is proposed that *PfAdoMetDC* activity is modulated through interdomain protein-protein interactions with *PfODC*, the hinge region and parasite-specific inserts in the heterotetrameric bifunctional complex (152, 195).

Furthermore, *PfAdoMetDC* contains three parasite-specific inserts, A1-A3 (194) (Figure 2.1). The first insert, A1 (residues 57-63), occurs before the S73 residue in the  $\beta$ -subunit of the protein (194). The A2 (residues 110-137) and A3 inserts (residues 259-408) were not modelled in the homology model due to the absence of appropriate templates. These two inserts were proposed to form large flexible loops extending away from the protein surface, as have been observed in other *Plasmodium* proteins (194, 202, 221). Gene sections transcribing these inserts evolved by rapid gene divergence such that highly hydrophilic residues, with a particular bias towards Asn and Lys residues, are repeated in the protein itself (199, 222). These properties result in the inserts being non-globular, flexible and located as unstructured loops on the protein surface (201). However, upon interaction with specific protein domains, these unstructured regions may mediate specific, conserved protein-protein



interactions that alter the conformations and activities of either of the interacting domains (195, 223).

The core catalytic domain of *PfAdoMetDC* is proposed to span residues 1-487 (152). However, since the exact start site of the hinge region is unknown due to low sequence homology with homologous proteins, the proposed start site of the hinge region on the C-terminus of *PfAdoMetDC* is residue 529 (194). Analysis showed that the C-terminal region of *PfAdoMetDC* (residues 487-529) contains two  $\alpha$ -helices and a  $\beta$ -sheet involved in interdomain interactions directly responsible for modulating activities of the two domains (196), specifically the *PfODC* domain (152, 174, 195).

Due to the decarboxylase activities of *PfAdoMetDC*/ODC residing on independent protein domains (151), *PfAdoMetDC* can be expressed and characterised as a monofunctional protein (192). Expression from wild-type gene sequence for monofunctional *PfAdoMetDC* resulted in low recombinant protein yields and equimolar co-elution of *E. coli* heat shock protein 70 (Hsp70) (207). In an earlier study, the core catalytic domain of the *PfAdoMetDC* gene was codon harmonised (encoding residues 1-487) (207). However, since the exact start site of the hinge region for *PfAdoMetDC* is unknown (194), an additional 255 wild-type nucleotides (encoding residues 488-572) were added to yield a partially codon-harmonised construct of monofunctional *PfAdoMetDC* (152, 192). Codon harmonisation of *PfAdoMetDC* not only improved soluble protein yield but also significantly reduced the amount of co-eluted *E. coli* Hsp70 (192). However, heterologous expression of this 572-residue protein had poor sample homogeneity as a result of dimeric and tetrameric complex formation of the heterologous protein. Although the oligomeric status for *PfAdoMetDC* has not been confirmed, superimposition with dimeric human AdoMetDC (211) indicated that *PfAdoMetDC* dimerises via an edge-on interaction by disulphide bond formation at Cys505 on  $\beta$ -sheet 15. Site directed mutagenesis of Cys505 to Ser decreased homodimerisation significantly. However, apart from disulphide bridge formation by the C505 residue, other proposed mechanisms of non-specific heterologous *PfAdoMetDC* dimerisation includes tail-to-tail interactions by the hinge region residues located at the C-terminal of *PfAdoMetDC* or side-to-side interactions mediated by the A3 parasite-specific insert and a hydrophobic patch. Simultaneous dimerisation mediated by these mechanisms may thus lead to formation of the homotetrameric complex also observed for monofunctional *PfAdoMetDC* (192) (Figure 2.2). The formation of these protein complexes results in an expressed protein with low sample homogeneity thus making it unsuitable for protein crystallography studies.

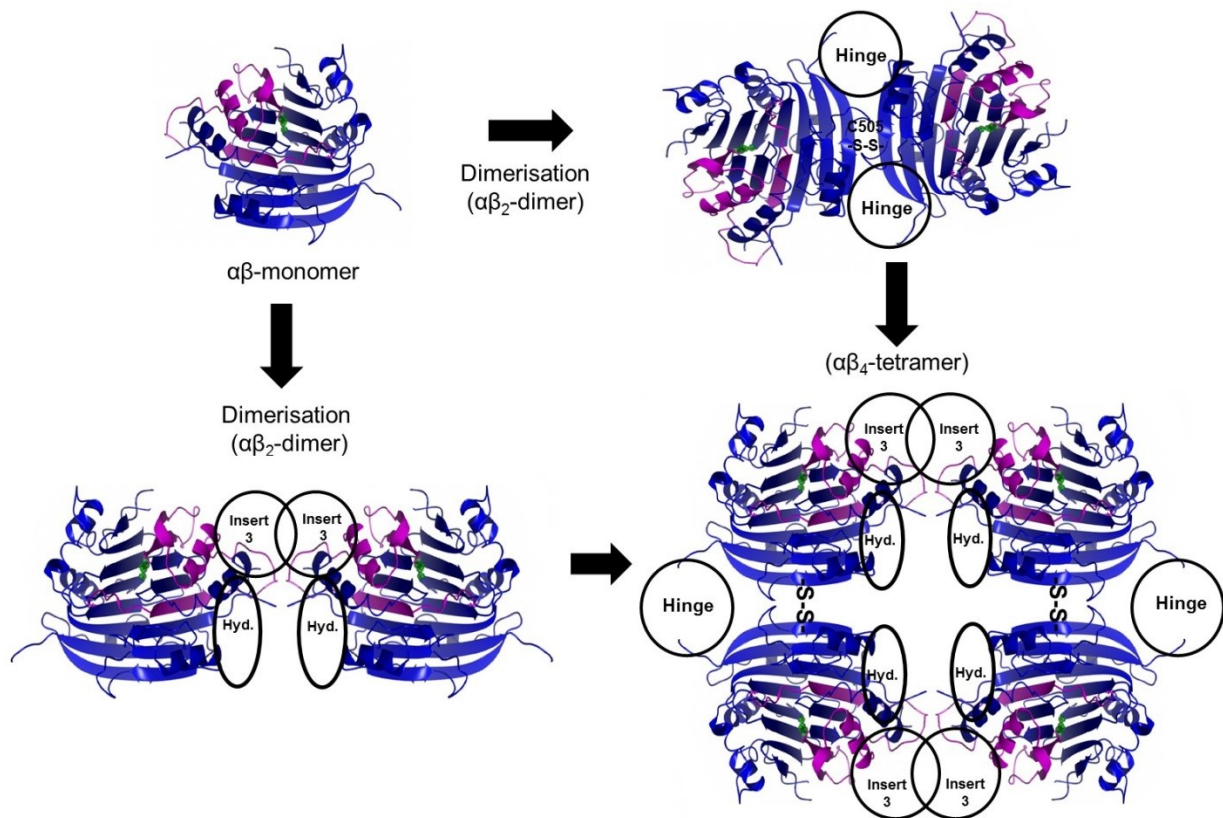


**Figure 2.2: Proposed mechanisms of heterologous monofunctional *PfAdoMetDC* oligomerisation *in vitro*.** The protomer undergoes autocatalytic serinolysis yielding the processed  $\alpha\beta$ -monomer ( $\alpha$ -subunit shown in blue and  $\beta$ -subunit shown in purple). Heterologous monofunctional *PfAdoMetDC* is proposed to dimerise ( $\alpha\beta_2$ -dimer) via two independent mechanisms 1) a tail-to-tail interaction by disulphide bond formation mediated by Cys residues at the proposed dimer interface (C50S residue (192) or the C-terminal hinge region) 2) a side-to-side interaction mediated by protein-protein interactions of the A3 parasite-specific insert (Insert 3) or interactions mediated by the hydrophobic patch (Hyd.). Simultaneous side-to-side and tail-to-tail interactions also lead to the formation of homotetrameric heterologous *PfAdoMetDC* complexes. Adapted from (207).

In this study, some of the above-mentioned structural and functional uncertainties of monofunctional *PfAdoMetDC* were investigated. Heterologous expression of a deletion mutant of the A3 parasite-specific insert resulted in an increased yield, purity, and sample homogeneity, whilst maintaining protein functionality and structural integrity. This confirms previous speculations that the parasite-specific inserts have no immediate structural and functional impact on monofunctional *PfAdoMetDC*, but instead mediate surface protein-protein intra- and interdomain interactions. However, truncation of the proposed non-essential hinge region resulted in low-level expression of insoluble protein aggregates and a complete loss of protein activity, indicating that the hinge region is essential for monofunctional *PfAdoMetDC* structural integrity and functionality. Furthermore, the improvement in expression and purity after deletion of the A3 parasite-specific insert resulted in the first-ever crystallisation trials for monofunctional *PfAdoMetDC*.

## 2.2 Materials and Methods

### 2.2.1 *In silico* analysis of *PfAdoMetDC*

Kyte and Doolittle hydrophobicity analysis of the residues removed from the A3 insert in  $\Delta$ A3 *PfAdoMetDC* was performed using CLC Bio Protein Workbench 6 (224). The plot indicates the ratio of hydrophobicity to hydrophilicity for each residue depending on the residue's hydrophobicity score. Prediction of LCRs was performed with the Wootton and Federhen algorithm (SEG algorithm) (225) using CLC Bio Protein Workbench 6. Protein unstructured regions were predicted with the IUPred server (226) ([iupred.enzim.hu/pred.php](http://iupred.enzim.hu/pred.php)) according to the algorithm described (227), and the graph analysed with JpGraph software (Appendix 5).

### 2.2.2 Cloning of codon harmonised *PfAdoMetDC* constructs

In an earlier study (152, 192), nucleotides 1-1461 representing the 487 residue core catalytic domain from *PfAdoMetDC* were codon harmonised, by replacing *Plasmodium* specific codons with synonymous codons, that equalised the codon usage frequency of the *P. falciparum* gene to that of the *E. coli* host (228, 229). At the C-terminus of the construct, 85 unharmonised codons of the *PfAdoMetDC*/ODC hinge region were cloned in addition to the 487 codon harmonised *PfAdoMetDC* residues into the pASK-IBA3 expression vector (Invitrogen). The partially codon harmonised *PfAdoMetDC*-hinge, 1716 nucleotide gene sequence (572 residues) (192) in this text is referred to as wild-type *pfadometdc* and translates wild-type, monofunctional *PfAdoMetDC* (Figure 2.3). From the wild-type *pfadometdc* construct, a second construct containing a Cys505Ser point mutation was cloned, expressing the mutant protein, C505S *PfAdoMetDC* (192, 208) (Figure 2.3). The C505S mutagenic construct was designed to reduce *in vitro* protein dimerisation as a result of disulphide bridge formation. Both the wild-type and C505S mutant proteins were expressed in a previous study (192), and are, therefore, used only for comparative analysis in this study. In the third construct, 100 residues (residues 264-364) of the 149-residue A3 parasite-specific insert were deleted from the wild-type *pfadometdc* construct (nucleotides 795-1095 deleted) (Marni Williams, unpublished work 2010), resulting in the expression of a  $\Delta$ A3 *PfAdoMetDC* mutant protein (Figure 2.3). As a fourth deletion mutant, the 85 unharmonised residues from the C-terminal of the *PfAdoMetDC*/ODC hinge region (residues 487- 572) were removed, producing a complete 487 residue *PfAdoMetDC* core protein, expressed from a fully codon harmonised gene, referred to as  $\Delta$ H *PfAdoMetDC* (Figure 2.3). The C505S mutant was not employed in the  $\Delta$ A3 mutant such that the sole effect of deletion of the A3 insert could be determined. For

comparative purposes, as a fifth construct the  $\Delta H$  deletion was also included in the  $\Delta A3$  mutant, producing a 387-residue construct referred to as  $\Delta A3\Delta H$  *PfAdoMetDC* (Figure 2.3).

The  $\Delta H$  and  $\Delta A3\Delta H$  constructs were produced by amplifying 3 pmol of harmonised *pfadometdc* and 3.5 fmol of  $\Delta A3$  *PfAdoMetDC* with 2 pmol and 10 pmol sense (5'-ATGGTAGGTCTCAAATGAATGGCATTTCGAAGGCATTG-3') and antisense (5'-ATGGTAGGTCTCAGCGCTCATATTATTAAGACTCCTCG-3') primers using TaKaRa Ex-Taq™ (TAKARA Bio Inc.), according to the manufacturer's specifications. These primers incorporated an Eco31I (*Bsa*1) restriction site at the respective start codon and  $\Delta H$  deletion site, for subsequent restriction enzyme digestion and sub-cloning into the pASK-IBA3 vector (Invitrogen). The cycling conditions were as follows: initial denaturation at 94°C for 3 min, followed by 35 cycles of 94°C for 30 sec, 61°C for 30 sec and 68°C for 2.5 min with a final elongation step of 68°C for 10 min. The PCR products were visualised by GelRed™ (Biotium) using agarose gel electrophoresis (Appendix 2), and the correct sized bands were purified using the Wizard® SV Gel and PCR Clean-up system kit (Promega). The PCR fragments (1 µg) were digested with 2 U of FastDigest Eco31I (*Bsa*1) (Fermentas) for 1 h at 37°C and heat inactivated for 15 min at 65°C. In addition, the pASK-IBA3 expression vector (1 µg) was digested with 2 U Eco31I (*Bsa*1) for 1 h at 37°C, and heat inactivated for 15 min at 65°C. The 5' and 3' phosphate groups of the vector were dephosphorylated with 5.5 U FastAP™ Thermo sensitive Alkaline Phosphatase (Fermentas) directly added to the digestion reaction for 45 min at 37°C, and heat inactivated for 10 min at 75°C. Following restriction digestion the PCR product and plasmid were ligated in a 5:1 insert: vector ratio with 2 U T4 DNA Ligase (Fermentas) for 16 h at 16°C and heat inactivated for 10 min at 65°C. The ligated products were transformed into heat shock competent *E. coli* DH5α cells and incubated for 14 h at 37°C on a LB-Ampicillin (100 µg/ml) agar plate. The amp resistance selection marker on the vector enabled selection of positive clones, which were inoculated into LB-Ampicillin (50 µg/ml) and grown for 16 h at 37°C. Colony PCR was performed to verify positive clones (230, 231) using 10 pmol pASK-IBA sequencing primers (forward: 5'-GAGTTATTTTACCACTCCCT-3' and reverse: 5'-CGCAGTAGCGGTAAACG-3' (Invitrogen)) with 2 x KAPA Taq ReadyMix PCR kit (KAPABiosystems, USA). The following temperature cycling parameters were used; 95°C for 30 min, with 25 cycles of 95°C for 30 sec, 55°C for 30 sec, 72°C for 4 min and a final denaturation step of 72°C for 5 min. Isolations of  $\Delta H$  and  $\Delta A3\Delta H$  *PfAdoMetDC* plasmids were performed using the Zyppy™ Plasmid Miniprep Kit (Zyppy). Positive clones were verified by restriction enzyme digestion with HndIII, XbaI and KpnI (Promega) (Appendix 3) and Sanger dideoxy sequencing using the above mentioned pASK-IBA sequencing primers (Inqaba Biotech, South Africa) (Appendix 4). Sequences were aligned using UniProt.

For comparative reasons, all five *PfAdoMetDC* constructs (harmonised, C505S,  $\Delta$ A3,  $\Delta$ H and  $\Delta$ A3 $\Delta$ H) were cloned into the pASK-IBA3 expression vector containing a *tet*-promoter, amp resistance gene, and a C-terminal *Strep*-tag II for affinity chromatography purification (Figure 2.3, Plasmid maps Appendix 1).

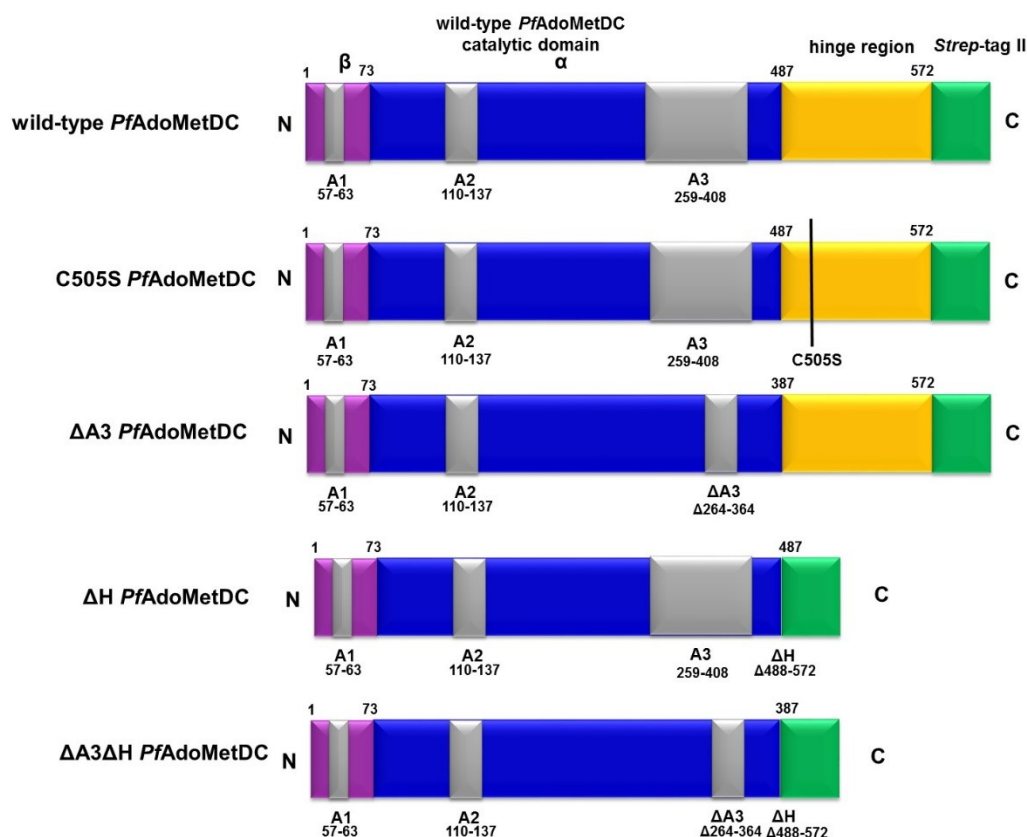


**Figure 2.3: Schematic diagram of the *PfAdoMetDC* wild-type protein and various mutant proteins created in this study to allow comparative structure-activity analyses.** Five proteins were comparatively expressed in this study: wild-type *PfAdoMetDC* consisting of the 487 catalytic  $\alpha$ - $\beta$ -monomer in purple and blue, A1, A2 and A3 parasite-specific inserts (grey), the 85 residue hinge region (yellow) and the C-terminal *Strep*-tag II (green) (192). The C505S mutant that was cloned via site-directed mutagenesis from the wild-type *PfAdoMetDC* construct (192). The novel *PfAdoMetDC* mutants cloned for this study include the  $\Delta$ A3 mutant, where 100 residues (residues 264-364) from the A3 parasite-specific insert were deleted. For the  $\Delta$ H mutant, the 85 hinge residues (residues 487-572) were deleted from wild-type *PfAdoMetDC*. For the  $\Delta$ A3 $\Delta$ H double mutant, the 85 hinge residues (residues 487-572) were deleted from the  $\Delta$ A3 mutant.



### 2.2.3 Analysis of recombinantly expressed and purified *PfAdoMetDC*

The pASK-IBA3 vectors containing harmonised *pfadometdc*, and the four mutated constructs, C505S,  $\Delta A3$ ,  $\Delta H$  and  $\Delta A3\Delta H$ , were transformed into *E. coli* BL21 Star<sup>TM</sup> (DE3) heat shock competent cells (Invitrogen) and incubated for 16 h at 37°C on LB-Ampicillin (100 µg/ml) agar plates. A single colony was inoculated into LB-Ampicillin (50 µg/ml) and incubated for 16 h at 37°C. The culture was subsequently diluted to 1:100 in LB-Ampicillin (50 µg/ml) and grown to  $OD_{600} = 0.5$ . Protein expression was induced with 200 µg anhydrotetracycline (AHT, Invitrogen), incubated for 4 h at 37°C and cells were harvested at 5 000g with a Beckman J-6 centrifuge (Beckman, USA) at 4°C. Protein purification was performed as previously described (192, 195) by re-suspending harvested cell pellets in 10 ml wash buffer (buffer W; 100 mM Tris-HCl pH 8.0, 10 mM EDTA, 150 mM NaCl, 10% Glycerol, 10 mM DTT and 0.02% Brij-35) and lysozyme per litre of culture. The inclusion of 10 mM DTT reduces covalent disulphide bridges (232) and subsequently, protein oligomerization whereas Brij-35, a non-ionic polyoxyethylene surfactant, assists in protein solubilisation by concealing surface hydrophobic patches (152, 174, 233). The cell suspensions were incubated on ice for 30 min, followed by sonification with a Sonifier cell disruptor B-30 (Instralab, South Africa). Lysates were ultracentrifuged at 100 000g for 1 h at 4°C with a Beckman Avanti J-25 ultracentrifuge (Beckman, USA) to segregate the soluble proteins in the supernatant from the insoluble fractions in the cellular pellet. Subsequently, the soluble *PfAdoMetDC* *Strep*-tagged proteins were loaded onto a column containing *Strep*-Tactin<sup>®</sup> Sepharose<sup>®</sup> affinity matrix for affinity chromatography, which was performed at 4°C (195). The cell pellets and superantants were kept at 4°C for later analysis by reducing SDS-PAGE. The *Strep*-tag // bound proteins were eluted in Buffer W containing 10 mM DTT, 0.02% Brij-35 and 2.5 mM desthiobiotin (Invitrogen). The eluted proteins were stored at 4°C pending further analysis.

Following affinity chromatography, protein yield was determined using the Bradford assay (234), with Quick Start<sup>TM</sup> Bradford dye reagent (Bio-Rad Laboratories) and absorbance measurements at 595 nm with a Multiscan ascent scanner (ThermoScientific Labsystems, USA). The yield of each independent *PfAdoMetDC* construct was determined in duplicate for three individual purified cell lysates to determine the average yield in mg/L culture.

The supernatants and pellets obtained after ultracentrifugation along with affinity chromatography purified *PfAdoMetDC* proteins were analysed by reducing SDS-PAGE (235) using AnyKD<sup>TM</sup> Mini-PROTEAN<sup>®</sup> TGX<sup>TM</sup> Precast Gels with the Mini-Protean Tetra-cell system (Bio-Rad) according to manufacturer's specifications. Bands were visualised with colloidal Coomassie-Blue (Sigma-Aldrich) staining (236).

For the detection of *PfAdoMetDC* proteins, Western immunodetection was performed using monoclonal *Strep*-tag II mouse antiserum conjugated to horseradish peroxidase (Invitrogen) (195). In addition, after easy nano-liquid chromatography coupled to LTQ Orbitrap Velos Mass Spectrometry at the Central Analytical Facility (CAF) Proteomics Laboratory at Stellenbosch University, South Africa ([www.sun.ac.za/saf](http://www.sun.ac.za/saf)), the identities of  $\Delta A3$  *PfAdoMetDC* bands visualized after reducing SDS-PAGE, were established by database searches of PlasmoDB 7.1 using Proteome Discover 1.2 and MASCOT ([www.matrixscience.com](http://www.matrixscience.com)).

A calibration curve for protein molecular mass determination by size-exclusion chromatography (SEC) on a Superdex S200 10/300 GL SE column (Tricorn, GE Healthcare) was established with a phosphate buffer (50 mM  $\text{KH}_2\text{PO}_4$ , pH 7.4, 150 mM NaCl) on a Äkta Explorer System (Amersham Pharmacia Biotech). The elution volumes ( $V_e$ ) of a 15 mg/ml high molecular weight (HMW) protein chromatography calibration kit (Tricorn, GE Healthcare) was determined at a 0.3 ml/min flow rate. This HMW protein mixture consisted of 3 mg/ml ovalbumin (44 kDa), 3 mg/ml conalbumin (75 kDa), 3 mg/ml aldolase (158 kDa), 3 mg/ml ferritin (440 kDa) and 3 mg/ml thyroglobulin (669 kDa). The void volume ( $V_o$ ) of the column was determined with 2 mg/ml 2000 kDa Dextran Blue eluted at a 0.3 ml/min flow rate.

To determine the native oligomeric status of the affinity chromatography purified *PfAdoMetDC* proteins, the SEC column was equilibrated with filtered and degassed buffer W containing 10 mM DTT and 0.02% Brij-35 and loaded with ~2 mg/ml affinity chromatography purified protein and eluted at a 0.3 ml/min flow rate. Protein containing fractions were collected and analysed by reducing SDS-PAGE as described above. Fractions of the monomeric protein peak were pooled and concentrated with an Ultracel 3K Amicon® filter (MWCO 3000, Millipore) and the concentration determined with the Bradford method (234).

#### 2.2.4 *PfAdoMetDC* activity determination

The specific activities of the various affinity chromatography purified *PfAdoMetDC* proteins were determined with a [ $^{14}\text{C}$ ]-AdoMet bioassay as described previously (151, 195, 237). Reactions were performed in duplicate with 5  $\mu\text{g}$  protein in assay buffer consisting of 10 mM EDTA, 10 mM DTT, 500  $\mu\text{M}$  S-(5'-adenosyl)-L-methionine chloride (Sigma-Aldrich) and 50 nCi [ $^{14}\text{C}$ ]-AdoMet [S-(5'-adenosyl-[carboxy- $^{14}\text{C}$ ]-L-methionine (55 mCi/mmol, ARC, Amersham Biosciences) adjusted to a final volume of 250  $\mu\text{l}$  with 50 mM  $\text{KH}_2\text{PO}_4$ , pH 7.5. The reactions were incubated for 30 min at 37°C with agitation in order to capture released  $^{14}\text{CO}_2$  produced



during the catalytic reaction on hyamine hydroxide soaked Whatman® filter paper. The reactions were terminated by precipitating the protein with 500 µl of a 5% (w/v) trichloroacetic acid solution. Captured  $^{14}\text{CO}_2$  was quantified with a Tri-carb series TR liquid scintillation fluid counter (PE Applied biosystems), with a 60 min count time or count termination at 10 000 counts per minute (cpm;  $\theta$  Sigma with 1% Relative standard deviation (RSD)). The results represent three independent experiments performed in duplicate and expressed in nmoles/min/mg for each independent *PfAdoMetDC* protein.

### 2.2.5 Analysis of mutated *PfAdoMetDC* secondary structure content with far-UV Circular Dichroism Spectroscopy

The influence of deletion mutagenesis on the secondary structure composition of the SEC-purified  $\Delta\text{A3}$  *PfAdoMetDC* deletion mutant was determined by far-UV CD. The C505S mutant was used as a control since previous far-UV CD results of this mutant compared to human AdoMetDC, showed that the proteins had similar secondary structure content. Following SEC, *PfAdoMetDC* fractions were pooled and dialysed overnight into a phosphate buffer (10 mM  $\text{KH}_2\text{PO}_4$  pH 7.7, 50 mM NaF) at 4°C with Slide-A-Lyzer® mini dialysis units (3.5 kDa MM cut-off, Thermo Scientific) to remove  $\text{Cl}^-$  ions, which have optical activity in far-UV spectra (238). Following dialysis the proteins were concentrated to 0.5 mg/ml with an Ultracel 3K Amicon® filter. Far-UV spectra was determined at a wavelength range of 190 to 250 nm at 20°C with 0.5 nm intervals and a bandwidth of 1 nm at a scanning speed of 20 nm/min with a Jasco J815 CD instrument using a 0.1 cm<sup>2</sup> cuvette. Absorbance readings were taken in duplicate and the background readings were subtracted from these average readings. Data points indicating the protein's molar ellipticity ( $[\theta]_M$ ) were analysed in deg.cm<sup>2</sup>.dmol<sup>-1</sup> (193).

### 2.2.6 Analysis of *PfAdoMetDC* protein flexibility with small angle X-ray scattering

Small angle X-ray scattering (SAXS) of the  $\Delta\text{A3}$  mutagenic *PfAdoMetDC* was performed and compared to the C505S mutant to determine whether the predicted intrinsically unstructured regions (IURs) influenced the proteins flexibility. Following SEC-purification, *PfAdoMetDC* fractions were pooled and concentrated with an Ultracel 3K Amicon® filter to 1, 2.5, 5 and 7.5 mg/ml. For each concentration a 1:1, 1:10, 1:25, 1:50, and 1:100 dilution with a 10 mM  $\text{Co}^{2+}$  buffered solution was prepared. Measurements were taken at the Synchrotron facility at Hamburg University, Germany and data analysis were performed by Janina Sprenger (Lund University, Sweden, unpublished work) as previously described (239). Briefly, the dimensionless Kratky plot was transformed with Guinier parameters, which is the relation

between scattering intensities ( $I(\theta)$ ) and the level of gyration ( $R_g$ ), to derive the Porod-Debye graph using structural parameters of the Porod-Debye law. The law is an approximation occurring within a limited range of scattering angles suggesting decay of a particle as indicated in the equation below:

$$I(q) \approx \Delta\rho^2 \times \frac{2\pi}{q^4} \times S$$

Porod-Debye law, where  $I(q)$  determines the volume of the scattering particle (Porod volume,  $V_p$ ),  $S$  is the surface area of the scattering particle  $\Delta\rho$  concentration of the scattering particle, and  $q$  is the normalising value.

### 2.2.7 Determination of the polydispersity index of SEC purified proteins with Dynamic Light Scattering

Dynamic light scattering (DLS) was performed to determine the hydrodynamic radius ( $R_H$ ) and polydispersity index (PDI) of SEC purified *PfAdoMetDC* proteins after deletion mutagenesis of specific regions of *PfAdoMetDC*. Pooled SEC-purified fractions were concentrated with an Ultracel 3K Amicon® filter to ~1 mg/ml and centrifuged at 10 000g for 10 min at 4°C to remove any protein aggregates. Prior to measurements protein samples were either incubated with 5 mM TCEP (tris-2(carboxyethyl phosphine), 10 mM DTT or 0.02% Brij-35 and kept on ice for 30 min. Measurements were obtained with a Zetasizer Nano S instrument (Malvern instruments) at default settings with a 3 mm precision cell curvette (Hellma). The PDI was calculated using Zetasizer Nano Software Version 6.01.

### 2.2.8 Determination of optimal protein crystallisation conditions with differential scanning fluorimetry

Prior to crystallisation trials of *PfAdoMetDC*, differential scanning fluorimetry (DSF) was performed to determine the optimal buffering condition in which the protein was the most stable. DSF relies on the binding of SYPRO orange dye to the hydrophobic regions of the target protein as the protein denatures and unfolds during increases in the temperature. Therefore, the lowest absorbance readings at the highest temperatures yields a  $T_m$  value corresponding to the equilibrium between folded and unfolded protein (240). Fractions of SEC-purified *PfAdoMetDC* were pooled and concentrated to 1 mg/ml in 20 mM Tris-HCl buffer, pH 8 (without 10 mM DTT and 0.02% Brij-35) with an Ultracel 3K Amicon® filter. A buffer screen was set-up as described by Niesen *et al.* (241). Briefly, concentrated *PfAdoMetDC* was diluted 10-fold in 20 mM Tris-HCl buffer, pH 8, which also contained 1000-fold diluted SYPRO orange (Sigma-Aldrich). A screen of 24 buffers were aliquoted (8  $\mu$ l) in duplicate in a

96-well ABgene® PCR plate (Thermo Scientific) and 24 µl of the protein solution was added in a 3:1 protein to buffer ratio. Two additional buffers were also screened: 1) 150 mM Tris-HCl, pH 8 and 2) 150 mM Tris-HCl, pH 8, 0.02% Brij-35, 10 mM DTT. Protein stability was assayed using the Mx3005P qPCR system (Stratagene) with a temperature range from 25-95°C. Fluorescence readings were taken at 1 min intervals with excitation and emission wavelengths of 492 nm and 610 nm, respectively, and data were analysed with MXPro Software (241).

### 2.2.9 $\Delta A3$ PfAdoMetDC crystallisation trials

Affinity chromatography purified PfAdoMetDC was further purified by SEC under two different reducing buffering conditions providing the highest protein stability as identified by DSF: 1) buffer W, with 10 mM DTT and 0.02% Brij-35 and 2) 100 mM HEPES, pH 7.4, 150 mM NaCl, 1 mM EDTA, 10 mM DTT and 0.02% Brij-35. Fractions of the monomeric peak under reducing SEC conditions for each buffering condition were pooled and concentrated with an Ultracel 3K Amicon® filter to 3-7 mg/ml. The concentrated proteins were centrifuged for 10 min at 10 000g at 4°C to remove protein aggregates. Protein crystallisation screens were performed either with the Apo-form of  $\Delta A3$  PfAdoMetDC or after pre-incubation with 250 µM of the AdoMetDC specific inhibitor, MDL73811 (10-fold higher than the protein molar concentration), for 30 min at 4°C. Initially, a manual sparse-matrix crystal screen was set up with a Hampton Research crystal screen HR 2-110 kit (Hampton Research, USA) using the hanging drop vapour diffusion method and incubation at 4°C and 20°C. Additionally, high-throughput crystallisation screens (HTS) were performed at the Max-Lab crystallisation facility (Lund University, Sweden) using the vapour diffusion method with a Mosquito MD11-11 robotics system (LabTech). Four independent crystallisation screens were performed: PACTpremier™ MD1-29, JCSG-plus™ MD1-37, ProPlex™ HT-96 and the Structure screen I+II HT96 MD1-30 (Molecular Dimensions). Plates were incubated at 20°C and crystals analysed under polarising light to determine birefringence with a CrystalPro™ 2 microscope and CrystalLIME™ (TriTek) software.

### 2.2.10 Statistical analyses

All data are representative of at least three independent biological experiments ( $n \geq 3$ ), each performed in duplicate. Data were analysed using GraphPad Prism 5.0. Statistical analyses were performed using the unpaired Student's *t*-test at a least 95% confidence level.

## 2.3 Results

### 2.3.1 *In silico* analysis of *PfAdoMetDC* reveals unique sequence characteristics of the A3 parasite-specific insert and the C-terminal hinge region

A homology model for monofunctional *PfAdoMetDC*, based on human (211) and plant (242) templates shows that the protein contains two central  $\beta$ -sheets of eight antiparallel  $\beta$ -sheets, flanked by several  $3_{10}$   $\alpha$ -helices, conforming to the  $\alpha\beta\alpha$ -fold observed for plant and human *PfAdoMetDC* (Figure 2.1) (194). However, structural characteristics of the A2 and A3 parasite-specific inserts were not modelled due low sequence homology with template models (194). Secondary structure prediction (Figure 2.4) showed no structures for the A1 and A2 inserts but the A3 insert was shown to contain five  $\beta$ -sheets. In addition, secondary structure prediction of the C-terminal hinge region of *PfAdoMetDC* (residues 487-572) showed a  $\beta$ -sheet and two  $\alpha$ -helices (Figure 2.4). These  $\alpha$ -helices correspond to previously predicted secondary structures within the hinge region (196).

Analysis of the sequence characteristics of the A3 insert with the Seg algorithm complexity plot (Appendix 5, Figure 5) identified four LCRs, which did not overlap with the predicted  $\beta$ -sheets (Figure 2.4). Protein unstructured regions were also predicted with the IUPred server (Appendix 5, Figure 8) of which five regions were identified. Interestingly, most of these overlapped with predicted LCRs (Figure 2.4). Furthermore, within the predicted LCRs and unstructured regions, five sequences of two to three tandem Asn repeats were identified (Figure 2.4) indicating selective bias for this residue in the A3 parasite-specific insert (Appendix 5, Figure 5) (243, 244). The Asn repeats along with the high content of polar and charged residues such as Thr, His, Arg and Ser are highly abundant in the A3 insert compared, to the rest of the conserved *PfAdoMetDC* sequence. The low content of hydrophobic and aromatic residues such as Leu, Met and Phe (confirmed by Kyte and Doolittle hydrophobicity plot analysis; Appendix 5, Figure 6) substantiates the hydrophilic nature of the A3 insert, similar to other parasite-specific inserts in proteins of *Plasmodium* parasites (199). Although not characterised as a parasite-specific insert, the hinge region also resembles the sequence specific characteristics of the A3 insert since it contains two tandem Asn repeats as well as a high content of hydrophilic residues (Kyte and Doolittle hydrophobicity plot; Appendix 5, Figure 6).

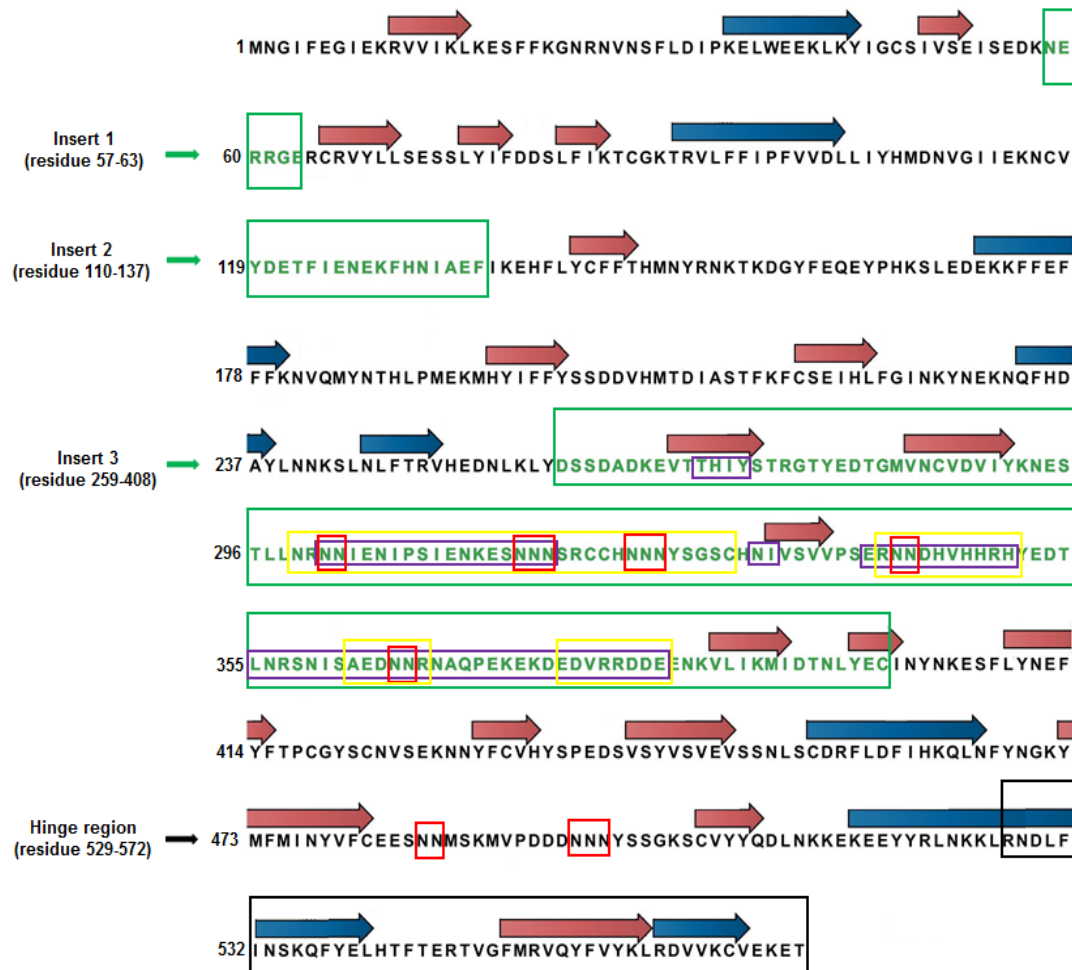


**Figure 2.4: Secondary structure prediction of *PfAdoMetDC*.** Blue arrows indicate  $\alpha$ -helices and red arrows indicate  $\beta$ -sheets. The secondary structure prediction without the A2 and A3 inserts as well as that of the hinge is similar to that of the homology model of *PfAdoMetDC* (194) with the exception of three  $\beta$ -sheets and two  $\alpha$ -helices. The secondary structures of the parasite-specific inserts (A1, A2 and A3) are indicated in green boxes and the hinge region as a black box. For insert A3, five tandem Asn repeats were identified (red boxes), which overlapped with four LCRs (yellow boxes) and five unstructured regions (purple boxes).

LCRs and disordered regions have been shown to interfere with protein crystallisation strategies (245). In this study, the A3 parasite-specific insert was partially deleted due to its large size, the predicted non-essential role in protein structure and function (194) and the high abundance of hydrophilic residues. (194) Furthermore, the C-terminal hinge region was also truncated based on similar considerations and presently unknown structural and functional role in monofunctional *PfAdoMetDC*.

### 2.3.2 Expression and purification of deletion constructs reveals unique characteristics of the A3 insert and the hinge region for monofunctional *PfAdoMetDC*

#### 2.3.2.1 Deletion of the A3 insert improves heterologous expression of monofunctional *PfAdoMetDC*

The specific structural and functional features of the A3 insert and the hinge region on dimerisation and oligomerisation of monofunctional *PfAdoMetDC* needed to be identified and understood. Three deletion mutants,  $\Delta A3$ ,  $\Delta H$  and  $\Delta A3\Delta H$ , were constructed from a codon harmonised version of wild-type *pfadometdc*. The A3 insert contains 149 amino residues (194) but only the central 100 residues (residues 264-364) were removed and is referred to as the  $\Delta A3$  mutant in this study. For the  $\Delta H$  mutant, the 85 residues of the hinge region at the C-terminal were removed, which left only the core catalytic domain of *PfAdoMetDC* (487 residues) (152). In order to increase the sequence homology of *PfAdoMetDC* to human *AdoMetDC*, a third deletion mutant was constructed containing both the  $\Delta A3$  and  $\Delta H$  deletions and named the  $\Delta A3\Delta H$  double mutant. Protein constructs were expressed from the pASK-IBA3 expression vector with a C-terminal *Strep*-tag II, as with the wild-type and C505S mutants (204). The amino acid sequence alignments of these constructs are shown in Figure 2.5 (Plasmid maps; Appendix 1, restriction enzyme mapping; Appendix 3, Sanger dideoxy sequencing results, Appendix 4).



Harm.	1	MNGIFEGIEKRVVVKLKESEFFKGNRNVNSFLDIPKELWEEKLKYIGCSIVSEISEDKNER	60
C505S	1	MNGIFEGIEKRVVVKLKESEFFKGNRNVNSFLDIPKELWEEKLKYIGCSIVSEISEDKNER	60
ΔA3	1	MNGIFEGIEKRVVVKLKESEFFKGNRNVNSFLDIPKELWEEKLKYIGCSIVSEISEDKNER	60
ΔH	1	MNGIFEGIEKRVVVKLKESEFFKGNRNVNSFLDIPKELWEEKLKYIGCSIVSEISEDKNER	60
ΔA3ΔH	1	MNGIFEGIEKRVVVKLKESEFFKGNRNVNSFLDIPKELWEEKLKYIGCSIVSEISEDKNER	60
*****			
Harm.	61	RGERCRVYLLSESSLYIFDSSLFIKTCGKTRVLFPIPFVVDLLIYHMDNVGIEKNCVYD	120
C505S	61	RGERCRVYLLSESSLYIFDSSLFIKTCGKTRVLFPIPFVVDLLIYHMDNVGIEKNCVYD	120
ΔA3	61	RGERCRVYLLSESSLYIFDSSLFIKTCGKTRVLFPIPFVVDLLIYHMDNVGIEKNCVYD	120
ΔH	61	RGERCRVYLLSESSLYIFDSSLFIKTCGKTRVLFPIPFVVDLLIYHMDNVGIEKNCVYD	120
ΔA3ΔH	61	RGERCRVYLLSESSLYIFDSSLFIKTCGKTRVLFPIPFVVDLLIYHMDNVGIEKNCVYD	120
*****			
Harm.	121	ETFIENEKFHNIAEFIKEHFLYCFFTHMNYRNKTKDGYFEQEPHKSLEDEKFFEFFFK	180
C505S	121	ETFIENEKFHNIAEFIKEHFLYCFFTHMNYRNKTKDGYFEQEPHKSLEDEKFFEFFFK	180
ΔA3	121	ETFIENEKFHNIAEFIKEHFLYCFFTHMNYRNKTKDGYFEQEPHKSLEDEKFFEFFFK	180
ΔH	121	ETFIENEKFHNIAEFIKEHFLYCFFTHMNYRNKTKDGYFEQEPHKSLEDEKFFEFFFK	180
ΔA3ΔH	121	ETFIENEKFHNIAEFIKEHFLYCFFTHMNYRNKTKDGYFEQEPHKSLEDEKFFEFFFK	180
*****			
Harm.	181	NVQMYNTHLPMEKMHYIFFYSSDDVHMTDIASFKFCSEIHLFGINKYNEKNQFHDAYLN	240
C505S	181	NVQMYNTHLPMEKMHYIFFYSSDDVHMTDIASFKFCSEIHLFGINKYNEKNQFHDAYLN	240
ΔA3	181	NVQMYNTHLPMEKMHYIFFYSSDDVHMTDIASFKFCSEIHLFGINKYNEKNQFHDAYLN	240
ΔH	181	NVQMYNTHLPMEKMHYIFFYSSDDVHMTDIASFKFCSEIHLFGINKYNEKNQFHDAYLN	240
ΔA3ΔH	181	NVQMYNTHLPMEKMHYIFFYSSDDVHMTDIASFKFCSEIHLFGINKYNEKNQFHDAYLN	240
*****			
A3 start site: D259			
Harm.	241	NKSLNLFTRVHEDNLKLYDSSDADKEVTTHIYSTRGTIEDTMVNCVDVIYKNESTLLNR	300
C505S	241	NKSLNLFTRVHEDNLKLYDSSDADKEVTTHIYSTRGTIEDTMVNCVDVIYKNESTLLNR	300
ΔA3	241	NKSLNLFTRVHEDNLKLYDSSDAD-----	264
ΔH	241	NKSLNLFTRVHEDNLKLYDSSDADKEVTTHIYSTRGTIEDTMVNCVDVIYKNESTLLNR	300
ΔA3ΔH	241	NKSLNLFTRVHEDNLKLYDSSDAD-----	264
*****			
ΔA3 start site: K264			
Harm.	301	NNIENIPSIENKESNNNSRCCNNNYSVSGSCHNIVSVVPSERNNDHVHRRHYEDTLNRSNI	360
C505S	301	NNIENIPSIENKESNNNSRCCNNNYSVSGSCHNIVSVVPSERNNDHVHRRHYEDTLNRSNI	360
ΔA3	265	-----	264
ΔH	301	NNIENIPSIENKESNNNSRCCNNNYSVSGSCHNIVSVVPSERNNDHVHRRHYEDTLNRSNI	360
ΔA3ΔH	265	-----	264
*****			
Harm.	361	SAEDNNRNAQPEKEKDEDVRRDDEENKVLKIMIDTNLYECINYNKESFLYNEFYFTPCGY	420
C505S	361	SAEDNNRNAQPEKEKDEDVRRDDEENKVLKIMIDTNLYECINYNKESFLYNEFYFTPCGY	420
ΔA3	265	---NNRNAQPEKEKDEDVRRDDEENKVLKIMIDTNLYECINYNKESFLYNEFYFTPCGY	320
ΔH	361	SAEDNNRNAQPEKEKDEDVRRDDEENKVLKIMIDTNLYECINYNKESFLYNEFYFTPCGY	420
ΔA3ΔH	265	---NNRNAQPEKEKDEDVRRDDEENKVLKIMIDTNLYECINYNKESFLYNEFYFTPCGY	320
*****			
		ΔA3 end site: D364	A3 end site: C408
Harm.	421	SCNVSEKNYFCVHYPEDSVSVSVSVSSNLSCDRFLDFIHKQLNFYNGKYMFMINYVF	480
C505S	421	SCNVSEKNYFCVHYPEDSVSVSVSVSSNLSCDRFLDFIHKQLNFYNGKYMFMINYVF	480
ΔA3	321	SCNVSEKNYFCVHYPEDSVSVSVSVSSNLSCDRFLDFIHKQLNFYNGKYMFMINYVF	380
ΔH	421	SCNVSEKNYFCVHYPEDSVSVSVSVSSNLSCDRFLDFIHKQLNFYNGKYMFMINYVF	480
ΔA3ΔH	321	SCNVSEKNYFCVHYPEDSVSVSVSVSSNLSCDRFLDFIHKQLNFYNGKYMFMINYVF	380
*****			
C505			
Harm.	481	CEESNNMSKMPDDDDNNYSVSGKSCVYYQDLNKKEKEEYRLNKKLRNDFINSKQFYEL	540
C505S	481	CEESNNMSKMPDDDDNNYSVSGKSCVYYQDLNKKEKEEYRLNKKLRNDFINSKQFYEL	540
ΔA3	381	CEESNNMSKMPDDDDNNYSVSGKSCVYYQDLNKKEKEEYRLNKKLRNDFINSKQFYEL	440
ΔH	481	CEESNNM-----	487
ΔA3ΔH	381	CEESNNM-----	387
*****			
Δhinge start site: S489			
Harm.	541	HTFTERTVGFMRVQYFVYKLRDVVKVEKETL	572
C505S	541	HTFTERTVGFMRVQYFVYKLRDVVKVEKETL	572
ΔA3	441	HTFTERTVGFMRVQYFVYKLRDVVKVEKETL	472
ΔH	488	-----	487
ΔA3ΔH	388	-----	387
*****			
ΔHinge end site: L572			

**Figure 2.5: Amino acid sequence alignments of wild-type, C505S, ΔA3, ΔH and ΔA3ΔH *PfAdoMetDC*.** Sequence alignments were performed with UniProt. \* indicate sequence identity for all 5 sequences; – indicate the gaps created via deletion mutagenesis, for the ΔA3 (indicated in green, with the remaining flanking residues of the A3 insert indicated in blue) and ΔH mutants (indicated in purple). The position of the C505S point mutation is indicated in red.



Soluble protein yield was determined by the Bradford method (Figure 2.6A), following heterologous expression in *E. coli* BL21 Star™ cells and purification of the cell lysates by *Strep*-tag II affinity chromatography. Wild-type and C505S *PfAdoMetDC* showed similar yields ( $1.83 \pm 0.20$  mg/L and  $2.33 \pm 0.48$  mg/L culture, compared to a significant increase observed for the  $\Delta A3$  mutant ( $3.13 \pm 0.52$  mg/L ( $n=6$ ,  $P=0.04$ , unpaired student t-test)) (Figure 2.6B). In contrast to the  $\Delta A3$  mutant, negligible protein yields were obtained for the  $\Delta H$  and  $\Delta A3\Delta H$  mutants ( $0.02 \pm 0.004$  mg/L for both  $\Delta H$  and  $\Delta A3\Delta H$  *PfAdoMetDC* ( $n=3$ ,  $P<0.01$ , unpaired students t-test)) (Figure 2.6B).

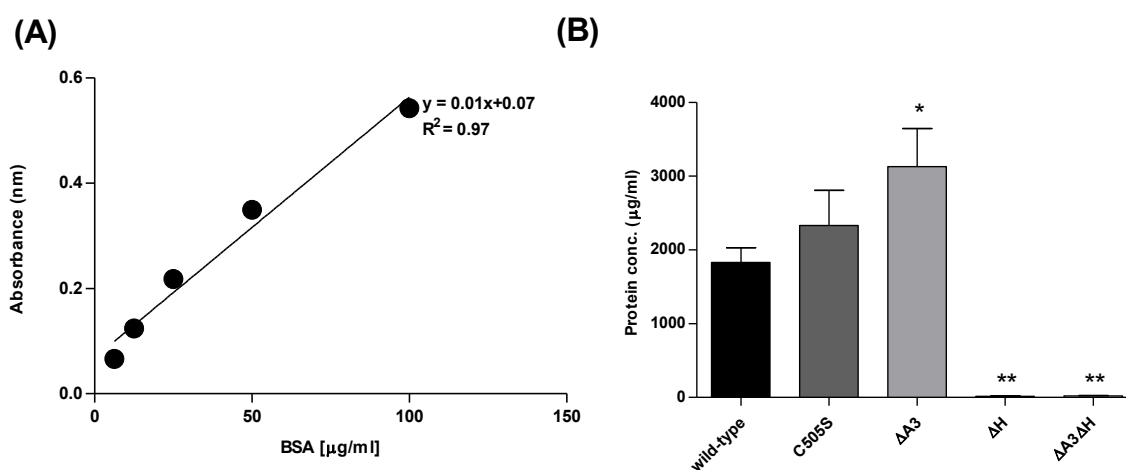


**Figure 2.6: Protein concentration and yield determination of soluble protein from wild-type and mutant (C505S,  $\Delta A3$ ,  $\Delta H$  and  $\Delta A3\Delta H$ ) *PfAdoMetDC*.** (A) Standard curve for quantifying protein concentration with the Bradford method. (B) Mean protein concentration in  $\mu\text{g/ml}$  of wild-type, C505S,  $\Delta A3$ ,  $\Delta H$  and  $\Delta A3\Delta H$  heterologous *PfAdoMetDC*. Protein yield per L of culture of the deletion mutants were compared to wild-type and C505S *PfAdoMetDC*. Data are representative of six independent experiments performed in duplicate ( $n = 6$  for harmonised, C505S and  $\Delta A3$  and  $n=3$  for  $\Delta H$  and  $\Delta A3\Delta H$ ,  $*P<0.05$  and  $**P<0.01$ , error bars indicate  $\pm$  SEM). Where not shown, error bars fall within the symbols.

Reducing SDS-PAGE of affinity chromatography purified wild-type and C505S *PfAdoMetDC* showed the processed monomeric  $\alpha$ -subunit as the major band at  $\sim 60$  kDa and the dissociated  $\beta$ -subunit at  $\sim 9$  kDa (192) (Figure 2.7). Due to removal of the A3 insert residues, the processed monomeric  $\alpha$ -subunit for  $\Delta A3$  *PfAdoMetDC* was present at  $\sim 50$  kDa with the dissociated  $\beta$ -subunit at  $\sim 9$  kDa (Figure 2.7). For the wild-type, C505S and  $\Delta A3$  *PfAdoMetDC* proteins, minor bands of the unprocessed forms of the protein, previously identified by LC-MS/MS (207), were observed at  $\sim 69$  and  $\sim 59$  kDa, respectively (Figure 2.7). The presence of unprocessed proteins in the soluble fractions of wild-type, C505S and  $\Delta A3$  *PfAdoMetDC* indicated incomplete post-translational processing for the heterologous protein. The *E. coli* heat shock protein 70 (Hsp70), previously identified with LC-MS/MS (207), also co-eluted with the  $\Delta A3$  mutant and as minor contaminant of the wild-type and C505S mutants. Furthermore, a  $\sim 100$  kDa band co-eluted with the  $\Delta A3$  mutant and is presumed to be a homodimer of this

protein (Figure 2.7). Since no dimerisation of the wild-type or C505S mutants were observed under these conditions, it may indicate that the  $\Delta A3$  mutant has a dimerisation mechanism independent of the C505S residue or hydrophobic based interactions (192). Therefore, although the soluble protein yield of the  $\Delta A3$  mutant was improved the sample homogeneity of the affinity chromatography purified protein was not improved due to co-elution of the unprocessed monomer and *E. coli* Hsp70 contaminant as well as the formation of a ~100 kDa dimer.

ProtParam sequence analysis predicted the sizes of processed forms of  $\Delta H$  and  $\Delta A3\Delta H$  to be ~50 and ~39 kDa, respectively. However, reducing SDS-PAGE showed these proteins were unprocessed, due to band sizes corresponding to ~59 and ~48 kDa and absence of the dissociated ~9 kDa  $\beta$ -subunits (Figure 2.7). In addition, Hsp70 identified by LC-MS/MS (207), co-eluted with  $\Delta H$  and  $\Delta A3\Delta H$  in higher amounts compared to the other *PfAdoMetDC* constructs (Figure 2.7). Furthermore, an unidentified ~18 kDa protein was associated with the  $\Delta H$  and the  $\Delta A3\Delta H$  mutants that was not observed for the wild-type, C505S or  $\Delta A3$  *PfAdoMetDC* proteins.

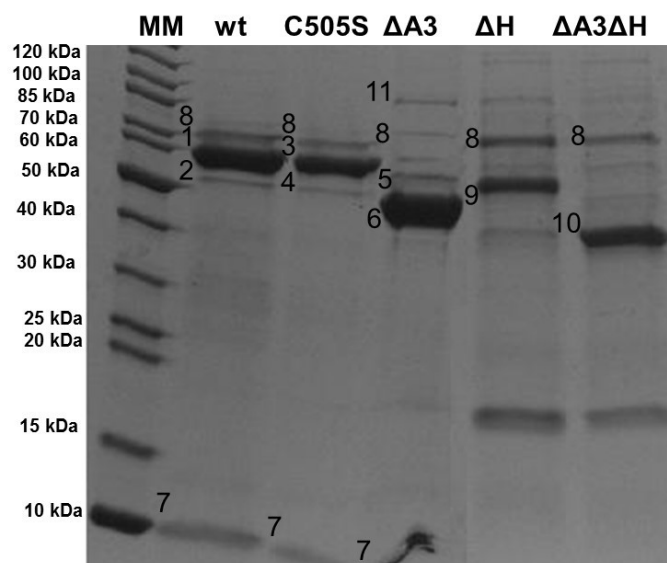


**Figure 2.7: Reducing SDS-PAGE of 5  $\mu$ g affinity chromatography purified wild-type, C505S,  $\Delta A3$ ,  $\Delta H$  and  $\Delta A3\Delta H$  *PfAdoMetDC*.** MM: unstained protein marker; lane 2: soluble wild-type (wt) *PfAdoMetDC*; lane 3: soluble C505S *PfAdoMetDC*; lane 4: soluble  $\Delta A3$  *PfAdoMetDC*; lane 5: soluble  $\Delta H$  *PfAdoMetDC* and lane 6: soluble  $\Delta A3\Delta H$  *PfAdoMetDC*. Processed and unprocessed  $\alpha$ -subunits are indicated at ~60 and ~69 kDa for wild-type and C505S *PfAdoMetDC* (numbers 1, 2, 3 and 4, respectively) and unprocessed and processed proteins at ~59 and ~50 kDa for  $\Delta A3$  *PfAdoMetDC* (numbers 5 and 6, respectively). The ~100 kDa  $\Delta A3$  *PfAdoMetDC* homodimer is represented by number 11. Processed  $\beta$ -subunits are indicated at ~9 kDa (number 7). Monomeric  $\Delta H$  and  $\Delta A3\Delta H$  are indicated at ~50 kDa and ~40 kDa (numbers 9 and 10), respectively, and *E. coli* Hsp70 at ~70 kDa (number 8).

Analysis by reducing PAGE of wild-type *PfAdoMetDC* showed no significant quantities of the monomeric *PfAdoMetDC* protein in the insoluble fractions and cell lysates (Figure 2.8A). The C505S mutant presented a similar profile compared to the wild-type protein (therefore not included in Figure 2.8). Interestingly, although the  $\Delta A3$  mutant showed a higher soluble protein yield, a substantial amount of the processed monomer was also present in the insoluble inclusion body fraction (Figure 2.8B). This may be attributable to nutrient depletion in *E. coli* due to the high expression levels of the  $\Delta A3$  mutant that could lead to aggregation of the proteins into inclusion bodies (246). Both  $\Delta H$  mutants (Figure 2.8C and D) showed unprocessed monomers aggregated in inclusion bodies but significantly lower soluble protein yields were observed compared to the  $\Delta A3$  mutant. This also explains the increased amount of co-eluted Hsp70 into the soluble fraction, as inclusion bodies are substrates for *E. coli* Hsp70 (246, 247).

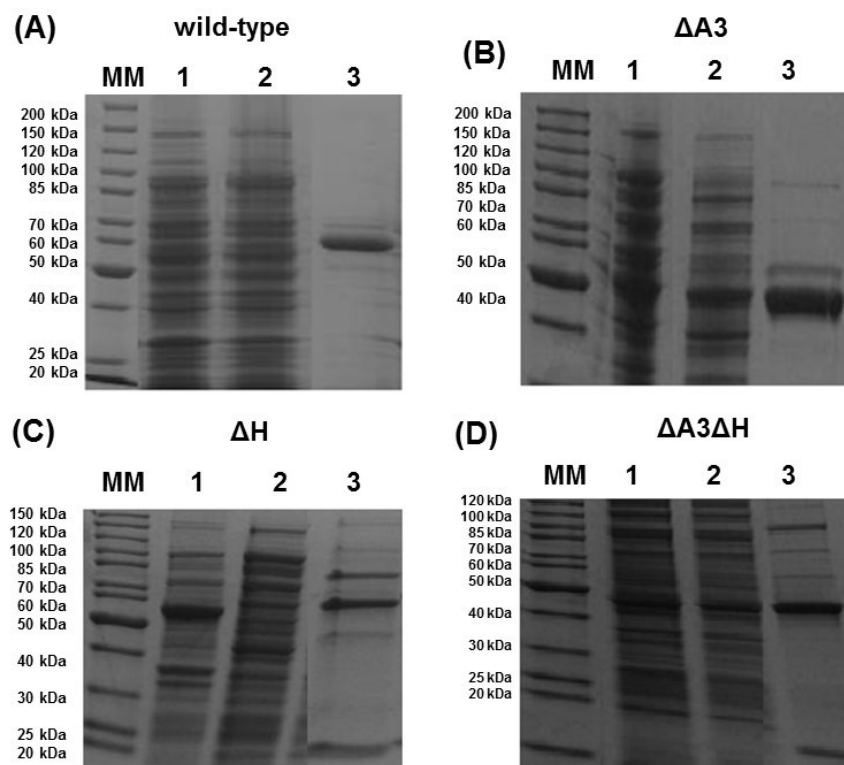


**Figure 2.8: Reducing SDS-PAGE analysis of *PfAdoMetDC* cell lysates, soluble and insoluble fractions.** (A) Wild-type *PfAdoMetDC*. Due to the similar purification profiles between the wild-type protein and the C505S mutant, the C505S mutant protein was not included in the figure. (B)  $\Delta A3$  *PfAdoMetDC*, (C)  $\Delta H$  *PfAdoMetDC* and (D)  $\Delta A3\Delta H$  *PfAdoMetDC*. MM: unstained protein marker, lane 1: pellet of lysed cells (10 x dilution), lane 2: cell lysate 10 x dilution, lane 3: 5  $\mu$ g purified *PfAdoMetDC*.

The specific activities of wild-type and C505S *PfAdoMetDC* ( $58.53 \pm 2.89$  and  $55.29 \pm 2.86$  nmol/min/mg, respectively,  $n=3$ ) were significantly lower than that of  $\Delta A3$  *PfAdoMetDC* ( $95.06 \pm 1.16$  nmol/min/mg,  $n=3$ ,  $P<0.01$ , unpaired student t-test) (Figure 2.9). Thus, removal of the A3 insert from wild-type *PfAdoMetDC* resulted in conformational changes that positively affected the active site and turnover rate of *PfAdoMetDC*.

The specific activities of  $\Delta H$  ( $0.15 \pm 0.15$  nmol/min/mg,  $n=4$ ) and  $\Delta A3\Delta H$  ( $0.67 \pm 0.25$  nmol/min/mg,  $n=4$ ) were marginal in comparison to specific activities of wild-type, C505S and  $\Delta A3$  *PfAdoMetDC* ( $n=4$ ,  $P<0.01$ , unpaired students t-test, Figure 2.9). Therefore, deletion of the 85 C-terminal hinge region residues were not only detrimental to soluble protein expression and post-translational processing, but also resulted in an essentially inactive enzyme. Thus, based on the unfolded, unprocessed oligomeric status of the  $\Delta H$  mutants, these proteins were not further investigated as candidates for protein crystallisation trials.

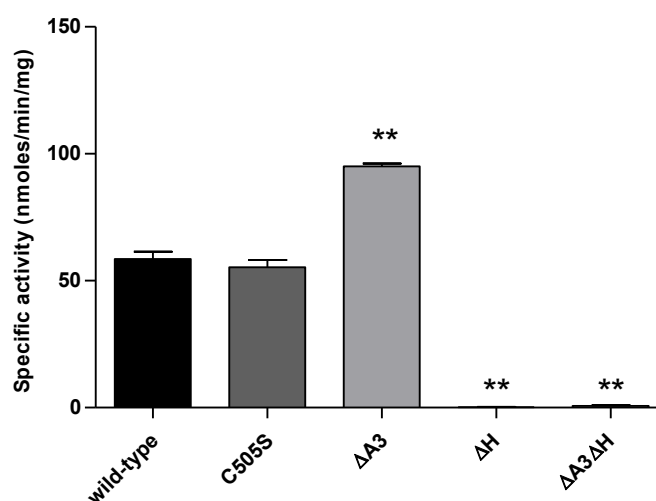


**Figure 2.9: Specific activities of soluble wild-type, C505S,  $\Delta A3$ ,  $\Delta H$  and  $\Delta A3\Delta H$  *PfAdoMetDC*.** Data are representative of three or four independent experiments performed in duplicate. Error bars indicate SEM, \*\*= $P<0.01$ , unpaired t-test. Where not observed error bars fall within symbols.

The presence of the monomeric and dimeric forms observed for soluble  $\Delta A3$  *PfAdoMetDC* was confirmed in subsequent studies. Western immunodetection of 5  $\mu$ g *Strep*-tag II bound  $\Delta A3$  *PfAdoMetDC* (Figure 2.10) following reducing SDS-PAGE analysis, identified the ~59 unprocessed and ~50 kDa processed monomeric protein bands. A third band at ~100 kDa indicated the homodimeric form. The ~9 kDa  $\beta$ -subunit was not visible on the immunoblot, due to the *Strep*-tag II being covalently bound to the C-terminus of the  $\alpha$ -subunit of *PfAdoMetDC*.

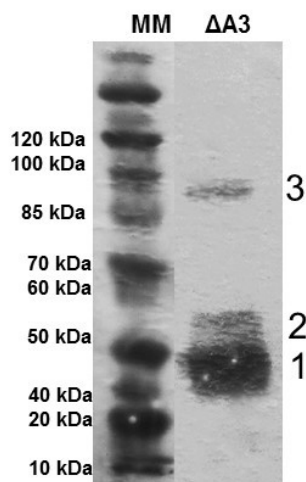


**Figure 2.10: Detection of  $\Delta A3$  *PfAdoMetDC* homodimer observed by reducing SDS-PAGE through Western immunodetection.** (A) Western immunoblot of 5  $\mu$ g soluble affinity chromatography purified  $\Delta A3$  *PfAdoMetDC*. MM: unstained protein marker; lane 2: Soluble  $\Delta A3$  *PfAdoMetDC* (~ 5  $\mu$ g). (1) Processed ~50 kDa monomer, (2) Unprocessed ~60 kDa monomer and (3) ~100 kDa homodimer.

Furthermore, MALDI-TOF MS performed on the most prevalent bands of a Coomassie stained reducing SDS-PAGE of ~50  $\mu$ g  $\Delta A3$  *PfAdoMetDC* confirmed the results observed by Western immunodetection (Table 2.1) (Appendix 10). The faint ~70 kDa band co-purified with *PfAdoMetDC* was previously identified by LC-MS MS as *E. coli* DnaK (Hsp70) (Table 2.1) to (192).

**Table 2.1: MALDI-TOF MS analysis of ~50  $\mu$ g affinity chromatography purified soluble  $\Delta A3$  *PfAdoMetDC*.** MALDI-TOF MS of the ~50, ~59, ~70 and ~100 kDa peptide sequences (depicted in figure below table) using the MASCOT search engine identified *P. falciparum* AdoMetDC/ODC and *E.coli* DnaK proteins.

	MM	$\Delta A3$	No.	Band	Accession	Description	MASCOT	%
							Score	Coverage
			1	60 kDa	PF10_0322	<i>P. falciparum</i> AdoMetDC/ODC ( <i>Pf3D7_10:1324130-1328434(-)</i> )	11806.48	19.87
			2	50 kDa	PF10_0322	<i>P. falciparum</i> AdoMetDC/ODC ( <i>Pf3D7_10:1324130-1328434(-)</i> )	4647.56	15.20
			3	70 kDa	A7ZHA4	Chaperone protein DnaK (OS= <i>Escherichia coli</i> O139:H28)	2237.87	31.97
			4	100 kDa	PF10_0322	<i>P. falciparum</i> AdoMetDC/ODC ( <i>Pf3D7_10:1324130-1328434(-)</i> )	5833.12	11.99

### 3.3.2.2 The oligomeric status and sample homogeneity of monofunctional *PfAdoMetDC*

The sample homogeneity and oligomeric status of wild-type, C505S and  $\Delta A3$  *PfAdoMetDC* was also determined by SEC under reducing conditions. A linear regression standard curve using the  $V_e$  of HMW proteins (Figure 2.11A) with a regression coefficient of  $R^2 = 0.98$ , was used to determine the MM of protein samples (Figure 2.11B).

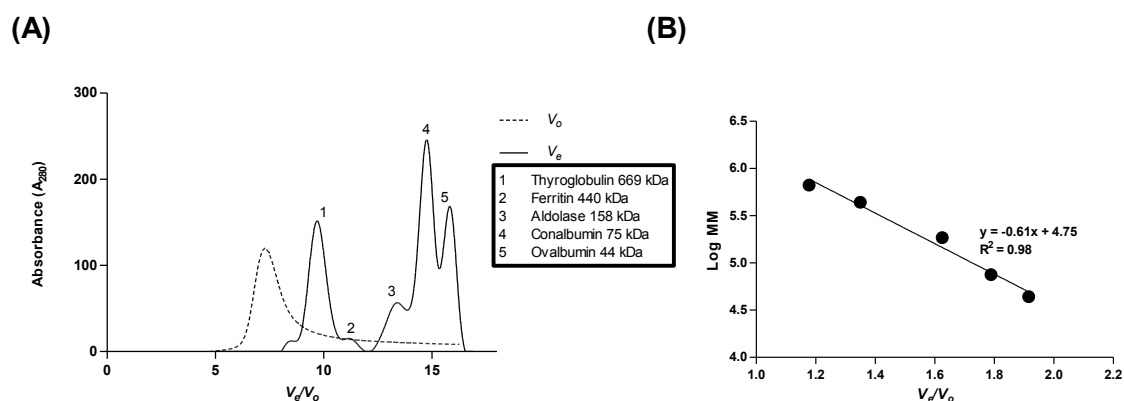


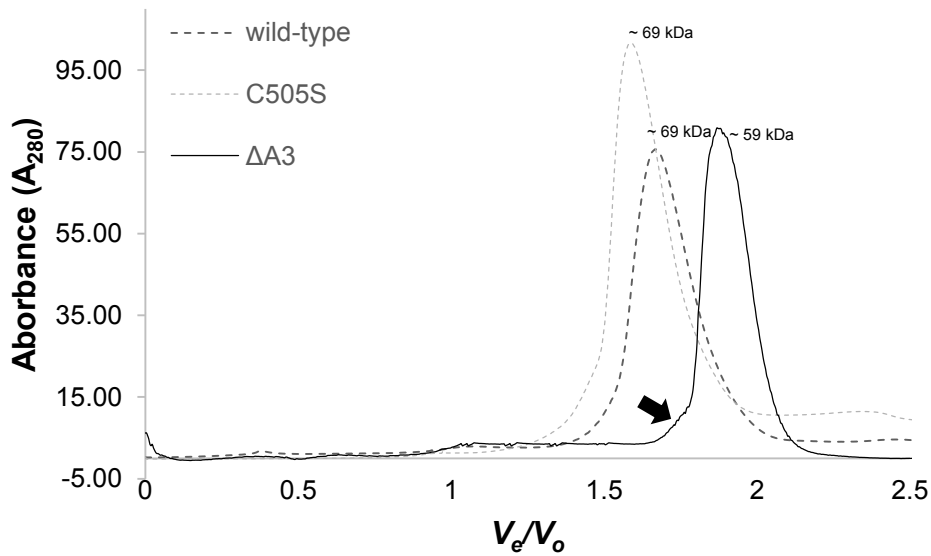
**Figure 2.11: HMW standard curve for analytical SEC (44-669 kDa).** Analytical SEC was performed with a Superdex 75 10/300 200 GL column. (A) Chromatogram of 2mg/ml dextran blue (2000 kDa) depicting the void volume ( $V_o$ , dotted line) at 8.255ml ( ) and the elution volumes ( $V_e$ , solid line) of the HMW markers (44 -699 kDa). (B) Standard curve obtained by plotting the Log molecular mass values of HMW proteins against the  $V_e/V_o$  values.

Following column equilibration with buffer W under reducing conditions (10 mM DTT and 0.02% Brij-35) ~2 mg affinity chromatography purified *PfAdoMetDC* was loaded for SEC analysis. These reducing and detergent conditions were included based on a previous study that showed that the sample homogeneity of monomeric *PfAdoMetDC* decreased as a result of dimerisation via disulphide bond formation and oligomerisation via hydrophobic interactions (207). Under these conditions ~2 mg wild-type ( $V_e/V_o = 1.56$ ) and C505S *PfAdoMetDC* ( $V_e/V_o = 1.59$ ) appeared as single peaks of the  $\alpha\beta$ -monomers at ~69 kDa (Figure 2.12A). In a previous study these proteins loaded at ~1 mg eluted as tetrameric, dimeric and monomeric forms (192). However, although not apparent on the chromatograms, collected peak fractions of wild-type and C505S *PfAdoMetDC* analysed by reducing SDS-PAGE, showed the processed and unprocessed  $\alpha\beta$ -monomers at ~60 and ~69 kDa, as well as faint bands that correspond to the homodimer of wild-type *PfAdoMetDC* and the heterotetrameric forms of wild-type and C505S *PfAdoMetDC* (Figure 2.12B) (192). The presence of these bands were however, only detected at protein concentrations higher than 5  $\mu$ g, and were not resolved in the presence of 0.02% Brij-35 that was included to prevent hydrophobic interactions and oligomerisation.

The  $\Delta A3$  mutant primarily eluted as the  $\alpha\beta$ -monomer at  $\sim 59$  kDa ( $V_e/V_o = 1.88$ ), however, a pre-eluted shoulder was detected that corresponds to a dimeric form at  $\sim 100$  kDa, not observed for wild-type or C505S *PfAdoMetDC* (Figure 2.12A). Reducing SDS-PAGE of the collected peak fraction confirmed the presence of the  $\sim 100$  kDa dimer co-eluting with the monomer (Figure 2.12B) also shown by Western immunoblotting and MADLI-TOF MS. Since SEC was performed under reducing conditions, the dimerisation observed could be due to non-obligatory isologous disulphide bonds, not completely reduced by DTT or hydrophobic interactions, not prevented by Brij-35. However, the absence of homotetrameric complexes for  $\Delta A3$  *PfAdoMetDC* indicated that protein oligomerisation of wild-type and C505S *PfAdoMetDC*, seen in Figure 2.12B, may have been caused by interdomain protein-protein interactions mediated by the A3 parasite-specific insert. Separation of the oligomeric and dimeric complexes for wild-type, C505S and  $\Delta A3$  *PfAdoMetDC* was not achieved with SEC due to poor column resolution at the flow-rate used to elute proteins.



(A)



(B)

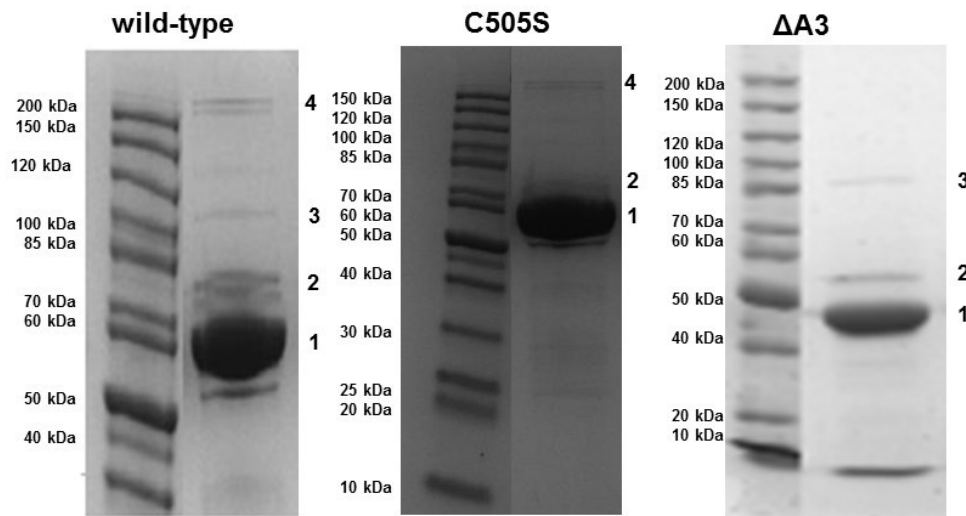


**Figure 2.12: Analytical SEC purification under reducing conditions followed by reducing SDS-PAGE of collected peak fractions of wild-type, C505S and  $\Delta A3$  PfAdoMetDC.** (A) Comparative chromatogram of affinity purified wild-type, C505S and  $\Delta A3$  PfAdoMetDC analysed by SEC. PfAdoMetDC proteins (~2 mg) were analysed in buffer W under reducing conditions (10 mM DTT and 0.02% Brij-35). Wild-type and C505S PfAdoMetDC eluted at ~69 kDa, and the  $\Delta A3$  mutant eluted at ~59 kDa with pre-eluting shoulder indicated by the black arrow. (B) Reducing SDS-PAGE of collected peak fractions following reducing SEC. The molecular markers are indicated in lane 1 and analysed wild-type, C505S and  $\Delta A3$  PfAdoMetDC peak fractions in lane 2. The processed (1), unprocessed (2), dimeric (3) and heterotetrameric (4) forms of the protein are indicated.

To establish the mechanism of dimerisation of the  $\Delta A3$  mutant and if this dimerisation was concentration dependent, the protein was further analysed by SEC under both reducing (Buffer W, 10 mM DTT and 0.02% Brij-35) and non-reducing conditions (Buffer W, no DTT or Brij-35 added) at a higher concentration (~4 mg compared to ~2 mg in Figure 2.12A) (Figure 2.13). At the increased concentration and under reducing conditions, a single peak representing the  $\alpha\beta$ -monomer at ~59 kDa was obtained. However, under non-reducing conditions a shoulder correlating to the ~100 kDa homodimer was observed, suggesting that dimerisation is due to disulphide bridge formation between surface cysteine residues C505 and C566 at the proposed dimerisation interface and/or other unknown interactions. However, since the C-terminal truncation, which included these residues, resulted in insoluble *PfAdoMetDC* expression, the role of these residues in dimerisation of the  $\Delta A3$  mutant could not be verified by this mutation. Although the level of dimerisation increased under non-reducing conditions, the increase in protein concentration to ~4 mg did not result in a shift from the monomeric form to the dimeric form, unlike that observed for wild-type and C505S *PfAdoMetDC* (192). This indicates that  $\Delta A3$  *PfAdoMetDC* has a lower propensity to dimerise compared to these proteins.

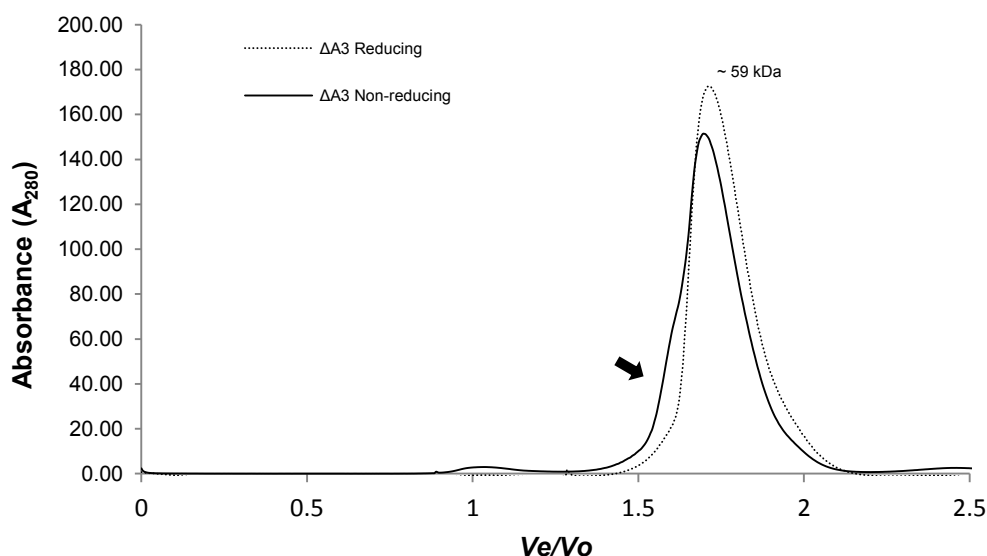


**Figure 2.13: Analytical SEC of affinity chromatography purified  $\Delta A3$  *PfAdoMetDC* under reducing and non-reducing conditions.** The protein (~4 mg) was analysed in buffer W under reducing (10 mM DTT and 0.02% Brij-35) and non-reducing conditions (without DTT and Brij-35). The proteins eluted at ~59 kDa with pre-eluting shoulder indicated by the black arrow.

The decreased propensity of the  $\Delta A3$  mutant to oligomerise or dimerise seems related to the removal of the disordered regions and LCRs contained within the A3 the insert. This may indicate that the oligomeric association of monofunctional wild-type and C505S *PfAdoMetDC*

(leading to tetrameric complexes) is mediated by the A3 insert and is independent of the disulphide bond created by the C505 residue. The increased yield, purity and sample homogeneity observed for the mutant, while maintaining activity makes it amenable for protein crystallisation trials and was therefore, studied in subsequent experiments.

### 2.3.3 Analysis of $\Delta$ A3 *PfAdoMetDC* reveals novel structural characteristics of the parasite-specific insert

#### 2.3.3.1 Deletion of the A3 insert does not influence *PfAdoMetDC* structural integrity

Following dialysis into a phosphate buffer, far-UV CD analysis performed on SEC purified  $\Delta$ A3 *PfAdoMetDC* in comparison to the C505S mutant revealed a similar secondary structure profile and fold for both mutants (Figure 2.14). This suggests that removal of the A3 insert did not induce gross changes in the secondary structure of *PfAdoMetDC*. The only difference in the protein spectra was observed between 195-200 nm, possibly due to removal of the three  $\beta$ -sheets predicted in the A3 insert (Figure 2.4), although detections at these low wavelengths are notoriously unreliable.

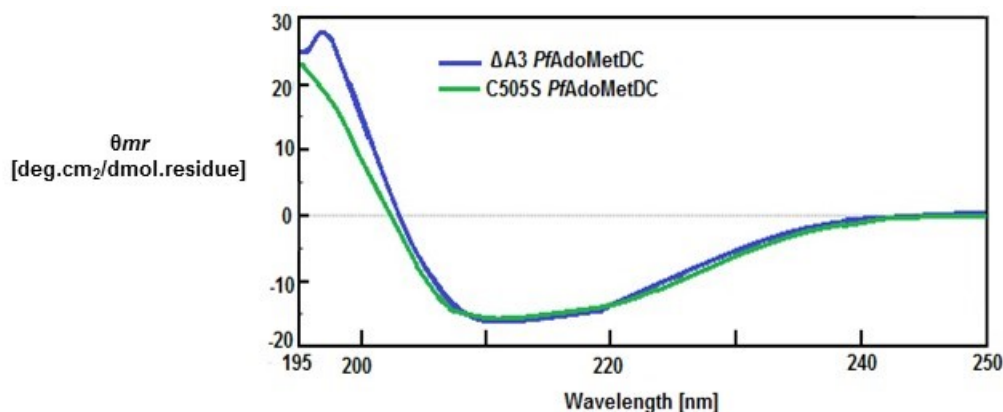


**Figure 2.14: Far-UV CD analysis of C505S and  $\Delta$ A3 *PfAdoMetDC*.** Far-UV CD analysis at 195-250 nm against the mean molar ellipticity per residue for C505S and  $\Delta$ A3 *PfAdoMetDC*.

The role of the A3 insert on protein flexibility and shape composition was determined with SAXS measurements. The plateau of the Kratky graph following an initial parabolic peak represents random coil movement of particles (Figure 2.15A). The low level baseline detected for C505S and  $\Delta$ A3 *PfAdoMetDC* indicated low protein flexibility and, stable protein structures for both proteins.

A transformed Kratky plot using Guinier parameters ( $R_g$ ) produced the Porod-Debye plot (Figure 2.15B) in which the plateau, referred to as the Porod-plateau observed for the BSA control, is an indication of the folded conformational states of a protein. The level of each plateau is specific to the conformation of the protein (248). The observed Porod-plateaus for C505S and  $\Delta A3$  *PfAdoMetDC* indicate comprehensively folded conformational states when compared to the completely folded BSA control (Figure 2.15B). As previously shown for parasite-specific inserts, the A3 insert was predicted to be a hydrophilic non-globular loop on the protein surface (195) and its presence or absence as expected does not appear to affect protein flexibility or the native protein fold, indicating that it does not interact with the protein core (200, 202).

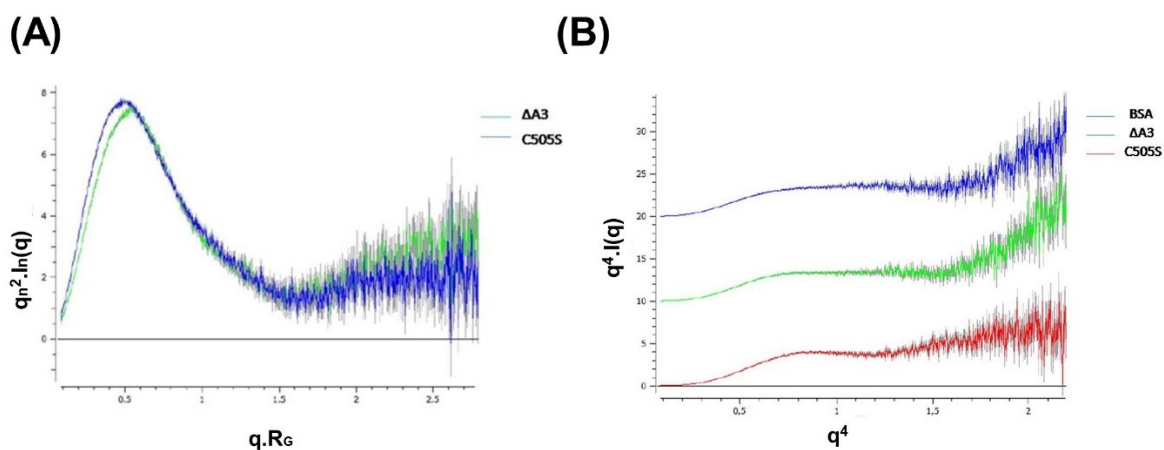


**Figure 2.15: SAXS analysis of C505S and  $\Delta A3$  *PfAdoMetDC*.** (A) Kratky plot of the C505S and the  $\Delta A3$  mutant. The scattering angle ( $q$ ) and radius of gyration using Guinier parameters ( $R_g$ ) is plotted against the particle volumes detected as derived from resolution ( $qn^2 \cdot \ln(q)$ ). (B) The Porod-Debye plot transformed from the Kratky plot by the Porod-Debye law, of the C505S and the  $\Delta A3$  mutants, with a BSA control. The plot is derived by transformation of the scattering data  $q^4 \cdot I(q)$  against  $q^4$ , where  $I(q)$  represents the association between  $q$  and resolution (248).

### 3.3.4 Deletion of residues of the A3 parasite-specific insert aids in protein crystal formation

For optimal crystallisation conditions a protein sample should preferably be monodisperse(249). Previously, DLS analysis of wild-type and C505S *PfAdoMetDC* showed that they were polydisperse (192). The  $R_H$  for  $\Delta A3$  *PfAdoMetDC* was lower compared to that of the C505S mutant, which is attributable to the smaller hydrodynamic size of the protein. However, the Pdl was nearly 2-fold lower than the C505S mutant indicating that the  $\Delta A3$  mutant is more monodisperse (Table 2.2). Despite the  $\Delta A3$  *PfAdoMetDC* showing a lower propensity to dimerise, the mutant was however still polydisperse as determined by DLS (Table 2.2).

Dimerisation of the  $\Delta A3$  mutant was still detectable following SEC under reducing conditions and the presence of Brij-35. Under non-reducing conditions and in the absence of Brij-35, however, there was an increased propensity of the protein to dimerise as shown by SEC, possibly either through disulphide bonds or hydrophobic interactions or both. Therefore, for comparative purposes the C505S and  $\Delta A3$  mutants were incubated with a stronger reducing agent, TCEP, to establish whether sample monodispersity could be further improved. The stronger reducing action of TCEP is due to its higher resistance to oxidation and thus higher stability under oxidising conditions compared to DTT (250). With this reducing agent the C505S mutant showed a ~2-fold increase in the  $R_H$  of the protein and the ~3-fold increase in the sample polydispersity as indicated (Table 2.2). This suggests that this reducing agent may have disrupted internal disulphide links, which led to conformational changes in protein structural integrity (251). The  $\Delta A3$  mutant in contrast showed an insignificant deviation in its  $R_H$  value but a ~2-fold increase in its polydispersity index in the presence of TCEP. These results suggest that  $\Delta A3$  mutant has a more stable and robust native fold than the C505S mutant that is not as easily disrupted. The effect of DTT on the  $R_H$  or Pdl of C505S and  $\Delta A3$  *PfAdoMetDC* was similar but much less substantial than TCEP. No significant deviation was observed in either the  $R_H$  or PDI in the presence or absence of 0.02% Brij-35 (Table 2.2) for either protein. Although the presence of 10 mM DTT slightly increased the polydispersity index of the  $\Delta A3$  mutant, it was included in crystallisation trials since it decreased protein dimerisation propensity as shown by reducing SEC.

**Table 2.2: Protein hydrodynamic radii ( $R_H$ ) and polydispersity index (Pdl) determined under reducing conditions for C505S and  $\Delta A3$  *PfAdoMetDC*.** Sample monodispersity, in terms of  $R_H$  and the Pdl with SEC purified C505S and  $\Delta A3$  *PfAdoMetDC* under reducing conditions was analysed by DLS, following pre-incubation with reducing agents (DTT and TCEP) and the non-ionic detergent, Brij-35.

Sample Conditions	[Protein] (mg/ml)	$R_H$ ( $\pm$ SD) (nm)	Pdl	Estimated ( $\pm$ SD) (kDa)	MM	Peak Polydispersity
C505S <i>PfAdoMetDC</i>	1.6	6.2	0.29	238 $\pm$ 127.5		Polydisperse
C505S <i>PfAdoMetDC</i> 5 mM TCEP	1.6	14.2	0.90	1660 $\pm$ 1.6 x 10 <sup>3</sup>		Polydisperse
C505S <i>PfAdoMetDC</i> 0.02% Brij-35	1.6	6.0	0.27	226 $\pm$ 117.4		Polydisperse
C505S <i>PfAdoMetDC</i> 10 mM DTT	1.6	6.7	0.35	319 $\pm$ 188.8		Polydisperse
$\Delta A3$ <i>PfAdoMetDC</i>	1.6	4.7	0.17	127 $\pm$ 52.8		Polydisperse
$\Delta A3$ <i>PfAdoMetDC</i> 5 mM TCEP	1.6	5.7	0.35	194 $\pm$ 114.9		Polydisperse
$\Delta A3$ <i>PfAdoMetDC</i> 0.0% Brij-35	1.6	4.7	0.17	126 $\pm$ 52.1		Polydisperse
$\Delta A3$ <i>PfAdoMetDC</i> 10 mM DTT	1.6	5.1	0.29	150 $\pm$ 80.7		Polydisperse

DSF performed on wild-type *PfAdoMetDC* showed that it is most stable ( $T_m$  of 61°C) when buffered with Buffer W (207). However, the internal stability of the  $\Delta A3$  mutant was higher at a  $T_m$  of 65.3°C than wild-type *PfAdoMetDC* under the same buffering condition (0.1 mg/ml). The same  $T_m$  (65.3°C) was obtained with 0.1 mg/ml  $\Delta A3$  *PfAdoMetDC* in a HEPES buffer (100 mM HEPES, pH 7.4, 150 mM NaCl) in the absence of DTT and Brij-35 (Figure 2.16). Under reducing conditions (10 mM DTT and 0.02% Brij-35) however, the  $T_m$  of the  $\Delta A3$  mutant decreased to 60°C (10 mM DTT, 0.02% Brij-35) (Figure 2.16), which may be due to the reduction of the additional surface covalent disulphide bonds by DTT (compared to slight changes in values in Table 2.2), resulting in a more temperature sensitive protein. Based on the internal stability under both the HEPES and reduced buffer W buffering conditions,  $\Delta A3$  *PfAdoMetDC* was pre-incubated in both buffers prior to protein crystallisation trials.

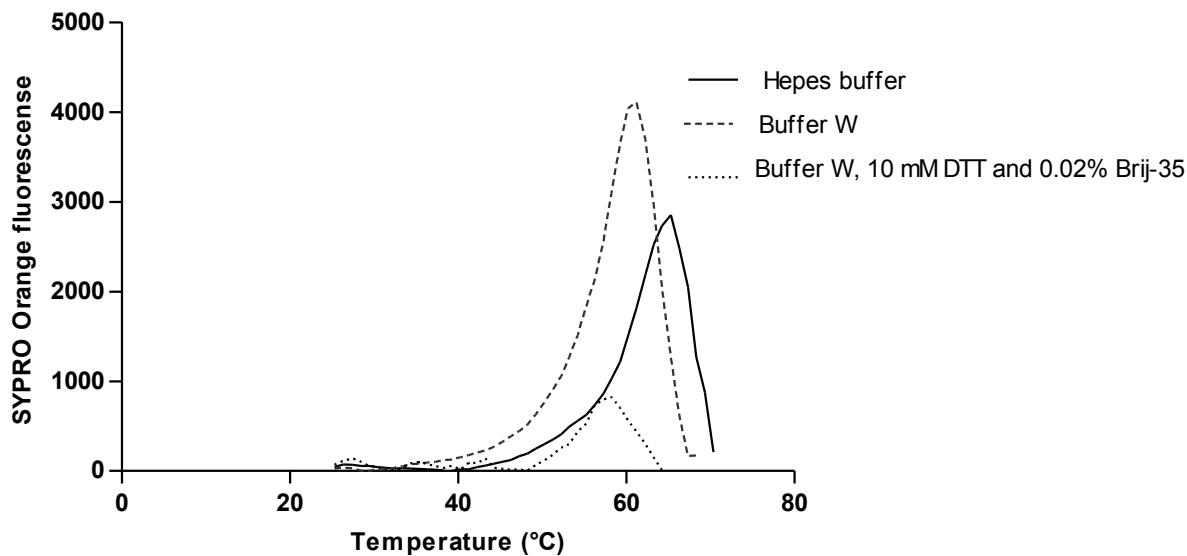
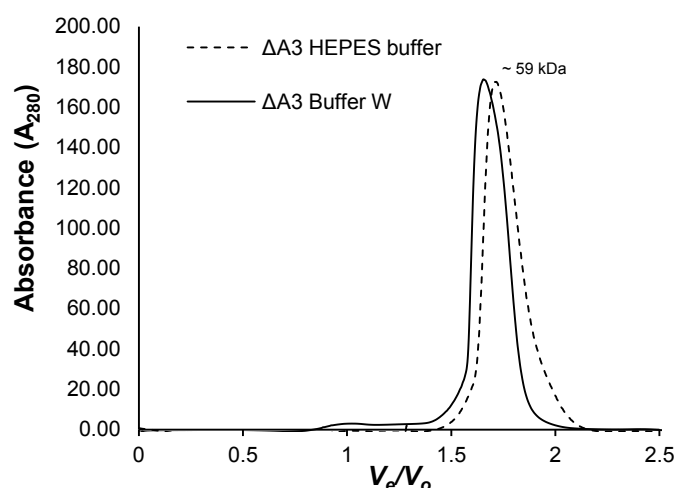


**Figure 2.16: Differential scanning fluorimetry (DSF) of SEC purified  $\Delta A3$  PfAdoMetDC under different buffering conditions.** The highest  $T_m$  observed for the protein was for Buffer W (purple line, 50 mM Tris-HCl, pH 8.0, 150 mM NaCl) and HEPES buffer (green line, 100 mM HEPES-NaOH, pH 7.4, 150 mM NaCl). Addition of 10 mM DTT and 0.02% Brij-35 to Buffer W decreased  $T_m$  to 60°C (blue line).

Prior to protein crystallisation trials, the  $\Delta A3$  PfAdoMetDC mutant was purified by reducing SEC in either Buffer W or HEPES buffer (identified by DSF) (Figure 2.17A). An elution rate of 0.1 ml/min was used and fractions containing the monofunctional form of the protein, e.g., fractions collected after fraction 30 (Figure 2.17B) were pooled and concentrated to ~4.6 - 17 mg/ml aliquots and screened for crystal formation, either in the Apo-form or co-incubated with MDL73811.



(A)



(B)

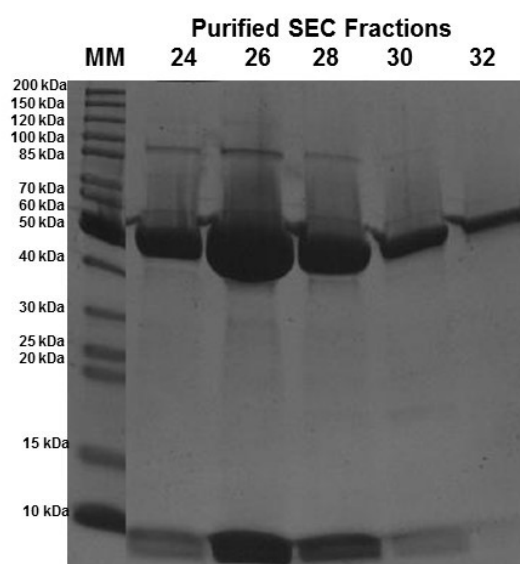


**Figure 2.17: Reducing SEC of ~4 mg  $\Delta A3$  *PfAdoMetDC* with buffer W and HEPES buffer.** (A) Reducing SEC-purification of affinity chromatography purified  $\Delta A3$  *PfAdoMetDC* under reducing conditions with either buffer W (50 mM Tris-HCl, pH 8.0, 150 mM NaCl, 10 mM DTT and 0.02% Brij-35) or HEPES buffer (100 mM HEPES, pH 7.4, 150 mM NaCl, 10 mM DTT and 0.02% Brij-35). (B) Reducing SDS-PAGE of collected peak fractions following reducing SEC. Fractions after fraction 30 contained the monomeric form of  $\Delta A3$  *PfAdoMetDC*. Similar results were obtained with either buffer W or HEPES buffered conditions.

In total, six crystallisation conditions all yielded birefringent protein crystals all presenting a needle cluster morphology (Figure 2.18). The crystals all developed under similar Tris and sodium citrate buffered crystallisation conditions with a pH range of 6-8.5 with corresponding sulphate and acetate salts and a high percentage of PEG polymers over periods from 24 h to 2 weeks at 20°C (Table 2.3). However, although these were birefringent protein crystals, no x-ray diffraction data were obtained. Interestingly, the 0.1 M Tris pH 8.5, 8% w/v PEG 8000 condition producing the needle clusters is the same crystallisation condition that produced

human AdoMetDC crystals (211). This may indicate a correlation between the structural homology of the human and *P. falciparum* protein, although the human protein crystallises as a dimer (252, 253).

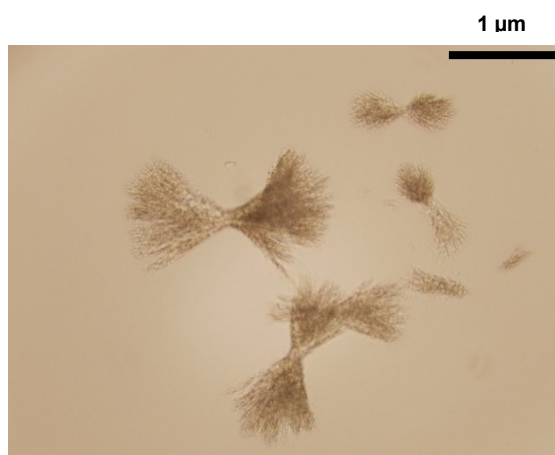


**Figure 2.18:  $\Delta A3$  PfAdoMetDC needle clusters.** Birefringent needle clusters of  $\Delta A3$  PfAdoMetDC obtained by the hanging drop vapour diffusion method. All crystals obtained in conditions described in Table 2.3, bear this morphology.

**Table 2.3: Protein crystallisation conditions for  $\Delta A3$  PfAdoMetDC.** Protein crystallisation trials with various crystal screen kits were set up with SEC purified  $\Delta A3$  PfAdoMetDC in either HEPES buffer or Buffer W. Protein crystals with needle cluster morphology were obtained in concentration ranging from 4.6 – 17 mg/ml in six different crystallisation conditions.

Protein buffer	Crystal screen kit	Final [protein] (mg/ml)	Crystallisation condition
Buffer W	Hampton Research crystal screen HR-2-110	17 mg/ml	0.1 M Tris, pH 8.5, 8% w/v PEG 8000
Buffer W	Proplex Screen	6.2 mg/ml	0.2 M Li <sub>2</sub> SO <sub>4</sub> , 0.1 M MES pH 6.0, 20% w/v PEG 4000
Buffer W	Proplex Screen	4.6 and 7.0 mg/ml	0.1 M MgCl <sub>2</sub> , 0.1 M MES pH 6.0, 8% w/v PEG 4000
HEPES	JCSG-1 Screen	4.6 and 7.0 mg/ml	0.2 M MgCl <sub>2</sub> , 0.1M Tris, pH 7.0, 10% w/v PEG 8000
HEPES	PACT Screen	4.6 and 7.0 mg/ml	0.2 M Na <sub>2</sub> SO <sub>4</sub> , 0.1 M Bis-Tris propane, pH 7.5, 20% w/v PEG 3350
HEPES	Proplex Screen	6.2 mg/ml	0.2 M CH <sub>3</sub> COONa, 0.1 M Sodium citrate, pH 5.5, 10% w/v PEG 4000

Optimisation of these crystallisation conditions to produce more planar crystals was attempted by varying protein concentrations, precipitant concentration, crystallisation buffer; pH and concentration and temperature as well as seeding experiments of crushed needle clusters. However, following up to 2 months incubation no optimised planar crystal formation was detected possibly due to the crystals presenting distinct biochemical signatures resulting in highly polymorphic formations (210).

## 2.4 Discussion

The bifunctional organisation of *PfAdoMetDC/ODC* not only uniquely distinguishes this protein complex structurally, but also functionally from the homologous human proteins. As *PfAdoMetDC* activity is not regulated by putrescine, unlike the human homologue (194), the bifunctional assembly induces inter- and intradomain interactions and associated conformational changes, which indirectly modulates the independent decarboxylase activities on the respective protein domains (195). The development of homology models and the functional characterisation of both bifunctional *PfAdoMetDC/ODC* and monofunctional *PfAdoMetDC* have provided limited insight into the structural and functional characteristics of this enzyme complex. However, in order to develop novel highly unambiguous and pharmacokinetically favourable compounds specifically targeting *PfAdoMetDC*, the crystal structure and functional characteristics must be determined. However, *PfAdoMetDC* structural determination has been challenged due to the poor heterologous expression levels of bifunctional *PfAdoMetDC/ODC* (206), co-purification of contaminating *E. coli* proteins and unstable truncated forms of the protein. Subsequently, heterologous expression of monofunctional *PfAdoMetDC* showed improved purity and yield with gene codon harmonisation, however, low sample homogeneity was still a limiting factor in attempts to crystallise the monofunctional form of *PfAdoMetDC*.

Homology modelling and sequence analysis identified three parasite-specific inserts for *PfAdoMetDC* (194). These parasite-specific inserts not only resemble LCRs found in many eukaryotic proteins (200), but they also have sequence characteristics similar to other types of protein inserts, for example, intrinsically unstructured regions (IURs) (223, 254) and intrinsically disordered regions (IDPs) (255). As a result of these similar sequence specific features, these regions have been found to sometimes overlap in *Plasmodium* parasite-specific inserts (256) as shown for the A3 insert in this chapter. Parasite-specific inserts are hydrophilic, non-globular domains proposed to extend away from the protein surface as non-globular unstructured loops (203, 243, 257, 258). The inserts are highly divergent (259) and usually consist of tandem amino acid (TAAs) repeats (243) of hydrophilic residues with a bias towards Asn and Lys (243, 244, 255), also observed for the A3 insert. Interestingly, similar to the A3 insert, the hinge region contains some LCRs sequence characteristics, with several tandem Asn repeats with a bias towards hydrophilic residues (196). Due to the unique side chain properties of Lys and Asn residues, their high abundance results in low steric hindrance with increased rotation around the phi- and psi-angles of the peptide bonds, contributing to the increased flexibility and unstructured nature associated with these inserts (260). Due to

the hydrophilic nature, increased flexibility as well as their surface localisation, parasite-specific inserts are not expected to be involved in the functional folding of the protein core (261), as observed for other *Plasmodium* parasite-specific inserts in bifunctional *PfDHFR-TS* (202). Instead, similarly to *PfDHFR/TS* (202), these inserts have been shown to mediate long-range intra- and interdomain interactions to stabilise the formation of the bifunctional *PfAdoMetDC/ODC* complex (195, 209, 260, 262).

Parasite-specific inserts A3 and O1 have been shown to stabilise interdomain interactions in the bifunctional complex (195) and monofunctional *PfODC* (207), since their deletion showed significant decreases in protein activity across both domains. However, the structural and functional roles of the A3 parasite-specific insert remains unknown for monofunctional *PfAdoMetDC*. In addition, the hinge region covalently linking the N-terminal *AdoMetDC* domain to the C-terminal *ODC* domain is also proposed to be essential for interdomain interactions for stabilising the bifunctional complex in forming active enzymes (152, 174), since deletion of the central hinge in bifunctional *PfAdoMetDC/ODC* also influenced the protein activities of both domains (195). However, in the absence of the correct binding site i.e. the *PfODC* domain, these surface localised hydrophilic inserts and C-terminal hinge region can mediate intra- and interdomain interactions for heterologously expressed monofunctional *PfAdoMetDC*. These non-obligatory interactions can result in non-obligatory protein complex formation of monomeric subunits for monofunctional *PfAdoMetDC* into dimeric or heterotetrameric complexes. Such non-specific protein oligomerisation leads to low sample heterogeneity and polydispersity, making protein structural studies increasingly difficult (249, 263-265). Therefore, this study not only focussed on characterising the structural and functional role of parasite-specific inserts and the hinge region for monofunctional *PfAdoMetDC* but also determined their influence on heterologous protein purify and homogeneity.

The three-dimensional structure of full-length bifunctional *PfDHFR-TS* was obtained after removal of non-essential residues within the junction region of this protein (202). In addition, several studies on *Plasmodium* proteins have shown that truncating non-homologous N- or C-termini, considerably improves heterologous protein expression (102, 249). In a previous study on monofunctional *PfAdoMetDC* it was shown that truncation of 87 residues of the C-terminal hinge region of *PfAdoMetDC* (residues 660-572) resulted in increased protein activity, purity and yield (152, 192). Therefore, in an attempt to improve the heterologous expression and sample homogeneity of *PfAdoMetDC* for crystallisation studies a similar strategy was followed in this study. However, in this study deletion of the entire C-terminal hinge region (residues 487-572) resulted in the low-level expression of insoluble, inactive, unfolded

monofunctional *PfAdoMetDC* unable to undergo post-translational autocatalytic serinolysis, identifying an essential structure-function role for the hinge region in monofunctional *PfAdoMetDC*.

Apart from the annotated  $\beta$ 15- and  $\beta$ 16-sheets (194), secondary structure predictions for the deleted hinge region identified two non-annotated  $\alpha$ -helices and a  $\beta$ -sheet. In a previous study disruption of these secondary structures in the bifunctional complex influenced *PfODC* activity more substantially in comparison to *PfAdoMetDC* (196), showing that *PfODC* is more dependent on the hinge region for structural integrity and activity (174). Intra- and interdomain interactions mediated through secondary structures within junction/hinge regions have been shown to be imperative for the stabilisation of other *P. falciparum* bifunctional proteins, e.g. the cross-over helix in the hinge junction region for *PfDHFR/TS* (266) and *PfPPPK/DHPS* (262). Therefore, the secondary structures present within the hinge region may resemble such conserved cross-over linking regions required for intradomain interactions to stabilise not only monofunctional *PfAdoMetDC*, but also bifunctional *PfAdoMetDC/ODC*. Future studies should include sectional truncations or deletions of these secondary structures within the C-terminal hinge region in order to derive their structural and functional role for monofunctional *PfAdoMetDC*.

Heterologous expression and purification of  $\Delta$ A3 *PfAdoMetDC* in comparison to wild-type, C505S and  $\Delta$ H *PfAdoMetDC*, showed a discernible increase in soluble protein yield, purity, stability and activity. Furthermore, as shown with the far-UV CD analysis, the overall secondary structure conformation of the protein remained grossly similar to the C505S construct, proposing that it may essentially be a non-globular domain (195). However, the positive conformational changes resulting in the  $\sim$ 2-fold increase in protein activity compared to wild-type *PfAdoMetDC* observed with the  $\Delta$ A3 mutant indicates that this parasite-specific insert mediates intradomain protein-protein interactions fundamental to protein structure and activity. Kinetic analysis of bifunctional *PfAdoMetDC/ODC* showed that *PfODC* in the bifunctional complex with *PfAdoMetDC* limits the latter's activity as evidenced by the 3-fold higher specific activity observed for monofunctional *PfAdoMetDC* (192). This observation in combination with the study performed by Birkholtz *et al.* 2004 (195), showing that deletion of parasite-specific inserts influenced the activity of opposing domains, suggests that the A3 parasite-specific insert is most likely involved with inter- and intradomain interactions between *PfAdoMetDC* and *PfODC*, co-ordinately regulating *PfAdoMetDC* and possibly *PfODC* activities (195).

Deletion of the A3 parasite-specific insert showed improved monofunctional *PfAdoMetDC* sample homogeneity due to the absence of the heterotetrameric complex observed for the wild-type protein. However, the sample showed heterogeneity due to the low level formation of the ~100 kDa homodimer. Human AdoMetDC is an obligate dimer with two monomeric domains associating via edge-on interactions, mediated by mainchain-mainchain and sidechain-sidechain hydrogen bonds between the  $\beta 7$  and  $\beta 15$  sheets (211). *PfAdoMetDC* has been proposed to dimerise via the same edge-on interaction (192), also mediated by these  $\beta$ -sheets. However, the Gln311 residue in the human AdoMetDC dimer interface, which may mediate hydrogen bonding, is replaced by a Cys505 residue in *PfAdoMetDC*. Therefore, *PfAdoMetDC* dimerisation may instead be mediated by disulphide bridge formation at the dimer interface, as shown by the shift to the monomeric form in the monomer-dimer equilibrium for the C505S mutant under reducing conditions (192). The dimer observed with the  $\Delta A3$  mutant was more abundant under non-reducing conditions, indicating that dimerisation is *inter alia* mediated by disulphide bridge formation by oxidised surface Cys residues for example, that of the C505 residue. Interestingly, C481 on  $\alpha$ -helix 10 and C454 on  $\alpha$ -helix 9 are also replaced by Gln residues in human AdoMetDC (194). These three Cys residues (C481, C454 and C505) are on the same plane as the proposed *PfAdoMetDC* dimerisation site and could thus form part of a cysteine-rich interdomain region, a highly polymorphic site responsible for mediating protein oligomerisation (267).

However, apart from C505, carbamidomethyl-modified surface Cys residues showed that these residues were not alkylated under reducing conditions upon MS analysis of the monomeric band of monofunctional *PfAdoMetDC* (192), indicating that they may form internal rather than surface mediated disulphide bonds. The only other surface Cys residues, that were not carbamidomethyl-modified, which may mediate dimerisation via disulphide bridge formation for of the  $\Delta A3$  mutant is the C566 residue in the hinge region or the C399 residue present within the residual residues of the A3 insert. This site could also have accounted for the residual dimerisation observed with the C505S mutant shown previously (192). In the bifunctional conformation, C566 and C399 may form essential disulphide bonds for intra- and interdomain interactions between the *PfAdoMetDC* and *PfODC* domains or may mediate dimerisation of *PfAdoMetDC* into its obligate homodimer. However, in obtaining a homogenous monomeric protein sample these residues may thus contribute to formation of the ~100 kDa dimer producing a heterogeneous protein sample. Residues C505 and C566 residues were removed with deletion of the hinge region, however, due to the low-level insoluble expression of these mutants it could not be verified whether these residues play a role in dimerisation of monofunctional *PfAdoMetDC*. Therefore, future studies should not only incorporate the C505S mutation in combination with the  $\Delta A3$  mutant, but also that of the other

proposed surface Cys residues in an aim to improve sample homogeneity for protein structural studies. However, other non-specific protein-protein interactions mediated by the A1, A2, and the ~50 remaining residues of the A3 insert cannot be excluded.

Williams *et al.* 2011 (192) showed that both wild-type and C505S *PfAdoMetDC* oligomerised into dimers and tetramers in a concentration-dependent monomer-dimer equilibrium. However, these heterogeneous SEC elution profiles could not be reproduced in this study, analysis of SEC purified *PfAdoMetDC* with SDS-PAGE confirmed the presence of homodimers. The formation of these protein complexes was proposed to be due to the exposed hydrophobic interaction site of *PfODC* (192). However, no homotetrameric complexes were observed for the  $\Delta A3$  mutant. This indicated that in addition to hydrophobic interactions, non-specific protein-protein interactions resulting in homotetrameric complex formation are also partially mediated A3 insert. These results indicate that the A3 insert may form part of an interdomain interaction with the *PfODC* domain, similar to that observed for insert 1 of *PfDHFR* interacting with the *PfTS* domain in bifunctional complex formation (202).

Despite the presence of the ~100 kDa homodimer producing a polydisperse protein sample, crystallisation trials showed the formation of birefringent protein needle clusters, the first ever hit conditions obtained for a domain from the *PfAdoMetDC/ODC* complex. Therefore, deletion of parasite-specific inserts may provide a viable strategy in aiding the structural determination of *Plasmodium* proteins.



## 2.5 Conclusion

This study focussed on determining the structural and functional characteristics of monofunctional *PfAdoMetDC*. Truncation of the C-terminal hinge region resulted in an unfolded, inactive protein indicating that this region mediates essential structural and functional roles for monofunctional *PfAdoMetDC*. On the other hand, deletion of one of the largest of the parasite-specific inserts, the A3 insert, did not influence the structural integrity or functionality of the enzyme, but improved the heterologous yield and homogeneity of the protein. This led to the formation of protein crystals, indicating that deletion of parasite-specific inserts provides a unique strategy in obtaining the crystal structure of *PfAdoMetDC* for structure-based drug design of novel *PfAdoMetDC* inhibitors.

## Chapter 3

# **Novel S-adenosyl-L-methionine decarboxylase inhibitors as potent antiproliferative agents against intra-erythrocytic *Plasmodium falciparum* parasites**

The work in this chapter has been published as follows:

Dina le Roux, Pieter Burger, Jandeli Niemand, Robert Barker, Anne Grobler, Patricia Urbán, Xavier Fernández-Busquets, Abraham I. Louw, Lyn-Marie Birkholtz. (2014) Novel derivatives of MDL 73811 inhibit *Plasmodium falciparum* S-adenosyl-L-methionine decarboxylase. International Journal for Parasitology: Drugs and Drug resistance, 4, 28-36

### **3.1 Introduction**

Polyamines (putrescine, spermidine and spermine) are critical components of cell growth and division, particularly in rapidly proliferating cells that include cancerous cells and numerous parasites (114, 116). A number of enzymes in the biosynthesis of polyamines have been validated as suitable drug targets including ornithine decarboxylase (ODC) (141) and S-adenosyl-L-methionine decarboxylase (AdoMetDC) (142) as the two major enzymatic activities. Protozoan infections resulting in human parasitic diseases such as African sleeping sickness (caused by subspecies of *Trypanosoma brucei*), Chagas disease (*Trypanosoma cruzi*), leishmaniasis (*Leishmania* spp) and malaria (*Plasmodium* spp) are highly reliant on substantial amounts of polyamines for development and proliferation (117, 144). Of these diseases, malaria has a high disease incidence in most tropical regions of the world, with *Plasmodium falciparum* parasites being the most lethal.

AdoMetDC catalyses a chokepoint reaction to produce decarboxylated S-adenosyl-L-methionine (dcAdoMet) that is exclusively used for polyamine biosynthesis. The irreversible AdoMetDC inhibitor, 5'-{[(Z)-4-amino-2-butenyl]methylamino}-5'-deoxyadenosine (MDL73811), is 100-fold more effective than the ODC inhibitor, DL- $\alpha$ -difluoromethylornithine (DFMO), in curing murine *T. b. brucei* and *T. b. rhodesiense* infections. Treatment of *T. brucei* parasites with MDL73811 causes an intracellular hypermethylated state due to accumulation of S-adenosyl-L-methionine (268) in addition to the detrimental depletion of trypanothione (the principal polyamine-dependent thiol in trypanosomes) (269, 270). AdoMetDC is considered

an attractive drug target in *P. falciparum* parasites due to its unique association with ODC in a heterotetrameric bifunctional protein complex, PfAdoMetDC/ODC (144, 160, 192). MDL73811 inhibits *in vitro* intra-erythrocytic *P. falciparum* parasite proliferation (162, 177), however, this does not result in a hypermethylated state but only depletes intracellular polyamine levels, leading to cellular cytostasis (144, 160, 271).

MDL73811, however, is not clinically useful against parasitic infectious due to poor blood brain barrier penetration, a short plasma half-life, poor oral bioavailability and limited metabolic activity (162, 177, 272). Structure-guided design of MDL73811 derivatives, modified on the ribose and purine moieties through addition of halogens and methyl groups, resulted in a series of compounds with improved ADME toxicity profiles. These included improved aqueous solubility, decreased rates of hepatocyte and microsome clearance, minimal CYP inhibition and half the plasma protein binding capacity compared to MDL73811 (272-274). Methylation of position 8 of the adenine group resulting in 8-methyl-5'-{[(Z)-4-aminobut-2-enyl]methylamino}-5'-deoxyadenosine (Genz-644131) displayed an increased inhibitory potency against heterologous TbAdoMetDC. This compound showed improved cellular toxicity against different *T. brucei* parasite strains, with a longer plasma half-life and improved blood brain barrier penetration in *in vivo* mice (272, 273). Here, the MDL73811 derivatives were assessed for inhibitory activity against heterologous PfAdoMetDC as well as for inhibition of intra-erythrocytic *P. falciparum* parasite proliferation *in vitro*.

## 3.2 Methods and materials

### 3.2.1 MDL73811 and derivatives

MDL73811 (5'-{[(Z)-4-amino-2-butenyl]methylamino}-5'-deoxyadenosine), Genz-644131 (8-methyl-5'-{[(Z)-4-amino-2-butenyl]methylamino}-5'-deoxyadenosine), Genz-644043 (2'-fluoro-5'-{[(Z)-4-amino-2-butenyl]methylamino}-5'-deoxyadenosine), and Genz-644053 (2-chloro-5'-{[(Z)-4-amino-2-butenyl]methylamino}-5'-deoxyadenosine) (Table 3.1) were synthesised by the Genzyme Corporation ([www.genzyme.com](http://www.genzyme.com), 2013; (274)).

### 3.2.2 Recombinant *PfAdoMetDC* enzyme inhibition assays

The monofunctional form of wild-type *PfAdoMetDC* (from a harmonised gene construct, described in chapter 2) as well as bifunctional *PfAdoMetDC/ODC* were heterologously expressed in *Escherichia coli* BL21 Star™ (DE3) cells and purified via *Strep*-tag II affinity chromatography as previously described (144, 192). To determine the enzyme inhibition activity of the MDL73811 derivatives, an isotope-based bioassay that measures the release of radiolabeled CO<sub>2</sub> (144, 192) was performed with 5 µg of either monofunctional *PfAdoMetDC* or bifunctional *PfAdoMetDC/ODC* in the presence of 1 µM of each derivative. Results were normalised to the specific activity (nmol/min/mg) of an uninhibited control to determine % inhibition.

### 3.2.3 Determination of the inhibition constant of Genz-644131 against *PfAdoMetDC*

The apparent inhibition constant ( $K_{app}$ ) of Genz-644131 was determined with Kitz and Wilson time dependent enzyme kinetics for irreversible inhibitors as described (275). Using the isotope-based bioassay described above (chapter 2 section 2.2.4), residual enzyme activity was measured following pre-incubation (37°C) at fixed time intervals (2, 4 and 6 min) with varying inhibitor concentrations (0.02, 0.05 and 0.1 µM) and 1 µg of either monofunctional *PfAdoMetDC* or bifunctional *PfAdoMetDC/ODC*, each in duplicate. The reciprocal of the slope in the primary graph ( $k_{app}$ ) was plotted against the reciprocal of the inhibitor concentrations to yield the secondary plot, from which the  $k_{inact}$  and the  $K_{app}$  values were derived.

### 3.2.4 Homology modelling and conformational analysis

*P. falciparum* and *T. brucei* homology models were generated using the human AdoMetDC crystal structure (PDBid 3DZ2) as template similar to a previously described model (194).

Molecular shape-based alignment between MDL73811 derivatives and the homology model was performed with vROCS (v3.1.0 OpenEyeScientific Software, Inc., Santa Fe, NM, USA, [www.eyesopen.com](http://www.eyesopen.com), 2010) (Appendix 7; Supplemental data; Fig S1 and Table S1). Conformational analysis was performed using Conformation Search and the Minimisation module of Discovery Studio 3.0 suite (Accelrys, Inc.). Detailed methods for homology modelling, molecular shape based alignment and conformational analysis are provided in Supplemental data, S1.

### 3.2.5 *In vitro* cultivation of intra-erythrocytic *P. falciparum* parasites and IC<sub>50</sub> determination of MDL73811 derivatives

Intra-erythrocytic *P. falciparum* parasites (strain 3D7; chloroquine sensitive) were maintained in *P. falciparum* culture media as described (276). Intra-erythrocytic parasites were synchronised to a 95% ring stage population with a 5% sorbitol solution. The effect of MDL73811 derivatives on the proliferation of intra-erythrocytic *P. falciparum* parasites at 37°C for 96 h was determined using a SYBR Green I-based fluorescence assay as described (276). MDL73811 and Genz-644131 were dissolved in 1xPBS and Genz-644043 and Genz-644053 in DMSO and incubated with ring stage intra-erythrocytic *P. falciparum* parasites (1% parasitaemia, 1% haematocrit) at specific concentrations, serially diluted 2-fold in culture medium (final 0.1% (v/v)) non-lethal DMSO concentration (277). Sigmoidal dose–response curves were fitted to the data using SigmaPlot 11.0 with non-linear regression yielding the IC<sub>50</sub> values (concentration at which 50% inhibition of parasite proliferation was observed).

### 3.2.6 Determining parasite recovery following Genz-644131 inhibition

The ability of the products of polyamine metabolism to rescue parasites from the inhibitory effect of Genz-644131 was determined. Ring stage intra-erythrocytic *P. falciparum* parasites (1% parasitaemia 1% haematocrit) were treated with Genz-644131 (2xIC<sub>50</sub>) in the presence of exogenous spermidine trichloride (non-toxic concentration, 250 µM, results not shown) and 500 µM of the polyamine oxidase inhibitor, aminoguanidine (278), for 96 h at 37°C. Parasite proliferation determined with a SYBR Green I-based assay (279, 280).

Subsequently, to determine the ability of ring stage intra-erythrocytic *P. falciparum* parasites (1% parasitaemia, 1% haematocrit) to recover after Genz-644131 treatment, the latter was withdrawn following 24 h incubation at 37°C at 2xIC<sub>50</sub>, the parasites were washed and subsequently resuspended in normal culture media. Samples were removed at 12 h intervals

over 96 h and DNA content was determined for the treated, untreated and the Genz-644131 withdrawn parasite populations using a SYBR Green I-based assay.

### 3.2.7 Spermidine uptake in intra-erythrocytic *P. falciparum* parasites

Intra-erythrocytic *P. falciparum* parasites were purified to  $\geq 95\%$  parasitaemia with magnetic separation (281, 282). [<sup>3</sup>H]spermidine uptake was initiated by combining equal volumes of cell suspension and radiolabelled solution (1  $\mu$ Ci/ml [<sup>3</sup>H]spermidine at 5 nM extracellular concentration, PerkinElmer, in 125 mM NaCl, 5 mM KCl, 20 mM glucose, 25 mM HEPES and 1 mM MgCl<sub>2</sub>, pH 7.1). At predetermined time intervals following incubation at 37°C, the reactions were terminated by dibutyl phthalate sedimentation. A 10  $\mu$ l sample of the aqueous phase was transferred to a scintillation vial to determine the extracellular concentration of [<sup>3</sup>H]spermidine. The remaining cell pellet was lysed with 0.1% (v/v) Triton X-100, the proteins precipitated with 5% w/v trichloroacetic acid and cell debris (including membrane fractions) removed with centrifugation before measuring the radioactivity present in the aqueous supernatant. The rapid initial association of radiolabel with the cells, due to polyamines trapped in the extracellular space as well as adhering to the cell surface was determined and subtracted from the total measured radioactivity (cmps) to determine the intracellular concentration of polyamines. The data are given as a distribution ratio of intracellular to extracellular spermidine (283).

### 3.2.8 Comparative IC<sub>50</sub> determination of Genz-644131 incorporated with Pheroid® technology

A micellar formulation of a nanoparticle structure, Pheroid®, consisting mainly of 43.8% plant and essential ethylated and PEGylated polyunsaturated fatty acids, was prepared in incomplete RPMI 1640 medium as described (284, 285). The suspension was subsequently filtered (0.22  $\mu$ m), diluted 50x with sterile water and homogenised with Genz-644131 powder to yield an encapsulated suspension with a final compound concentration of 23.75 mM. The encapsulation efficiency of Pheroid® was analysed with confocal laser scanning microscopy (Appendix 10) (286). Subsequently, ring stage intra-erythrocytic *P. falciparum* parasites (1% parasitaemia, 1% haematocrit) were treated with Genz-644131 encapsulated Pheroid® at a 20-fold dilution (24  $\mu$ M initial starting concentration) and incubated for 96 h at 37 C. Parasite proliferation of cell suspensions treated with Genz-644131 encapsulated into Pheroid® was determined, and normalised against non Genz-644131 encapsulating Pheroid® suspension in order to derive the IC<sub>50</sub> value using the SYBR Green I-based assay.

### 3.2.9 Comparative IC<sub>50</sub> determination of Genz-644131 with immunoliposomes

Immunoliposomes were prepared by the lipid film hydration method (287) and covalently functionalised with IgG antibody fragments prepared specifically for intra-erythrocytic *P. falciparum* parasites (288). For encapsulation of Genz-644131, 1.74 mg of the compound was incorporated into a 1.5 ml immunoliposome suspension to give a final concentration of encapsulated Genz-644131 at 30 µM (10% encapsulation efficiency). Ring stage intra-erythrocytic *P. falciparum* parasites (1% parasitaemia, 1% haematocrit) were treated with Genz-644131 encapsulated immunoliposomes at a 50-fold dilution (0.6 µM starting concentration) and incubated for 96 h at 37°C. Parasite proliferation of cell suspensions treated with Genz-644131 encapsulated into immunoliposomes was determined as described above.

### 3.2.10 Statistical analyses

All data are representative of at least three independent biological experiments ( $n \geq 3$ ), each performed in triplicate. Statistical analysis was performed using either paired or unpaired Student's *t*-tests. Data were analysed using GraphPad Prism 5.0 or SigmaPlot 11.0.

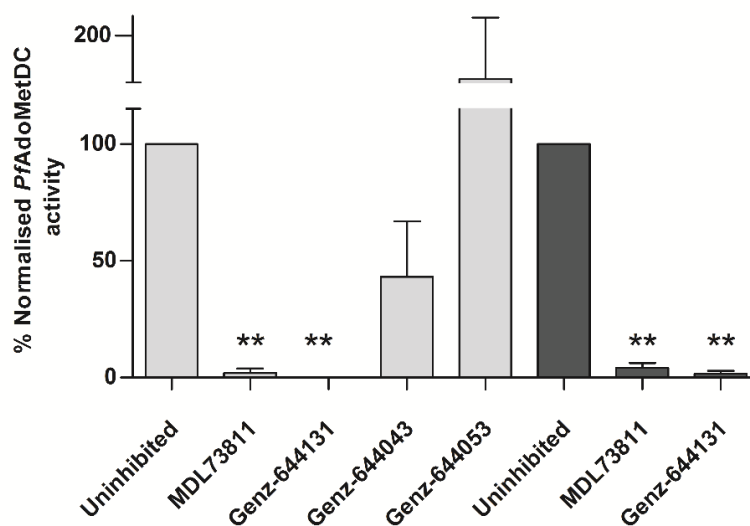


### 3.3. Results

#### 3.3.1 Inhibitory effect of MDL73811 derivatives on heterologous monofunctional *PfAdoMetDC* and bifunctional *PfAdoMetDC/ODC*

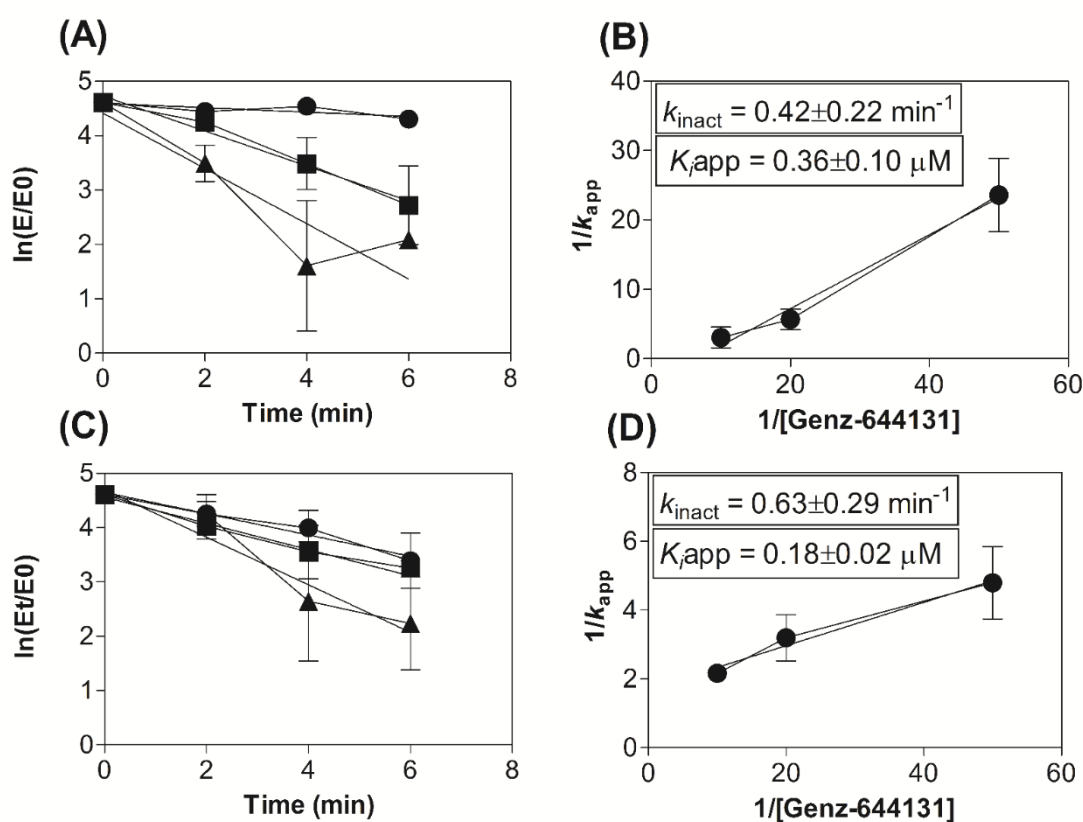
In Chapter 2, structure-activity analyses of various deletion mutants of monofunctional *PfAdoMetDC* indicated the essential nature of the hinge region, but that the A3 insert could be removed without obvious impacts on the proteins activity. However, in the absence of an atomic resolution crystal structure of this mutant form of *PfAdoMetDC*, it was decided not to use the A3 deletion mutant for the work presented here. Rather wild-type monofunctional *PfAdoMetDC* was compared to the protein in its bifunctional association with *PfODC*.

MDL73811 and Genz-644131 showed the highest percentage inhibition of monofunctional *PfAdoMetDC* at 98% and 100%, respectively ( $n = 3$ ,  $P < 0.01$ , paired Student's *t*-test) (Figure 3.1). The inhibition of the *PfAdoMetDC* domain of heterologous bifunctional *PfAdoMetDC/ODC* was similar at 96% and 98%, respectively ( $n = 3$ ,  $P < 0.01$ , paired Student's *t*-test) (Figure 3.1). By contrast, Genz-644043 only inhibited monofunctional *PfAdoMetDC* by 57% ( $n = 3$ ,  $P = 0.14$ , paired Student's *t*-test) whereas Genz-644053 had no inhibitory effect (Figure 3.1).



**Figure 3.1: The inhibitory activities of MDL73811 derivatives against monofunctional *PfAdoMetDC* (grey) and the *PfAdoMetDC* domain of bifunctional *PfAdoMetDC/ODC* (black).** MDL73811 and the three derivatives (1  $\mu$ M) were incubated with either 5  $\mu$ g monofunctional *PfAdoMetDC* or bifunctional *PfAdoMetDC/ODC* for 30 min at 37°C. Specific activity (nmol/min/mg) of the monofunctional and bifunctional *PfAdoMetDC* domains were normalised against the uninhibited enzymes. Data are representative of three independent experiments performed in triplicate,  $\pm$ SEM. \*\* $P < 0.01$ , paired Student's *t*-test. Where not shown, the error bars fall within the symbols.

The activity of *PfAdoMetDC* decreased in a concentration dependent manner following pre-incubation with Genz-644131 for both monofunctional and bifunctional forms of the protein (Figure 3.2A and C). A non-significant increase in the  $K_{app}$  value of  $0.36 \pm 0.10 \mu\text{M}$  ( $n = 3$ ,  $P > 0.05$ , unpaired Student's  $t$ -test) was determined for Genz-644131 on monofunctional *PfAdoMetDC* (Figure 3.2B) compared to  $0.22 \pm 0.09 \mu\text{M}$  for MDL73811 ( $n=2$ , Appendix 8). However, there was a significant difference in the inhibition of bifunctional *PfAdoMetDC*/ODC by Genz-644131 ( $K_{app}$  at  $0.18 \pm 0.02 \mu\text{M}$  (Figure 3.2D) compared to MDL73811 ( $0.53 \pm 0.09 \mu\text{M}$ ,  $n=2$ , Appendix 8) ( $n = 3$ ,  $P = 0.02$ , unpaired Student's  $t$ -test).

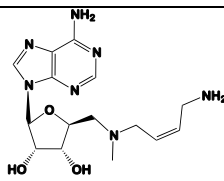
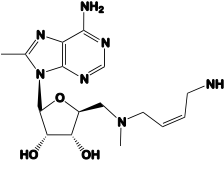
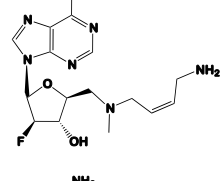
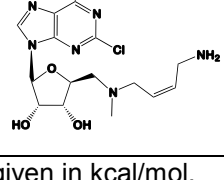


**Figure 3.2: Enzyme kinetics of Genz-644131 against monofunctional and bifunctional *PfAdoMetDC*.** Kitz-Wilson inhibition kinetics was used to determine the  $K_{app}$  for Genz-644131 against monofunctional (A and B) and bifunctional *PfAdoMetDC* (C and D). Percentage activity was determined from residual enzyme activity, following pre-incubation with Genz-644131 at 0.02 (circles), 0.05 (squares) or 0.1  $\mu\text{M}$  (triangles) concentrations ( $[I]$ ) at specific time intervals (0–6 min) ( $E_t$ ). The  $\ln(E_t/E_0)$  of the activity at a specific inhibitor concentration was plotted against the pre-incubation time points using non-linear regression. The reciprocal of the slopes ( $1/k_{app}$ ) of the primary plots (A and C) was plotted against the reciprocal of the specific inhibitor concentrations using non-linear regression (B and D), from which the  $k_{inact}$  (inverse of the y-intercept) and the  $K_{app}$  (slope multiplied by  $k_{inact}$ ) were derived (275). Data are representative of three independent experiments performed in triplicate,  $\pm$ SEM and all values fell into the 95% confidence interval of the mean. Where not shown, the error bars fall within the symbols.

The efficiency of inactivation (depicted by the  $k_{\text{inact}}/K_{\text{iapp}}$  ratio) of MDL73811 compared to Genz-644131 against monofunctional *PfAdoMetDC* was not significantly different at 1.91 and 1.17  $\mu\text{M}^{-1}\text{min}^{-1}$ , respectively. However, the inactivation efficiency for Genz-644131 against the *PfAdoMetDC* domain of bifunctional *PfAdoMetDC/ODC* is 1.6-fold higher ( $k_{\text{inact}}/K_{\text{iapp}} = 3.50 \mu\text{M}^{-1}\text{min}^{-1}$ ) compared to MDL73811 ( $k_{\text{inact}}/K_{\text{iapp}} = 2.19 \mu\text{M}^{-1}\text{min}^{-1}$ ). Moreover, there was a ~3-fold increase in the inactivation efficiency of Genz-644131 against bifunctional *PfAdoMetDC/ODC* compared to monofunctional *PfAdoMetDC* ( $k_{\text{inact}}/K_{\text{iapp}}$  ratios of 3.50 vs. 1.17  $\mu\text{M}^{-1}\text{min}^{-1}$ ), respectively. Genz-644131 seems to therefore be a more effective inhibitor of *PfAdoMetDC* compared to MDL73811, with marked preference for the protein when found in its native conformation in bifunctional *PfAdoMetDC/ODC*.

Due to the observed differences in the inhibition of MDL73811 and its derivatives against *PfAdoMetDC*, the binding capacity of these compounds to *PfAdoMetDC* was analysed *in silico*. A new homology model was prepared to enable accurate binding pose analyses. Previously, it was shown that purine nucleoside AdoMetDC inhibitors adopt unusual *syn* conformations and that modification of these inhibitors does not only affect protein ligand interactions but also alter conformational preferences (289) (Appendix 7; Supplemental data S1). MDL73811 has an energy difference of 7.6 kcal/mol between the lowest energy conformation and its bioactive *syn* conformation (Table 3.1). However, the 8-methyl substitution on the purine ring of MDL73811, yielding Genz-644131, increases the conformational preference for the bioactive *syn* conformation of the latter (energy difference equal to 2.2 kcal/mol, Table 1). By contrast, the energy differences for both the halogen substituted Genz-644043 and Genz-644053 derivatives were higher, with the latter also showing a distorted *N*-(*Z*)-4-aminobutenyl-*N*-methyl tail conformation due to interference of the chlorine substitution at position 2 of the purine ring (Appendix 7; Supplemental data S1).

**Table 3.1: Conformational search analysis of MDL73811 and its derivatives.**

		Lowest overall energy conformation <sup>#</sup>	Lowest <i>syn</i> energy conformation <sup>#</sup>	Number of conformations generated <sup>#</sup>	Bioactive <i>syn</i> conformational number <sup>*,#</sup>
<b>MDL73811</b>		-131.6	-124.0	200	22
<b>Genz-644131</b>		-132.9	-130.7	207	7
<b>Genz-644043</b>		-131.0	-117.8	193	106
<b>Genz-644053</b>		-136.0	-127.8	209	64

<sup>#</sup> All energies are given in kcal/mol.

<sup>\*</sup> Generated conformations were ranked from the lowest to highest energy i.e. the bioactive *syn* conformation of Genz-644131 was ranked the 7<sup>th</sup> lowest energy conformation from 207 conformations generated.

The selected binding pose of Genz-644131 (Figure 3.3A) shows similar interactions to other AdoMetDC substrate analogues (Figure 3.3B) (290). Moreover, conformational search analysis of the *N*-(*Z*)-4-aminobutenyl-*N*-methyl tail of Genz-644131 showed that the lowest absolute energy of the Genz-644131 *syn* conformation is reached when the tail assumes the predicted binding conformation (-126.9 kcal/mol) (Figure 3.3C). Notably, the 8-methyl substitution on the purine ring does not show any steric hindrance within the protein active site and therefore would not negatively affect ligand binding.

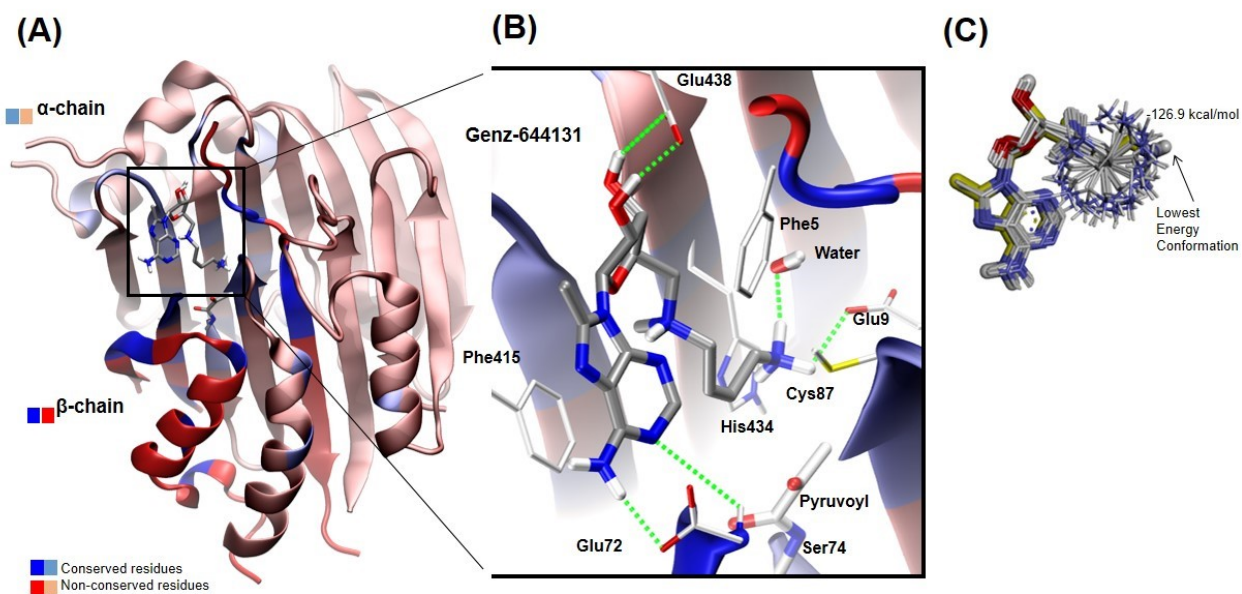


**Figure 3.3: A predicted binding pose for Genz-644131 to *PfAdoMetDC* highlighting conserved residues with *T. brucei* and human protein equivalents.** (A) A homology model of *PfAdoMetDC* bound with Genz-644131 in the active site. The ribbon representing the  $\beta$ -chain is coloured either bright blue or red indicating conserved and non-conserved residues. Likewise, the  $\alpha$ -chain ribbon is coloured in a lighter shade. (B) The interacting residues between *PfAdoMetDC* and Genz-644131. Green lines represent hydrogen bonds formed between the protein and ligand. (C) Representation of the systematic conformational search of the [(Z)-4-amino-2-butenyl] methylamino tail with the lowest energy conformations in yellow. (For interpretation of the references to colour in this figure legend, the reader is referred to the web version of this article: <http://dx.doi.org/10.1016/j.ijpddr.2013.11.003>)

### 3.3.2 Genz-644131 is active against *in vitro* intra-erythrocytic *P. falciparum* parasites

The  $IC_{50}$  of the MDL73811 derivatives was determined on intra-erythrocytic *P. falciparum* parasites *in vitro* (96 h incubation at 37°C) (dose response curves; Appendix 9). Treatment of intra-erythrocytic *P. falciparum* parasites with Genz-644131 resulted in a significant, 2-fold decrease in the  $IC_{50}$  compared to MDL73811 ( $IC_{50} = 0.97 \pm 0.06 \mu\text{M}$  vs.  $2.21 \pm 0.07 \mu\text{M}$ ,  $n = 5$ ,  $P < 0.01$ , unpaired Student's *t*-test). The  $IC_{50}$  values of Genz-644043 and Genz-644053 against intra-erythrocytic *P. falciparum* parasites were significantly higher ( $25.6 \pm 8.4$  and  $22.4 \pm 7.5 \mu\text{M}$ ;  $n = 4$ ,  $P > 0.05$ , unpaired Student's *t*-test) than that of the parent compound, MDL73811 (dose-response  $IC_{50}$  curves, Appendix 9).

The ability of exogenous polyamines to rescue the inhibitory effect of Genz-644131 on intra-erythrocytic *P. falciparum* parasites was established by determining the  $IC_{50}$  of Genz-644131 in the presence and absence of exogenous spermidine (250  $\mu\text{M}$ ). No significant change in

the  $IC_{50}$  value of Genz-644131 in the presence ( $IC_{50} = 0.94 \pm 0.03 \mu M$ ) or absence ( $IC_{50} = 0.97 \pm 0.06 \mu M$ ) of spermidine ( $n = 3$ ,  $P = 0.89$ , paired Student's  $t$ -test) was observed (Figure 3.4A), indicating that spermidine could not antagonise the inhibitory effect of Genz-644131. However, *P. falciparum* infected erythrocytes are capable of taking up exogenous spermidine, with [ $^3H$ ]spermidine reaching a distribution ratio of  $1.4 \pm 0.4$  ( $n = 6$ ) following 60 min incubation (Figure 3.4B).

The recovery of intra-erythrocytic *P. falciparum* parasites (1% parasitaemia, 1% haematocrit) after limited exposure to Genz-644131 ( $2 \times IC_{50}$ ) for 24 h was determined after washing out the compound, followed by additional incubation of parasite cultures for a further 96 h before measuring DNA content as an indicator of parasite proliferation. There was a significant increase in DNA levels observed for untreated parasites over the two life cycles analysed (Figure 3.4C). Genz-644131 treated ring-stage intra-erythrocytic *P. falciparum* parasites ( $2 \times IC_{50}$ ) were able to recover after 24 h of drug pressure and continue to proliferate following drug removal (Figure 3.4C). However, continuous exposure of intra-erythrocytic *P. falciparum* parasites to Genz-644131 ( $2 \times IC_{50}$ ) for 96 h resulted in a stage-specific inhibition of parasite proliferation, with parasites arrested in the trophozoite stage ( $\sim 24$  h post-invasion) within the first life cycle (Figure 3.4D).

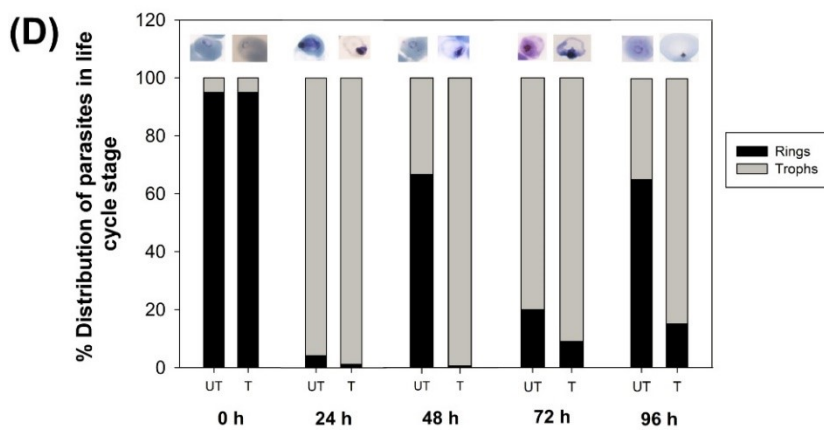
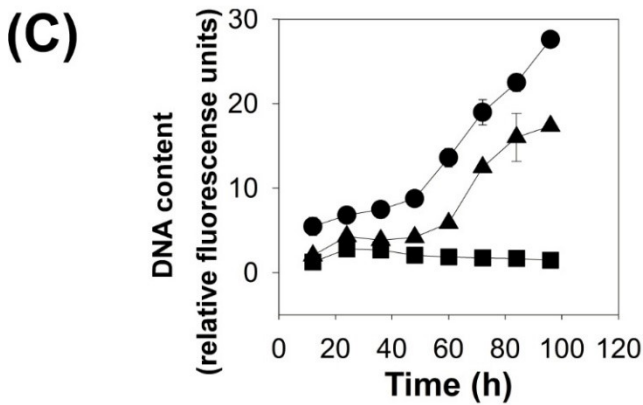
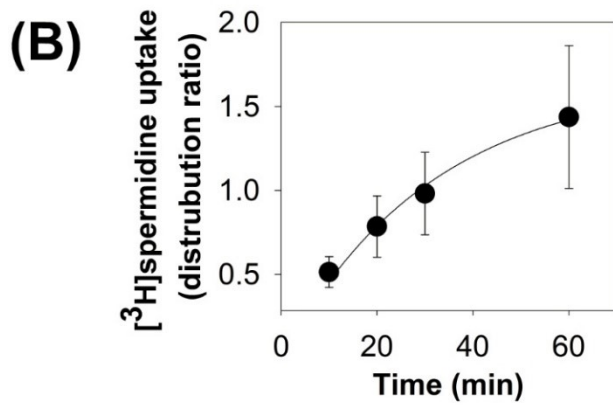
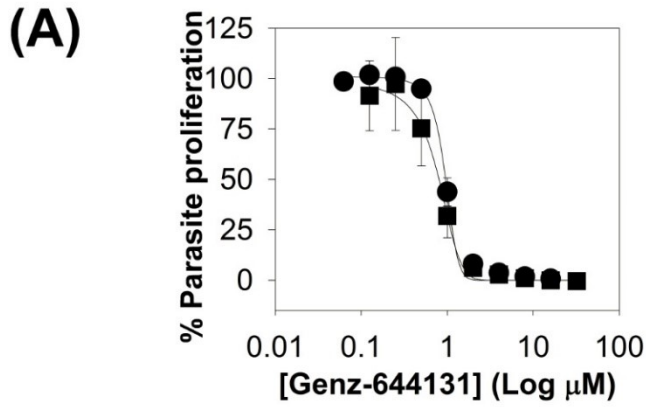




**Figure 3.4: Uptake of [<sup>3</sup>H]spermidine, with rescue and reversibility of Genz-644131 inhibited intra-erythrocytic *P. falciparum* parasites *in vitro*.** (A) Initial ring stage intra-erythrocytic *P. falciparum* parasites were treated with Genz-644131 (serial dilution) alone (squares) or in the presence of 250 μM spermidine (circles, 0.5 μM aminoguanidine present) for 96 h at 37°C. Parasite proliferation is expressed as a percentage of untreated parasite proliferation at 100%. Data are representative of  $n \geq 3$  independent experiments performed in triplicate,  $\pm$  SEM. (B) Time course for the uptake of [<sup>3</sup>H]spermidine (5 nM extracellular concentration) into intra-erythrocytic *P. falciparum* parasites (circles) at 37°C over 60 min averaged from five independent experiments and shown  $\pm$  SEM. A distribution ratio of  $1.4 \pm 0.4$  was obtained, where a ratio of 1 indicates that the radiolabelled polyamine has equilibrated to levels equal to the extracellular levels. (C) Initial ring stage intra-erythrocytic *P. falciparum* parasites were either treated with Genz-644131 ( $2 \times IC_{50}$ , squares) for 96 h at 37°C or treated with Genz-644131 ( $2 \times IC_{50}$ , triangles) for 24 h at 37°C before replacing the culture media thereby removing the Genz-644131 before incubating the parasites for a further 96 h at 37°C. Untreated initial ring stage intra-erythrocytic *P. falciparum* parasites (circles) incubated at 37°C for 96 h was included as a positive control for parasite proliferation. Samples were taken every 12 h and DNA content was measured as relative fluorescence units using SYBR Green I-based assay. Data are representative of  $n \geq 3$  independent experiments performed in triplicate,  $\pm$ SEM. Where not shown, the error bars fall within the symbol. (D) Morphological monitoring of the stage specificity of parasites treated with Genz-644131 ( $2 \times IC_{50}$ ), analysing percentage distribution in each life cycle stage. Treated parasites indicated that Genz-644131 arrested parasite development during the trophozoite stage compared to untreated parasites.

### 3.3.3. Effect of Genz-644131 encapsulated in nanovectors on *in vitro* antiplasmodial activity

To improve membrane translocation of Genz-644131 and possibly the *in vitro* activity against intra-erythrocytic *P. falciparum* parasites, Genz-644131 was encapsulated into two types of nanovectors, a submicron micellar emulsion formulation, Pheroid® (284), and a parasite targeting immunoliposome system (288). The compound encapsulated into Pheroid® did not show a significant decrease in the *in vitro* IC<sub>50</sub> ( $0.97 \pm 0.06 \mu\text{M}$  compared to  $0.67 \pm 0.29 \mu\text{M}$ ;  $n = 4$ ,  $P > 0.05$ , unpaired Student's *t*-test; Figure 5A). By contrast, Genz-644131 encapsulated immunoliposomes showed a significant 32-fold decrease in the *in vitro* IC<sub>50</sub> compared to non-encapsulated Genz-644131 ( $0.97 \pm 0.06 \mu\text{M}$  vs.  $0.031 \pm 0.004 \mu\text{M}$ ;  $n = 3$ ,  $P < 0.01$ , unpaired Student's *t*-test) (Figure 5B).

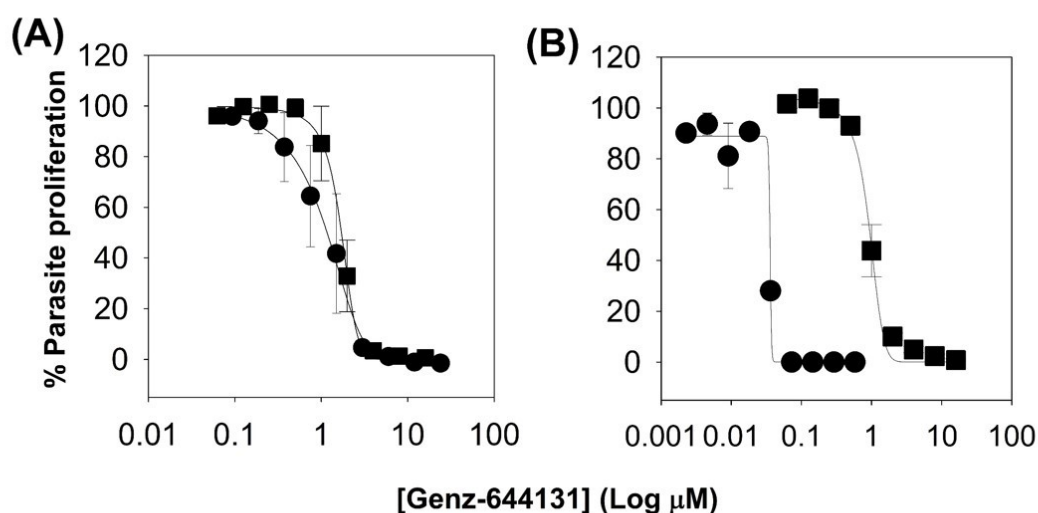


**Figure 3.5: The effect of encapsulation of Genz-644131 in different nanovectors on its *in vitro* anti-plasmodial activity.** Parasite proliferation of ring stage intra-erythrocytic *P. falciparum* parasites was monitored with a SYBR Green I-based assay over 96 h at 37°C and IC<sub>50</sub> determined from dilution series. Dose–response curves for Genz-644131 alone (squares) compared to incorporated into (A) Pheroid® or (B) immunoliposomes (circles). Data are representative in each instance of three independent experiments performed in triplicate or quadruplicate,  $\pm$ SEM. Where not shown, the error bars fall within the symbols.

### 3.4 Discussion

Polyamine biosynthesis enzymes have been the target of various parasitic disease intervention strategies (144) as highlighted by the clinical treatment of *T. brucei* infections through DFMO inhibition of ODC activity (164). Of the other enzymatic activities associated with polyamine biosynthesis, inhibition of AdoMetDC shows promise as a therapeutic target in *P. falciparum*, with MDL73811 being a 1000-fold more potent against intra-erythrocytic *P. falciparum* parasites compared to DFMO (177). Although MDL73811 is an irreversible inhibitor of AdoMetDC activity, it has poor drug-like characteristics for *Plasmodium* (177) and *Trypanosoma* parasites (272), which led to the synthesis of pharmacokinetically amenable derivatives. These derivatives of MDL73811 were used here to determine (1) their efficacy in inhibiting the *PfAdoMetDC* protein and (2) their antiproliferative activity against intra-erythrocytic *P. falciparum* parasites *in vitro*.

Several comparisons can be drawn between the treatment of *P. falciparum* and *T. brucei* parasites with the lead derivative, Genz-644131. Firstly, the AdoMetDC protein from both these parasites responds similarly to Genz-644131 treatment. *PfAdoMetDC* has a near conserved active site compared to AdoMetDC homologues from human and *T. brucei* parasites, despite an overall low sequence identity (21% and 23%, respectively (194)). As a result, MDL73811 inhibits AdoMetDC from both *P. falciparum* and *T. brucei* parasites at comparable levels and in a similar manner as indicated by their respective micromolar  $K_{app}$  values (162, 192, 291). However, Genz-644131 potently inhibits monofunctional and bifunctional *PfAdoMetDC* similarly to *TbAdoMetDC* (272) with  $K_{app}$  values in the nanomolar range (272).

The 1.6-fold decrease in  $K_{app}$  between MDL73811 and Genz-644131 observed for the bifunctional *PfAdoMetDC*/ODC is explained by the 8-methyl substitution on the purine ring of Genz-644131, which promotes the preferred bioactive *syn* conformation (142). However, Genz-644131 is ~7-fold less effective in inhibiting monofunctional *PfAdoMetDC* compared to the *T. brucei* enzyme ( $k_{inact}/K_{app}$  ratios of  $1.17 \mu\text{M}^{-1} \text{min}^{-1}$  for *PfAdoMetDC* compared to  $7.78 \mu\text{M}^{-1} \text{min}^{-1}$  for *TbAdoMetDC* (272)). The association of *PfAdoMetDC* with ODC in the biologically relevant bifunctional protein, *PfAdoMetDC*/ODC, has been shown to result in the modulation of plasmodial AdoMetDC activity (144, 192). Rate-limiting and equimolar synthesis of putrescine and dcAdoMet by the ODC and AdoMetDC activities is enabled by a decrease in AdoMetDC activity when associated in the bifunctional complex with ODC in comparison to its monofunctional *PfAdoMetDC* form, respectively (192). Here, although comparative inactivation efficiencies are seen for Genz-644131 for the monofunctional and

bifunctional proteins, this inhibitor shows a ~3-fold increase in specificity and rate of inhibition of the AdoMetDC domain of the bifunctional protein. This can be attributed to the lower substrate  $K_m$  of PfAdoMetDC in the bifunctional protein compared to the monofunctional protein, which probably reflects differences between active site conformations of these two proteins and consequently, their binding affinities for Genz-644131 (192). Interestingly, the simultaneous inhibition of both activities of the bifunctional PfAdoMetDC/ODC with Genz-644131 and DFMO is additive as was also shown for MDL73811 and DFMO on *in vitro* *P. falciparum* parasites (160, 177) (Appendix 7; Supplemental data S2).

In contrast to the marked improvement (>10-fold) in the *in vitro* antiproliferative efficacy of *T. brucei* parasites treated with Genz-644131 compared to MDL73811 (272), Genz-644131 only shows marginal (2-fold) improvement in the *in vitro* IC<sub>50</sub> against intra-erythrocytic *P. falciparum* parasites. The antiproliferative effect observed with Genz-644131 was not plasmodicidal to the parasite, similar to treatment with MDL73811 and DFMO, with parasite proliferation recovering after limited Genz-644131 exposure (24 h at 2× IC<sub>50</sub>). Both MDL73811 and DFMO treatment result in a cytostatic effect since inhibition is negated by the uptake of exogenous polyamines (162, 168). Co-treatment of parasites with MDL73811 and exogenous spermidine did not abolish the inhibitory effect of MDL73811 on parasite proliferation, and it was previously suggested that intra-erythrocytic *P. falciparum* parasites are incapable of spermidine uptake, since exogenously supplied putrescine, but not spermidine, was capable of overcoming biosynthesis inhibition caused by a variety of inhibitors (162, 168). Likewise, co-treatment of parasites with Genz-644131 and exogenous spermidine also did not abolish the inhibitory effect of Genz-644131 on parasite proliferation. However, recent work clearly indicates that exogenous spermidine is taken up by isolated *P. falciparum* trophozoite-stage parasites (154). Once inside the infected erythrocyte unit, the parasite is able to efficiently take up spermidine across the plasma membrane in a concentration dependent manner, mediated by an electrogenic process energised by the parasite's membrane potential (154). In addition, here we report that exogenous spermidine is taken up by *P. falciparum* infected erythrocytes. Therefore, the inability of spermidine to abolish Genz-644131 inhibition does not appear to be due to the inability of the parasite to take up spermidine. Genz-644131 shows improved *in vivo* cellular toxicity against different *T. brucei* parasite strains (272, 273). When this compound was tested in a murine malaria model for *in vivo* antimalarial activity, Genz-644131 significantly ( $P < 0.001$ ) reduced *P. berghei* parasitaemia by 89% when dosed in the Peters model for 4 days at 100 mg/kg/day. Animals dosed with 20 mg/kg/day showed a 37% ( $P = 0.002$ ) reduction. However, in no case was there sterile cure, as all animals had detectable parasitaemia levels on day 4 (Appendix 7; Supplemental data S3). This may be due to the cytostatic effect described above.

The evidence provided does however not exclude the possibility of off target effects of Genz-644131 on *P. falciparum* parasites including its binding to purine deaminases and polyamine oxidases as observed for MDL73811 (274), particularly to *P. falciparum* adenosine deaminases (292) and erythrocytic polyamine oxidases (268). However, Genz-644131 (at 2× IC<sub>50</sub>) arrested parasite development in a stage-specific manner during the trophozoite stages (18–26 h post invasion), as previously described for MDL73811 (177). This corresponds to the requirement of polyamines due to the stage-specific expression of *PfAdoMetDC/ODC* (18–30 h post-invasion) during the trophozoite stage of the asexual cycle (160). The parasite arrested temporal phenotype induced by Genz-644131 therefore corresponds to the expression profile of *PfAdoMetDC* in the parasite as the target for this compound.

Another explanation for the relatively poor activity of Genz-644131 against intra-erythrocytic *P. falciparum* parasites may be due to the poor membrane permeability of the compound itself, as low membrane permeability was previously shown to be the only inferior *in vitro* ADME characteristic of the MDL73811 derivatives (272). Additionally, for any compound to access the intra-erythrocytic *P. falciparum* parasites, they would need to cross the parasite plasma membrane (PPM), parasitophorous vacuolar membrane (PVM) and erythrocyte membrane (293). Extracellular *T. brucei* parasites are surrounded by only a single plasma membrane (294, 295) and cannot synthesise purines *de novo*, and therefore have to acquire host purines (296). Adenosine, of which MDL73811 is a structural analogue, is actively transported into *T. brucei* parasites by the *T. brucei* nucleotide transporter 1 (*TbNT1*) (297) and the *T. brucei* aminopurine transporter (*TbAT1* or *P<sub>2</sub>*). The latter transporter has been confirmed to actively transport MDL73811 (298, 299), which could explain the low nanomolar *in vitro* IC<sub>50</sub> values of MDL73811 in these parasites. As in *T. brucei*, *Plasmodium* parasites also do not synthesise purines *de novo* and has to recruit exogenous purines from the host (300). In contrast to *T. brucei*, multiple transport mechanisms enable the uptake of purines into intra-erythrocytic *P. falciparum* parasites including host purine transporters (301) as well as parasite derived transporters, *PfNT1* and *PfNT4* localised in the PPM (302, 303). Although the latter are low-affinity transporters (300), their ability to transport MDL73811 and derivatives needs further investigation.

The development of novel lipid based nanovectors provides a solution for the challenges facing malaria chemotherapeutics, since it has the potential to mediate sustained, targeted drug release thereby increasing the drug plasma half-life, lowering dosage requirements and reducing drug toxicity (304). Additionally, lipid-based nanovectors has been shown to eliminate off-target effects by delivery to specific targeted cells, thereby improving the therapeutic efficacy of the compound (305). This makes lipid-based nanovector drug delivery

systems ideal for treatment of intracellular pathogens (304, 306, 307). Previous encapsulations of chloroquine (288) and fosmidomycin (308) resulted in a 10- and 7.5-fold decrease in the *in vitro* IC<sub>50</sub> values of these compounds.

To investigate possible enhancement of the uptake of Genz-644131 into intra-erythrocytic *P. falciparum* parasites, the compound was incorporated into two nanovector drug delivery systems: Pheroid<sup>®</sup> and immunoliposomes (285, 288). The Pheroid<sup>®</sup> system is a nanovector carrier developed from a submicron micellular emulsion formulation, typically ranging in size from 80 to 300 nm (285). These micellular structures can be manipulated in terms of structure, size and morphology to enhance the solubility properties of intended compounds, by entrapment and delivery of compounds across cellular membranes (285). Liposomes are synthetic lipid bilayers of up to 200 nm that have the ability to increase drug bioavailability by encapsulating compounds into the hydrophilic core of the lipid bilayer system. Moreover, the liposomal preparations were orientated with half anti-glycophorin A antibodies, specific for intra-erythrocytic *P. falciparum* parasites, enhancing the selectivity of Genz-644131 to the parasite (288). Here, the 32-fold decrease observed in the *in vitro* IC<sub>50</sub> of immunoliposome encapsulated Genz-644131 against intra-erythrocytic *P. falciparum* parasites suggests that the uptake of Genz-644131 by itself into intracellular *P. falciparum* parasites is restricted. However, the activity of compounds can be improved by either enhancing the chemical pharmacokinetic properties through medicinal chemistry, or encapsulating the compound into drug delivery systems. Although the Genz-644131 immunoliposome combination has not been tested *in vivo*, other immunoliposomal drug suspensions tested against murine mice infections improved the pharmacokinetic profiles of the drugs tested (309, 310). Encapsulation of Genz-644131 with immunoliposomes may also reduce non-specific off-target effects and in a sustainable release of the drug to prolong its plasma half-life.

The combination of Genz-644131 with a novel nanovector drug delivery system therefore provides the most promising result obtained thus far with this nanovector delivery system against intra-erythrocytic *P. falciparum* parasites *in vitro*, and could be evaluated in novel antimalarial drug development.

## Chapter 4

### Concluding discussion

Effective malaria elimination and eradication requires the implementation of both disease prevention and treatment strategies (1). However, vector resistance formation to current IRS and the lack of safe and efficient vaccines consequently places a high dependency on drug prophylaxis and treatment as a final resolution to malaria control (32). Despite the collection of available antimalarials, the parasite is acquiring resistance towards drugs targeted against it at an alarmingly high rate (78). This creates a pressing need to identify and characterise novel drug targets for drug development to expand the near-depleted supply of current antimalarials.

Based on the parasite's dependency on polyamines for cellular proliferation during the IDC (114) and the unique distinctions in polyamine metabolism and the polyamine biosynthetic enzymes between the human host and the parasite (144), polyamine biosynthesis has been identified and validated as a possible drug target in *P. falciparum* parasites (117, 311). Although a wide variety of inhibitors targeting polyamine biosynthetic enzymes has been developed, no compound has produced a sterile cure in murine mice models (144). One of the most effective inhibitors targeting polyamine biosynthesis in *P. falciparum* parasites is MDL73811, a substrate analogue targeting *PfAdoMetDC*, which showed a 1000-fold improved potency compared to parasite proliferation inhibition with DFMO (162). The improved efficacy of this compound as well as the catalysis of a chokepoint reaction by this enzyme (86) makes *PfAdoMetDC* a promising drug target in *P. falciparum* parasites. However, regardless of the *in vitro* potency of *AdoMetDC* inhibitors, additional research is required to identify an antimalarial compound, which can effectively inhibit polyamine biosynthesis. This study focused on the characterisation of *PfAdoMetDC* as a drug target in *P. falciparum* parasites by dissecting the structure-function paradigm of monofunctional *PfAdoMetDC* as well as identifying novel pharmacokinetically favourable MDL73811 derivatives as potent inhibitors of the protein in developing a potential antimalarial therapeutic strategy.

Heterologous expression of active monofunctional *PfAdoMetDC* enabled determination of unique structural and functional characteristics of the enzyme, such as the autocatalytic processing mechanism, activity regulation through complex formation with the *PfODC* domain independent of allosteric putrescine binding as well as its classification into a novel class of adenosyl decarboxylases (192, 194). However, the structural and functional role of the large



A3 parasite-specific insert and the C-terminal hinge region for monofunctional *PfAdoMetDC* was unknown (192, 194). Deletion mutagenesis of residues within the A3 insert showed no gross influence on the structural integrity, however, indicated positive conformational changes to enzyme functionality for monofunctional *PfAdoMetDC*. In a similar study performed on bifunctional *PfAdoMetDC/ODC*, deletion of a similar region concerning a parasite-specific insert in *PfAdoMetDC* showed a significant decrease in both *PfAdoMetDC* and *PfODC* activity. Thus, indicating that the A3 insert may be a surface localised domain that does not influence functional folding of the core *PfAdoMetDC* domain (195), but rather mediates long-range intra- and interdomain interactions between *PfAdoMetDC* and *PfODC* to stabilise the bifunctional complex essential for the coordinated regulation of the enzyme activities (195) (Figure 4.1). This is similarly to the first parasite-specific insert in bifunctional *PfDHFR/TS* is not involved in functional folding of the *PfDHFR* core structure, but in mediating the *PfDHFR* interdomain interactions with the *PfTS* domain in stabilising the bifunctional complex (202).

In contrast to results obtained with the A3 parasite-specific insert, the hinge region is essential for the structural and functional integrity of monofunctional *PfAdoMetDC* as observed with deletion of this region. More specifically, the functional role of this section of the hinge could be attributed to one of the  $\alpha$ -helices or  $\beta$ -sheets predicted to be present within this region. This assumption is based on the role of  $\alpha$ -helices present in the junction regions of various *P. falciparum* bifunctional proteins such as *PfDHFR/TS* and *PfPPPK/DHPS*, which have been shown to mediate critical interdomain interactions in bifunctional complex assembly and activity (262, 266). Due to the essentiality indicated with these structures in the hinge region in maintaining the conformational stability and activity of monofunctional *PfAdoMetDC*, disruption of the protein-protein interactions mediated by these secondary structures may thus be a more ideal and unique target, than *PfAdoMetDC* activity (312) (Figure 4.1). Disruption of such important and specific protein-protein interactions within a protein have been proposed to be an ideal therapeutic intervention strategy, and is a new field being intensively investigated in Biochemistry (313).

However, in order to investigate such protein-protein interactions and develop new novel compounds specific to *PfAdoMetDC*, through structure based drug design strategies, the crystal structure of this protein is required. This has been challenging for *PfAdoMetDC* due low level heterologous expression and poor sample homogeneity. Deletion of the A3 insert was shown to improve sample homogeneity since it may have prevented the formation of the non-obligatory protein-protein interactions leading to heterologous protein complex formation of a heterotetrameric complex. This improved heterologous protein stability and sample homogeneity resulted in protein crystallisation of the  $\Delta$ A3 mutant, the first ever hit conditions

identified for this protein domain. Therefore, truncation of such low complexity regions in *PfAdoMetDC* may provide an ideal strategy in determining the crystal structure of the monofunctional domain (249), and may thus be a key strategy to be implemented in structural studies for the complete bifunctional complex or other *Plasmodium* parasite proteins.

Solving the structure of monofunctional *PfAdoMetDC* will provide a starting point for designing of inhibitors targeting *PfAdoMetDC*. However, other drug development strategies has also been followed for the development of AdoMetDC inhibitors, such as rational analogue-based drug design approach. This strategy produced effective substrate analogue inhibitors for AdoMetDC such as, CGP4866A, MDL73811 and the most recent and potent Genz-644131. The *in vitro* and *in vivo* potency of Genz-644131 against *TbAdoMetDC* and *T. rhodesiense* parasites lead to the first ever clinical trials in development of an AdoMetDC drug (273).

Based on the specificity and activity observed with this compound, the chemical scaffold may be used as a starting point in developing more potent *PfAdoMetDC* inhibitors, upon determination of the three-dimensional protein crystal structure. This combinatory strategy will provide a novel approach to develop specific *PfAdoMetDC* inhibitors. The high rate of parasite resistance formation of malaria parasites is apparent through derivative based drug design strategies that have been applied in the development of antimalarial drugs (100). Therefore, the introduction of a unique chemical scaffold developed against a validated drug target through rational structure-based drug design, may delay parasite resistance formation extending antimalarial life span.

The comparative study performed with Genz-644131 between *P. falciparum* and *T. brucei* parasites revealed unique antiparasitic activity characteristics between these protozoans. The similar enzyme specificities for Genz-644131 against the target enzymes of both parasites were contradicted by the >1000-fold lower *in vitro* activity of Genz-644131 against *P. falciparum* parasites. This observation indicated that antimalarial compounds have an intrinsic challenge in reaching their intracellular target due to poor membrane permeability into infected erythrocytes (294, 295). However, the encapsulation of Genz-644131 into the immunoliposomal based drug delivery system significantly increased the antiplasmodial activity of Genz-644131, making this the most effective compound targeting *P. falciparum* polyamine biosynthesis *in vitro* to date. This drug delivery system provides targeted drug release against *P. falciparum* infected erythrocytes, avoiding host AdoMetDC assimilation, improving drug plasma half-life and lowering dosage requirements (288, 308), which is required for antimalarials as stipulated by the Medicines for Malaria Venture ([www.mmv.org](http://www.mmv.org)). Although the *in vivo* activity of Genz-644131 encapsulated with immunoliposomes remains to

be determined, this study confirmed that the use of nanotechnology drug delivery systems might be an ideal tool for antimalarial drug development (51, 305). The improved potency of Genz-644131 observed in this study, against recombinant *PfAdoMetDC* and *P. falciparum* parasites validated the enzyme as a drug target. Furthermore, it iterated that polyamine biosynthesis, through targeting *PfAdoMetDC*, is a viable antimalarial strategy.

In conclusion, this study has validated *PfAdoMetDC* as a potential drug target in *P. falciparum* parasites through the identification of novel inhibitors as well the validation of a novel therapeutic strategy with an immunoliposomal drug delivery system. However, additional research is required to identify compounds that may serve as specific *PfAdoMetDC* inhibitors. For structure-based drug discovery, the structural and functional characteristics of bifunctional *PfAdoMetDC/ODC* remains to be determined. This study identified various unique protein specific properties of monofunctional *PfAdoMetDC*, which may give insight into the essential regions of this domain required for interdomain interactions and modulation in the bifunctional heterotetrameric complex as shown in Figure 4.1. The *PfODC* domains of two heterodimeric *PfAdoMetDC/ODC* polypeptides interact to form the basis of the bifunctional complex (203). The *PfAdoMetDC* domains are also proposed to form a homodimer mediated by disulphide bridge formation at the proposed dimer interface (192). The A3 parasite-specific insert interacts with the *PfODC* domain, indirectly linking the *PfAdoMetDC* domain to the *PfODC* domain. The hinge regions of the polypeptides stabilises the complex through protein-protein interactions mediated by conserved  $\alpha$ -helices or  $\beta$ -sheets. Furthermore, the characterisation of these protein specific properties not only gave rise to strategies in obtaining the protein crystal structure, but also identified peptide regions forming essential interactions for protein structural integrity. The disruption of such interactions, for example with a small molecule specific to the interaction site, it may inhibit the bifunctional complex assembly thereby affecting both decarboxylase activities. This would result in a unique exploitation of the bifunctional nature of *PfAdoMetDC/ODC* to effect inhibition through targeting protein-protein interactions, an application not yet observed in targeting malaria parasites.

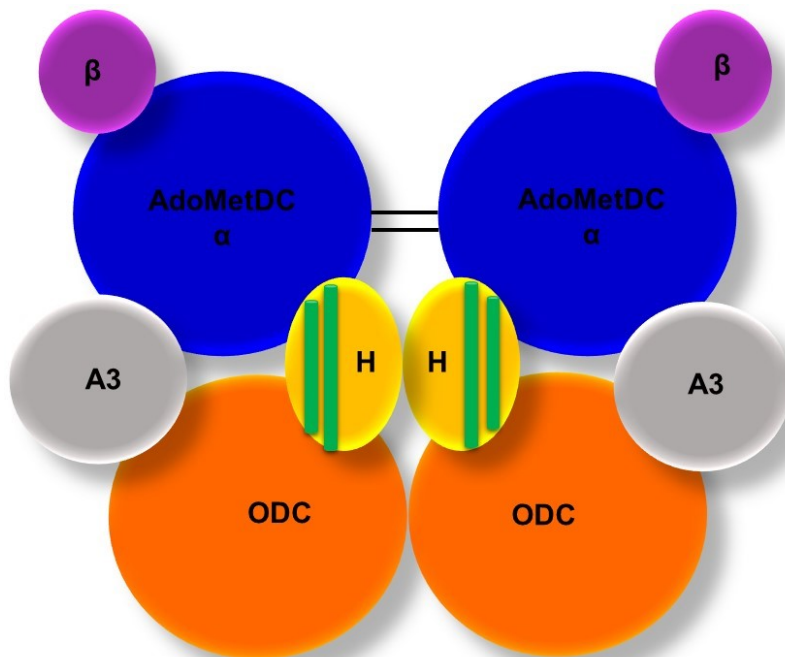


**Figure 4.1: The proposed spatial organisation of heterotetrameric bifunctional *PfAdoMetDC/ODC*.** The diagram depicts two heterodimeric *PfAdoMetDC/ODC* polypeptides that interacts directly via the *PfODC* domain (orange). The hinge region (yellow) connects the *PfODC* domain to the *PfAdoMetDC* domain, stabilising the complex via  $\alpha$ -helices or  $\beta$ -sheets (green). *PfAdoMetDC* ( $\alpha$ -subunit, blue and  $\beta$ -subunit, purple) forms a homodimer via disulphide bridges at the proposed dimer interface, while indirectly interacting with the *PfODC* domain via protein-protein interactions mediated by the A3 parasite-specific insert (grey).

Based on the observations in this study, future studies should include the structural and functional characterisation of the A3 parasite-specific insert in context of the bifunctional complex. Moreover, since deletion of the A3 parasite-specific insert has shown to improve heterologous protein expression, further optimisation and deletion mutagenesis of parasite-specific inserts should be applied to optimise the expression of not only monofunctional *PfAdoMetDC*, but also bifunctional *PfAdoMetDC/ODC*. In addition, the presence of an  $\alpha$ -helix essential to bifunctional complex stabilisation through interdomain interactions should be validated and characterised for *PfAdoMetDC/ODC*, as it may provide a novel drug target site for this protein. Lastly, with the *in vitro* success achieved with Genz-644131 encapsulated with immunoliposomes the validation of this nanotechnology drug delivery system *in vivo* can lead to the development of a potential antimalarial chemotherapeutic strategy.

## References

1. WHO. (2013) World Malaria Report 2013.
2. Murray, C. J. L., Rosenfeld, L. C., Lim, S. S., Andrews, K. G., Foreman, K. J., Haring, D., Fullman, N., Naghavi, M., Lozano, R., and Lopez, A. D. (2012) Global malaria mortality between 1980 and 2010: a systematic analysis. *Lancet*. 379, 413-431.
3. Wellems, T. E., and Miller, L. H. (2003) Two worlds of malaria. *N. Eng. J. Med.* 349, 1496-1498.
4. Suh, K. N., Kain, K. C., and Keystone, J. S. (2004) Malaria. *Can. Med. Assoc. J.* 170, 1693-1702.
5. Sachs, J., and Malaney, P. (2002) The economic and social burden of malaria. *Nature*. 415, 680-685.
6. Myrvang, v. (2010) A fifth *Plasmodium* that can cause malaria. *Tidsskr Nor Laegeforen.* 130, 282-283.
7. Snounou, G., Viriyakosol, S., Jarra, W., Thaithong, S., and Brown, K. N. (1993) Identification of the four human malarial species in field samples by the polymerase chain reaction and detection of a high prevalence of mixed infections. *Mol. Biochem. Parasitol. Res.* 58, 283-292.
8. Hoffman, S. L., Subramanian, G. M., Collins, F. H., and Venter, J. C. (2002) *Plasmodium*, human and *Anopheles* genomics and malaria. *Nature*. 415, 702-709.
9. Rodriguez, M. H., and Hernández-Martínez, S. (2004) Insect malaria parasites infections: The salivary gland. *Insect biochemistry and molecular biology. Insect. Biochem. Molec. Biol.* 34, 615-624.
10. Garcia, J. E., Puentes, A., and Patarroyo, M. E. (2006) Developmental Biology of Sporozoite-Host Interactions in *Plasmodium falciparum* Malaria: Implications for Vaccine Design. *Clin. Microbiol. Rev.* 19, 686-707.
11. Schwartz, E., Parise, M., Kozarsky, P., and Cetron, M. (2003) Delayed onset of malaria-implications for chemoprophylaxis in travelers. *N. Engl. J. Med.* 349, 1510-1516.
12. Warrell, D. A., Molyneux, M. E., and Beales, P. F. (1990) Severe and complicated malaria. Second edition. World Health Organization Division of Control of Tropical Diseases *Trans. Roy. Soc. Trop. Med. Hyg.* 84, 1-65.
13. World Health Organization, C. D. C. (2000) Severe falciparum malaria. *Trans. Roy. Soc. Trop. Med. Hyg.* 94.

14. Pongponratn, E., Riganti, M., Punpoowong, B., and Aikawa, M. (1991) Microvascular sequestration of parasitized erythrocytes in human *falciparum* malaria: a pathological study. *Amer. J. Trop. Med. Hyg.* 44, 168-175.
15. Rogerson, S. J., Grau, G. E., and Hunt, N. H. (2004) The microcirculation in severe malaria. *Microcirculation.* 11, 559-576.
16. Goodman, R. A., Foster, K. L., Trowbridge, F. L., and Figueroa, J. P. (1998) Global Disease Elimination and Eradication as Public Health Strategies. *Sci. J.* 76.
17. Bousema, T., Griffin, J. T., Sauerwein, R. W., Smith, D. L., Churcher, T. S., Takken, W., Ghani, A., Drakeley, C., and Gosling, R. (2012) Hitting Hotspots: Spatial Targeting of Malaria for Control and Elimination. *PLoS Med.* 9, e1001165.
18. Greenwood, B., and Koram, K. (2014) Malaria control in Africa: progress but still much to do. *The Lancet.*
19. Russell, P. F. (1946) Lessons in malariology from World War II *Am. J. Trop. Med. Hyg.* s1-26, 5–13.
20. Greenwood, B. M., Bojang, K., Whitty, C. J. M., and Targett, G. A. T. (2005) Malaria. *Lancet.* 365, 1487-1498.
21. Programme, U. N. E. (2001) Stockholm Convention on Persistent Organic Pollutants. (Text, C., Ed.), Geneva.
22. Board, I. D. A. (1956) Malaria Eradication: Report and Recommendations of the International Development Advisory Board. International Cooperation Agency, Washington, DC.
23. Packard, R. M. (1998) 'No other logical choice': global malaria eradication and the politics of international health in the post-war era. *Parasitologia.* 40, 217-229.
24. Heppner, D. G. (2013) The malaria vaccine – Status quo 2013. *Travel. Med. Infect. Dis.* 11, 2-7.
25. Bairwa, M., Rajput, M., Khanna, P., Rohilla, R., Verma, R., and Chawla, S. (2012) Malaria vaccine: A bright prospect for elimination of malaria. *Hum. Vaccin. Immunother.* 8, 6.
26. Todryk, S. M., and Hill, A. V. S. (2007) Malaria vaccines: the stage were at. *Nature Rev. Microbiol.* 5, 487-489.
27. Ballou, W. R. (2009) The development of the RTS,S malaria vaccine candidate: challenges and lessons. *Parasite Immunol.* 31, 492-500.
28. Bojang, K., Milligan, P., Pinder, M., Doherty, T., Leach, A., Ofori-Anyinam, O., Lievens, M., Kester, K., Schaecher, K., Ballou, W. R., and Cohen, J. (2009) Five year safety and immunogenicity of GlaxoSmithKline's candidate malaria vaccine RTS,S/AS02

following administration to semi-immune adult men living in a malaria-endemic region of The Gambia. *Hum. Vaccin.* . 5, 242-247.

29. Graves, P. M., and Gelband, H. (2006) Vaccines for preventing malaria. *Cochrane Database Syst. Rev.* . 4.
30. Spring, M. D., Cummings, J. F., Ockenhouse, C. F., Dutta, S., Reidler, R., Angov, E., Bergmann-Leitner, E., Stewart, V. A., Bittner, S., Juompan, L., Kortepeter, M. G., Nielsen, R., Krzych, U., Tierney, E., Ware, L. A., Dowler, M., Hermsen, C. C., Sauerwein, R. W., de Vlas, S. J., Ofori-Anyinam, O., Lanar, D. E., Williams, J. L., Kester, K. E., Tucker, K., Shi, M., Malkin, E., Long, C., Diggs, C. L., Soisson, L., Dubois, M. C., Ballou, W. R., Cohen, J., and Heppner, D. G., Jr. (2009) Phase 1/2a Study of the Malaria Vaccine Candidate Apical Membrane Antigen-1 (AMA-1) Administered in Adjuvant System AS01B or AS02A. *PLoS One.* 4, e5254.
31. Ferreira, M. U., Ribeiro, W. L., Tonon, A. P., Kawamoto, F., and Rich, S. M. (2003) Sequence diversity and evolution of the malaria vaccine candidate merozoite surface protein-1 (MSP-1) of *Plasmodium falciparum*. *Gene.* 304, 65-75.
32. WHO. (2012) World Malaria Report 2012.
33. Kain, K. C., Harrington, M. A., Tennyson, S., and Keystone, J. S. (1998) Imported malaria: prospective analysis of problems in diagnosis and management. *Clin. Infect. Dis.* 27, 142-149.
34. Moody, A. (2002) Rapid diagnostic tests for malaria parasites. *Clin. Microbiol. Rev.* 15, 66-78.
35. Wongsrichanalai., C. (2001) Rapid diagnostic techniques for malaria control. *Trends in Parasitol. Res.* 17 307-309.
36. Van Vianen, P. H., van Engen, A., Thaithong, S., van der Keur, M., Tanke, H. J., and van der Kaay, H. J. (1993) Flow cytometric screening of blood samples for malaria parasites *Cytometry.* 14, 276-280.
37. Hanscheid, T., Valadas, E., and Grobusch, M. P. (2000) Automated malaria diagnosis using pigment detection. *Parasitol.Today.* 16, 549-551.
38. Nwaka, S., and Ridley, R. G. (2003) Virtual drug discovery and development for neglected diseases through public-private partnerships. *Nature Rev. Drug. Discov.* 2, 919-928.
39. Ridley, R. G. (2002) Medical need, scientific opportunity and the drive for antimalarial drugs. *Nature.* 415, 686-693.
40. Leete, E. (1969) Biosynthesis of quinine and related alkaloids *Acc. Chem. Res.* 2, 59-64.



41. Warhurst, D. C., Craig, J. C., Adagu, I. S., Guy, R. K., Madrid, P. B., and Fivelman, Q. L. (2007) Activity of Piperaquine and other 4-Aminoquinoline Antiplasmodial Drugs against Chloroquine-sensitive and Resistant blood stages of *Plasmodium falciparum*. Role of beta-haematin inhibition and drug concentration in vacuolar water-and lipid phases. *Biochem. Pharmacol.* 73, 1910-1926.
42. Fitch, C. D. (2004) Ferriprotoporphyrin IX, phospholipids and the antimalarial actions of quinoline drugs. *Life Sci.* 74, 1957-1972.
43. Deharo, E., Garcia, R. N., Oporto, P., Gimenez, A., Sauvian, M., Jullian, V., and Ginsburg, H. (2002) A non-radiolabelled ferriprotoporphyrin (FP) IX biomineralisation inhibition test for high throughput screening of antimalarial drugs. *Exp. Parasitol.* 252, 252-256.
44. Fidock, D. A., Nomura, T., Talley, A. K., Cooper, R. A., Dzekunov, S. M., Ferdig, M. T., Ursos, L. M. B., bir Singh Sidlhu, A., Naude, B., and Deistch, K. W. (2000) Mutations in the *Plasmodium falciparum* digestive vacuole transmembrane protein PfCRT and evidence for their role in chloroquine resistance. *Mol. Cell.* 6, 861-871.
45. Cooper, R. A., Ferdig, M. T., Su, X., Ursos, L. M. B., Mu, J., Nomura, T., Fujioka, H., Fidock, D. A., Roepe, P. D., and Wellems, T. E. (2001) Alternative Mutations at Position 76 of the Vacuolar Transmembrane Peorwin PfCRT are associated with Chloroquine Resistance and Unique Stereospecific Quinine and Quinidine Responses in *Plasmodium falciparum* *Mol. Pharmacol.* 61, 35-42.
46. Na-Bangchang, K., and Karbwang, J. (2009) Current status of malaria chemotherapy and the role of pharmacology in antimalarial drug research and development. *Fundam. Clin. Pharmacol.* 23, 387-409.
47. Vale, N., Moreira, R., and Gomes, P. (2009) Primaquine revisited six decades after its discovery. *Eur. J. Med. Chem.* 27, 25-61.
48. Hawley, S. R., Bray, P. G., O'Neill, P. M., Park, B. K., and Ward, S. A. (1996) The role of Drug Accumulation in 4-Aminoquinoline Antimalarial potency - the Influence of Structural substitution and Physiochemical Properties. *Biochem. Pharmacol.* 52, 723-733.
49. Schlitzer, M. (2007) Malaria chemotherapeutics part I: History of antimalarial drug development *Chem. Med. Chem.* 2, 944-986.
50. Trenholme, C. M., Williams, R. L., Desjardins, R. E., Frischer, H., Carson, P. E., Rieckman, K. H., and Canfield, C. J. (1975) Mefloquine (WR 142, 490) in the treatment of human malaria *Science.* 190, 792-794.
51. Santos-Magalhães, N. S., and Mosqueira, V. C. F. (2010) Nanotechnology applied to the treatment of malaria. *Adv. Drug Deliv. Rev.* 62, 560-575.
52. Vangapandu, S., Jain, M., Kaur, K., Patil, P., Patel, S. R., and Jain, R. (2007) Recent advances in antimalarial drug development. *Med. Res. Rev.* 27, 65-107.

53. Olliaro, P., and Wells, T. N. C. (2009) The global portfolio of new antimalarial medicines under development. *Clin. Pharmacol. Ther.* 85, 879-891.
54. O'Neill, P. M., Barton, V. E., Ward, S. A., and Chadwick, J. (2012) 4-Aminoquinolines: Chloroquine Amodiaquine and Next-Generation Analogues. Springer Basel AG. 19, 44.
55. O'Neill, P. M., Park, B. K., Shone, A. E., Maggs, J. L., Roberts, P., Stocks, P. A., Biagini, G. A., Bray, P. G., Gibbons, P., Berry, N., Winstanley, P. A., Mukhtar, A., Bonar-Law, R., Hindley, S., Bamba, I. R. B., Davis, C. B., Bates, M., Hart, T. K., Gresham, S. L., Lawrence, R. M., Brigandi, R. A., Gomez-delas-Heras, F. M., Gargallo, D. V., and Ward, S. A. (2009) Candidate selection and preclinical evaluation of N-tert-butyl isoquine (GSK369796), an affordable and effective 4-aminoquinoline antimalarial for the 21st century. *J. Med. Chem.* 52, 1408–1415.
56. Nasveld, P. E., Edstein, M. D., Reid, M., Brennan, L., Harris, I. E., Kitchener, S. J., Leggat, P. A., Pickford, P., Kerr, C., Ohrt, C., and Prescott, W. (2010) Tafenoquine Study Team, Randomized, double-blind study of the safety, tolerability, and efficacy of tafenoquine versus mefloquine for malaria prophylaxis in nonimmune subjects. *Antimicrob. Agents Chemother.* 54, 792–798.
57. Wang, J. Y., Cao, W. C., Shan, C. Q., Zhang, M., Li, G. F., Ding, D. B., Shi, Y. I., and Wu, B. (2004) Naphthoquine phosphate and its combination with artemisinin. *Acta Trop.* 89, 375–381.
58. Kurth, F., Belard, S., Basra, A., and Ramharter, M. (2011) Pyronaridine-artesunate combination therapy for the treatment of malaria. *Curr. Opin. Infect. Dis.* 24, 564-569.
59. Marfurt, J., Chalfein, F., Prayoga, P., Wabiser, F., Kenangalem, E., Piera, K. A., Machunter, B., Tjitra, E., Anstey, N. M., and Price, R. N. (2011) *Ex vivo* drug susceptibility of ferroquine against chloroquine-resistant isolates of *Plasmodium falciparum* and *P. vivax*. *Antimicrob. Agents Chemother.* 55, 4461–4464.
60. Ivanetich, K. M., and Santi, D. V. (1990) Thymidylate synthase-dihydrofolate reductase in protozoa. *Exp. Parasitol.* 70, 367-371.
61. Warhurst, D. C. (1999) Antimalarial drug discovery: development of inhibitors of dihydrofolate reductase active in drug resistance. *Drug Discov. Today.* 3, 538–546.
62. Olliaro, P. (2001) Mode of action and mechanisms of resistance for antimalarial drugs. *Pharmacol. Ther.* 89, 207-219.
63. Ivanetich, K. M., and Santi, D. V. (1990) Bifunctional thymidylate synthase-dihydrofolate reductase in protozoa. *FASEB J.* 4, 1591-1597.
64. Wang, C. C., Lee, C. S., Bayoumi, R., Djimde, A., Duombo, O., Swedberg, G., Dao, L. D., Mshinda, H., Tanner, M., Watkins, W. M., Sims, P. F., and Hyde, J. E. (1997) Resistance to antifoaltes in *Plasmodium falciparum*, monitored by sequence analysis of Dihydropteroate synthase and Dihydrofolate reductase alleles in a large number of field samples of diverse origins. *Mol. Biochem. Parasitol.* 8, 161-177.

65. Plowe, C. V., Kublin, J. G., and Doumbo, O. K. (1998) *Plasmodium falciparum* dihydrofolate reductase and dihydropteroate synthase mutations: epidemiology and role in clinical resistance to antifolates. *Drug Resist. Updat.* 1, 389-396.
66. Sirawaraporn, W., Sathitkul, T., Sirawaraporn, R., Yuthavong, Y., and Santi, D. V. (1997) Antifolate-resistant mutants of *Plasmodium falciparum* dihydrofolate reductase. *Proc. Natl. Acad. Sci.(USA)*. 94, 1124-1129.
67. Cowman, A. F., and Lew, A. M. (1990) Chromosomal rearrangements and point mutations in the DHFR/TS gene of *Plasmodium chabaudi* under antifolate selection. *Mol. Biochem. Parasitol.* 42, 21-29.
68. Plowe, C., Cortese, J. F., Djimde, A., Nwanjanwu, O. C., Watkins, W. M., Winstanley, P. A., Estrada-Franco, J. G., Mollinedo, R. E., Avila, J. C., Cespedes, J. L., Carter, D., and Doumbo, O. K. (1997) Mutations in *Plasmodium falciparum* dihydrofolate reductase and dihydropteroate synthase and epidemiologic patterns of pyrimethamine-sulphadoxine use and resistance. *J. Infect. Dis.* 176, 1590-1596.
69. Thera, M. A., Sehdev, P. S., Coulibaly, D., Traore, K., Garba, M. N., Cissoko, Y., Kone, A., Guindo, A., Dicko, A., Beavogui, A. H., Djimde, A. A., Lyke, K. E., Diallo, D. A., Doumbo, O. K., and Plowe, C. V. (2005) Impact of Trimethoprim-Sulfamethoxazole Prophylaxis on *Falciparum* Malaria Infection and Disease. *J. Infect. Dis.* 192, 1823-1829.
70. Mather, M. W., Daarouzet, E., Valkova-Valchanova, M., Cooley, J. W., McIntosh, M. T., Daldal, F., and Vaidya, A. B. (2005) Uncovering the molecular mode of action of the antimalarial drug atovaquone using a bacterial system *J. Biol. Chem.* 280, 27458-27465.
71. Korsinczky, M., Chen, N. H., Kotecka, B., Saul, A., Rieckmann, K., and Cheng, Q. (2000) Mutations in *Plasmodium falciparum* cytochrome *b* that are associated with atovaquone resistance are located at a putative drug-binding site. *Antimicrob. Agents Chemother.* 44, 2100-2108.
72. Deye, G. A., Miller, R. S., Miller, L., Salas, C. J., Tosh, D., Macareo, L., Smith, B. L., Francisco, S., Clemens, E. G., Murphy, J., Sousa, J. C., Dumler, J. S., and Magill, A. J. (2012) Prolonged Protection Provided by a Single Dose of Atovaquone-Proguanil for the Chemoprophylaxis of *Plasmodium falciparum* Malaria in a Human Challenge Model. *Clin. Infect. Dis.* 54, 232-239.
73. Klayman, D. L. (1985) Qinghaosu (Artemisinin): an antimalarial drug from China. *Science.* 228, 1049-1055.
74. Luo, X. D., and Shen, C. C. (1987) The chemistry, pharmacology and clinical applications of qinghaosu and its derivatives. *Med. Res. Develop.* 7, 29-52.
75. Clark, I. A., Hunt, N. H., W.B.; C., Maxwell, L. E., and Mackie, E. J. (1984) Radical-mediated damage to parasites and erythrocytes in *Plasmodium vinckei* infected mice after injection of t-butyl hydroperoxide. *Clin. Exp. Immunol.* 56, 524-530.

76. Eckstein -Ludwig, U., Webb, R. J., van Goethem, I. D. A., East, J. M., Lee, A. G., Kimura, M., O'Neill, P. M., Bray, P. G., Ward, S. A., and Krishna, S. (2003) Artemisinins target the SERCA of *Plasmodium falciparum*. *Nature*. 424, 957-961.
77. Wang, J., Huang, L., Li, J., Fan, Q., Long, Y., Li, Y., and Zhou, B. (2010) Artemisinin Directly targets Malarial Mitochondria through its specific Mitochondrial Activation PLoS One. 5, e9582.
78. Noedl, H., Se, Y., Sriwichai, S., Schaecher, K., Teja-Isavadharm, P., Smith, B. L., Rutvisuttinunt, W., Bethell, D., Surasri, S., Fukuda, M. M., Socheat, D., and Chan, T. L. (2010) Artemisinin Resistance in Cambodia: A Clinical Trial Designed to Address an Emerging Problem in Southeast Asia. *Clin. Infect. Dis.* 51, e82.
79. Dondorp, A. M., Nosten, F., Yi, P., Das, D., Phyo, A. P., Tarning, J., Lwin, K. M., Arieu, F., Hanpithakpong, W., Lee, S. J., Ringwald, P., Silamut, K., Imwong, M., Chotivanich, K., Lim, P., Herdman, T., An, S. S., Yeung, S., Singhasivanon, P., Day, N. P. J., Lindegardh, N., Socheat, D., and White, N. J. (2009) Artemisinin Resistance in *Plasmodium falciparum* Malaria. *New Eng. J. Med.* 361, 455-467.
80. Arieu, F., Witkowski, B., Amaratunga, C., Beghain, J., Langlois, A. C., Khim, N., Kim, S., Duru, V., Bouchier, C., Ma, L., Lim, P., Leang, R., Duong, S., Sreng, S., Suon, S., Chhor, C. M., Bout, D. M., Menard, S., Rogers, W. O., Genton, B., Fandeur, T., Miotto, O., Ringwald, P., Le Bras, J., Berry, A., Barale, J. C., Fairhurst, R. M., Benoit-Vical, F., Mercereau-Puijalon, O., and Menard, D. (2014) A molecular marker of artemisinin-resistant *Plasmodium falciparum* malaria. *Nature*. 505, 50-55.
81. Olliaro, P. L., and Taylor, W. R. J. (2003) Antimalarial compounds: from bench to bedside. *J. Exp. Biol.* 206, 3753-3759.
82. Charman, S. A., Arbe-Barnes, S., Bathurst, I. C., Brun, R., Campbell, M., Charman, W. N., Chiu, F. C. K., Chollet, J., Craft, J. C., Creek, D. J., Dong, Y., Matile, H., Maurer, M., Morizzi, J., Nguyen, T., Papastogiannidis, P., Scheurer, C., Shackelford, D. M., Sriraghavan, K., Stingelin, L., Tang, Y., Urwyler, H., Wang, X., White, K. L., Wittlin, S., Zhou, L., and Vennerstrom, J. L. (2011) Synthetic ozonide drug candidate OZ439 offers new hope for a single-dose cure of uncomplicated malaria PNAS Early Edition. 108, 4400-4405.
83. Nagelschmitz, J., Voith, B., Wensing, G., Roemer, A., Fugmann, B., Haynes, R. K., Kotecka, B. M., Rieckmann, K. H., and Edstein, M. D. (2008) First assessment in humans of the safety, tolerability, pharmacokinetics, and *ex vivo* pharmacodynamic antimalarial activity of the new artemisinin derivative artemisone. *Antimicrob. Agents Chemother.* 52, 3085-3091.
84. Haynes, R. K., Fugmann, B., Stetter, J., Rieckmann, K., Heilmann, H. D., Chan, H. W., Cheung, M. K., Lam, W. L., Wong, H. N., Croft, S. L., Vivas, L., Rattray, L., Stewart, L., Peters, W., Robinson, B. L., Edstein, M. D., Kotecka, B., Kyle, D. E., Beckermann, B., Gerisch, M., Radtke, M., Schmuck, G., Steinke, W., Wollborn, U., Schmeer, K., and Romer, A. (2006) Artemisone-a highly active antimalarial drug of the artemisinin class. *Angew. Chem. Int. Ed. Engl.* 45, 2082-2088.

85. Dahl, E. L., and Rosenthal, P. J. (2008) Apicoplast translation, transcription and genome replication: targets for antimalarial antibiotics. *Trends Parasitol.* 24, 279-284.
86. Yeh, E., and DeRisi, J. L. (2011) Chemical rescue of malaria parasites lacking an apicoplast defines organelle function in blood-stage *Plasmodium falciparum* *PLOS Biology.* 9, e1001138.
87. van Eijk, A. M., and Terlouw, D. J. (2011) Azithromycin for Treating Uncomplicated Malaria. *Cochrane Database Syst. Rev.*, 2.
88. Dahl, E. L., and Rosenthal, P. J. (2007) Multiple antibiotics exert delayed effects against *Plasmodium falciparum* apicoplast. *Antimicrob. Agents Chemother.* 51, 3485-3490.
89. Wiesner, J., Reichenberg, A., Heinrich, S., Schlitzer, M., and Jomaa, H. (2008) The plastid-like organelle of apicomplexan parasites as drug target. *Current Pharm. Des.* 14, 855-871.
90. Kremsner, P. G., and Krishna, S. (2004) Antimalarial combinations. *Lancet.* 364, 285-294.
91. Bell, A. (2005) Antimalarial drug synergism and antagonism: Mechanistic and clinical significance. *FEMS Microbiol.* 253, 171-184.
92. Dorsey, G., Vlahos, J., Kanya, M. R., Staedke, S. G., and Rosenthal, P. J. J. (2003) Prevention of increasing rates of treatment failure by combining sulfadoxine-pyrimethamine with artesunate or amodiaquine for the sequential treatment of malaria. *Infect. Dis.* 188, 1231-1238.
93. White, N. (1999) Antimalarial drug resistance and combination chemotherapy. *Phil. Trans. Roy. Soc.*, 739-749.
94. WHO. (2010) Guidelines for the treatment of malaria. 194.
95. Lell, B., Lehman, L. G., Schmidt-Ott, J. R., Sturchler, D., Handschin, J., and Kremsner, P. G. (1998) Malaria chemotherapy trial a minimal effective dose of mefloquine/sulphadoxine/pyrimethamine compared with equivalent doses of sulphadoxine/pyrimethamine or mefloquine alone. *Am. J. Trop. Med. Hyg.* 58, 619-624.
96. von Seidlein, L., Millgran, P., and Pinder, M. (2000) Efficacy of artesunate plus pyrimethamine-sulphadoxine for uncomplicated malaria in Gambian children: a double-blind, randomised, controlled trial. *Lancet.* 355, 352-357.
97. McCollum, A. M., Poe, A. C., Hamel, M., Huber, C., Zhou, Z. Y., Shi, Y. P., Ouma, P., Vulule, J., Bloland, P., and Slutsker, L. (2006) Antifolate resistance in *Plasmodium falciparum*: multiple origins and identification of novel *dhfr* alleles. *J. Infect. Dis.* 194, 189-197.

98. Metzger, W., Mordmuller, B., Graninger, W., Bienzle, U., and Kremsner, P. G. (1995) High efficacy of short-term quinine-antibiotic combinations for treating adult malaria patients in an area in which malaria is hyperendemic. *Antimicrob. Agents Chemother.* 39, 245-246.
99. Wiesner, J., Henschker, D., Hutchinson, D. B., Beck, E., and Jomaa, H. (2002) *In vitro* and *in vivo* Synergy of fosmidomycin, a Novel Antimalarial drug, with Clindamycin. *Antimicrob. Agents Chemother.* 46, 2889-2894.
100. Bloland, P. B. (2001) Drug resistance in malaria. World Health Organization, Chamblee, GA.
101. Oyakhirome, S., Potschke, M., Schwarz, N., Dornemann, J., Laengin, M., Salazar, C., Lell, B., Kun, J. F., Kremsner, P. G., and Grobusch, M. P. (2007) Artesunate - amodiaquine combination therapy for *falciparum* malaria in young Gabonese children. *Malaria J.* 6, 29.
102. Vedadi, M., Lew, J., Artz, J., Amani, M., Zhao, Y., Dong, A., Wasney, G. A., Gao, M., Hills, T., Brokx, S., Qiu, W., Sharma, S., Diassiti, A., Alam, Z., Melone, M., Mulichak, A., Wernimont, A., Bray, J., Loppnau, P., Plotnikova, O., Newberry, K., Sundararajan, E., Houston, S., Walker, J., Tempel, W., Bochkarev, A., Kozieradzki, I., Edwards, A., Arrowsmith, C., Roos, D., Kain, K., and Hui, R. (2007) Genome-scale protein expression and structural biology of *Plasmodium falciparum* and related Apicomplexan organisms. *Mol. Biochem. Parasitol.* 151, 100-110.
103. Gardner, M. J., Hall, N., Fung, E., White, O., Berriman, M., Hyman, R. W., Carlton, J. M., Pain, A., Nelson, K. E., and Bowman, S. (2002) Genome sequence of the human malaria parasite *Plasmodium falciparum*. *Nature.* 419, 498-511.
104. Olliaro, P. (2005) Drug Resistance Hampers Our Capacity to Roll Back Malaria. *Clin. Infect. Dis.* 41, S247-S257.
105. Wells, T. N., and Poll, E. M. (2010) When is enough enough? The need for a robust pipeline of high-quality antimalarials. *Discov. Med.* 9, 389-398.
106. Krishna, S., Eckstein-Ludwig, U., Joet, T., Uhlemann, A. C., Morin, C., Webb, R., Woodrow, C., Kun, J. F., and Kremsner, P. G. (2002) Transport processes in *Plasmodium falciparum* infected erythrocytes: potential as new drug targets. *Int. J. Parasitol.* 32, 1567-1573.
107. Greenbaum, D. C., Baruch, A., Grainger, M., Bozdeek, Z., Medzihradzky, K. F., Engel, J., DeRisi, J., Holder, A. A., and Bogyo, M. (2002) A role for the protease falcipain 1 in host cell invasion by the human malaria parasite. *Science.* 298, 2002-2006.
108. Bell, A. (1998) Microtubule inhibitors as potential antimalarial agents. *Parasitol. Res. Today.* 14, 234-240.



109. Murphy, S. C., Harrison, T., Hamm, H. E., Lomasney, J. W., Mohandas, N., and Haldar, K. (2006) Erythrocyte G protein as a novel target for malarial chemotherapy. *PLoS Med.* 3, e528.
110. Roberts, F., Roberts, C. W., Johnson, J. J., Kyle, D. E., Krell, T., Coggins, J. R., Coombs, G. H., Milhous, W. K., Tzipori, S., Ferguson, D. J., Chakrabarti, D., and McLeod, R. (1998) Evidence for the shikimate pathway in apicomplexan parasites. *Nature.* 393, 801–805.
111. Bauer, N. L., Bendale, K., Rivas, P., Yokoyama, K., Buckner, F. S., and Chakrabarti, D. (2005) Protein farnesyltransferase inhibitors exhibit potent antimalarial activity. *J. Med. Chem.* 48, 3704–3713.
112. Cameron, A., Read, J., Tranter, R., Winter, V., Sessions, R., and Brady, R. L. (2004) Identification and activity of a series of azolebased compounds with lactate dehydrogenase directed antimalarial activity. *J. Biol. Chem.* 279, 31429–31439.
113. Sufrin, J. R., Meshnick, S. R., Spiess, A. J., Garofalohannan, J., Pan, X. Q., and Bacchi, C. J. (1995) Methionine recycling pathways and antimalarial drug design. *Antimicrob. Agents Chemother.* 39, 2511–2515.
114. Heby, O., Persson, L., and Rentala, M. (2007) Targeting the polyamine biosynthetic enzymes: a promising approach to therapy of African sleeping sickness, Chagas' disease and leishmaniasis. *Amino Acids.* 33, 359-366.
115. Calderera, C. M., Barbiroli, B., and Moruzzi, G. (1965) Polyamines and nucleic acids during development of the chick embryo. *Biochem. J.* 97, 84-88.
116. Casero, R. A., and Marton, L. J. (2007) Targeting polyamine metabolism and function in cancer and other hyperproliferative diseases. *Nat. Rev. Drug. Discov.* 6, 373-390.
117. Heby, O., Roberts, S. C., and Ullman, B. (2003) Polyamine biosynthetic enzymes as drug targets in parasitic protozoa. *Biochem. Soc. Trans.* 31, 415–419.
118. Hamana, K., and Matsuzaki, S. (1992) Polyamines as a chemotaxonomic marker in bacterial systematics. *Crit. Rev. Microbiol.* 18.
119. Pegg, A. E., and McCann, P. P. (1982) Polyamine metabolism and function. *Am. J. Physiol.* 243, 212-221.
120. Tabor, C. W., and Tabor, H. (1984) Polyamines. *Annu. Rev. Biochem.* 53, 749-790.
121. D'Agostino, L., and Luccia, A. D. (2002) Polyamines interact with DNA as molecular aggregates. *Eur. J. Biochem.* 269, 4315-4325.
122. Matthews, H. R. (1993) Polyamines, chromatin structure and transcription. *BioEssays.* 15, 561-567.



123. Childs, A. C., Metha, D. J., and Gerner, E. W. (2003) Polyamine dependent protein expression. *Cell. Mol. Life Sci.* 60, 1394-1406.
124. Behe, M., and Felsenfeld, G. (1981) Effects of methylation on a synthetic polynucleotide: the B to Z transition in poly(dG-m<sup>5</sup>dC).poly(dG-m<sup>5</sup>dC). *Proc. Natl. Acad. Sci. (USA)*. 78, 1619-1623.
125. Basu, H. S., Feuerstein, B. G., Deen, D. F., Lubich, W. P., Bergeron, R. J., Samejima, K., and Marton, L. J. (1989) Correlation between the effects of polyamines analogues on DNA conformation and cell growth. *Cancer Res.* 49, 5591-5597.
126. Beninati, S., Gentile, V., Caraglia, M., Lentini, A., Tagliaferri, P., and Abbruzzese, A. (1998) Tissue transglutaminase expression affect hypusine metabolism in BALB/c3T3 cells. *FEBS Letters.* 437, 34-38.
127. Williams, K. (1997) Interactions of polyamines with ion channels. *Biochem. J.* 325, 289-297.
128. Schuber, F. (1988) Influence of polyamines on membrane function. *Biochem. J.* 260, 1-10.
129. Meksuriyen, D., Fukuchi-Shimogori, T., Tomitori, H., Kashiwagi, K., Toida, T., Imanari, T., Kawai, G., and Igarashi, K. (1998) Formation of a Complex Containing ATP, Mg<sup>2+</sup>, and Spermine. *J. Biol. Chem.* 273, 30939-30944.
130. Park, M. H. (2006) The Post-Translational Synthesis of a Polyamine-Derived Amino Acid, Hypusine, in the Eukaryotic Translation Initiation Factor 5A (eIF5A). *J. Biochem.* 139, 161-169.
131. Cooper, H. L., Park, M. H., Folk, J. E., Safer, B., and Braverman, R. (1983) Identification of the hypusine-containing protein hy<sup>+</sup> as translation initiation factor eIF-4D. *Proc. Natl. Acad. Sci. (USA)*. 80, 1854-1857.
132. Molitor, I. M., Knöbel, S., Dang, C., Spielmann, T., Alléra, A., and König, G. M. (2004) Translation initiation factor eIF-5A from *Plasmodium falciparum*. *Mol. Biochem. Parasitol.* 137, 65-74.
133. Wright, R. K., Buehler, B. A., Schott, S. N., and Rennert, O. M. (1978) Spermine and spermidine, modulators of the cell surface enzyme adenylate cyclase. *Pediatr. Res.* 12.
134. Igarashi, K., and Morris, D. R. (1984) Physiological Effects in Bovine Lymphocytes of Inhibiting Polyamine Synthesis with Ethylglyoxal Bis(guanylhydrazone). *Cancer Res.* 44, 5332-5337.
135. Pohjanpelto, P., and Hölttä, E. (1996 ) Phosphorylation of Okazaki-like DNA fragments in mammalian cells and role of polyamines in the processing of this DNA. *EMBO J.* 15, 1193–1200.

136. Johansson, V. M., Stina, M., Oredsson, S. M., and Alm, K. (2008) Polyamine Depletion with Two Different Polyamine Analogues Causes DNA Damage in Human Breast Cancer Cell Lines. *DNA Cell Biol.* 27, 511-516.
137. Nitta, T., Igarashi, K., and Yamamoto, N. (2002) Polyamine Depletion Induces Apoptosis through Mitochondria-Mediated Pathway. *Exp. Cell Res.* 276, 120-128.
138. Tome, M. E., Fiser, S. M., Payne, C. M., and Gerner, E. W. (1997) Excess putrescine accumulation inhibits the formation of modified eukaryotic initiation factor 5A (eIF-5A) and induces apoptosis. *Biochem. J.* 328, 847-854.
139. He, Y., Kashiwagi, K., Fukuchi, J., Terao, K., Shirahata, A., and Igarashi, K. (1993) Correlation between the inhibition of cell growth by accumulated polyamines and the decrease of magnesium and ATP. *Eur. J. Biochem.* 217, 89-96.
140. Igarashi, K., and Kashiwagi, K. (2000) Polyamines: mysterious modulators of cellular functions. *Biochem. Biophys. Res. Com.* 271, 559-564.
141. Pegg, A. E. (2006) Regulation of Ornithine decarboxylase. *J. Biol. Chem.* . 281, 14529-14532.
142. Pegg, A. E. (2009) S-adenosylmethionine decarboxylase. *Essays Biochem.* 46, 25-45.
143. Ikeguchi, Y., Bewley, M. C., and Pegg, A. E. (2006) Aminopropyltransferases: Function, structure and genetics. *J. Biochem.* 139, 1-9.
144. Birkholtz, L., Williams, M., Niemand, J., Louw, A. I., Persson, L., and Heby, O. (2011) Polyamine homeostasis as a drug target in pathogenic protozoa: peculiarities and possibilities. *Biochem. J.* . 438, 229-244.
145. Krauth-Seigel, R. L., and Comini, M. A. (2008) Redox control in trypanosomatids, parasitic protozoa with trypanothione-based thiol metabolism. *Biochem. Biophys. Acta.* 1780, 1236-1248.
146. Berman, J. (2006) Visceral leishmaniasis in the New World and Africa. *Indian J. Med. Res.* 123, 289-294.
147. Roberts, S. C., Jiang, Y., Jardim, A., Carter, N. S., and Heby, O. (2001) Genetic analysis of Spermidine Synthase from *Leishmania donovani* *Mol. Biochem. Parasitol.* 115, 217-226.
148. Stuart, K., Brun, R., Croft, S., Fairlamb, A., Gurtler, R. E., McKerrow, J., Reed, S., and Tarlton, R. (2008) Kinetoplastids: related protozoan pathogens, different diseases. *J.Clin. Invest.* 118, 1301-1310.
149. Hunter, K. J., Le Quesne, S. A., and Fairlamb, A. H. (1994) Identification and biosynthesis of N<sup>1</sup>,N<sup>9</sup>-bis (glutathionyl) aminopropylcadaverine (homotrypanothione) in *Trypanosoma cruzi*. *Eur. J. Biochem.* 79, 525-532.

150. Haider, N., Eschbach, M., de Souza Dias, S., Gilberger, T., Walter, T. D., and Luersen, K. (2005) The spermidine synthase of the malaria parasite *Plasmodium falciparum*: Molecular and biochemical characterisation of the polyamine synthesis enzyme. *Mol. Biochem. Parasitol.* 142, 224–236.
151. Muller, S., Da' dara, A., Luersen, K., Wrenger, C., Das Gupta, R., Madhubala, R., and Walter, R. D. (2000) In the Human Malaria Parasite *Plasmodium falciparum*, Polyamines are synthesized by a Bifunctional Ornithine decarboxylase, S-Adenosylmethionine decarboxylase. *J. Biol. Chem.* 275, 8097-8102.
152. Wrenger, C., Luersen, K., Krause, T., Muller, S., and Walter, R. D. (2001) The *Plasmodium falciparum* Bifunctional Ornithine Decarboxylase, S-Adenosylmethionine Decarboxylase, enables a well balanced Polyamine Synthesis without Domain-Domain interaction. *J. Biol. Chem.* 276, 29651-29656.
153. Singh, S., Puri, S. K., Singh, S. K., Srivastava, R., Gupta, R. C., and Pandey, V. C. (1997) Characterization of simian malarial parasite (*Plasmodium knowlesi*)-induced putrescine transport in rhesus monkey erythrocytes. A novel putrescine conjugate arrests *in vitro* growth of simian malarial parasite (*Plasmodium knowlesi*) and cures multidrug resistant murine malaria (*Plasmodium yoelii*) infection *in vivo*. *J. Biol. Chem.* 272, 13506-13511.
154. Niemand, J., Louw, A. I., Kirk, K., and Birkholtz, L. (2012) Polyamine uptake by the intraerythrocytic malaria parasite, *Plasmodium falciparum*. *Int. J. Parasitol.* 42, 921-929.
155. Palmer, A. J., and Wallace, H. M. (2010) The polyamine transport system as a target for anticancer drug development. *Amino Acids.* 38, 415-422.
156. Casero, R. A., and Pegg, A. (2009) Polyamine catabolism and disease. *Biochem. J.* 421, 232-338.
157. Shi, W., Ting, L. M., and Kicska, G. A. (2004) *Plasmodium falciparum* purine nucleoside phosphorylase: crystal structures, immucillin inhibitors, and dual catalytic function. *J. Biol. Chem.* 279, 18103-18106.
158. Ting, L. M., Shi, W., Lewandowicz, A., Singh, V., Mwakingwe, A., Birck, M. R., Ringia, E. A., Bench, G., Madrid, D. C., Tyler, P. C., Evans, G. B., Furneaux, R. H., Schramm, V. L., and Kim, K. (2005) Targeting a novel *Plasmodium falciparum* purine recycling pathway with specific immucillins. *J. Biol. Chem.* 280, 9547-9554.
159. Assaraf, Y. G., Golenser, J., Spira, D. T., and Bachrach, U. (1984) Polyamine levels and the activity of their biosynthetic enzymes in human erythrocytes infected with the malarial parasite, *Plasmodium falciparum*. *Biochem. J.* 222, 815-819.
160. van Brummelen, A. C., Olszewski, K. L., Wilinski, D., Llinas, M. I., Louw, A. I., and Birkholtz, L. (2008) Co-Inhibition of *Plasmodium falciparum* S-Adenosylmethionine Decarboxylase/Ornithine Decarboxylase reveals Perturbation-Specific compensatory Mechanisms by Transcriptome, Proteome and Metabolome Analysis. *J. Biol. Chem.* 284, 4635-4646.

161. Reeksting, S. (2009) Metabolomic analyses of the malaria parasite after inhibition of polyamine biosynthesis. Thesis, University of Pretoria.
162. Das Gupta, R., Krause-Ihle, T., Bergmann, B., Müller, I. B., Khomut, A. R., Müller, S., Walter, R. D., and Lüersen, K. (2005) 1-Aminoxy-3-Aminopropane and Derivatives Have an Antiproliferative Effect on Cultured *Plasmodium falciparum* by Decreasing Intracellular Polyamine Concentrations Antimicrob. Agents Chemother. 49, 2857–2864.
163. Metcalf, B. W., Bey, P., Danzin, C., Jung, M. J., Casara, P. L., and Vevert, J. P. (1978) Catalytic irreversible inhibition of mammalian ornithine decarboxylase by substrate and product analogues. J. Am. Chem. Soc. 100, 2551-2552.
164. Van Nieuwenhove, S., Schechter, P. J., Declercq, J., Bone, G., Burke, J., and Sjoerdsma, A. (1985) Treatment of gambiense sleeping sickness in the Sudan with oral DFMO (DL- $\alpha$ -difluoromethylornithine), an inhibitor of ornithine decarboxylase: first field trial. Trans. Roy. Soc. Trop. Med. Hyg. 79, 692-698.
165. Bacchi, C. J., Nathan, H. C., Hutner, S. H., McCann, P. P., and Sjoerdsma, A. (1980) Polyamine metabolism: a potential therapeutic target in trypanosomes. Science. 210, 332-334.
166. Bitonti, A. J., Dumont, J. A., Bush, T. L., Edwards, M. L., Stemerick, D. M., McCann, P. P., and Sjoerdsma, A. (1989) Bis(benzyl)polyamine analogues inhibit growth of chloroquine resistant human malaria parasites (*Plasmodium falciparum*) *in vitro* and in combination with  $\alpha$ -difluoromethylornithine cure murine malaria. Proc. Natl. Acad. Sci. (USA). 86, 651-655.
167. Bitonti, A. J., McCann, P. P., and Sjoerdsma, A. (1987) *Plasmodium falciparum* and *Plasmodium berghei*: effects of ornithine decarboxylase inhibitors on erythrocytic schizogony. Exp. Parasitol. 64, 237-243.
168. Assaraf, Y. G., Golenser, J., Spira, D. T., Messer, G., and Bachrach, U. (1987) Cytostatic effect of DL- $\alpha$ -difluoromethylornithine against *Plasmodium falciparum* and its reversal by diamines and Spermidine. Parasitol. Res. 73, 313-318.
169. Park, M. H., Wolff, E. C., and Folk, J. E. (1993) Hypusine: It's Post-translational formation in the eukaryotic initiation factor 5A and it's potential in cellular regulation. Biofactors. 4, 95-104.
170. Singh, S., Mukherjee, A., Khomutov, A. R., Persson, L., Heby, O., Chatterjee, M., and Madhubala, R. (2007) Antileishmanial effect of 3-aminoxy-1-aminopropane is due to polyamine depletion. Antimicrob. Agents Chemother. 51, 528-534.
171. Rathaur, S., and Walter, R. D. (1987) *Plasmodium falciparum*: S-Adenosyl-L-methionine decarboxylase Exp. Parasitol. 63, 227-232.
172. Bacchi, C. J., Brun, R., Croft, S. L., Alicea, K., and Bühler, Y. (1996) *In vivo* trypanocidal activities of new S-Adenosylmethionine decarboxylase inhibitors. Antimicrob. Agents Chemother. 40, 1448-1453.

173. Brun, R., Buhler, Y., Sanfmeier, U., Kaminsky, R., Bacchi, C., Ranttendi, D., Lane, S., Croft, S. L., Snowden, D., and Yardley, V. (1996) *In vitro* antitrypanocidal activities of new S-adenosylmethionine decarboxylase inhibitors. *Antimicrob. Agents Chemother.* 40, 1442-1447.
174. Krause, T., Lüersen, K., Wrenger, C., Gilberger, T. W., Müller, S., and Walter, R. D. (2000) The ornithine decarboxylase domain of the bifunctional ornithine decarboxylase/S-adenosylmethionine decarboxylase of *Plasmodium falciparum*: recombinant expression and catalytic properties of two different constructs. *Biochem. J.* 1, 287–292.
175. Shantz, L. M., Stanley, B. A., Secrist, J. A., and Pegg, A. E. (1992) Purification of human S-adenosylmethionine decarboxylase expressed in *Escherichia coli* and use of this protein to investigate the mechanism of inhibition by the irreversible inhibitors, 5'-deoxy-5'-[(3-hydrazinopropyl)methylamino]adenosine and 5'-{[(Z)-4-amino-2-butenyl]methylamino}-5'-deoxyadenosine. *Biochemistry.* 31, 6848-6855.
176. Byers, T. L., Ganem, B., and Pegg, A. E. (1992) Cytostasis induced in L1210 murine leukaemia cells by the S-adenosyl-L-methionine decarboxylase inhibitor 5'-[(Z)-4-amino-2-butenyl]methylamino)-5'-deoxyadenosine may be due to hypusine depletion. *Biochem. J.* 287, 717–724.
177. Wright, P. S., Byers, T. L., Cross-Doersen, D. E., McCann, P. P., and Bitonti, A. J. (1991) Irreversible Inhibition of S-Adenosylmethionine Decarboxylase in *Plasmodium falciparum*-infected erythrocytes: Growth Inhibition *In Vitro*. *Biochem. Pharmacol.* 41, 1713-1718.
178. Becker, J. V., Mtwisha, L., Crampton, B. G., Stoychev, S., van Brummelen, A. C., Reeskting, S., Louw, A. I., Birkholtz, L. M., and Mancama, D. T. (2010) *Plasmodium falciparum* Spermidine synthase inhibition results in unique perturbation-specific effects observed on transcript, protein and metabolite levels. *B. C. Genomics.* 11, 235.
179. Wu, H., Min, J., Ikeguchi, Y., Zeng, H., Dong, A., Loppnau, P., Pegg, A., and Plotnikov, A. N. (2007) Structure and mechanism of Spermidine Synthases. *Biochemistry.* 46, 8331-8339.
180. Shirahata, A., Takashi, N., Beppu, T., Hosoda, H., and Samejima, K. (1993) Effects of inhibitors of spermidine synthase and spermine synthase on polyamine synthesis in rat tissues. *Biochemical. Pharmacol.* 45, 1897-1903.
181. Niemand, J. (2011) Biochemical characterisation of putrescine and spermidine uptake as a potential therapeutic target against the human malaria parasite, *Plasmodium falciparum*. Thesis, University of Pretoria.
182. Shirahata, A., Morohohi, T., Fukai, M., Akatsu, S., and Samejima, K. (1991) Putrescine or spermidine binding site of aminopropyltransferases and competitive inhibitors. *Biochem. Pharmacol.* 41, 205-512.

183. Müller, I. B., Das Gupta, R., Lüersen, K., Wrenger, C., and Walter, R. D. (2008) Assessing polyamine metabolism of *Plasmodium falciparum*, as chemotherapeutic target Mol. Biochem. Parasitol. 1016.
184. Dufe, V. T., Qui, W., Müller, I. B., Hui, R., Walter, R. D., and Al-Karaghadi, S. (2007) Crystal structure of *Plasmodium falciparum*, Spermidine synthase in Complex with the Substrate Decarboxylated S-Adenosylmethionine and the potent inhibitors 4-MCHA and AdoDATO. J. Mol. Biol. 373, 167-177.
185. Burger, P. B., Birkholtz, L., Joubert, F., Haider, N., Walter, R. D., and Louw, A. I. (2007) Structural and mechanistic insights into the action of *Plasmodium falciparum* Spermidine Synthase. Bioorg. Med. Chem. 15, 1628-1637.
186. Bitonti, A. J., Kelly, S. E., and McCann, P. P. (1984) Characterization of Spermidine synthase from *Trypanosoma brucei brucei*. Mol. Biochem. Parasitol. 13, 21-28.
187. Casero, R. A., and Woster, P. M. (2009) Recent advances in the development of polyamine analogues as antitumor agents. J. Med. Chem. 52, 4551-4573.
188. Das, B., Gupta, R., and Madhubala, R. (1995) Combined action of inhibitors of S-adenosylmethionine decarboxylase with an antimalarial drug, chloroquine, on *Plasmodium falciparum*. J. Eukaryot. Microbiol. 44, 12-17.
189. Clark, K., Niemand, J., Reeksting, S., Smit, S., van Brummelen, A. C., Williams, M., Louw, A. I., and Birkholtz, L. (2009) Functional consequences of perturbing polyamine metabolism in the malaria parasite, *Plasmodium falciparum*. Amino Acids. 10.
190. Klenke, B., Barret, M. P., Brun, R., and Gilbert, I. H. (2003) Antiplasmodial activity of a series of 1,3,5-triazine substituted polyamines. J. Antimicrob. Chemother. 52, 290-293.
191. Labadie, G. R., Choi, S. R., and Avery, M. A. (2004) Diamine derivatives with antiparasitic activities. Bioorg. Med. Chem. Lett. 14, 615-619.
192. Williams, M., Sprenger, J., Human, E., Al-Karadaghi, S., Persson, L., Louw, A. I., and Birkholtz, L. (2011) Biochemical Characterization and Novel Classification of Monofunctional S-Adenosylmethionine Decarboxylase of *Plasmodium falciparum*. Mol. Biol. Parasitol. 180, 17-26.
193. Bale, S., Lopez, M. M., Makhatadze, G. I., Fang, Q., Pegg, A. E., and Ealick, S. E. (2008) Structural basis for putrescine activation of human S-adenosylmethionine decarboxylase. Biochemistry 47, 13404-13417.
194. Wells, G. A., Birkholtz, L., Joubert, F., Walter, R. D., and Louw, A. I. (2006) Novel properties of malarial S-adenosylmethionine decarboxylase as revealed by structural modelling. J. Mol. Graph. Model. 24, 307-318.
195. Birkholtz, L., Wrenger, C., Joubert, F., Wells, G. A., Walter, R. D., and Louw, A. (2004) Parasite-specific inserts in the bifunctional S-adenosylmethionine



- decarboxylase/ornithine decarboxylase of *Plasmodium falciparum* modulate catalytic activities and domain interactions. *Biochem. J.* 15, 439-448.
196. Roux, S. (2006) Modulation of functional properties of bifunctional Sadenosylmethionine decarboxylase/ornithine decarboxylase of *Plasmodium falciparum* by structural motifs in parasite-specific inserts. Thesis, University of Pretoria.
  197. Gilberger, T. W., Schirmer, R. H., Walter, R. D., and Muller, S. (2000) Deletion of the parasite-specific insertions and mutation of the catalytic triad in glutathione reductase from chloroquin-sensitive *Plasmodium falciparum* 3D7. *Mol. Biochem. Parasitol.* 107, 169-179.
  198. Luersen, K., Walter, R. D., and Muller, S. (1999) The putative  $\gamma$ -glutamylcysteine synthetase from *Plasmodium falciparum* contains large insertions and a variable tandem repeat. *Mol. Biochem. Parasitol.* 98, 131-142.
  199. Pizzi, E., and Frontali, C. (2000) Divergence of Noncoding Sequences and of inserts Encoding Nonglobular Domains at a Genomic Region Well Conserved in *Plasmodia*. *J. Mol. Evol.* 50, 474-480.
  200. Pizzi, E., and Frontali, C. (2001) Low-Complexity regions in *Plasmodium falciparum* proteins. *Genome Res.* 11, 218-229.
  201. Zilversmit, M. M., Volkman, S. K., DePristo, M. A., Wirth, D. F., Awadalla, P., and Hartl, D. L. (2010) Low-Complexity Regions in *Plasmodium falciparum*: Missing Links in the Evolution of an Extreme Genome. *Mol. Biol. Evol.* 27, 2198-2209.
  202. Yuvaniyama, J., Chitnumsub, P., Kamchonwongpaisan, S., Vanichtanankul, J., Sirawaraporn, W., Taylor, P., Walkinshaw, M. D., and Yuthavong, Y. (2003) Insights into antifolate resistance from antimalarial DHFR-TS structures. *Nature Struct. Biol.* 10, 357-365.
  203. Birkholtz, L., Joubert, F., Neitz, A. W. H., and Louw, A. I. (2003) Comparative properties of a three-dimensional model of *Plasmodium falciparum* ornithine decarboxylase. *Proteins.* 50, 464-473.
  204. Williams, M., Louw, A. I., and Birkholtz, L. (2007) Deletion mutagenesis of large areas in *Plasmodium falciparum* genes: a comparative study. *Malar. J.* 6.
  205. Smit, S. (2010) Functional consequences of the inhibition of malaria S-adenosylmethionine decarboxylase as a key regulator of polyamine and methionine metabolism. Thesis, University of Pretoria.
  206. Niemand, J. (2007) A phage display of interacting peptide binding partners of malarial S-adenosylmethionine Decarboxylase/ Ornithine Decarboxylase. Thesis, University of Pretoria.



207. Williams, M. (2011) Biochemical and structural characterisation of novel drug targets regulating polyamine biosynthesis in the human malaria parasite, *Plasmodium falciparum*. Thesis, University of Pretoria.
208. Sprenger, J. (2010) Structural studies on S-adenosylmethionine decarboxylase from *Plasmodium falciparum*. Thesis, Universität Potsdam.
209. Shallom, S., Zhang, K., Jiang, L., and Rathod, K. R. (1999) Essential Protein-Protein Interactions between *Plasmodium falciparum* Thymidylate Synthase and Dihydrofolate Reductase domains. *J. Biol. Chem.* 274, 37781-37786.
210. Luft, J. R., and De Titta, G. T. (2003) A deliberate approach to screening or initial crystallisation conditions of biological macromolecules. *J. Struc. Biol.* 142, 170-179.
211. Ekstrom, J. L., Mathews, I. I., Stanley, B. A., Pegg, A. E., and Ealick, S. E. (1999) The crystal structure of human S-adenosylmethionine decarboxylase at 2.25 Å resolution reveals a novel fold. *Structure.* 7, 583-595.
212. Almrud, J. J., Oliveira, M. A., Kern, A. D., Grishin, N. V., Phillips, M. A., and Hackert, M. L. (2000) Crystal structure of human ornithine decarboxylase at 2.1 Å resolution: Structural insights to antizyme binding. *J. Mol. Biol.* 295, 7-16.
213. Bale, S., and Ealick, S. E. (2010) Structural Biology of S-adenosylmethionine decarboxylase. *Amino Acids.* 2, 451-460.
214. Bennett, E. M., Ekstrom, J. L., Pegg, A. E., and Ealick, S. E. (2002) Monomeric S-Adenosylmethionine Decarboxylase from Plants Provides an Alternative to Putrescine Stimulation. *Biochemistry.* 41, 14509-14517.
215. Clyne, T., Kinch, L. N., and Phillips, M. A. (2002) Putrescine Activation of *Trypanosoma cruzi* S-Adenosylmethionine Decarboxylase. *Biochem.* 41, 13207-13216.
216. Jackson, L. K., Goldsmith, E. J., and Phillips, M. A. (2003) X-ray Structure Determination of *Trypanosoma brucei* Ornithine Decarboxylase Bound to d-Ornithine and to G418: Insights into substrate binding and ODC conformational flexibility. *J. Biol. Chem.* 278, 22037-22043.
217. Xiong, H., Stanley, B. A., and Pegg, A. E. (1999) Role of Cysteine-82 in the Catalytic Mechanism of Human S-Adenosylmethionine Decarboxylase. *Biochemistry.* 38, 2462-2470.
218. Stanley, B. A., Pegg, A. E., and Holm, I. (1989) Site of pyruvate formation and processing of mammalian S-adenosylmethionine decarboxylase proenzyme. *J. Biol. Chem.* 264, 21073-21079.
219. Stanley, B. A., and Pegg, A. E. (1991) Amino acid residues necessary for putrescine stimulation of human S-adenosylmethionine decarboxylase proenzyme processing and catalytic activity. *J. Biol. Chem.* 266, 18502-18506.

220. Ekstrom, J. L., Tolbert, W. D., Xiong, H., Pegg, A. E., and Ealick, S. E. (2001) Structure of a Human S-Adenosylmethionine Decarboxylase Self-Processing Ester Intermediate and Mechanism of Putrescine Stimulation of Processing As Revealed by the H243A Mutant. *Biochemistry*. 40, 9495-9504.
221. Yuthavong, Y., Yuvaniyama, J., Chitnumsub, P., Vanichtanankul, J., Chusacultachai, S., Tarnchompoo, B., Vilaivan, T., and Kamchonwongpaisan, S. (2005) Malarial (*Plasmodium falciparum*) dihydrofolate reductase-thymidylate synthase: structural basis for antifolate resistance and development of effective inhibitors. *Parasitol. Res.* 130, 249-259.
222. DePristo, M. A., Zilversmit, M. M., and Hartl, D. L. (2006) On the Abundance, amino acid composition, and evolutionary dynamics of Low-complexity Regions in Proteins. *Gene*. 378, 19-30.
223. Feng, Z., Zhang, X., Han, P., Arora, N., Anders, R., and Norton, R. S. (2006) Abundance of Intrinsically Unstructured Proteins in *Plasmodium falciparum* and other Apicomplexan Parasite Proteomes. *Mol. Biochem. Parasitol.* 150, 256-267.
224. Altschul, S. F., Gish, W., Miller, W., Myers, E. W., and Lipman, D. J. (1990) Basic local alignment search tool. *J. Mol. Biol.* 215, 403-410.
225. Wootton, J. C., and Federhen, S. (1993) Statistics of local complexity in amino acid sequences and sequence databases. *Comput. Chem.* 17, 149-163.
226. Dosztanyi, Z., Czismok, V., Tompa, P., and Simon, I. (2005) IUPred: web server for the prediction of intrinsically unstructured regions of proteins based on estimated energy content. *Bioinformatics*. 21.
227. Thomas, P. D., and Dill, K. A. (1996) An iterative method for extracting energy-like quantities from protein structures. *PNAS Early Edition*. 93.
228. Angov, E., Hillier, C. J., Kincaid, R. L., and Lyon, J. A. (2008) Heterologous Protein Expression Is Enhanced by Harmonizing the Codon Usage Frequencies of the Target Gene with those of the Expression Host. *PLoS One*. 3, e2189.
229. Birkholtz, L., Blatch, G., Coetzer, T. L., Hoppe, H. C., Human, E., Morris, E. J., Ngcete, Z., Oldfield, L., Roth, R., Shonai, A., Stephens, L., and Louw, A. I. (2008) Heterologous expression of *Plasmodial* proteins for structural studies and functional annotation. *Malar. J.* 197.
230. Sladek, F. M., Zhong, W., Lai, E., and Darnell, J. E. (1990) Liver-enhanced transcription factor HNF-1 is a novel member of the steroid hormone receptor superfamily. *Genes Dev.* 4, 2353-2365.
231. Dallas-Yang, Q., Jiang, G., and Sladek, F. M. (1998) Avoiding false positives in Colony PCR. *Biotechniques*. 34, 580-581.

232. Ben-Haim, D., Dreyer, F., and Peper, K. (1975) Acetylcholine receptor: Modification of synaptic gating mechanism after treatment with a disulfide bond reducing agent. *Pflugers Arch.* 355, 19-26.
233. Ashani, Y., and Catravas, G. N. (1980) Highly reactive impurities in Triton X-100 and Brij 35: partial characterization and removal. *Anal. Biochem.* 109, 55-62.
234. Bradford, M. M. (1967) A Rapid and Sensitive Method for the Quantitation of Microgram Quantities of Protein Utilizing the Principle of Protein-Dye Binding. *Anal. Biochem.* 72, 248-254
235. Laemmli, U. K. (1970) Cleavage of structural proteins during assembly of the head of bacteriophage T4. *Nature.* 227, 680–685.
236. Chrambach, A., Reisfeld, R. A., Wyckoff, M., and Zaccari, J. (1967) A procedure for rapid and sensitive staining of protein fractionated by polyacrylamide gel electrophoresis. *Anal. Biochem.* 20, 150-154.
237. Pegg, A. E. (1986) Recent advances in the biochemistry of polyamines in eukaryotes. *Biochem. J.* 234, 246-262.
238. Greenfield, N. J. (2006) Using circular dichroism spectra to estimate protein secondary structure. *Nature Prot.* 1, 2876-2890.
239. Tainer, J. A., and Rambo, R. P. (2011) Characterizing Flexible and Intrinsically Unstructured Biological Macromolecules by SAS Using the Porod-Debye Law. *Biopolymers.* 95, 559-571.
240. Vedadi, M., Niesen, F. H., Allali-Hassani, A., Fedorov, O. Y., Finerty, P. J., Wasney, G. A., Yeung, R., Arrowsmith, C., Ball, L. J., Berglund, H., Hui, R., Marsden, B. D., Nordlund, P., Sundstrom, M., Weigelt, J., and Edwards, A. M. (2006) Chemical screening methods to identify ligands that promote protein stability, protein crystallization, and structure determination. *Proc. Nat. Aca.Sci. (USA).* 103, 15835-15840.
241. Niesen, F. H., Berglund, H., and Vedadi, M. (2007) The use of differential scanning fluorimetry to detect ligand interactions that promote protein stability. *Nat Protoc.* 2, 2212 - 2221.
242. Bennet, E. M., Ekstrom, J. L., Pegg, A. E., and Ealick, S. E. (2002) Monomeric S-Adenosylmethionine Decarboxylase from Plants Provides an Alternative to Putrescine Stimulation. *Biochemistry.* 41, 14509-14517.
243. Dalby, A. R. (2009) A Comparative Proteomic Analysis of the Simple Amino Acid Repeat Distributions in *Plasmodia* Reveals Linage Specific Amino Acid Selection. *PLoS One.* 4, e6231.
244. Muralidharan, V., Oksman, A., Iwamoto, M., Wandless, T. J., and Goldberg, D. E. (2011) Asparagine repeat function in a *Plasmodium falciparum* protein assessed via a regulatable fluorescent affinity tag. *PNAS Early Edition.* 108, 4411-4416.

245. Dosztányi, Z., and Tompa, P. (2008) Prediction of Protein Disorder, Structural Proteomics (Kobe, B., Guss, M., and Huber, T., Eds.), pp 103-115, Humana Press.
246. Villaverde, A., and Carrio, M. M. (2003) Protein aggregation in recombinant bacteria: biological role of inclusion bodies. *Biotechnol. Lett.* 25, 1385–1395.
247. Mogk, A., Mayer, M. P., and Deuerling, E. (2002) Mechanisms of protein folding: molecular chaperones and their application in biotechnology. *B. C.* 3, 807–814.
248. Rambo, R. P., and Tainer, J. A. (2011) Characterizing Flexible and Intrinsically Unstructured Biological Macromolecules by SAS Using the Porod-Debye Law. *Biopolym.* 95, 559-571.
249. Structural Genomics Consortium, Architecture et Fonction des Macromolécules Biologiques, Berkeley Structural Genomics Center, China Structural Genomics Consortium, Integrated Center for Structure and Function Innovation, Israel Structural Proteomics Center, Joint Center for Structural Genomics, Midwest Center for Structural Genomics, New York Structural GenomiX Research Center for Structural Genomics, Northeast Structural Genomics Consortium, Oxford Protein Production Facility, Protein Sample Production Facility, M. D. C. f. M. M., and SPINE2-Complexes, R. S. G. P. I. (2008) Protein production and purification. *Nat. Methods.* 5, 135-146.
250. Burmeister, G. E., Ming, X., Chakrabarty, T., Cooke, R., and Selvin, P. R. (1999) A Comparison between the Sulfhydryl Reductants Tris(2-carboxyethyl)phosphine and Dithiothreitol for Use in Protein Biochemistry. *Anal. Biochem.* 273, 73-80.
251. Li, X., Han, Y., and Pan, X. M. (2001) Cysteine-25 of Adenylate Kinase reacts with Dithiothreitol to form an Adduct upon aging of the enzyme. *FEBS Letters.* 507, 169-173.
252. Chayen, N. E., and Saridakis, E. (2008) Protein crystallisation: from purified protein to diffraction-quality crystal. *Nat. Methods.* 5, 147-153.
253. Derewenda, Z. S. (2004) Rational Protein Crystallization by Mutational Surface Engineering. *Structure.* 12, 529-535.
254. Tompa, P. (2003) Intrinsically unstructured proteins evolve by repeat expansion. *Bioassays.* 25, 847-855.
255. Simon, M., and Hancock, J. H. (2009) Tandem and Cystic Amino Acid Repeats Accumulate in Disordered Regions of Proteins. *Genome Biol.* 10, Article 59.
256. Brown, C. J., Johnson, A. K., Dunker, A. K., and Daughdrill, G. W. (2011) Evolution and disorder. *Curr. Opin. Struct. Biol.* 21, 441- 446.
257. Aravind, L., Lyer, L. M., Wellems, T. E., and Miller, L. H. (2003) *Plasmodium* biology genomic gleanings. *Cell.* 115, 771-785.
258. Singh, G. P., Chanda, B. R., Bhattacharya, A., Akhouri, R. R., Singh, S. K., and Sharma, A. (2004) Hyper-Expansion of Asparagines Correlates with an Abundance of

- Proteins with Prion-like Domains in *Plasmodium falciparum*. Mol. Biochem. Parasitol. 137, 307-319.
259. Frontali, C. (1994) Genome plasticity in *Plasmodium* Genetica. 94, 91-100.
  260. Wright, P. E., and Dyson, H. J. (1999) Intrinsically unstructured proteins: Re-assessing the protein structure-function paradigm. J. Mol. Biol. 293, 321-331.
  261. Wootton, J. C. (1994) Non-globular domains in protein sequences: automated segmentation using complexity measures. J. Comput. Chem. 18, 269-285.
  262. de Beer, T. A. P., Louw, A. I., and Joubert, F. (2006) Elucidation of sulfadoxine resistance with structural models of the bifunctional *Plasmodium falciparum* dihydropterin pyrophosphokinase–dihydropteroate synthase. Bioorg. Med. Chem. 14, 4433-4443.
  263. Romero, P., Obradovic, Z., Kissinger, C., Villafranca, J. E., and Dunker, A. K. (1997) Identifying disordered regions in proteins from amino acid sequence. The 1997 IEEE International conference on neural networks Proc. 1, 90-95.
  264. Peti, W., and Page, R. (2007) Strategies to maximize heterologous protein expression in *Escherichia coli* with minimal cost. Protein Expr. Purif. 51, 1-10.
  265. Linding, R., Jensen, L. J., Diella, F., Bork, P., Gibson, T. J., and Russell, R. B. (2003) Protein Disorder Prediction: Implications for Structural Proteomics. Structure. 11, 1453-1459.
  266. Chaianantakul, N., Sirawaraporn, R., and Sirawaraporn, W. (2013) Insights into the role of the junctional region of *Plasmodium falciparum* dihydrofolate reductase-thymidylate synthase. Malar. J. 12, 91-104.
  267. Klein, M. M., Gittis, A. G., Su, H., Makobongo, M. O., Moore, J. M., Singh, S., Miller, L. H., and Garboczi, D. N. (2008) The Cysteine-Rich Interdomain Region from the Highly Variable *Plasmodium falciparum* Erythrocyte Membrane Protein-1 Exhibits a Conserved Structure. PLOS Path. . 4, 1.
  268. Byers, T. L., Bush, T. L., McCann, P. P., and Bitonti, A. J. (1991) Antitrypanosomal Effects of Polyamine Biosynthesis Inhibitors correlate with Increases in *Trypanosoma brucei brucei* S-adenosyl-L-methionine. Biochem. J. 274, 527-533.
  269. Yarlett, N., Quamina, A., and Bacchi, C. (1991) Protein methylases in *Trypanosoma brucei brucei*: activities and response to DL-a-difluoromethylornithine. J. Gen. Microbiol. 137, 717-724.
  270. Willert, E. K., and Phillips, M. A. (2008) Regulated expression of an essential allosteric activator of polyamine biosynthesis in African trypanosomes. PLoS Pathog. 4.
  271. Wallace, H. M., Fraser, A. V., and Hughes, A. (2003) A perspective of polyamine metabolism. Biochem. J. . 376, 1–14.

272. Barker, R. H., Hanlan, L., Hirth, B., Celatka, C. A., Fitzpatrick, R., Xiang, Y., Willert, E. K., Phillips, M. A., Kaiser, M., Bacchi, C. Y., Rodriguez, A., Yarlett, N., Klinger, J. D., and Sybertz, E. (2009) Novel S-adenosylmethionine Decarboxylase Inhibitors for the treatment of Human African Trypanosomiasis. *Antimicrob. Agents Chemother.* 53, 2052-2058.
273. Bacchi, C. J., Barker, R. H., Rodriguez, A., Hirth, B., Rattendi, D., Yarlett, N., Hendrick, C. L., and Sybertz, E. (2009) Trypanocidal Activity of 8-Methyl-5'-[[Z]-4-Aminobut-2-enyl]-(methylamino)} Adenosine (Genz 644131), an Adenosylmethionine Decarboxylase Inhibitor. *Antimicrob. Agents Chemother.* 53, 3269-3271.
274. Hirth, B., Barker, R. H., Celatka, C. A., Klinger, J. D., Liu, H., Nare, B., Nijjar, A., Phillips, M. A., Sybertz, E., Willert, E. K., and Xiang, Y. (2009) Discovery of new S-adenosylmethionine decarboxylase inhibitors for the treatment of Human African Trypanosomiasis (HAT). *Bioorg. Med. Chem. Lett.* 19, 2916-2919.
275. Kitz, R., and Wilson, I. B. (1962) Esters of Methanesulfonic Acid as Irreversible Inhibitors of Acetylcholinesterase. *J. Biol. Chem.* 237, 3245-3249.
276. Verlinden, B. K., Niemand, J., Snyman, J., Sharma, S. K., Beattie, R. J., Woster, P. M., and Birkholtz, L. (2011) Discovery of Novel Alkylated (bis)Urea and (bis)Thiourea Polyamine Analogues with Potent Antimalarial Activities. *J. Med. Chem.* 54, 6624-6633.
277. Grobusch, M. P., Hanscheid, T., Gobels, K., Slevogt, H., Zoller, T., Rogler, G., and Teichmann, D. (1998) Comparison of three antigen detection tests for diagnosis and follow-up of *falciparum* malaria in travellers returning to Berlin, Germany. *Parasitol. Res.* 89, 354-357.
278. Niemand, J., Burger, P., Verlinden, B. K., Reader, J., Joubert, A. M., Kaiser, A., Louw, A. I., Kirk, K., Phantsiel, O., and Birkholtz, L. (2013) Anthracene-Polyamine Conjugates Inhibit In Vitro Proliferation of Intraerythrocytic *Plasmodium falciparum* Parasites *Antimicrob. Agents Chemother.* 57, 2874-2877.
279. Stjernborg, L., and Persson, L. (1993) Stabilization of S-adenosylmethionine decarboxylase by aminoguanidine. *Biochem. Pharmacol.* 45, 1174-1176.
280. Lee, P., Ye, Z., Van Dyke, K., and Kirk, R. G. (1988) X-ray microanalysis of *Plasmodium falciparum* and infected red blood cells: effects of qinghaosu and chloroquine on potassium, sodium, and phosphorus composition. *Am. J. Trop. Med. Hyg.* 39, 157 - 165.
281. Trang, D. T. X., Huy, N. T., Kariu, T., Tajima, K., and Kamei, K. (2004) One-step concentration of malarial parasite-infected red blood cells and removal of contaminating white blood cells. *Malar. J.* 3.
282. Teng, R. W., Junankar, P. R., Bubb, W. A., Rae, C., Mercier, P., and Kirk, K. (2009) Metabolite profiling of the intraerythrocytic malaria parasite *Plasmodium falciparum* by H-1 NMR spectroscopy. *NMR Biomed.* 22, 292-302.



283. Saliba, K. J., Horner, H. A., and Kirk, K. (1998) Transport and metabolism of the essential vitamin pantothenic acid in human erythrocytes infected with the malaria parasite *Plasmodium falciparum*. *J. Biol. Chem.* 273, 10190-10195.
284. Grobler, A., Kotzé, A., and Du Plessis, J. (2008) The design of a skin-friendly carrier for cosmetic compounds using Pheroid™ technology. *Allured*. Ed. Johann Wiechers, 283-311.
285. Steyn, J. D., Wiesner, L., du Plessis, L. H., Grobler, A. F., Smith, P. J., Chan, W.-C., Haynes, R. K., and Kotzé, A. F. (2011) Absorption of the novel artemisinin derivatives artemisone and artemiside: Potential application of Pheroid™ technology. *Int. J. Pharm.* 414, 260-266.
286. Wiechers, J. W. (2008) *Science and Applications of Skin Delivery Systems*
287. MacDonald, R. C., MacDonald, R. I., Menco, B. P., Takeshita, K., Subbarao, N. K., and Hu, L. R. (1991) Small-volume extrusion apparatus for preparation of large, unilamellar vesicles. *Biochem. Biophys. Acta.* 1061, 297-303.
288. Urbán, P., Estelrich, J., Cortes, A., and Fernandez-Busquets, X. (2011a) A nanovector with complete discrimination for targeted delivery to *Plasmodium falciparum*-infected versus non-infected red blood cells *in vitro*. *J. Control Release.* 151, 202-211.
289. Tolbert, W. D., Ekstrom, J. L., Mathews, I. I., Secrist, J. A., Kapoor, P., Pegg, A. E., and Ealick, S. E. (2001) The structural basis for substrate specificity and inhibition of human S-adenosylmethionine decarboxylase. *Biochemistry.* 40, 9484-9494.
290. McCloskey, D. E., Bale, S., Secrist, J. A., Tiwari, A., Moss, T. H., Valiyaveetil, J., Brooks, W. H., Guida, W. C., Pegg, A. E., and Ealick, S. E. (2009) New insights into the design of inhibitors of human S-adenosylmethionine decarboxylase: studies of adenine C(8) substitution in structural analogues of S-adenosylmethionine. *J. Med. Chem.* 52, 1388–1407.
291. Bitonti, A. J., Byers, T. L., Bush, T. L., Casara, P. J., Bacchi, C. J., Clarkson, A. B. J., McCann, P. P., and Sjoerdsma, A. (1990) Cure for *Trypanosoma brucei brucei* and *Trypanosoma brucei rhodesiense* infections in mice with an irreversible inhibitor of S-adenosylmethionine decarboxylase. *Antimicrob. Agents Chemother.* 34, 1485-1490.
292. Reyes, P., Rathod, P. K., Sanchez, D. J., Mrema, J. E., Rieckamn, K. H., and Heidrich, H. G. (1982) Enzymes of purine and pyrimidine metabolism from the human malaria parasite, *Plasmodium falciparum*. *Mol. Biochem. Parasitol.* 5, 275–290.
293. Lingelbach, K., and Joiner, K. A. (1998) The parasitophorous vacuole membrane surrounding *Plasmodium* and *Toxoplasma*: an unusual compartment in infected cells. *J. Cell. Sci.* 111, 1467-1475.
294. Vennerstrom, J. L., Arbe-Barnes, S., Brun, R., Charman, S. A., Chiu, F. C. K., Chollet, J., Dong, Y., Dorn, A., Hunziker, D., and Matile, H. (2004) Identification of an antimalarial synthetic trioxolane drug development candidate. *Nature.* 430, 900–904.



295. Orhan, I., Sener, B., Atici, T., Brun, R., Perozzo, R., and Tasdemir, D. (2006) Turkish freshwater and marine macrophyte extracts show *in vitro* antiprotozoal activity and inhibit FabI, a key enzyme of *Plasmodium falciparum* fatty acid biosynthesis. *Phytomed.* 13, 388–393.
296. Hassan, H. F., and Coombs, G. H. (1988) Purine and pyrimidine metabolism in parasitic protozoa. *FEMS Microbiol. Rev.* 54, 47-84.
297. de Koning, H. P., Bridges, D. J., and R.J., B. (2005) Purine and pyrimidine transport in pathogenic protozoa: from biology to therapy. *FEMS Microbiol. Rev.* 29, 987–1020.
298. Maser, P., Sutterlin, C. K., and Kraminsky, R. (1999) A nucleoside transporter from *Trypanosoma brucei* involved in drug resistance. *Science.* 285, 242–244.
299. Goldberg, B., Yarlett, N., Sufrin, J., LLoyd, D., and Bacchi, C. Y. (1997) A unique transporter of S-adenosylmethionine in African Trypanosomes. *FASEB J.* 11, 256-260.
300. Downie, M. J., Kirk, K., and Mamoun, C. B. (2008) Purine salvage pathways in the intraerythrocytic malaria parasite *Plasmodium falciparum*. *Eukaryot. Cell.* 7, 1231-1237.
301. Quashie, N. B., Ranford-Cartwright, L. C., and H.P., d. K. (2008) A comprehensive model of purine uptake by the malaria parasite *Plasmodium falciparum*: identification of four purine transport activities in intraerythrocytic parasites. *Biochem. J.* 411, 287–295.
302. Carter, N. S., Ben Mamoun, C., Liu, W., Silva, E. O., Landfear, S. M., Goldberg, D. E., and Ullman, B. (2000) Isolation and functional characterization of the *PFNT1* nucleoside transporter gene from *Plasmodium falciparum*. *J. Biol. Chem.* 275, 10683 - 10691.
303. Parker, M. D., Hyde, R. J., Yao, S. Y., McRobert, L., Cass, C. E., Young, J. D., McConkey, G. A., and Baldwin, S. (2000) Identification of a nucleoside/nucleobase transporter from *Plasmodium falciparum*, a novel target for anti-malarial chemotherapy. *Biochem. J.* 349, 67 - 75.
304. Maurer, N., Fenske, D. B., and Cullis, P. R. (2011) Developments in liposomal drug delivery systems. *Expert. Opin. Biol. Ther.* 1, 923-947.
305. Forrest, M. L., and Kwon, G. S. (2008) Clinical developments in drug delivery nanotechnology. *Adv. Drug Deliv. Rev.* 60, 861-862.
306. Alving, C. R. (1986) Liposomes as drug carriers in leishmaniasis and malaria. *Parasitol. Today.* 2, 101-107.
307. Armstead, A. L., and Bingyun, L. (2011) Nanomedicine as an emerging approach against intracellular pathogens. *Int. J. Nanomedicine.* 6, 3281–3293.

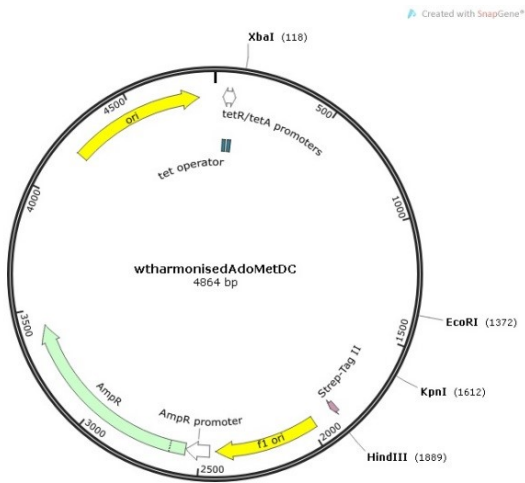
308. Urbán, P., Estelrich, J., Adeva, A., Cortés, A., and Fernández-Busquets, X. (2011b) Study of the efficacy of antimalarial drugs delivered inside targeted immunoliposomal nanovectors. *Nanoscale Res. Lett.* 6, 1-9.
309. Owais, M., Varshney, G. C., Choudhury, A., Chandra, S., and M., G. C. (1995) Chloroquine encapsulated in malaria-infected erythrocyte-specific antibody-bearing liposomes effectively controls chloroquine-resistant *Plasmodium berghei* infections in mice. *Antimicrob. Agents Chemother.* 39, 180-184.
310. Agrawal, A. K., and Gupta, C. M. (2000) Tuftsin-bearing liposomes in treatment of macrophage-based infections. *Adv. Drug Deliv. Rev.* 41, 135–146.
311. Fatumo, S., Plaimas, K., Mallm, J.-P., Schramm, G., Adebisi, E., Oswald, M., Eils, R., and König, R. (2009) Estimating novel potential drug targets of *Plasmodium falciparum* by analysing the metabolic network of knock-out strains *in silico*. *Infect., Gen. Evol.* 9, 351-358.
312. Wells, J. A., and McClendon, C. L. (2007) Reaching for high-hanging fruit in drug discovery at protein-protein interfaces. *Nature.* 450, 1001-1009.
313. Jubb, H., Higuero, A. P., Winter, A., and Blundell, T. L. (2012) Structural biology and drug discovery for protein-protein interactions. *Trends Pharma. Sci.* 33, 241-248.
314. Fivelman, Q. L., Adagu, I. S., and Warhurst, D. C. (2004) Modified Fixed-Ratio Isobologram Method for Studying In Vitro Interactions between Atovaquone and Proguanil or Dihydroartemisinin against Drug-Resistant Strains of *Plasmodium falciparum*. *Antimicrob. Agents Chemother.* 48, 4097-4102.
315. van Schalkwyk, D. A., Priebe, W., and Saliba, K. J. (2008) The Inhibitory Effect of 2-Halo Derivatives of d-Glucose on Glycolysis and on the Proliferation of the Human Malaria Parasite *Plasmodium falciparum*. *J. Pharmacol. Exp. Ther.* 327, 511-517.
316. Bacchi, C. J., Nathan, H. C., Yartlett, N., Goldber, B., McCann, P. P., Bitonti, A. J., and Sjoerdsma, A. (1992) Cure of Murine *Trypanosoma brucei rhodesiense* infections with and S-adenosylmethionine decarboxylase inhibitor *Antimicrob. Agents Chemother.* . 36, 2736-2740.

# Appendices

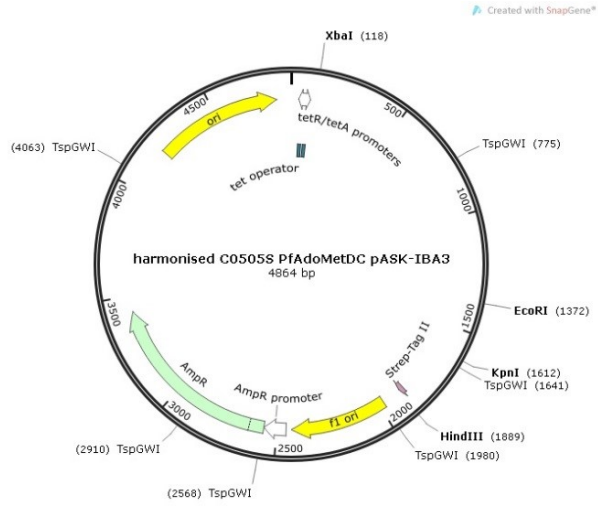
## Appendix 1

Plasmid maps of wild-type, C505S,  $\Delta A3$ ,  $\Delta H$  and  $\Delta A3\Delta H$  *PfAdoMetDC*.

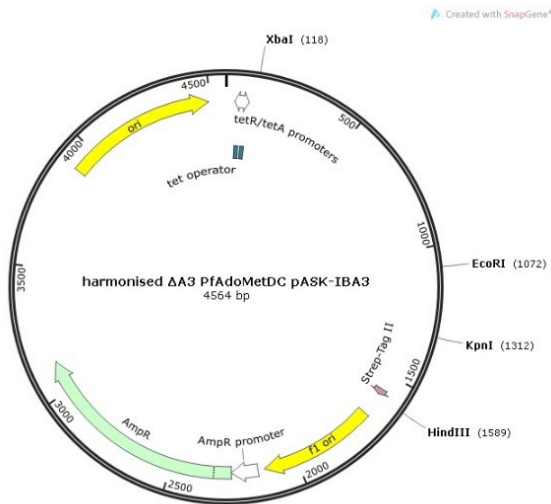
(A)



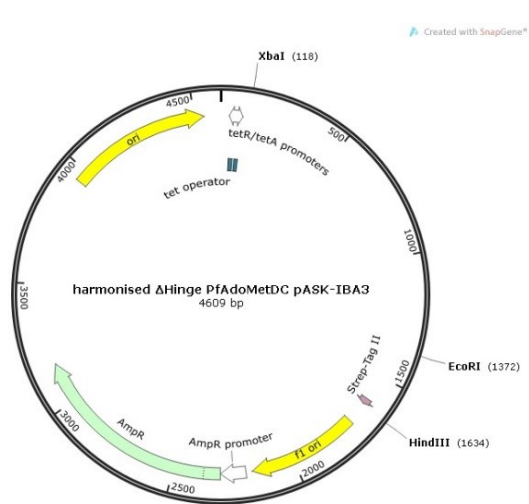
(B)



(C)



(D)



(E)

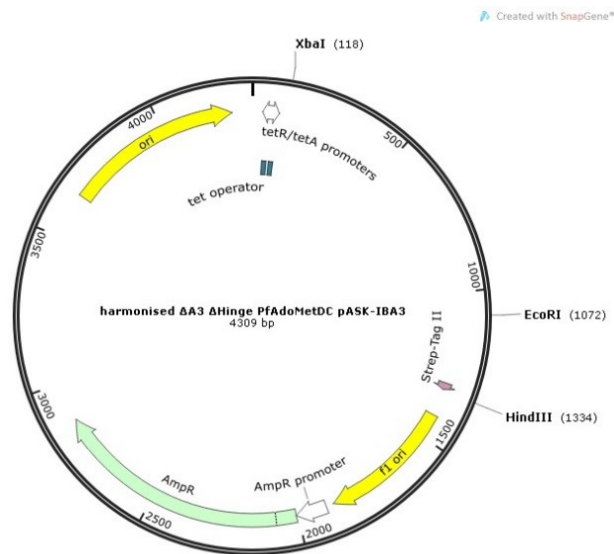


**Figure 1: Plasmid maps of codon wild-type *PfAdoMetDC* constructs used for recombinant expression in the pASK-IBA3 expression vector.** (A) Wild-type *PfAdoMetDC* (572 aa) cloned into pASK-IBA3 with C-terminal *Strep*-tag II. (B) C505S *PfAdoMetDC* (572 aa) cloned into pASK-IBA3 with C-terminal *Strep*-tag II. (C)  $\Delta$ A3 *PfAdoMetDC* (472 aa) cloned into pASK-IBA3 with C-terminal *Strep*-tag II. (D)  $\Delta$ H *PfAdoMetDC* (487 aa) cloned into pASK-IBA3 with C-terminal *Strep*-tag II. (E)  $\Delta$ A3 $\Delta$ H *PfAdoMetDC* (387 aa) cloned into pASK-IBA3 with C-terminal *Strep*-tag II.

## Appendix 2

### PCR products of $\Delta H$ and $\Delta A3\Delta H$ *PfAdoMetDC* recombinant cloning.

For recombinant cloning of  $\Delta H$  and  $\Delta A3\Delta H$ , *PfAdoMetDC* the PCR reaction was performed as described in section 2.2.1. In Figure 2, the respective bands of the PCR products of  $\Delta H$  (~1.5 kb) and  $\Delta A3\Delta H$  *PfAdoMetDC* (~1.2 kb) observed. The correct-sized bands were cut from the gel and the PCR product purified using the Wizard® SV Gel and PCR Clean-up system kit (Promega) and used in subsequent cloning reactions. Following identification of positive clones, the constructs were restriction enzyme mapped and sequenced, as described in Appendix 3 and 4.

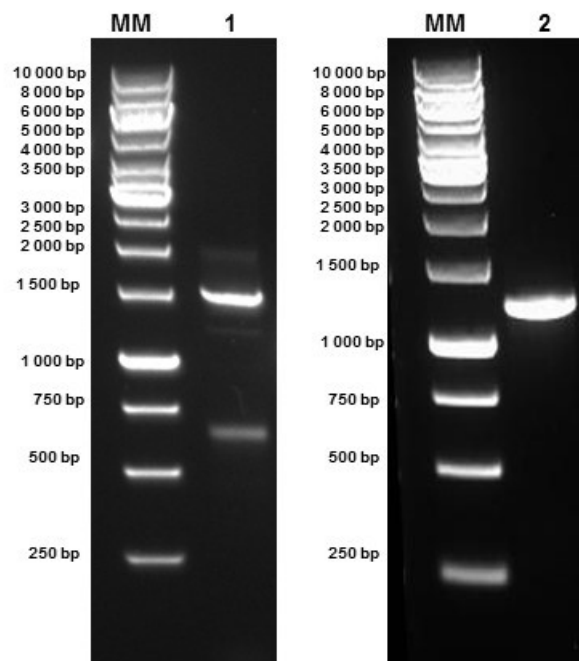


**Figure 2: Optimised PCR amplification of  $\Delta H$  and  $\Delta A3\Delta H$  *PfAdoMetDC* fragments for recombinant cloning into pASK-IBA3.** MM: O'Generuler 1 kbp DNA ladder. Lane 1: ~1461 bp amplified  $\Delta H$  *PfAdoMetDC*. Lane 2: ~1161 bp amplified  $\Delta A3\Delta H$  *PfAdoMetDC*. Bands were analysed on a 1% agarose gel and visualised with GelRed™.

## Appendix 3

### Restriction enzyme mapping of wild-type, C505S, $\Delta A3$ , $\Delta H$ and $\Delta A3\Delta H$ *PfAdoMetDC*.

The five codon wild-type *PfAdoMetDC* constructs in the pASK-IBA3 vector were transformed into heat shock competent *E. coli* DH5 $\alpha$  cells and grown overnight at 37°C on 1% agar plates (1% w/v LB-agar with 100  $\mu$ g/ml amp). A single colony was inoculated into 5 ml LB-Ampicillin and grown for overnight at 37°C with 200rpm rotation. Plasmids were isolated from cell cultures with the Zyppy™ Plasmid Miniprep kit (ZymoResearch, USA), as per manufacturer's instructions. DNA concentration was determined by a NanoDrop® (Agilent technologies) and stored at -20°C.

For restriction enzyme analysis of the *PfAdoMetDC* constructs, 1  $\mu$ g of purified plasmid DNA was 1) linearized with *HindIII* (Promega) and 2) double digested with *HindIII* and *XbaI* (Promega) restriction enzymes in buffer C (Promega) in the presence of 10  $\mu$ g/ $\mu$ l bovine serum albumin (BSA). The digest reaction was incubated for 3 h at 37°C, followed by inactivation at 65°C for 15 min. According to the vector maps in Appendix 1, *HindIII* and *XbaI* digestion removes the full recombinant *PfAdoMetDC* insert to produce two fragments; one of the cut plasmid and one of the *PfAdoMetDC* insert. The digested (1  $\mu$ g) plasmid fragments were run on a 1% Agarose DNA gel at 80V for 90 min Figure appendix 7A. To confirm the deletion of the C-terminal hinge region, 1  $\mu$ g of purified plasmid DNA was digested with *KpnI* and *EcoRI* (New England Biolabs) using NEB buffer 1. The digest reaction was incubated for 3 h at 37°C, followed by heat inactivation at 65°C for 20 min. The digested (1  $\mu$ g) plasmid fragments were run on a 1% Agarose DNA gel at 80V for 90 min Figure 3.

Plasmid restriction enzyme mapping was performed to verify that the correct PCR products were ligated into the recombinant site of the pASK-IBA3 vectors. Using the unique cut sites in the plasmids *XbaI* and *HindIII* (Appendix 1) the entire codon harmonised *PfAdoMetDC* gene fragment including the C-terminal *Strep*-tag II could be removed relating to the size of the cloned product. In Figure 3A, the plasmid linearized without any fragment was observed at 3.2 kb when double digested with *XbaI* and *HindIII* with the respective insert sizes at ~1.8 kb for harmonised and C505S, ~1.5 kb for  $\Delta A3$  and  $\Delta H$  and ~1.2 kb for  $\Delta A3\Delta H$  *PfAdoMetDC*. Furthermore, to confirm removal of the C-terminal hinge region for  $\Delta H$  and  $\Delta A3\Delta H$ , the unique cut site within this region, *KpnI*, in combination with another cut site *EcoRI* was used. For the wild-type, C505S and  $\Delta A3$  constructs the ~240 bp hinge insert was observed, however, for

the  $\Delta H$  and  $\Delta A3\Delta H$  no bands at  $\sim 240$  bp was observed, confirming the removal of this insert (Figure 3B).

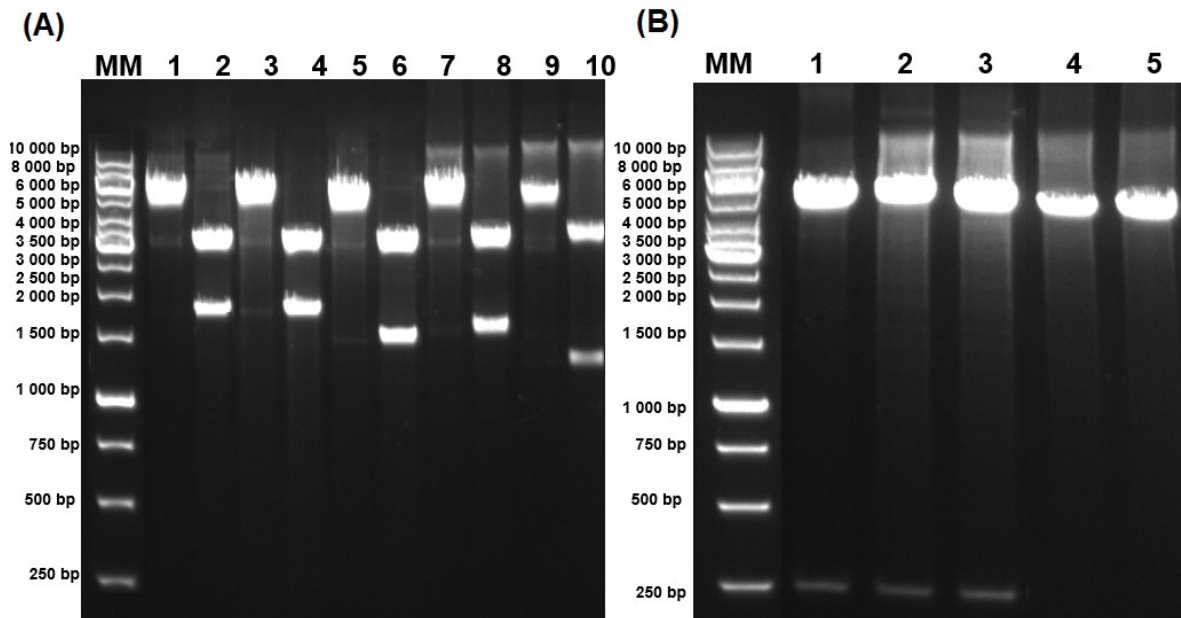


**Figure 3: Restriction enzyme mapping of wild-type, C505S,  $\Delta A3$ ,  $\Delta H$  and  $\Delta A3\Delta H$  *PfAdoMetDC* constructs in pASK-IBA3.** (A) Restriction mapping with XbaI and HindIII. Molecular marker (MM) is a 1 kb ladder. Lane 1: HindIII linearized harmonised *PfAdoMetDC* at  $\sim 4.9$  kb. Lane 2: HindIII and XbaI digested harmonised *PfAdoMetDC* in pASK-IBA3 at  $\sim 3.2$  kb for the plasmid and  $\sim 1.8$  kb for the harmonised *PfAdoMetDC* insert. Lane 3: HindIII linearized C505S *PfAdoMetDC* at  $\sim 4.9$  kb. Lane 4: HindIII and XbaI digested C505S *PfAdoMetDC* in pASK-IBA3 at  $\sim 3.2$  kb for the plasmid and  $\sim 1.8$  kb for the C505S *PfAdoMetDC* insert. Lane 5: HindIII linearized  $\Delta A3$  *PfAdoMetDC* at  $\sim 4.6$  kb. Lane 6: HindIII and XbaI digested *PfAdoMetDC* in pASK-IBA3 at  $\sim 3.2$  kb for the plasmid and  $\sim 1.5$  kb for the  $\Delta A3$  *PfAdoMetDC* insert. Lane 7: HindIII linearized  $\Delta H$  *PfAdoMetDC* at  $\sim 4.6$  kb. Lane 8: HindIII and XbaI digested  $\Delta H$  *PfAdoMetDC* at  $\sim 3.2$  kb for the plasmid and  $\sim 1.5$  kb for the  $\Delta H$  *PfAdoMetDC* insert. Lane 9: HindIII linearized  $\Delta A3\Delta H$  *PfAdoMetDC* at  $\sim 4.3$  kb. Lane 10: HndIII and XbaI digested  $\Delta A3\Delta H$  *PfAdoMetDC* at  $\sim 3.2$  kb for the plasmid and  $\sim 1.2$  kb for the  $\Delta A3\Delta H$  *PfAdoMetDC* insert. (B) Restriction mapping with KpnI and EcoRI. Molecular marker (MM) is a 1 kb ladder. Lane 1: KpnI and EcoRI digested harmonised *PfAdoMetDC* in pASK-IBA3 with a  $\sim 4.9$  kb plasmid and 240 bp hinge insert. Lane 2: KpnI and EcoRI digested C505S *PfAdoMetDC* in pASK-IBA3 with a  $\sim 4.9$  kb plasmid and 240 bp hinge insert. Lane 3: KpnI and EcoRI digested  $\Delta A3$  *PfAdoMetDC* in pASK-IBA3 with a  $\sim 4.6$  kb plasmid and 240 bp hinge insert. Lane 4: KpnI and EcoRI digested  $\Delta H$  *PfAdoMetDC* in pASK-IBA3 with a  $\sim 4.6$  kb linearized plasmid. Lane 5: KpnI and EcoRI digested  $\Delta A3\Delta H$  *PfAdoMetDC* in pASK-IBA3 with a  $\sim 4.3$  linearized plasmid.

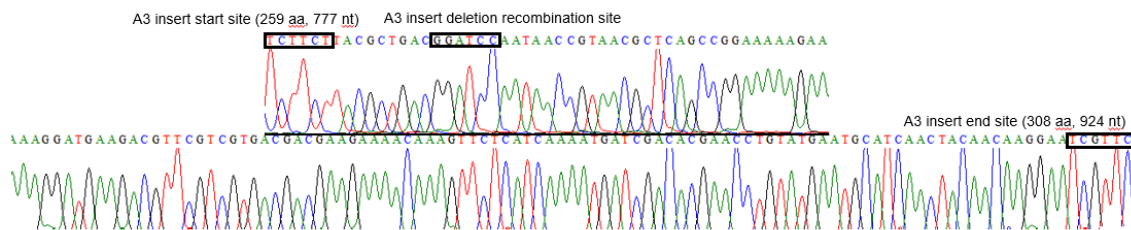


## Appendix 4

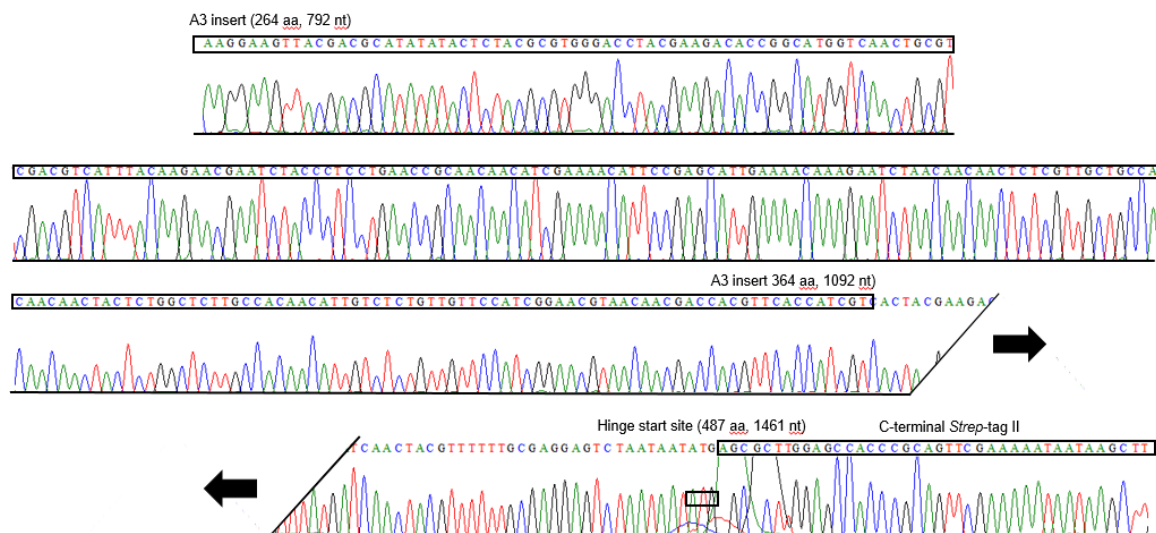
### Automated nucleotide sequencing of $\Delta A3$ , $\Delta H$ and $\Delta A3\Delta H$ *PfAdoMetDC*.

The  $\Delta A3$ ,  $\Delta H$  and  $\Delta A3\Delta H$  *PfAdoMetDC* plasmids were sequenced with Sanger-dideoxy chain terminator sequencing on a ABI 3130XL sequencer using the BigDye<sup>®</sup> terminator cycle sequencing kit at Inqaba Biotech<sup>™</sup>, SA. The plasmids were sequenced with pASK-IBA3 sequencing primers (Invitrogen); Forward 5'-GAGTTATTTTACCACTCCCT-3' and Reverse 5'-CGCAGTAGCGGTAAACG-3'. The sequencing reactions were analysed using the ABI Prism 3130<sup>®</sup> analyser and chromatograms analysed using BioEdit<sup>®</sup> sequence alignment editor. The chromatograms for  $\Delta A3$ ,  $\Delta H$  and  $\Delta A3\Delta H$  *PfAdoMetDC*, showing the respective point mutations are indicated in Figure 4.

(A)



(B)



(C)

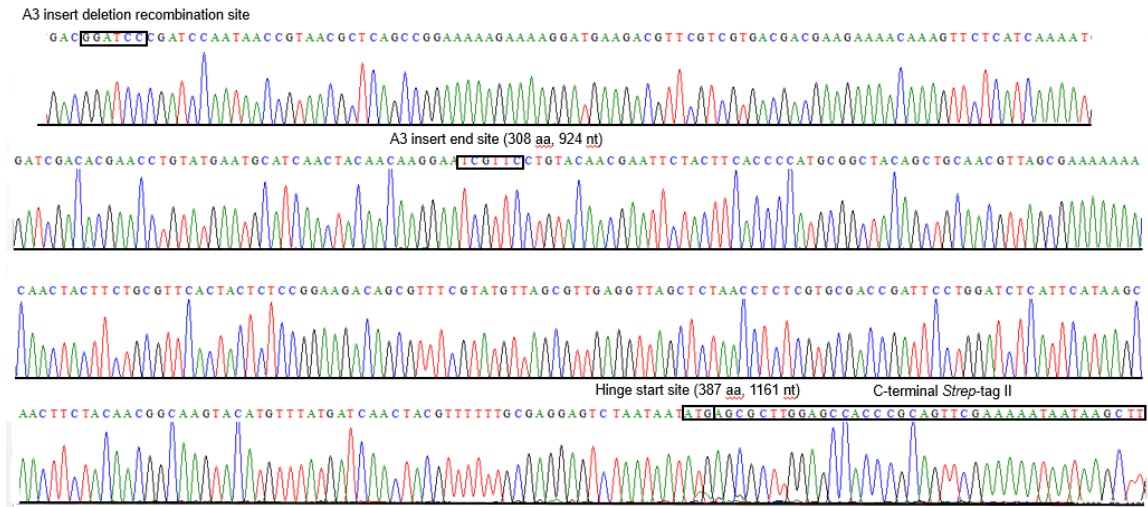


**Figure 4: Nucleotide sequences and chromatograms of dideoxy Sanger sequencing of  $\Delta A3$ ,  $\Delta H$  and  $\Delta A3\Delta H$  *PfAdoMetDC*.** (A) Nucleotide sequence and chromatogram of  $\Delta A3$  *PfAdoMetDC*. The chromatogram indicates the start site of the A3 parasite-specific insert at 777 bp (259 aa) with the 100 aa deletion being indicated with the A3 insert deletion recombination site 792 bp (264 aa). (B) Nucleotide sequence and chromatogram of  $\Delta H$  *PfAdoMetDC*. The chromatogram indicates the 100 aa residues removed for the  $\Delta A3$  mutant (792 bp, 264 aa to 1092 bp, 364 aa) and with the C-terminal *Strep*-tag II starting at 1461 bp (487 aa). (C) Nucleotide sequence and chromatogram of  $\Delta A3\Delta H$  *PfAdoMetDC*. The chromatogram indicates the A3 insert deletion recombination site 792 bp (264 aa) as well as the C-terminal *Strep*-tag II starting at 1161 bp (387 aa).

## Appendix 5

*PfAdoMetDC* A3 insert amino acid sequence analysis, Kyte and Doolittle hydrophobicity plot, complexity and disorder prediction.

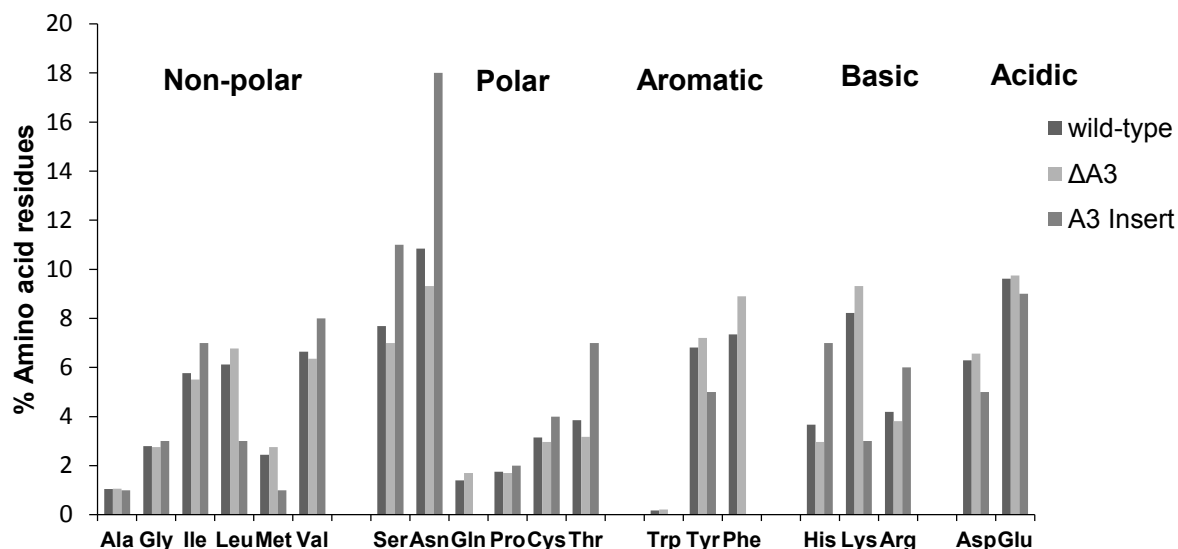


**Figure 5: Amino acid content analysis of full length wild-type *PfAdoMetDC*, the  $\Delta A3$  mutant, and the A3 insert.** The % amino acid composition of full length wild-type *PfAdoMetDC* was compared to the  $\Delta A3$  deletion mutant and the A3 insert, indicating amino acid selection bias for Asn residues and hydrophilic residues within the parasite-specific insert.

A Kyte and Doolittle hydrophobicity plot of the 100 amino acid residues removed from the A3 insert of  $\Delta A3$  *PfAdoMetDC* was determined using CLC Bio Protein Workbench 6 (Figure 6). The plot revealed the ratio of hydrophobic to hydrophilic amino acid residues scored for each residue depending on the residue's hydrophobicity (224). LCRs were predicted using the Wootton and Federhen algorithm (SEG algorithm) (225) with the CLC Bio Protein Workbench 6 (Figure 7). Protein unstructured regions were predicted with the IUPred server (226) ([iupred.enzim.hu/pred.php](http://iupred.enzim.hu/pred.php)) according the algorithm described by (227) and the graph was analysed with JpGraph software (Figure 8).

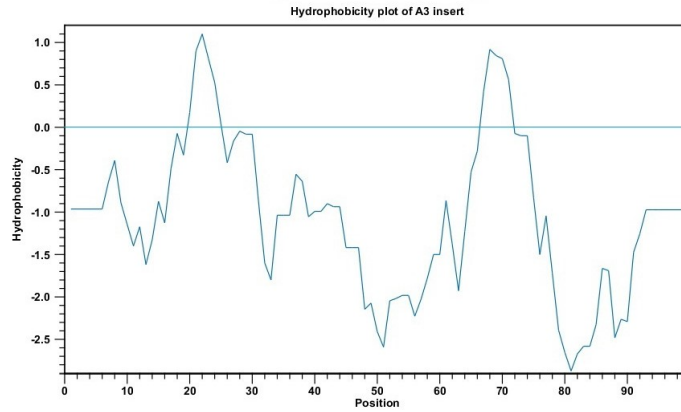


**Figure 6: Kyte and Doolittle hydrophobicity plot of the core residues removed from the A3 insert.** The plot predicted that most of the residues present in the A3 insert had a hydrophilic nature where hydrophobic residues have a positive value and hydrophilic residues a negative value.

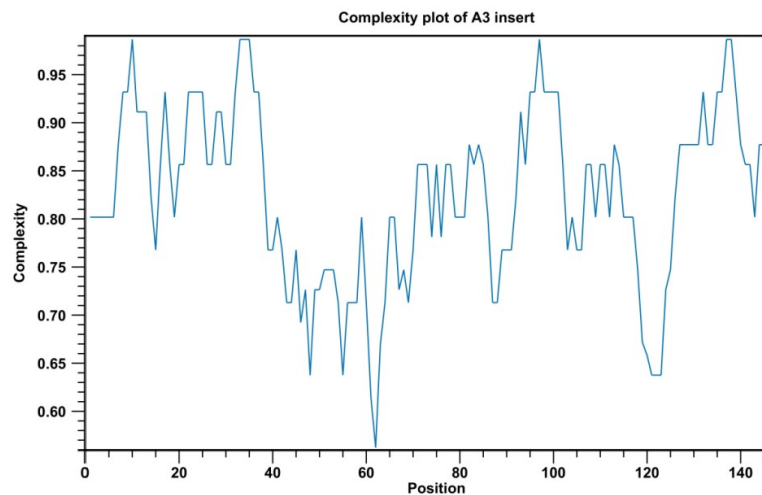


**Figure 7: Complexity plot of A3 *PfAdoMetDC* insert.** The plot predicted low-complexity regions (complexity 0.6-0.8) and high complexity regions (0.8-0.95) according to the Wootton and Fedheren Seg algorithm. LCR's were predicted for residues 39-70, 87-91, 103-106, 118-125.

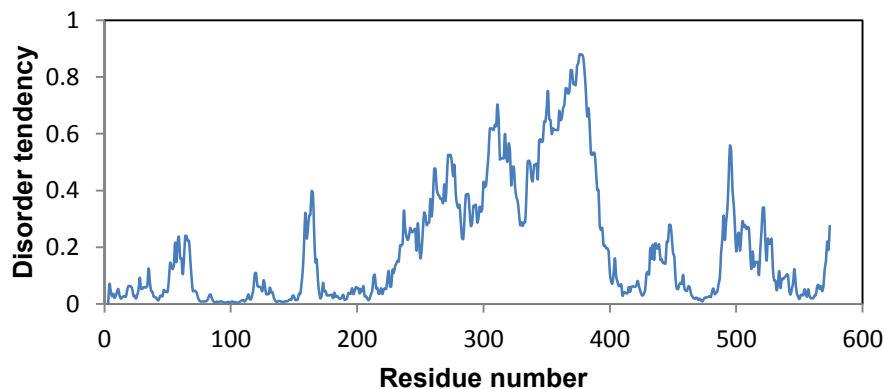


**Figure 8: IUPred prediction of intrinsically unstructured regions.** The plot represents the entire wild-type *PfAdoMetDC* sequence. Five unstructured regions were identified in the A3 insert (values >0.5).

## **Appendix 6**

### **MALDI-TOF MS analysis of $\Delta A3$ *PfAdoMetDC*.**

Soluble affinity chromatography purified (~50  $\mu$ g)  $\Delta A3$  *PfAdoMetDC* was separated by reducing SDS-PAGE followed by Coomassie blue staining. The major bands were analysed by MALDI-TOF MS. The ~100 kDa band was confirmed as a homodimer of  $\Delta A3$  *PfAdoMetDC*, and the ~59 and ~50 kDa bands as the unprocessed and processed  $\alpha\beta$  monomers, respectively. The faint ~70 kDa band was identified as the *E. coli* DnaK (Hsp70), previously identified by LC-MS MS to be co-purified with *PfAdoMetDC* (192).

## MALDI-TOF MS of ΔA3 PfAdoMetDC: Sequence analysis and MASCOT data

Verification of ΔA3 PfAdoMetDC with MALDI –TOF MS

Easy nano-Liquid Chromatography coupled to LTQ Orbitrap Velos Mass Spectrometry at the CAF Proteomics Laboratory at Stellenbosch University South Africa ([www.sun.ac.za/saf](http://www.sun.ac.za/saf)) was used to verify the presence of C505S ΔA3 PfAdoMetDC bands by SDS-PAGE analysis following SEC. Database searches of the peptide sequences were performed with PlasmDB 7.1 using the software packages; Proteome Discover 1.2 and MASCOT.

### 50 kDa band MASCOT database search

Accession	# AAs	MW [kDa]	calc. pI	Description	ΣCoverage	Σ# PSMs	Σ# Peptides	Score A5	Coverage A5	# PSM A5	# Peptides A5
PF10_0322	1434	168.1	6.37	organism=Plasmodium_falciparum_3D7   product=S-adenosylmethionine decarboxylase/ornithine decarboxylase   location=PF3D7_10:1324130-1328434(-)   length=1434	19.87	573	30	11806.48	19.87	573	30

### 50 kDa band sequence\*

```

MNGIFEGIEK RVVIKLKESF FKGRRNVNSF LDIPKELWEE KLKYIGCSIV SEISEDKNER RGERCRVYLL SESSLYIFDD
SLFIKTCGKT RVLFFPIPFV DILLIYHMDNV GIEKNCVYD ETFIENEKHF NIAEFIREHF LYCFPTHMNY RNKTRDGYFE
QEYPHRSLED EKKFFPEFFFK NVQMYNTHLP MERMHYIFY SDDVHMTDI ASTFKPCSEI

HLFGINKYNE KNQFHDAYLN NKSLSLNFTRV HEDNLKLYDS SDADKEVTH IYSTRGTIYED TGMVNCVDVI YKNESTLLNR
NNIENIPSEI NKESNNNSRC CHNNNSYSGC HNIVSVVPE RNDHVHHRH YEDTLNRSNI SAEDNNRNAQ LEKERDEVDV
RDDEENKVLK KMDITNLYEC INYNRESFLY NEFYFTPCGY SCNVSEKNNY FCVHYSPEDS

VSYVSVEVSS NLSCDRFLDF MHRQLNFYNG KYMFMINYVF CEESNNMSKM VPDDNNNNYS SGKSCVYQD LNKKEEY
RLNKKLRNDL FINSKQFYEL HTFERTVGF MRVQYFVYKL RDVVKCVEKE TLLARSSSCL FMFNKIRND VHDYVTKSS
NGGVIRQLTE RDVDDMYEYA LNFCKQNKIV VVDNTFFDA SKRKENLIK ERVQTNEKDE

YEKDEVYRR GNNELSSLDH LDSKNNLIHM YEKKNCDII NKDDENSTIA TNNNDNNNDN NNDSSSYDKS ITISRSSCN
NSHLSYSSFD NNHGNEKMKD YISVDENNNN NNNNNNNNNN NNNKNNVLL TLQRNSDDEN GKDKDNEKNV VLENMEKN
YKEEINWYIT KNKVEVKTLE KVLNENIDTS VVCINLQKIL AQYVRFKKNL PHVTPFYSVK

SNNDVVVIFK LYGLNCFNDC ASIGEISKVI KLLPNLSRDR IIFANTIKSI NSLIYARKEN INLCTFDNLD ELKKIYKYHP
KCSLILRINV DFKNYKSYMS SKYGANEYEW EEMLLIYAKKH NLNIVGVSFH VGSNTNLFDF FOLAIKLCDR VFDMSNNMGF
NFYIINLGGG YPEELEYNDA KKHDKIHYCT LSLQEIKKDI QKFLNEETFL KTYGYYSFE

KISLAINMSI DHYFISHMKDN LRVICEPGRY MVAASSTLAV KIIGKRRPT QGIMLKDLDK HYDPLNFAQQ ENKQDETKI
NHNDNNNDN DNDNNNDNI NNNNNQKGG QGNIMNDLII TSTNDSTNKK NDHSSSQVIQ NVSCTIRDKE GDNKINTHT
INNPNINGKE NTVGDGNIINI AHNIGNNFS SSNSKLGNI NIKKKVVNIN DNRNYFYSY

VSDSIYGCFS GIIFDEYNRC PIYVIKNNN PNQNFNFNL YLANVFGQSC DGLDMSINT YLPECYINDW LLYEYAGAYT
FVSSNENGF KKCKKVIYIF ESKPSLKGQP NKHW

```

\*Green and yellow letters indicate MS identified sequences aligned with *Pf*AdoMetDC sequence from PlasmoDB

### 60 kDa band MASCOT database search

Accession	# AAs	MW [kDa]	calc. pI	Description	ΣCoverage	Σ# PSMs	Σ# Peptides	Score A5	Coverage A5	# PSM A5	# Peptides A5
PF10_0322	1434	168.1	6.37	organism=Plasmodium falciparum_3D7   product=S-adenosylmethionine decarboxylase/ornithine decarboxylase   location=PF3D7_10:1324130-1328434(-)   length=1434	15.20	264	21	4647.56	15.20	264	21

### 60 kDa band sequence\*

```

MNGIFEGIEK RVIKILKESF FKGNRNVNSF LDIPKELWEE KLKYIGCSIV SEISEDKNER RGERCRVYLL SESSLYIFDD
SLFIKTCGKT RVLFFIPFVV

DLIIYHMDNV GIIEKNCVYD ETFIENEKPH NIAEFIKEHF LYCFFTHMNY RNKTKDGYFE QEYPHKSLED EKKFFEFFFK
NVQMYNTHLP MEKMHYIFFY

SSDDVHMIDI ASIFKFCSEI HLFGINKYNE KNQFHDAYLN NKSINLFRV HEDNLKLYDS SDADKEVTTH IYSTRGTYED
TGMVNCVDVI YKNESTLLNR

NNIENIPSIE NKESNNNSRC CHNNNYSGSC HNIIVSVVPSE RNNDHVHHRH YEDTLNRSNI SAEDNNRNAQ LEKEKDEDVR
RDDEENKVL I KMIDTNLYEC

INYNKESFLY NEFYFTPCGY SCNVSEKNY FCVHYPEDS VSYVSEVSS NLSCDRFLDF MHKQLNFYNG KYMFMINYVF
CEESNNMSK VPDDNNNYS

SGKSCVYYQD LNKKEKEEY RLNKKLRNDL FINSKQFYEL HTFTERTVGF MRVQYFVYKL RDVVKCVEKE TLLARSSSCL
FMFNKIRND VHDDYVTKSS

```



NGGVIKQLTE RDVDDMEYEA LNFCKQNKIV VVDNTFFDA SKRKENLIKLEKVTNEKDE YEEKDEVYRR GNNELSSLDH  
 LDSKNNLIHM YYEKNKCDII  
  
 NKDDENSTIA TNNNDNNNDN NNDSSSYDKS ITISRSSSCN NSHLSYSSFD NNHGNEKMKD YISVDENNNN NNNNNNNNNN  
 NNNKNNNVLL TLQRNSDDEN  
  
 GKDKDNEKND VSLENNMEKN YKEEIWNYIT KNKVEVKTLE KVLNENIDTS VVCINLQKIL AQYVRFKKNL PHVTPFFYSVK  
 SNNDEVVIKF LYGLNCFDC  
  
 ASIGEISKVI KLLPNLSRDR IIFANTIKSI NSLIYARKEN INLCTFDNLD ELKKIYKYP KCSLILRINV DFKNYKSYMS  
 SKYGANEYEW EEMLLYAKKH  
  
 NLNIVGVSPH VGSNTKNLFD FCLAIKLCRD VFDMSNMGF NFYIINLGGG YPEELEYDNA KKHDKIHYCT LSLQEIKKDI  
 QKFLNEETFL KTKYGYYSFE  
  
 KISLAINMSI DHYFSHMKDN LRVICEPRY MVAASSTLAV KIIGKRPTF QGIMLKDLKD HYDPLNFAQQ ENKKQDETKI  
 NNNNDNNNDN DNNNDNNNI  
  
 NNNNNQKGG QGNIMNDLII TSTNDSTNKK NDHSSQVIQ NVSCTIRDKE GDNIKINTHT INNPNINGKE NTVDGNINI  
 AHKNIGNNFS SSNSKLGIT  
  
 NIKKKVVNIN DNRNYFSY VSDSIYCFCS GIIFDEYNRC PIYVIKNNN PNQFMFNL YLANVFGQSC DGLDMINSIT  
 YLPECYINDW LLYEYAGAYT  
  
 FVSSNFNGF KKCKKVYIFP ESKPSLKGQP NKHW

## 70 kDa band MASCOT database search

Accession	# AAs	MW [kDa]	calc. pI	Description	$\Sigma$ Coverage	$\Sigma$ # PSMs	$\Sigma$ # Peptides	Score A2	Coverage A2	# PSM A2	# Peptides A2
P04264	644	66.0	8.12	Keratin, type II cytoskeletal 1 OS=Homo sapiens GN=KRT1 PE=1 SV=6 - [K2C1_HUMAN]	38.35	103	17	2879.66	38.35	103	17
A7ZHA4	638	69.1	4.97	Chaperone protein dnaK OS=Escherichia coli O139:H28 (strain E24377A / ETEC) GN=dnaK PE=2 SV=1 - [DNAK_ECO24]	33.39	191	18	2237.87	31.97	82	17
P35527	623	62.0	5.24	Keratin, type I cytoskeletal 9 OS=Homo sapiens GN=KRT9 PE=1 SV=3 - [K1C9_HUMAN]	20.71	60	8	2741.02	20.71	60	8
P00761	231	24.4	7.18	Trypsin OS=Sus scrofa PE=1 SV=1 - [TRYP_PIG]	16.45	32	3	557.27	16.45	32	3
P13645	584	58.8	5.21	Keratin, type I cytoskeletal 10 OS=Homo sapiens GN=KRT10 PE=1 SV=6 - [K1C10_HUMAN]	14.55	21	7	590.75	14.55	21	7
P02769	607	69.2	6.18	Serum albumin OS=Bos taurus GN=ALB PE=1 SV=4 - [ALBU_BOVIN]	14.33	16	8	256.20	14.33	16	8
P35908	639	65.4	8.00	Keratin, type II cytoskeletal 2 epidermal OS=Homo sapiens GN=KRT2 PE=1 SV=2 - [K22E_HUMAN]	13.62	31	6	894.41	13.62	31	6

## 100 kDa band MASCOT database search

Accession	# AAs	MW [kDa]	calc. pI	Description	ΣCoverage	Σ# PSMs	Σ# Peptides	Score A5	Coverage A5	# PSM A5	# Peptides A5
PF10_0322	1434	168.1	6.37	organism=Plasmodium_falciparum_3D7   product=S-adenosylmethionine decarboxylase/ornithine decarboxylase   location=Pf3D7_10:1324130-1328434(-)   length=1434	11.99	308	19	5833.12	11.99	308	19

## 100 kDa band sequence\*

MNGIFEGIEK RVVIKLESF FKGNRNVNSF **LDIPKELWEE** KLKYIGCSIV SEISEDKNER RGERCRVYLL SESSLYIFDD  
 SLFIKTCGKT RVLFFIPFV DLIYHMDNV **GIEKNCVYD** **ETFIENEKPH** **NIAEFIKEHF** LYCFFTHMNY RNK**TKDGYFE**  
**QEYPHKSLED** **EKKFFFEFFK** **NVQMYNTHLP** **MERMHYIFFY** SSDDVHMTDI ASTFK**FCSEI**

**HLFGINKYNE** **KNQPHDAYLN** **NKSLNLFTRV** HEDNLKLYDS SDADKEVTTH IYSTRGTYED TGMVNCVDVI YKNESTLLNR  
 NNENIPISIE NKESNNNSRC CHNNYSGSC HNIVSVVPE RNNHVVHHRH YEDTLNRSNI SAEDNNRQAQ LEKEKDEDVR  
**RDDEENKVL** **KMIDTNLYEC** **INYNKESFLY** NEFYFTPCGY SCNVSEKNNY FCVHYSPEDS

VSYVSEVSS NLSCDRFLDF MHKQLNFYNG KYMFMINYVF CEESNNMSKM **VPDDNNNYS** **SGKSCVYQD** **LNKKEKEEYY**  
 RLMKKLRNDL **FINSKQFYEL** **HTFTER**TVGF **MRVQYFVYKL** RDVVKCVEKE TLLARSSSCL FMFNNIKRD VHDYVTKSS  
 NGGVIKQLTE RDVDDMYEYA LNFCKQNKIV VVDINTFFDA SKRKENLIK ERVQTNEKDE

YEEKDEVYRR GNNELSSLDH LDSKNNLIHM YYEKNKCDII NKDDENSTIA TNNNDNNNDN NNDSSSYDKS ITISRSSSCN  
 NSHLSYSSFD NNHGNEKMKD YISVDENNNN NNNNNNNNNN NNNKNNVLL TLQRNSDDEN GKDKDNEKND VSLENNMEKN  
 YKEEIWNYYT KNKVEVKTLE KVLNENIDTS VVCINLQKIL AQYVRFKKNL PHVTPFYSVK

SNNDEVVIKF LYGLNCNFDC ASIGEISKVI KLLPNLSRDR IIFANTIKSI NSLIYARKEN INLCTFDNLD ELKKIYKYHP  
 KCSLILRINV DFKNYKSYMS SKYGANEYEW EEMLLYAKKH NLNIVGVSFH VGSNTKLNFD FCLAIKLCRD VFDMSNMGF  
 NFYIINLGGG YPEELEYDNA KKHDKIHYCT LSLQEIKKDI QKFLNEETFL KTKYGYYSFE

KISLAINMSI DHYFSHMKDN LRVICPEGRY MVAASSTLAV KIIGKRRPTF QGIMLKDLDK HDYPLNFAQQ ENKKQDETKI  
 NNNNDNNNDN DNNDNNNDNI NNNNNNQKGG QGNIMNDLII TSTNDSTNKK NDHSSSQVIQ NVSCTIRDKE GDNKINHTHT  
 INNPINGKE NTVDGDNINI AHKNIGNNFS SSKSLGNIT NIKKKVVNIN DNRYNYFSYY

VSDSIYGCFS GIIFDEYNRC PIYVIRKNN PNQNFMMFNL YLANVFGQSC DGLDMINSIT YLPECYINDW LLEYAGAYT  
 FVSSSNFNGF KRCKKVYIFP ESKPSLKGQP NKHW

## Appendix 7

### Chapter 3: Supplemental data for novel S-adenosyl-L-methionine decarboxylase inhibitors as potent antiproliferative agents against intra-erythrocytic *Plasmodium falciparum* parasites.

#### S1

Evaluation of the crystallised hAdoMetDC revealed 8 different substrate analogues, all co-crystallised in the *syn* conformation within 14 different structures ([www.rcsb.org](http://www.rcsb.org)). Compound 21c co-crystallised within the human hAdoMetDC (PDBID 3DZ2) were selected as the bioactive inhibitor conformation to which the MDL73811 derivatives were aligned, since it represents a molecular conformation similar to the conformation that will be assumed before a Schiff base can form. Conformational search analysis of these analogues and their comparison to compound 21c are denoted in Table S1. The best overlaying *syn* conformations with compound 21c found were Genz-644131 and MDL73811, which were ranked to be the 7<sup>th</sup> and 22<sup>nd</sup> lowest conformational energies when compared to the overall lowest energy conformation of the respective compounds. In addition, we calculated the binding free energy for each ligand prior to Schiff base formation and their ligand energies (Table S1). An overlay of compound 21c, MDL73811 and its derivatives after *in situ* optimisation within the *Pf*AdoMetDC structure are shown in figure S1.

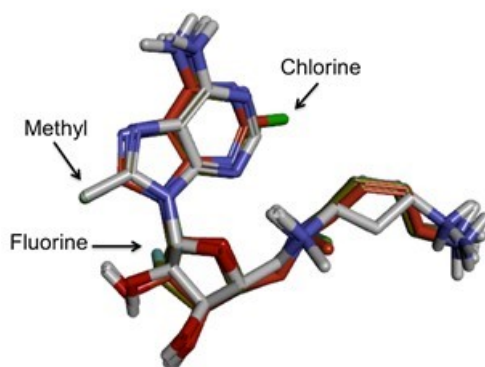


**Figure S1: The bioactive *syn* conformations of MDL73811 and its derivatives overlaid with compound 21c (white) post *in situ* optimisation.** The methyl, fluorine and chlorine substitutions of Genz-644131, Genz-644043 and Genz-644053 respectively are highlighted.

**Table S1: Conformational search analysis of the MDL73811 and its analogues.**

	ROCS Tanimoto Combo score	Conformational overlay similarity	Lowest energy conformation <sup>#</sup>	<i>syn</i> Lowest energy conformation <sup>#</sup>	Number of conformations generated <sup>#</sup>	Bioactive <i>syn</i> conformational number <sup>#</sup>	Binding free energy <sup>†</sup>	Ligand energy <sup>†</sup>
Compound 21c	--	0.97	-145.3	-148.8	215	31	-76.5	-131.6
MDL73811	1.58	0.95	-124.0	-131.6	200	22	-101.7	-105.8
Genz-644131	1.81	0.96	-130.7	-132.9	207	7	-112.1	-104.1
Genz-644043	1.56	0.95	-117.8	-131.0	193	106	-98.1	-98.0
Genz-644053	1.46	0.96	-127.8	-136.0	209	64	-108.5	-110.1

\* Generated conformations were ranked from lowest to highest energy. i.e. The bioactive *syn* conformation of Genz-644131 was the 7<sup>th</sup> lowest energy conformation from 207 generated.

# All conformational energies are given in kcal/mol.

† Binding free energy calculations were performed prior to Schiff base formation.

## **S2: Drug combination studies of Genz-644131 and other polyamine biosynthesis inhibitors**

Fixed-ratio isobole analysis (314) was performed to determine interactions between Genz-644131 with DFMO and the Spermidine synthase (SpdS) inhibitor; Trans-4-methylcyclohexylamine (4-MCHA). A fixed-ratio series of six drug combinations for Genz-644131:DFMO and Genz-644131:4-MCHA was established with the IC<sub>50</sub> of an independent drug present in the fourth serial dilution of a 96-well plate: 100% drug 1 to 0% of drug 2; 80% drug 1 to 20% drug 2; 60% drug 1 to 40% drug 2; 40% drug 1 to 60% drug 2; 20% drug 1 to 80% drug 2 and 0% drug 1 to 100% drug 2. Ring stage intra-erythrocytic *P. falciparum* parasites (1% haematocrit, 1% parasitaemia) were co-treated as such with Genz-644131 and either DFMO or 4-MCHA for 96 h and parasite proliferation was subsequently measured using the SYBR Green I-based assay. The fractionary inhibitory concentration (FIC) values were expressed as the IC<sub>50</sub> obtained for a drug combination compared to the IC<sub>50</sub> for the drug alone. Corresponding FIC values were plotted to obtain isobolograms (314, 315) with a straight line an additive effect, concave to the bottom drug synergism, and concave to the top drug antagonism. The magnitude of synergism or antagonism is indicated with SFIC, determined as the mid-point of the curve between the two drugs plotted in the isobologram; a value of >2-4 indicates antagonism, 1 additive and <0.5 a synergistic interaction (91, 314).

### **Genz-644131 displays similar *in vitro* antiplasmodial activity compared to MDL73811**

MDL73811 has shown synergistic interactions with DFMO in *in vivo* murine *T. b. rhodesiense* infections (316). However, the compounds showed an additive interaction in *in vitro* intra-erythrocytic *P. falciparum* parasites (SFIC=1.3, Figure S2A) (162). Additionally, Genz-644131 displayed an additive action when used in combination with either DFMO or 4-MCHA, with FIC values of 1.2 and 1.7, respectively (Figure S2B and S2C).

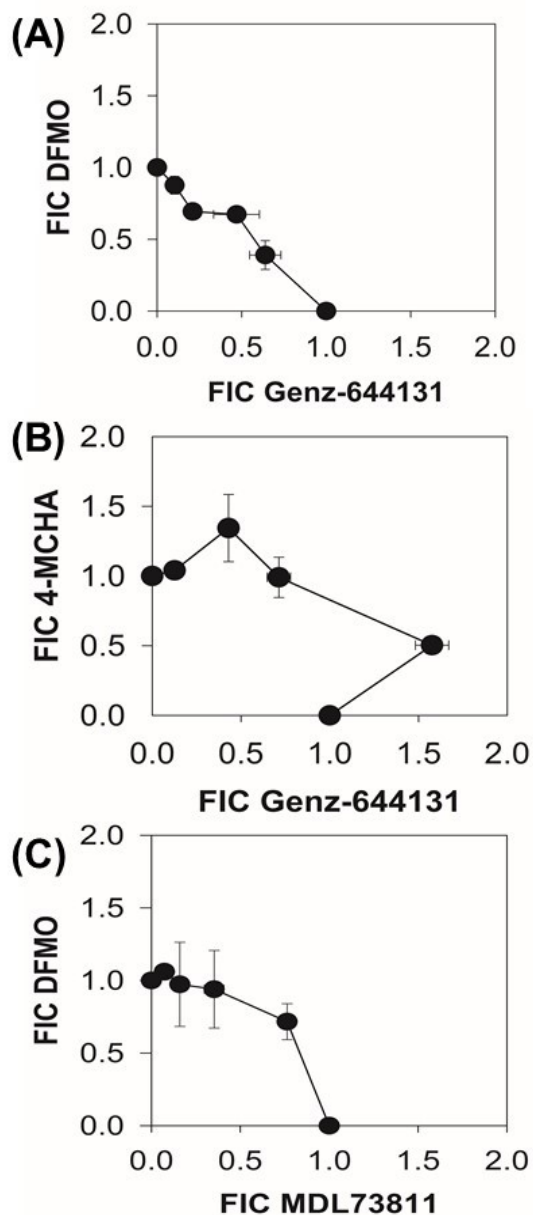


**Figure S2: Isobologram analysis of Genz-644131 with the ODC inhibitor DFMO and the SpdS inhibitor 4-MCHA.** Proliferation of ring stage intra-erythrocytic *P. falciparum* parasites was monitored over 96 h after initiating treatment on ring stage parasites at 37°C. (A) Isobologram of DFMO and MDL73811, indicating an additive effect between the two compounds with FIC = ~1.3. (B) Isobologram of DFMO and Genz-644131 indicating an additive effect between the two compounds with FIC = 0.12. (C) Isobologram of 4-MCHA and Genz-644131 indicating an additive effect between the two compounds with FIC = 1.7. Data are representative of three independent experiments performed in triplicate,  $\pm$  SEM. Where not shown, the error bars fall within the symbols.

### **S3: Efficacy of Genz-644131 against *P. berghei* in mice**

The acute *P. berghei* model in rodents is adapted from Peters' 4-day suppressive test using the *P. berghei* N strain. All studies were conducted under protocols approved by the IACUC of the Medical Sciences campus, University of Puerto Rico and in accordance with the Guide for the Care and Use of Laboratory Animals (National-Research-Council 1996. Guide for the Care and Use of Laboratory Animals. National Academy Press, Washington, DC.). Animals were maintained according to NIH guidelines and were allowed to acclimatise for 1 week prior to the commencement of studies. On Day 0, groups of 4-6-week old female Swiss Albino mice (n=5) were infected by tail vein injection with 0.2 ml heparinised blood diluted to contain  $1 \times 10^7$  N-clone parasites. Genz-644131 was formulated in 15% DMSO, 25% polyvinylpyrrolidone, 5% Tween 80 in water and was administered by oral gavage at either 20 or 100 mg/kg/day. On day 0, a single dose was given at 6 h post initial infection and over the subsequent 3 days the dose was split and administered b.i.d., with 6 h between doses. Animals in the Control group received vehicle alone. Dose concentration and frequency of dosing were based upon preliminary tolerability/exposure studies. On day 4 post-infection (5<sup>th</sup> day of assay) blood was collected by tail-nick, and thin smear microscope slides were prepared and stained using Diff Quick®. Parasitised erythrocytes were counted and compared with the total number of erythrocytes per microscopic field to determine the percent parasitaemia. A minimum of 350 erythrocytes was counted.

Results (Figure S3) indicate that Genz-644131 had a significant ( $P < 0.001$ ) parasite-suppressive effect at 100 mg/kg/day, reducing parasitaemia by 90% after 4 days' dosing and had some efficacy ( $P = 0.002$ ) when dosed at 20 mg/kg/day. Neither dose was curative, based upon the observation that all fields examined contained parasites (data not shown).



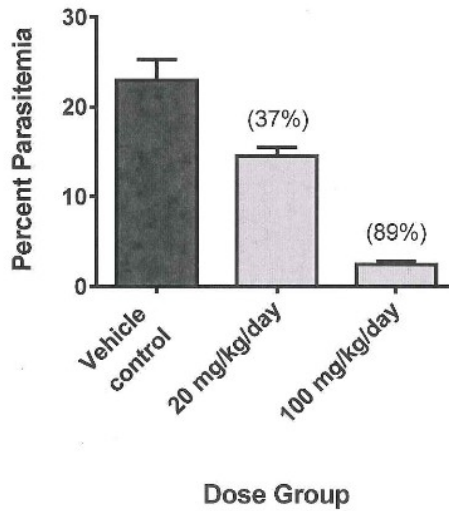


**Figure S3: Efficacy of Genz-644131 against *P. berghei* in mice.** Groups of 5 animals were infected on Day 0 and received a single treatment (half-dose) on that day at the doses indicated. For the next 3 days, animals were dosed b.i.d. Blood smears were made on Day 4 post infection and percentage parasitaemia was calculated based upon microscopic examination. Dark grey bars: animals received vehicle only; light grey bars: animals received 20 or 100 mg/kg/day. Values in parentheses indicate percentage reduction relative to vehicle-treated controls;  $\pm$  SEM. Where not shown, the error bars fall within the symbols.

## Appendix 8

### Kitz-Wilson enzyme kinetics analysis of MDL73811 against bifunctional and monofunctional *PfAdoMetDC*

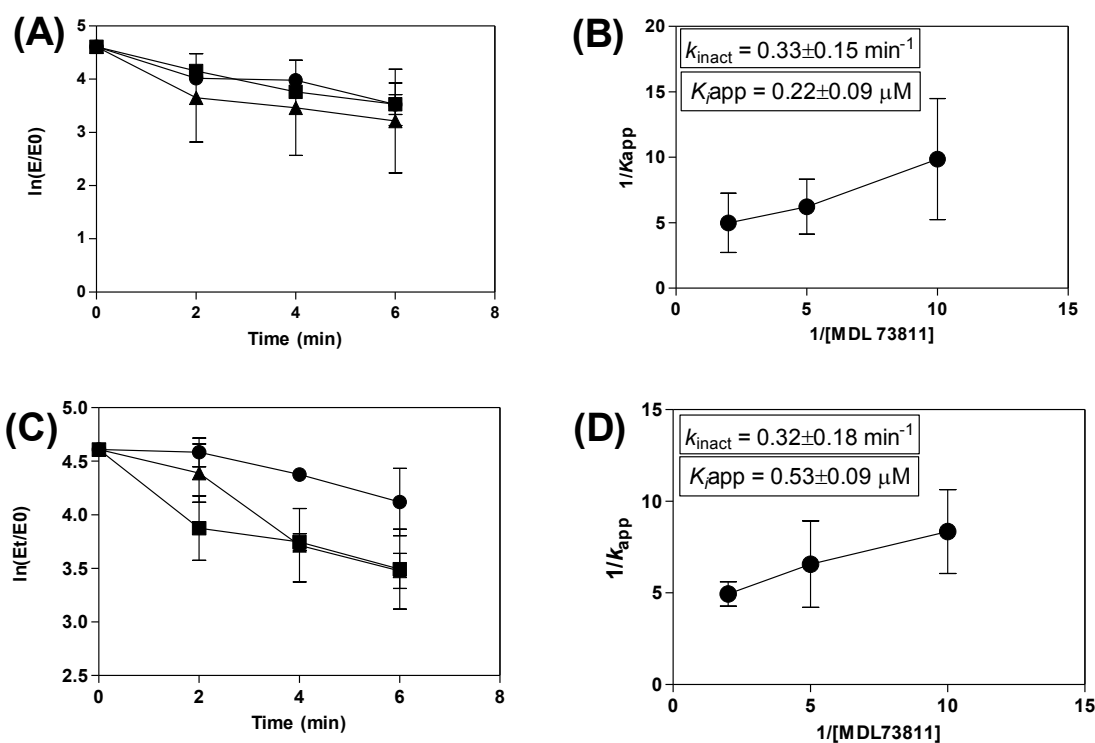


**Figure 9: Kitz-Wilson inhibition kinetics to determine the  $K_i$  for MDL 73811 against monofunctional and bifunctional *PfAdoMetDC*.** Kitz-Wilson inhibition kinetics was used to determine the  $K_{app}$  for MDL73811 against monofunctional (A and B) and bifunctional *PfAdoMetDC* (C and D). Percentage activity was determined from residual enzyme activity, following pre-incubation with MDL73811 at 0.02 (circles), 0.05 (squares) or 0.1  $\mu\text{M}$  (triangles) concentrations ( $[I]$ ) at specific time intervals (0–6 min) ( $E_t$ ). The  $\ln(E_t/E_0)$  of the activity at a specific inhibitor concentration was plotted against the pre-incubation time points using non-linear regression. The reciprocal of the slopes ( $1/k_{app}$ ) of the primary plots (A and C) was plotted against the reciprocal of the specific inhibitor concentrations using non-linear regression (B and D), from which the  $k_{inact}$  (inverse of the y-intercept) and the  $K_{app}$  (slope multiplied by  $k_{inact}$ ) were derived (275). Data are representative of three independent experiments performed in triplicate,  $\pm\text{SEM}$  and all values fell into the 95% confidence interval of the mean. Where not shown, the error bars fall within the symbols.

## Appendix 9

Dose response  $IC_{50}$  curves of MDL73811 derivatives as determined with the SYBR Green I-based assay

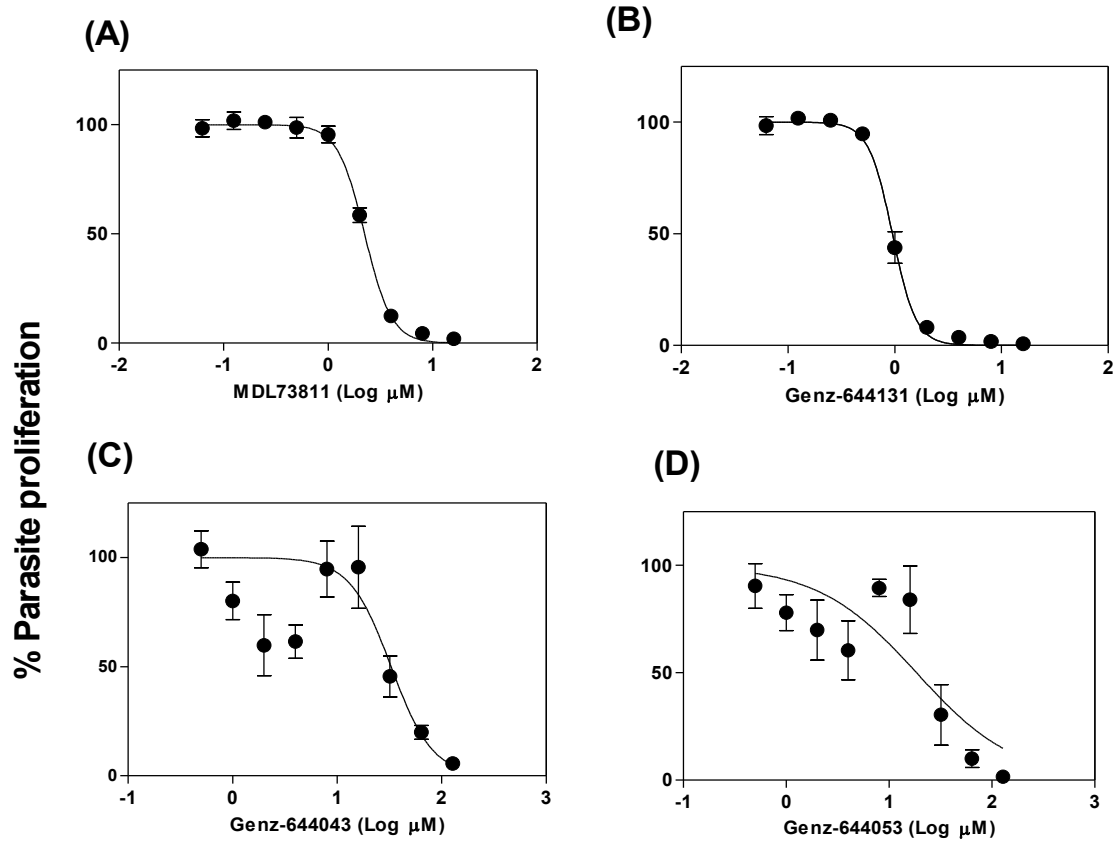


**Figure 9: Dose-response curves of MDL73811 derivatives showing the inhibitory effect on the *in vitro* proliferation of intra-erythrocytic *P. falciparum* parasites.** The  $IC_{50}$ 's of the MDL73811 derivatives were determined using the SYBR green I based assay. (A) Dose-response curve of MDL73811, (B) dose-response curve of Genz-644131, (C) dose-response curve of Genz-644043 and (D) dose-response curve of Genz-644053. Parasite proliferation values are normalised to untreated parasite proliferation at 100%. n=5, error bars indicate  $\pm$  SEM.

## Appendix 10

### Scanning Confocal Laser Microscopy (SCLM) of Pheroids® encapsulating Genz-644131

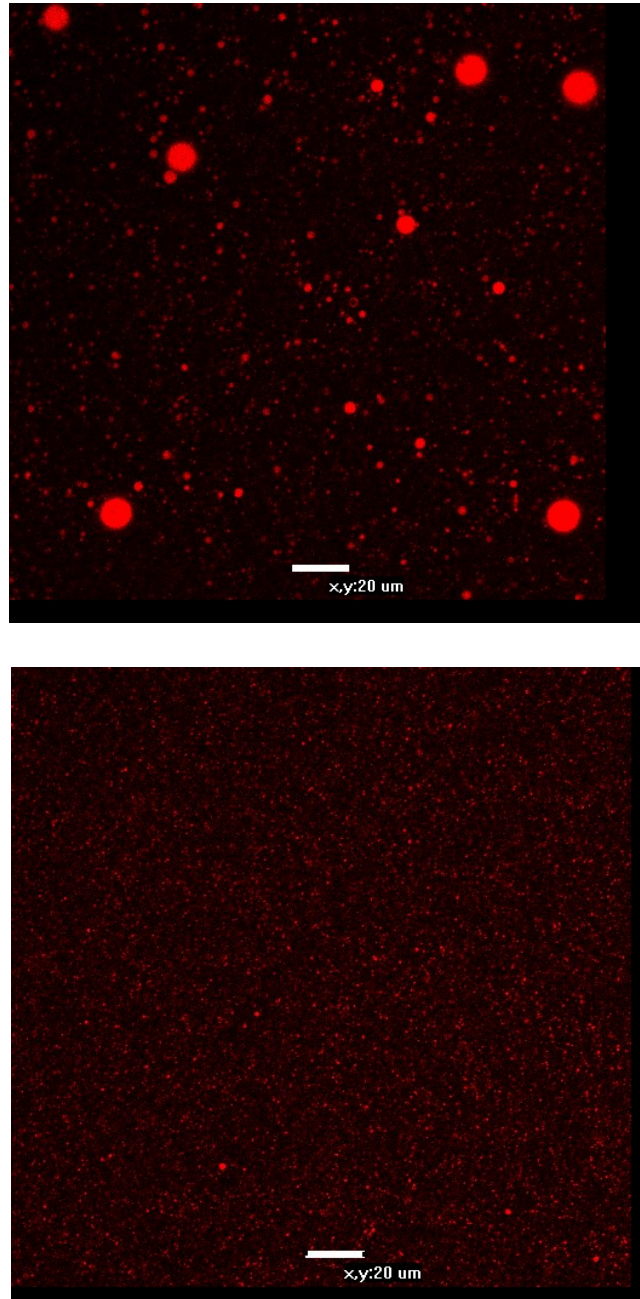


**Figure 10: SCLM of Pheroids® encapsulating Genz-644131.** Scanning Confocal Laser microscopy was performed to establish successful encapsulation of Genz-644131 within Pheroids® as described in (286). Red Fluorescent spheres are Pheroids® with encapsulated compound.